

Danshi Li

**Lightweight concept design
of economical FRTP-metal
multi-material vehicle doors**

**Lightweight concept design of economical
FRTP-metal multi-material vehicle doors**

Danshi Li

Siegener Schriftenreihe Automobiltechnik

Hrsg. von Xiangfan Fang

Band 8

Lightweight concept design of economical FRTP-metal multi-material vehicle doors

Von der Naturwissenschaftlich - Technischen Fakultät
der Universität Siegen
zur Erlangung des Grades eines Doktors
der Ingenieurwissenschaften
genehmigte Dissertation

vorgelegt von
Danshi Li, M.Sc.

Tag der mündlichen Prüfung:

02. November 2021

Referent:

Professor Dr.-Ing. Xiangfan Fang

Koreferent:

Professorin Dr.-Ing. Tamara Reinicke

Bibliografische Information der Deutschen Nationalbibliothek

Die Deutsche Nationalbibliothek verzeichnet diese Publikation in der Deutschen Nationalbibliografie; detaillierte bibliografische Daten sind im Internet über <http://dnb.dnb.de> abrufbar.

Impressum

Herausgeber:

Univ.-Prof. Dr.-Ing. Xiangfan Fang
Lehrstuhl für Fahrzeugleichtbau
Universität Siegen
Breite Straße 11
57076 Siegen
Telefon: +49 271 740 2384
Fax: +49 271 740 3786
E-Mail: info.flb@uni-siegen.de

Druck:

Uni Print, Universität Siegen

Siegen 2021: universi – Universitätsverlag Siegen
www.uni-siegen.de/universi

Gedruckt auf alterungsbeständigem holz- und säurefreiem Papier.

ISSN: 2568-0374 (Siegener Schriftenreihe Automobiltechnik)

ISBN: 978-3-96182-113-6

doi.org/10.25819/ubsi/10028

Die Publikation erscheint unter der
Creative Commons Lizenz CC-BY-SA



Acknowledgement

The present work originated during my work as the research assistant at the institute of automotive lightweight design (FLB). Throughout my research work and the writing of this dissertation, I have received a great deal of support and assistance.

First and foremost, I would like to express my sincere gratitude to my supervisor, Univ.-Prof. Dr.-Ing. Xiangfan Fang, for his invaluable advice, continuous support and patience at every stage of my research project and PhD study. His immense expertise and knowledge were invaluable for me in formulating the research topic and methodology. His insightful feedback brought my research work to a higher level. His “can-do” attitude on facing difficulties and challenges have encouraged me not only in the time of my research, but also in daily life.

I would like to offer my thanks to Univ.-Prof. Dr.-Ing. Tamara Reinicke for the acceptance as the second supervisor of my dissertation and her evaluation. In addition, I would like to thank Univ.-Prof. Dr.-Ing. Peter Kraemer and Prof. Dr.-Ing. habil. Chuanzeng Zhang for their participation of my PhD committee.

I would also like to extend my special thanks to my colleagues at FLB for their patient and effortless support, and stimulating discussion to my research work and life in Germany. Additionally, I would like to thank my Hiwis and the students, who support me through their Bachelor-, Master- and Diplom-work.

My deeply appreciation also goes to my parents. They are always there for me. Without their tremendous understanding, fully encouragement and unconditioned love in the past years, it would be impossible for me to complete my study. I would like to thank Mr. Xuefeng Wang for broadening my vision and his wise counsel and sympathetic ear. In additional, thank all my friends, who fill up my lonely time with many happy activities and memories.

Lastly, I would like to thank China Scholarship Council (CSC) for the scholarship and the general consulate of China in Düsseldorf for the continuous support during my PhD study time in Germany.

Siegen, Jun. 2021

Danshi Li

Zusammenfassung

Die Fahrzeugtür als große stahlintensive Klappe kann durch den Einsatz von Leichtbaumaterialien und neuen Konstruktionsprinzipien ein gewisses Gewichtseinsparpotenzial erzielen. Aufgrund der unterschiedlichen Steifigkeits- und Festigkeitsanforderungen an unterschiedliche Bereiche von Fahrzeugtüren unter statischen und Crash-Lastfällen kann die Multi-Material-Konstruktion eine der effektivsten Möglichkeiten sein, Leichtbau mit minimalen Zusatzkosten zu erreichen. Diese Arbeit zeigt einen Gestaltungsansatz von wirtschaftlichen Leichtbau-Multimaterial-Fahrzeugtürkonzepten auf Basis einer marktverfügbaren Stahlreferenz unter Berücksichtigung typischer statischer und Crash-Lastfälle. Es wird eine innovative Türstruktur vorgestellt, die eine tragende Ringstruktur und ein hochfunktionsintegriertes Innenblech umfasst. In der Struktur werden wirtschaftliche Leichtbaumaterialien wie Aluminium, langfaserverstärkte Thermoplaste und unidirektionale Tapes sowie entsprechende massenproduktionsorientierte Fertigungsmethoden eingesetzt. Die Anisotropieanalyse unter verschiedenen Belastungen garantiert einen effektiven Einsatz von unidirektionalen Tapes. Topologie- und Parameteroptimierungen liefern Designvorschläge für Rippenstrukturen aus langfaserverstärkten Thermoplasten. Die finalen Türkonzepte erreichen ca. 20% Gewichtsreduzierung und eine vergleichbare mechanische Leistung im Vergleich zur Stahlreferenztür. Speziell für den Crash-Lastfall wird zur Validierung der finalen Türkonzepte eine innovative Komponentenentwicklungsmethode eingesetzt, die das Crashverhalten nahe am Gesamtfahrzeugszenario mit begrenzten Umgebungskomponenten nachbildet.

Abstract

The vehicle door, as a major steel-intensive closure, can achieve a certain degree of weight-saving potential by the use of lightweight materials and new design principles. Due to the different stiffness and strength requirements on different areas of vehicle doors under static and crash loading conditions, multi-material construction can be one of the most effective ways to achieve lightweight design with minimal additional cost. This work illustrates an approach for the design of economical lightweight multi-material vehicle door concepts based on a market-available steel reference, while considering typical static and crash loading cases. An innovative door structure is introduced that includes a major load-bearing ring structure and a highly function-integrated inner panel. The structure incorporates economical lightweight materials, such as aluminum, long-fiber thermoplastics, and unidirectional tapes, and corresponding mass-production-oriented manufacturing methods. Anisotropy analysis under different loadings guarantees an effective use of unidirectional tapes. Topology and parameter optimizations provide design suggestions for rib structures of long-fiber-reinforced thermoplastics. The final door concepts achieve ca. 20% weight reduction and comparable mechanical performance compared to the steel reference door. Especially for the crash loading case, an innovative component development method is used to validate the final door concepts, which rebuilds the crash behavior close to the full-vehicle scenario with limited surrounding components.

Content

Acknowledgement.....	I
Zusammenfassung.....	II
Abstract.....	III
Content	IV
Abbreviation	VIII
Symbol	XI
1 Introduction	1
1.1 Motivation.....	1
1.2 Objective and structure of the work	3
2 State of the art.....	5
2.1 Fiber-reinforced thermoplastics for lightweight vehicles.....	5
2.1.1 Typical categories of FRTP material on lightweight vehicles	6
2.1.2 Typical mass-production-oriented manufacturing methods for FRTPs.....	16
2.2 Lightweight construction methods for FRP BIW components and applications	22
2.2.1 Integral and integrative construction.....	22
2.2.2 Multi-material construction.....	23
2.3 Typical construction of vehicle door.....	30
2.3.1 Door classification based on load-bearing structures.....	30
2.3.2 Door classification based on window frame structures	32
2.4 Door requirements definition	34
2.4.1 General requirements.....	34
2.4.2 Static loading cases	34
2.4.3 Crash loading cases.....	35
2.5 Existing lightweight studies and applications on vehicle doors	37
2.5.1 Lightweight door with steel	37

2.5.2	Lightweight door with light alloy	42
2.5.3	Lightweight door with fiber reinforced plastic (FRP).....	45
2.6	Mass-production-oriented joining techniques for FRTPs and multi-material components.....	53
2.6.1	General	53
2.6.2	Joining between FRTPs	54
2.6.3	Joining between FRTP and metal.....	57
2.7	Component development method with limited BIW data.....	62
2.8	Summary and cognition of the state-of-the-art technology.....	67
3	Concept, development process, and requirements	68
3.1	The multi-material door concept	68
3.1.1	Preliminary FLB concept (starting point).....	68
3.1.2	New concept ideas	69
3.1.3	Material choice and property – LFT and UD Tape	71
3.2	Development goal and process	75
3.3	Summary of general FEA modeling techniques.....	77
3.3.1	Static simulation with Abaqus (reference door).....	77
3.3.2	Topology-, parameter optimization, and static performance validation with OptiStruct (concept door)	78
3.3.3	Crash simulation with Ls-Dyna (reference and concept door).....	79
4	Reference door analysis.....	80
4.1	Structural analysis	80
4.2	Performance analysis	83
4.2.1	Static loading cases and anisotropy analysis	83
4.2.2	Crash loading cases.....	86
4.2.3	Implementable test bench design for a component development method.....	88
5	Structural development with topology optimization	99
5.1	Concept 1.....	99

5.1.1	Design space definition	100
5.1.2	Frame area design	101
5.1.3	Inner panel area design.....	107
5.2	Concept 2.....	117
5.2.1	Design space definition	117
5.2.2	Frame and inner panel area design.....	117
6	Door concept, structural validation, and parameter optimization.....	125
6.1	Concept 1.....	125
6.2	Concept 2.....	133
6.3	Comparison and evaluation of different door concepts	140
6.3.1	Weight and mechanical performance	140
6.3.2	Manufacturability and cost.....	140
6.4	Rapid prototyping with additive manufacturing	143
7	FRTP-metal multi-material door – opportunity and challenge in mass manufacturing ..	146
7.1	Cost for manufacturer.....	146
7.1.1	Investment cost.....	147
7.1.2	Material cost.....	147
7.1.3	Manufacturing cost.....	149
7.2	Reliability for customer use	151
7.3	Environment effect	152
7.3.1	Recycling	152
7.3.2	Life cycle analysis	152
8	Summary and outlook	154
8.1	Summary.....	154
8.2	Outlook.....	156
9	Reference.....	157
10	Appendix.....	169

10.1	Intrusion and intrusion velocity comparison of component development method ..	169
10.2	Bill of material of the FLB-concept.....	171
10.3	Detail of the FE model for the crash simulation	173
10.3.1	Important modeling requirement for the full vehicle crash simulation.....	173
10.3.2	*Mat_24 in Ls-Dyna with the stain rate dependency.....	174
10.3.3	Modeling UD-Tape with *Mat_54 in Ls-Dyna.....	175
10.4	Bill of material of the reference door	177
10.5	Schematics of the door static test bench (CAD)	179
10.6	Maximal intrusion comparison between concept 1 and the reference	181
10.7	Maximal intrusion comparison between concept 2 and the reference	184
10.8	Door material cost calculation and comparison	187
10.9	Life cycle analysis on automotive door outer panel.....	189

Abbreviation

AM	Additive Manufacturing
ATP	Automated Tape Placement
BIW	Body-In-White
BMC	Bulk-molding compound
BOM	Bill of material
CAD	Computer-aided design
CAE	Computer-aided engineering
CED	Cumulative energy demand
CF	Carbon fiber
CFRP	Carbon fiber reinforced plastic
COG	Center of gravity
DIW	Door-In-White
D-LFT	Direct long fiber thermoplastic compression molding process (sometimes as LFT-D)
DOF	Degree of freedom
DS	Design space
E-LFT	Direct endless and long fiber thermoplastic compression molding process
FDM	Fused Deposition Modeling
FDS	Flow drilling screw
FEA	Finite element analysis
FEM	Finite element method
FFF	Fused filament fabrication
FLB	Institute of Automotive Lightweight Design, University of Siegen
FMVSS	Federal Motor Vehicle Safety Standards
FRP	Fiber reinforced plastic

FRTTP	Fiber reinforced thermoplastic
GFxx	Glass fiber weight percent xx%
GHG	Greenhouse gas
G-LFT	Granulate long fiber thermoplastic injection molding process
GMT	Glass mat thermoplastics
HDT	Heat deflection temperature
IMA	In-Mold-Assembly
ITB	Implementable test bench model
LCA	Life cycle analysis
LFT	Long fiber thermoplastic
LGFxx	Long glass fiber reinforced thermoplastic with a fiber weight percent xx%
L3M	Level-3 model
MDB	Moving Deformable Barrier
MI	Metal insert
MIG	Metal Inert Gas
NCAP	New Car Assessment Program
NVH	Noise, Vibration, Harshness
OEM	Original Equipment Manufacturer (automobile)
PA	Polyamide
PMA	Post-Mold-Assembly
PP	Polypropylene
SDS	Sub-design space
SFT	Short fiber thermoplastics
SMC	Sheet-molding compound
TRL	Technology Readiness Level
UD	Unidirectional

Symbol

B/b	Width
d	Fiber diameter
E	E-modulus
F	Force
H/h	Height
I	Moment of inertia
l	Fiber length
m	Mass
M	Moment
T	Thickness
T_g	Glass transition temperature
T_m	Crystalline melting temperature
T_r	Rib thickness
T_s	Surface thickness
T_u	UD tape thickness
W''	Deflection
σ_{fu}	Fiber ultimate tensile strength
τ	Interfacial bonding strength between the fiber and the matrix
ρ	Density
σ_y	Yield stress
ε_{eff}^p	Effective plastic strain

1 Introduction

1.1 Motivation

Due to the trend of e-mobility and the increasingly stringent legislation requirements on vehicle emissions, lightweight design is now considered by the automotive industry as one of the most effective methods to help electric vehicles reach higher ranges or to reduce CO₂ emissions on traditional motor vehicles, in addition to management of the power train efficiency, aerodynamics, and electrical power [1]. According to the newest regulation from the European Union (EU), a value curve is defined in the “EU 2020-21 Target” [2] that sets a weight-related average CO₂ emission limit of 95 g/km for newly registered vehicles in 2021. This value is equal to a fuel consumption of ca. 4.1 L petrol or 3.6 L diesel per 100 km. Furthermore, to achieve a climate-neutral EU by 2050, a 37.5% CO₂ emission reduction from 2021 values has been set as an intermediate target for 2030 [3]. For OEMs, what should be more of a focus regarding the EU regulation is the increase in penalties for excess CO₂ emissions (up to 190 €/gram). According to a study [4], this penalty can be as high as 12000 € per vehicle sold (calculated based on 2010 vehicle models), which means that failure to fulfill the CO₂ target is no longer acceptable for OEMs.

The vehicle door, as a major steel-intensive closure component on a vehicle, has good potential for weight reduction through lightweight design. Typically, weight reductions on vehicle components are effectively achieved by lightweight material substitution and construction redesign. Currently, substituting lightweight materials is the only method applied to existing serial vehicle doors. Obviously, for OEMs, using material substitution on vehicle doors is a straightforward lightweight method that avoids making any significant changes in the conventional structure while removing a certain amount of weight. Although this method has been established for many years and is fully developed with lightweight materials, such as aluminum, magnesium, and even fiber-reinforced plastics (FRP) [5; 6; 7], the high additional material costs, which are a very sensitive issue for OEMs, remain the major obstacle for its application to serial productions by most economical vehicle manufacturers. Developing an economical lightweight design with a possibly lower additional cost for vehicle doors is therefore a concrete need of OEMs.

The development trends in the automotive industry and the prices of typical lightweight materials create difficulties for Body-In-Whites (BIW) with single lightweight materials, such as aluminum alloys or FRPs, to dominate the automotive market in the next few decades, and especially the in mass-production economical vehicle class. However, searching for an intelligent mixture of materials on BIWs is a promising way to find an answer to the dilemma between weight and cost [8], and is the reason why the multi-material design method has drawn so much attention among different lightweight methods.

As the philosophy of lightweight design says: use the right material in the right place. Multi-material design is undoubtedly one of the best ways to fulfill this philosophy economically. The principle of the multi-material design is to combine the strength of the substituted material and the construction redesign with consideration of the specific mechanical requirements of different structural regions. This then enables smart usage and integration between the innovative lightweight material and traditional structural materials, such as steels. This smart material use is the key factor for controlling the additional material, as well as the cost, of lightweight design. Nevertheless, multi-material design brings more challenges to the joining

techniques needed for different materials. Using constructive methods and innovative process combinations to solve the joining challenge is therefore an important research area for investigation.

For the reasons presented above, the major motivation of this work was to use a multi-material design method to solve the dilemma faced by OEMs between the demand for lightweight doors and the cost of vehicle doors. The basic idea underlying the multi-material door concept is to combine an innovative load-bearing door structure concept with the use of cost-efficient lightweight materials. Fang [9] has proposed the extensive use of long-fiber thermoplastics (LFTs), in addition to conventional lightweight materials such as aluminum, for crash-relevant structures in door concepts. Due to the completely different material behaviors and manufacturing methods between fiber-reinforced thermoplastics (FRTPs) and metals, a major investigation is made here on efficient methods for using FRTPs to achieve an optimum structure with a high level of component integration.

The whole development process of door concepts is accelerated in this work by the extensive incorporation of CAD and CAE in the design, optimization, and validation. To reproduce the door crash behavior close to the full vehicle (FV) simulation, Investigation is also made on the further development of a self-developed component development method with the limited surrounding BIW component information.

1.2 Objective and structure of the work

Compared to other conventional lightweight approaches, the multi-material design has the potential to achieve cost-neutral lightweight door concepts. The goal of this work is to develop a universal lightweight design approach for economical multi-material vehicle doors made with FRTPs. The door concepts should achieve the goal of weight reduction and reach comparable mechanical performance under given static and crash-loading conditions. The additional lightweight cost is maintained in the acceptable range of most OEMs by preferentially employing widely used lightweight materials and existing serial manufacturing methods.

The work has eight major parts. After a short introduction to the motivation, objectives, and structure of this concept development work, the topic-related state-of-the-art technologies are comprehensively illustrated in section 2. This includes the typical FRTP materials and their mass-production-oriented manufacturing methods, the typical lightweight construction methods and applications of FRTP BIW components, the typical constructions and requirements of vehicle doors, the existing lightweight studies and applications on vehicle doors, the typical joining techniques for FRTPs and multi-material components, and the component development method with limited BIW data.

In section 3, after a brief introduction of the preliminary concept of the Institute of Automotive Lightweight Design, University of Siegen (FLB), core innovation ideas on two new multi-material door concepts are illustrated with corresponding simplified sketches. The major material choice is also determined during idea generation. Due to the complexity of developing the multi-material door concepts, the specific development goal, process, and requirements are also given clearly in this section. Since the Finite Element Method (FEM) is the workhorse for this development work, the important Finite Element Analysis (FEA) modeling techniques are described as well, following the different loading cases and solvers.

Section 4 provides the analysis of the reference door. The FEA modeling techniques are also validated here with door static tests. The structural performance of the reference door is quantified and set as the inputs/objectives for the development of door concepts. This section further illustrates the anisotropy analysis on the reference door and further development of a component development method with limited BIW information; these fundamental methods are used throughout the whole concept development.

Section 5 describes in detail the structural development with the topology optimization method for two different door concepts. This includes a design space definition and a description of the specific innovative design approaches used for the frame and the inner panel area. A simplified calculation method allows determination of the mechanical performance and the rough material thickness range of the frame area without the need for the FEM. The design suggestion achieved from the topology optimization then provides guidance for the LFT rib construction.

Section 6 presents the structural validation, parameter optimization, and final construction for the two concepts. After fine-tuning the preliminary concepts, the final concepts are evaluated from the perspectives of the percentage of weight reduction and the structural performance under defined static and crash-loading cases compared to a reference door. Further comparisons of weight, mechanical performance, manufacturability, and cost between the two concepts are also made here. The possibilities of using additive manufacturing for the rapid prototyping of door concepts is also briefly discussed.

Section 7 is an analysis of the opportunities and challenges presented by the multi-material door as an industry product from the standpoint of manufacturers, customers, and the environment. It covers a variety of topics, such as cost, reliability, recycling, and life cycle analysis (LCA). The work ends with a summary and outlook on future development of the multi-material door concepts and other possible scenarios for using lightweight design approaches.

2 State of the art

2.1 Fiber-reinforced thermoplastics for lightweight vehicles

Fiber-reinforced thermoplastics (FRTPs), as a subgroup of fiber-reinforced plastics, have been widely used in the automotive industry for decades. Especially in the economy class of vehicles, FRTPs are used more often than fiber-reinforced thermosets. This is due to the longer cycle time required for the manufacture of components made of fiber-reinforced thermosets and the related higher cost as well as the recyclability. For this reason, fiber-reinforced thermosets are initially excluded from consideration in this work since they cannot meet the economic requirements. In this section, all mentioned techniques are oriented on FRTPs, including typical materials, manufacturing methods, and joining techniques.

On lightweight vehicles, most FRTPs are reinforced with E-glass fibers as these are available at low cost [10]. FRTPs inherit many attributes from their matrix materials, such as formability, weldability, damage resistance, and recyclability. The existence of fibers does not have any effect on the glass transition temperature (T_g) or the crystalline melting temperature (T_m) of thermoplastic polymers, which means that the thermoplastic matrix determines the performance of FRTPs at different temperatures [10]. However, the fibers do have some influence on some important properties of the composites, such as the modulus, strength, coefficient of thermal expansion, etc. Fibers can be incorporated into the thermoplastic matrix in many ways, and different methods can generate several types of fiber-reinforced thermoplastics [10]:

- Randomly oriented short fibers
- Randomly oriented long fibers
- Randomly oriented continuous fibers
- Unidirectional continuous fibers
- Bi-directional fabric

Randomly oriented short glass fiber reinforced thermoplastics are the most common thermoplastic matrix composites since they can be manufactured by traditional injection molding processing. They also behave more like an isotropic material because of the nearly random fiber orientation in the macroscopic scale. Unidirectional fibers and bi-directional fabric can add strength in certain directions, resulting in a higher anisotropic behavior of the structures. In structural applications like BIW, the use of continuous fibers is always preferred. In general, continuous fibers can provide more strength and better crash resistance to the whole structure if they applied in an appropriate way. Typically, continuous FRTPs are available as semi-finished products (prepreg).

The following typical mass-production-oriented FRTP categories will be illustrated in section 2.1.1:

- 1) Short fiber thermoplastics
- 2) Long fiber thermoplastics
- 3) Glass mat thermoplastics
- 4) Laminated thermoplastic composites

Correspondingly, since the fiber length and mechanical properties of FRTPs are strongly dependent on the manufacturing processes, two major manufacturing processes for FRTPs will be introduced in the following section 2.1.2:

- 1) Injection molding
- 2) Compression molding

2.1.1 Typical categories of FRTP material on lightweight vehicles

Generally, in existing automotive applications, short fiber thermoplastics (SFTs), long fiber thermoplastics (LFTs), glass mat thermoplastics (GMTs), and laminated thermoplastic composites are the most widely used types. Before going in depth into each specific type, the definition of short, long, and continuous fibers should be clarified. Since the fiber length is strongly dependent on the mode of manufacturing (see section 2.1.2), the boundary between a short and a long fiber is sometimes ambiguous. For example, some “long fibers” in the injection molding process can only be treated as “short fibers” in the compression molding process [11]. To avoid misunderstandings in this work, the classification suggested previously [12] is adopted (Table 2-1). Here, a continuous fiber refers to the semi-finished products, such as laminated thermoplastic composites, whose length is determined by the size of the components.

Group	Fiber length
Short fiber	0.1 to 1 mm
Long fiber	1 to 50 mm
Continuous fiber	>50 mm

Table 2-1 Definition of short, long, and continuous fibers [12]

Short fiber thermoplastics (SFTs)

SFTs typically contain randomly oriented short fibers less than 1 mm in length [10]. They can be manufactured by traditional injection molding processes in short cycle times. In most cases, an SFT shows a higher modulus, higher heat deflection temperature, lower coefficient of thermal expansion, and lower mold shrinkage than its original thermoplastic matrix materials. At the same time, yield strength, tensile strength, and impact strength are increased, and strain-to-failure is decreased. Table 2-2 shows a comparison between polypropylene (PP) and PP-GF30.

SFTs have three limitations due to the nature of the conventional injection molding process: 1) fiber content; 2) fiber length; and 3) fiber orientation [10]. A significant negative correlation exists between the fiber content and the viscosity of liquid polymers. Maintaining the melt-blended material flowing and ensuring that it fills complete parts requires that the maximum fiber content (maximum weight fraction) of the injection molded SFT be limited to about 60%.

During the injection molding process, the average fiber length decreases. The fiber length of SFTs is limited by the fiber breakage occurring during the injection molding process. This breakage reduces the strength of the SFT parts, since effective strengthening can only be achieved if the fiber length is greater than the critical fiber length (detailed in the following LFT section) [10; 13].

Property	PP	PP-GF30
Fiber weight (%)	0	30
Density (g/cm³)	0.9	1.12
Tensile modulus (GPa)	1.4	5.3
Tensile strength (MPa)	35	48.3
Strain-to-failure (%)	150	2
Notched Izod impact strength (J/m)	37	58.6
Heat deflection temperature (HDT) at 1.82 MPa (°C)	54	135
Coefficient of thermal expansion (10e-6/°C)	90	39.6
Mold shrinkage	1.7	0.6

Table 2-2 Properties of PP and PP-GF30 [10]

Under ideal injection molding conditions, fiber orientation is random in SFTs, so they can be treated as isotropic materials in the macroscopic scale. However, in practice, fibers tend to be oriented in a preferred direction that depends on the mold design, material thickness, and process parameters. This leads to material anisotropy in an SFT part, thereby affecting the performance of that part. Today, the fiber orientation can be estimated with the Moldflow simulation. As mentioned in [14], due to the change in the gating location in the injection molding process alone, two water pump housings made of the same SFT show completely different fiber orientations and significantly different displacement distributions at critical areas. Currently, seat pans, door trims, and some technical components in the engine compartment (Figure 2-1) are typical applications of SFTs. Finding SFTs on BIWs or even in semi-structured applications is rare in the automotive industry.



Figure 2-1 Transmission carrier of PA66-GF50 [15]

Long fiber thermoplastics (LFTs)

The LFTs typically contain randomly oriented discontinuous long fibers 5 to 25 mm in length. Compared to SFTs, LFTs have significantly better mechanical properties (Table 2-3) because their fiber length to diameter ratio is higher than the critical fiber aspect ratio (defined as Formula 2-1) [16; 17]. In this situation, instead of fiber pullout (a typical material failure form with SFTs), the stress on fibers in LFTs may reach the ultimate tensile strength, meaning that the fibers can possibly be used to their limit.

Property	SFT	LFT
Matrix material	PP	PP
Fiber weight (%)	30	30
Density (g/cm³)	1.12	1.12
Tensile modulus (GPa)	6.21	6.89
Tensile strength (MPa)	76	100
Tensile strain at failure (%)	4–5	2.5–3.5
Flexural modulus (GPa)	4.83	6.21
Flexural strength (MPa)	112	155
Notched Izod impact strength (J/m)	107	166

Table 2-3 SFT and LFT comparison (fiber type: unspecified) [10]

$$\left(\frac{l}{d}\right)_c = \frac{\sigma_{fu}}{2\tau}$$

Formula 2-1

l : fiber length; d : fiber diameter; σ_{fu} : fiber ultimate tensile strength; τ : interfacial bonding strength between the fiber and the matrix

As illustrated in Table 2-3, the fiber length plays an important role in determining the mechanical properties of LFTs [18; 19]. The relationship between the fiber length and several important mechanical properties of FRTPs is described in Figure 2-2. Clearly, the elastic modulus, strength, and impact resistance are increased with increasing fiber length. Note also that the processability of FRTPs and the fiber length show an opposite trend. If considering the mechanical performance and the processability at the same time, most LFTs possess a relatively optimum fiber length.

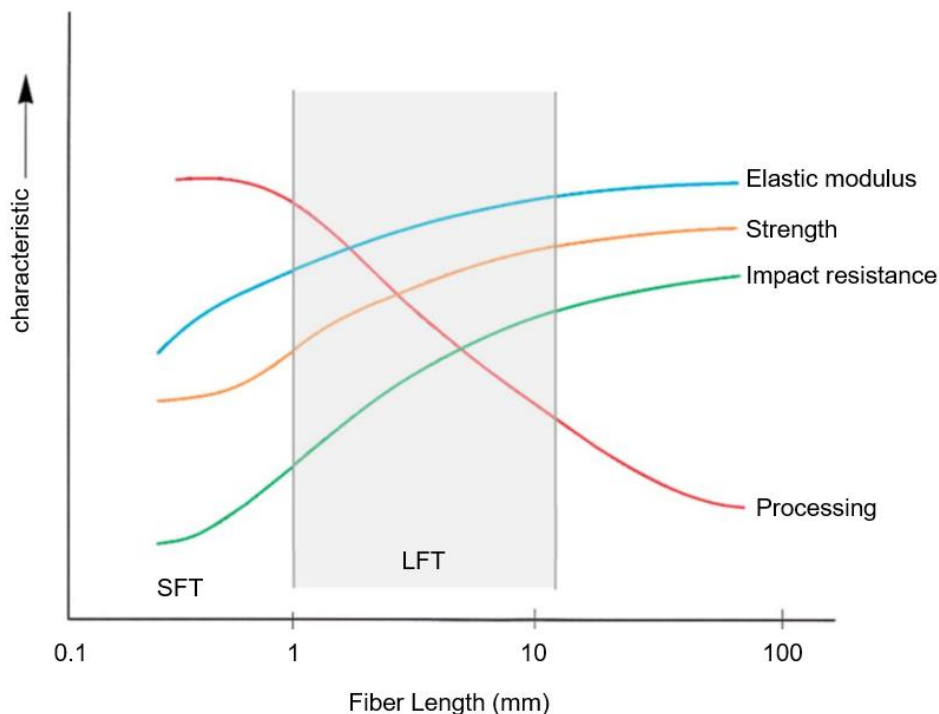


Figure 2-2 Relationship between the fiber length and several important mechanical properties of FRTPs [16; 17; 20; 21]

Typically, LFT components can be manufactured by either injection molding or compression molding processes. Considering the manufacturing efficiency, Granulate-LFT injection molding (G-LFT) and Direct-LFT compression molding (D-LFT) are widely used methods. Pre-compounded pellets are used in the G-LFT process, which means fibers are impregnated with the matrix material as pellets in a separate process by material suppliers. The length of standard pellets is normally 5–25 mm [22], but the pellet length can also be up to 40 mm, depending on the specific application requirements [10]. To reduce the fiber breakage to a large extent, the G-LFT process uses a conventional injection molding machine with some modifications to the screw design, the mold design, and the process parameters. The D-LFT process (section 2.1.2) reduces the fiber length degradation and can achieve a much higher average fiber length than the G-LFT process in the final component, making it the preferable

method for manufacturing LFT components. As illustrated in [22], the average fiber length of D-LFT compression molded parts can reach ca. 8–10 mm, whereas this length is only ca. 2–6 mm in G-LFT injection molded parts. For both manufacturing methods, it should be noted that the flow of LFTs leads to a preferable fiber orientation, which means LFTs cannot be treated as a type of isotropic material. Specifically, a higher level of fiber orientation in LFTs can be achieved with injection molding than with compression molding. The anisotropic property of LFTs between the flow and transverse direction is caused by this preferable fiber orientation (detail see section 3.1.3).

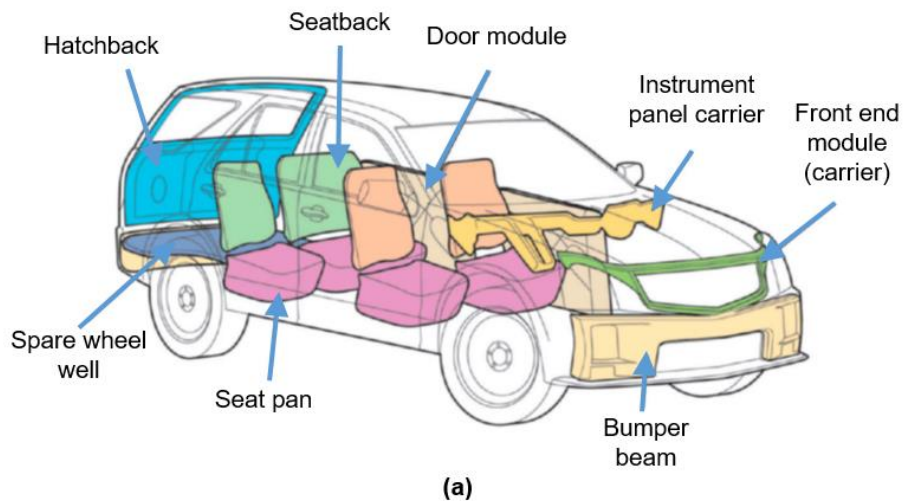


Figure 2-3 Typical LFT automotive component (a) [17]; Front end carrier for a VW Golf V (b) [15]

At present, automotive applications of LFTs can typically be found in semi-structural components (Figure 2-3a), such as seat structures [11; 23; 24; 25; 26; 27], door modules [11; 23; 24; 25; 28; 29; 30], front end carriers [11; 23; 24; 25; 28; 31; 32; 33; 34], instrumental panel carriers [11; 23; 24; 28; 31], bumper beams [11; 24; 25; 28; 35; 36], and spare-wheel wells [11; 24; 28]. For example, Figure 2-3b shows the front end carrier of a VW Golf V made of PP-LGF30 with metal sheet reinforcements (4.7 kg). The carrier shows good energy absorption, especially under oscillation, and good impact strength [15].

Glass mat thermoplastics (GMTs)

GMTs are normally available in sheet form and consist of a thermoplastic polymer mixed with E-glass fiber mats. The constitution of the fiber mat can be either randomly oriented chopped glass fibers (typical fiber length: 25–100 mm) or randomly oriented continuous glass fibers (Figure 2-4). Both types behave like isotropic materials. GMTs are also available in the form of unidirectional continuous glass fibers and bi-directional glass fiber mats, which show anisotropy behavior. These can be added to the layers of randomly oriented GMTs to increase the tensile modulus and strength in selected directions. Another type of high-performance GMT, the textile-reinforced GMT, is another good choice for the most demanding applications where traditional GMTs, LFTs, and many thermoset composites cannot compete [37]. Several properties of different types of GMTs with PP-matrixes are listed in Table 2-4. Polypropylene (PP) is the most commonly used thermoplastic matrix material for GMTs. One advantage worth mentioning here is that GMTs with a PP matrix and randomly oriented glass fibers have high stiffness and excellent impact resistance even at temperatures as low as -40°C . Other types of glass fiber-reinforced PPs are brittle at low temperatures, making them unfavorable or even unacceptable for some applications in the automotive branch.

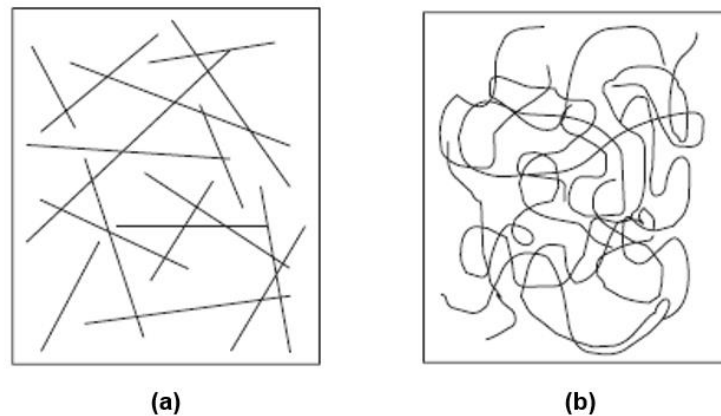


Figure 2-4 Glass mat thermoplastics (GMTs) with randomly oriented chopped fibers (a) and randomly oriented continuous fibers (b) [10]

Compression molding and thermo-stamping are common manufacturing processes for GMT parts. Typically, compression molding is always used to mold complex parts, such as the parts with ribs and bosses. However, due to the high viscosity, fibers cannot reach the whole extent of fine features, such as thin ribs and bosses, and this creates a higher design limitation for GMTs than for SFTs and LFTs for use with compression molding. As shown in Figure 2-5 [38], fibers in GMTs are prone to entanglement, jamming, and agglomeration in the lower parts of ribs. This can lead to fiber matrix separation and low fiber content in the upper part of the ribs, as well as subsequent local failure in some circumstances. This problem is more obvious with the use of GMTs with continuous fibers.

Property	Chopped fiber	Continuous fiber	Unidirectional fiber	
	GMT	GMT	GMT	
Matrix material	PP	PP	PP	
Fiber weight %	40	40	42	
Density (g/cm ³)	1.19	1.21	1.24	
Tensile modulus (GPa)	5.965	5.82	10.1 (L*)	5.31 (T*)
Tensile strength (MPa)	90.4	108	276 (L*)	60 (T*)
Strain-to-failure (%)	2.2	2.5	2.5 (L*)	2.3 (T*)

*L: longitudinal direction; T: transverse direction

Table 2-4 Mechanical properties of glass mat thermoplastics (GMTs) with a polypropylene (PP) matrix [10]

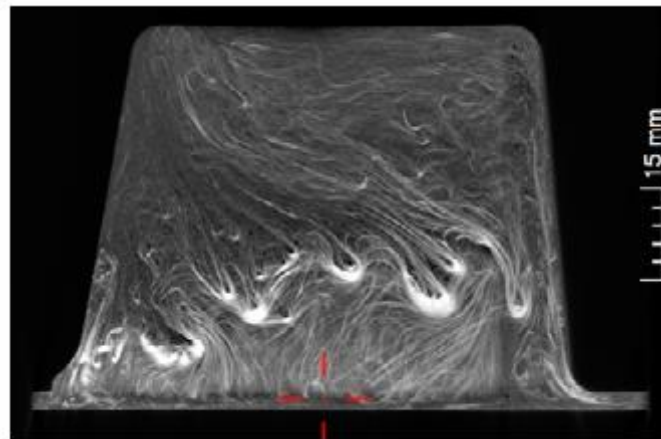


Figure 2-5 CT scan of a rib made of a GMT (lower part: light gray, fiber concentration; upper part: dark gray, fiber matrix separation) [38]

The application scenario of GMTs in the automotive industry is quite similar to that of the LFTs. As shown in Figure 2-6, semi-structural components on vehicles in the European market can be made either of GMTs or LFTs. A good example here is the front end carrier from the VW Golf 3 (Figure 2-7). In comparison to its predecessor, this GMT front end carrier achieves a 35% weight reduction (from 6.4 kg to 4.4 kg) and replaces 15 steel sheet parts with a highly integrated structure without any performance loss. Correspondingly, the 6% cost is reduced by virtue of the highly functional integrated structure.

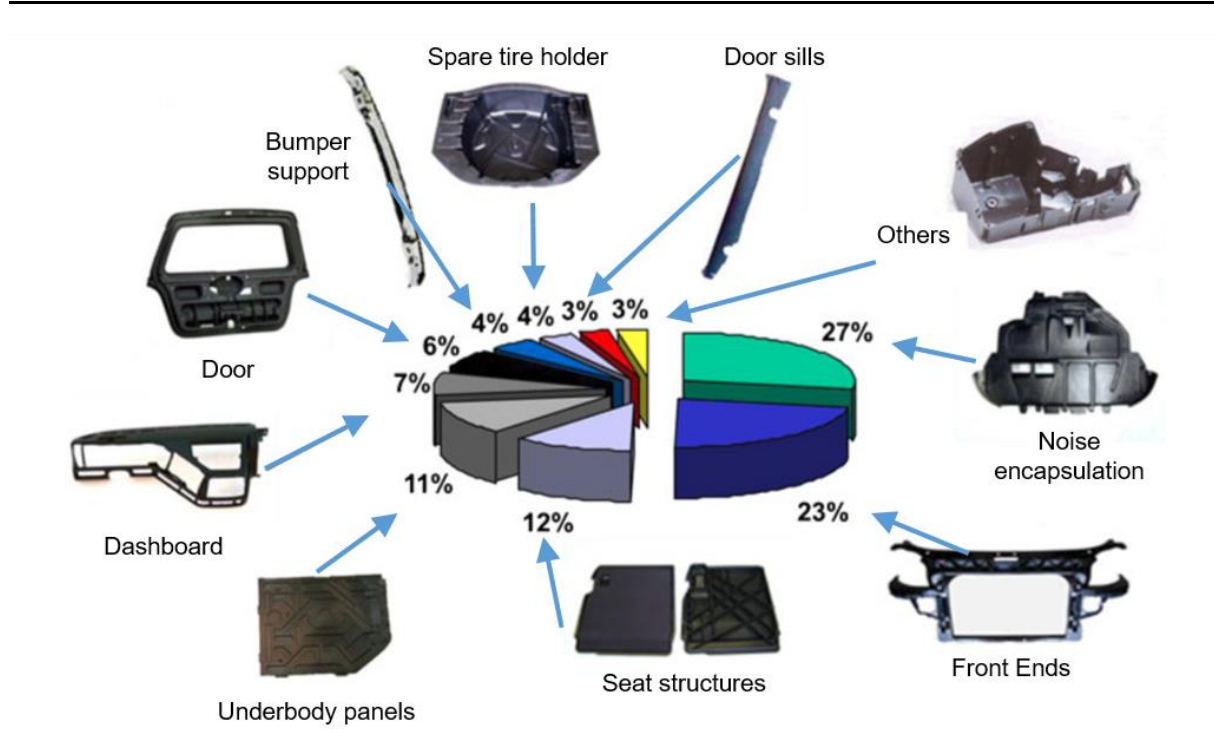


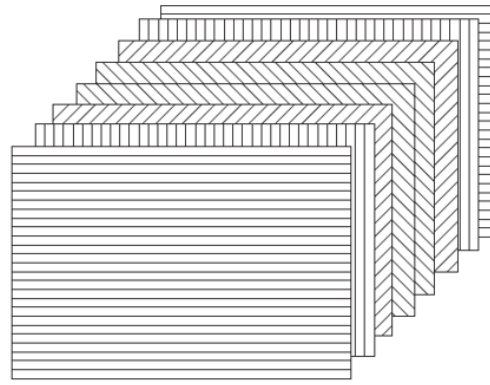
Figure 2-6 Final parts made from GMTs on European vehicles [24]



Figure 2-7 GMT front end carrier of the VW Golf 3 [39]

Laminated thermoplastic composites

Laminated thermoplastic composites are made by stacking several layers of preregs [10]. A prepreg is a layer of composite fibers pre-impregnated with a polymer matrix. Preregs are available in a variety of forms, such as unidirectional continuous fiber preregs (e.g., UD tape) and bi-directional fabric preregs (e.g., organo sheet). As shown in Figure 2-8, the stacking sequence and the number of layers of a laminated thermoplastic composite can be varied from application to application, which means laminated thermoplastic composites can be tailored based on the external loadings and the fiber orientation in each layer can be determined fully as needed.



An 8-layered continuous fiber laminate
with [0/90/+45/-45/-45/90/0]

Figure 2-8 An example of a laminated composite [10]

Organo sheets and UD tapes are two of the most widely used semi-finished products (prepregs) on FRTP components (Figure 2-9). The organo sheet is a type of flat thermoplastic bi-directional fabric prepreg. Typically, the fiber fabric of organo sheets lies in the direction of $0^\circ / 90^\circ$ with a fiber distribution ratio 50/50, 80/20, or 90/10, and the fiber content of organo sheets is up to 50%. Thanks to the superior mechanical properties (Table 2-5), organo sheets can often be seen on vehicle structural components. They are usually used as an insert on components and are formed and reinforced with ribs in the injection molding process (see section 2.1.2) since they are unable to flow even at the melting temperature. Good connection can be achieved between organo sheets and reinforcing ribs if the same matrix material is used. Typical matrix materials of organo sheets on vehicle components are PP and PA.

Name	Matrix material	Fiber distribution	Density (g/cm ³)	Strength (MPa)	E-modulus (GPa)
Tepex dynalite 104-RG600/47%	PP	50/50	1.68	430	20
Tepex dynalite 102-RG600/47%	PA6	50/50	1.8	380–390	18–23

Table 2-5 properties of organo sheets [40]

The UD tape [41] is a type of fiber-reinforced tape with endless unidirectional aligned fibers (glass or carbon) and is available in different widths. By arranging the fibers in only one preferred direction, UD tapes have the highest strengths of all semi-finished products and are typically used where components have high anisotropic loading. UD tapes come with either thermoplastic or thermoset matrixes. This work will focus only on the thermoplastic UD tapes. The use of a thermoplastic tape layup process allows these tapes to be placed following the load path in the component with a high level of automation (in-situ consolidation, e.g.,

Fiberforge from Dieffenbacher) [42; 43]. This process includes four major steps [44]: (1) tape selection; (2) tape lay-up; (3) consolidation; and (4) forming and molding (injection or compression molding).

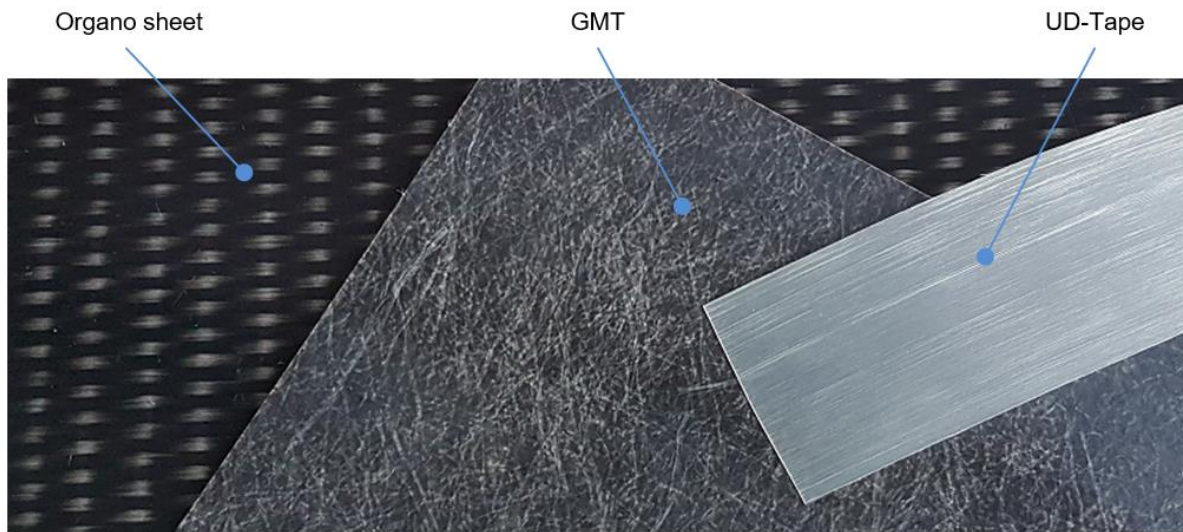


Figure 2-9 Examples of an organo sheet, GMT, and UD tape

Many applications of organo sheets and UD tapes can be found in automotive serial components or in research projects [45], such as the “Hybtuer” in section 2.5.3, the FRTP door carrier, and the air bag case. The use of organo sheets and UD tapes also brings the thermoplastic material into the region of high-demanding crash-relevant BIW components. One good example is the door side impact beam from project “SpriForm” (Figure 2-10) [46; 47]. The use of PA6-GF60 and an organo sheet with the “SpriForm” process (similar to “FiberForm” in section 2.1.2) resulted in a “SpriForm-beam” weighing 550g, for a 20% weight reduction compared to the aluminum reference. According to the drop tower test results (similar to 3-point bending tests), the stiffness and the maximal reaction force achieved from this “SpriForm beam” are comparable to the steel reference. However, the severe material failure of organo sheets on this component should be noted, as this is also a major obstacle for FRPs in crash-relevant components. Although this problem has been solved and no material failure has happened with the modified “SpriForm-beam,” a significant loss of performance is something that cannot be ignored. Similar applications and approaches can also be found in [48]. According to its simulation results under compression loading, the combination of UD tapes and organo sheets effectively reduces the stress concentration area on the FRTP door side impact beam, and only minor material failure is observed on the LFT ribs. Both studies show that organo sheets and UD tapes are important parts of crash-relevant components made of FRTPs. Finding a balance between the level of material failure and the structure stiffness is the key point for developing these structural components.



Figure 2-10 Door side impact beam from project “Spriform” [46]

2.1.2 Typical mass-production-oriented manufacturing methods for FRTPs

Injection molding and compression molding are the two dominant manufacturing methods for FRTPs, which are investigated and applied in this work.

Injection molding

Injection molding is a major method for the manufacture of FRTP parts because of its capability to form complex parts with good dimensional tolerance and excellent surface quality [10] within a short cycle time (maximal 60 seconds) [49]. Although injection mold tooling is a relatively large investment, this technology is always preferred in the automotive industry due to its fully automated process, high part counts, and the excellent reproducibility of its components [50]. In general, the injection molding process can be summarized as the following five steps:

- 1) Plasticize & dosing
- 2) Injecting
- 3) Holding pressure
- 4) Cooling
- 5) Demolding & ejecting

Manufacturing SFT parts and some of the LFT parts is possible with injection molding, depending on the required average fiber length in the final components. Figure 2-11 illustrates a typical injection molding machine, which consists of two major units: the clamping unit and the injection unit. The major responsibilities of the injection unit are the collection of liquid polymer from solid pellets and the generation of the required pressure for the injection process. The clamping unit is responsible for cooling and the shape of the part. The cavity is kept closed during the injection process. After the temperature of the part falls below the solidification temperature of the polymer, the cavity opens and the part is ejected. Cooling is the most important step in injection molding, and it determines the cycle time to a large extent.

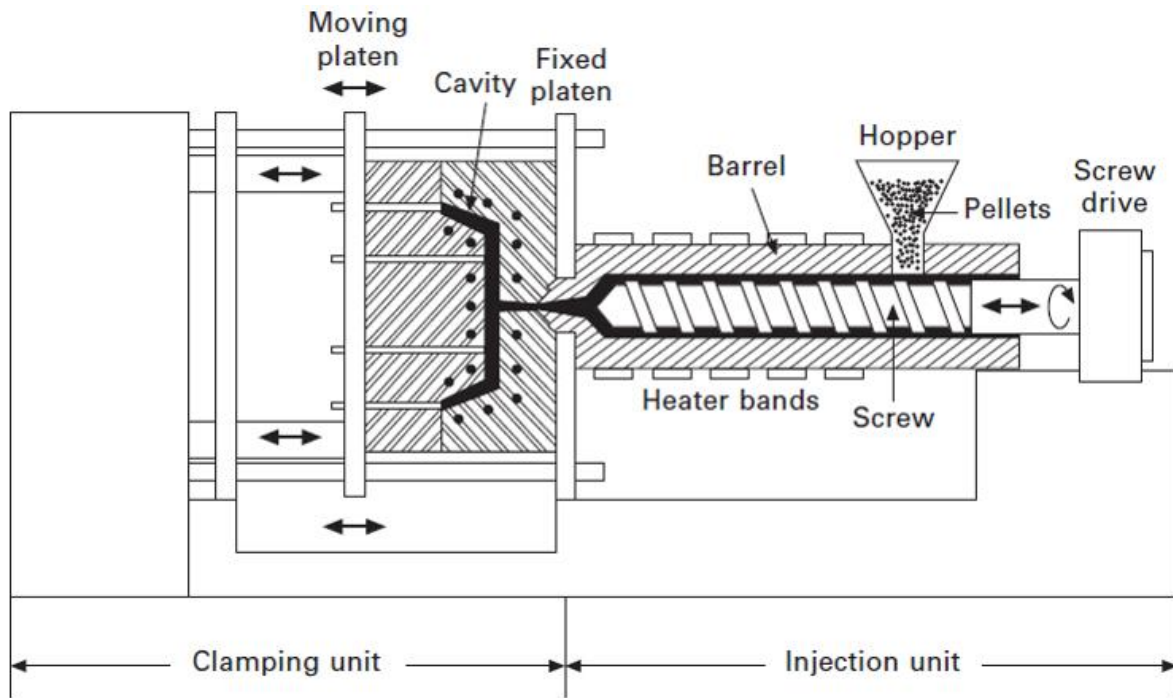


Figure 2-11 Typical injection molding machine [10]

For processing FRTPs, due to the small size of the passages (runners and gates), only discontinued fibers are suitable for injection molding. An obvious reduction in fiber length found during the “plasticizing & dosing” step is caused by the applied induced direction force and shear forces by the screw in the injection unit [50]. This fiber length degradation means that the maximal average fiber length in a typical fiber-reinforced injection molded component is ca. 3 mm. A strong fiber orientation can also be found in fiber-reinforced injection molded components and this orientation has a substantial influence on the mechanical performance. The high viscosity of thermoplastics limits the fiber weight fraction of injection molded thermoplastic composites to about 60% [49].

Many injection molding variations are available in the market. Among them, insert molding and outsert molding processes are highly related to this work. In the insert molding process, small components (different materials from the matrix), such as threaded metal inserts and pins, are placed into the mold before the injection step. In this way, the pre-placed small components will be over-molded (surrounded) by the polymer melt and simultaneously integrated into the final product during the injection molding process. For outsert molding, the process is essentially the same as for insert molding, but the size of the insert (e.g., volume, surface area) is larger than that of the polymers. Both processes can reduce assembly operations and time, while achieving considerable assembly cost reductions [10]. Applications of these two processes can be found in section 2.2.2.

Conventional injection molding is used in combination with other manufacturing processes as well. One well-known example is the “FiberForm” process [15; 51], which combines injection molding with the thermoforming of semi-finished continuous fiber-reinforced prepregs (e.g., organo sheets). In this process (Figure 2-12), the additional reinforcing “organo sheet” is preheated and seamlessly integrated into the FRTP component. This step has no influence on the injection-molded function elements (e.g., ribs) or on the total cycle time, making this highly favorable for mass production. This process combination leads to a strength increment in the

injection molded parts and potentially enables the application of injection molded parts in crash-related areas on vehicles. The door carrier mentioned in section 2.5.3 is made with this process.

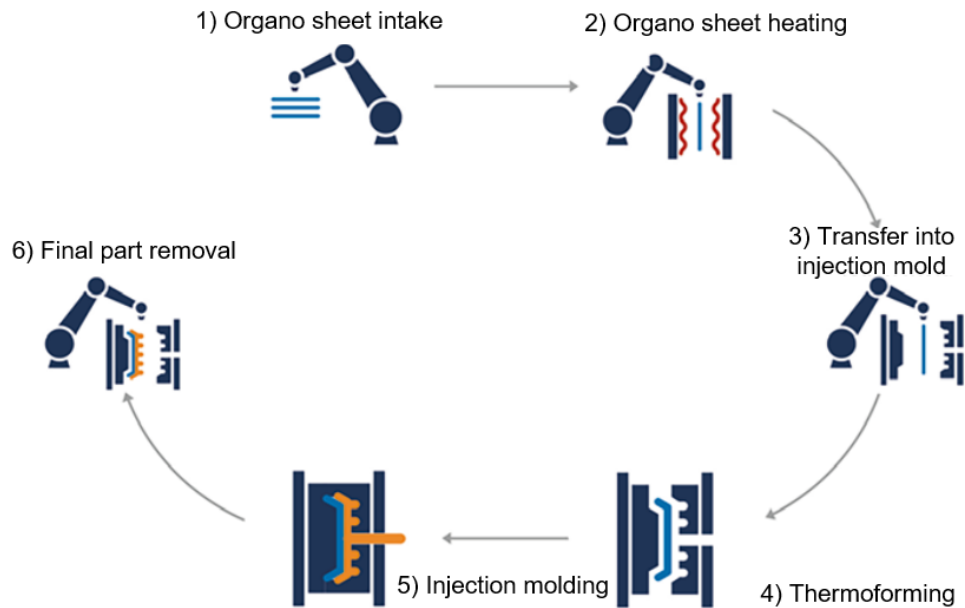


Figure 2-12 The FiberForm process (Thermoforming and injection molding) [15; 51]

The introduction of semi-finished continuous fiber-reinforced prepregs provides further lightweight potential. As shown in Figure 2-13, the use of an organo sheet reduces the airbag case weight [15; 52] by 30% compared to the reference series part made of polyamide 6 (PA 6). The thickness of the component is also reduced from 3–4 mm to 0.5–1 mm.



Figure 2-13 Air bag case with an organo sheet [52]

Compression molding

Compression molding has become another important forming method for FRTPs in the last decades. Initially, this method was developed for shaping sheet-molding compounds (SMCs) and bulk-molding compounds (BMCs), and it is able to produce large complex parts at a high rate with a high level of automation [13]. For this reason, the compression molding process is highly suitable for mass production of composite parts. In the last decades, the application of compression molding has expanded to FRTP applications, which is the point of interest of the

present work. In the domain of FRTPs, the typical semi-finished products used in the compression molding process are LFTs and GMTs.

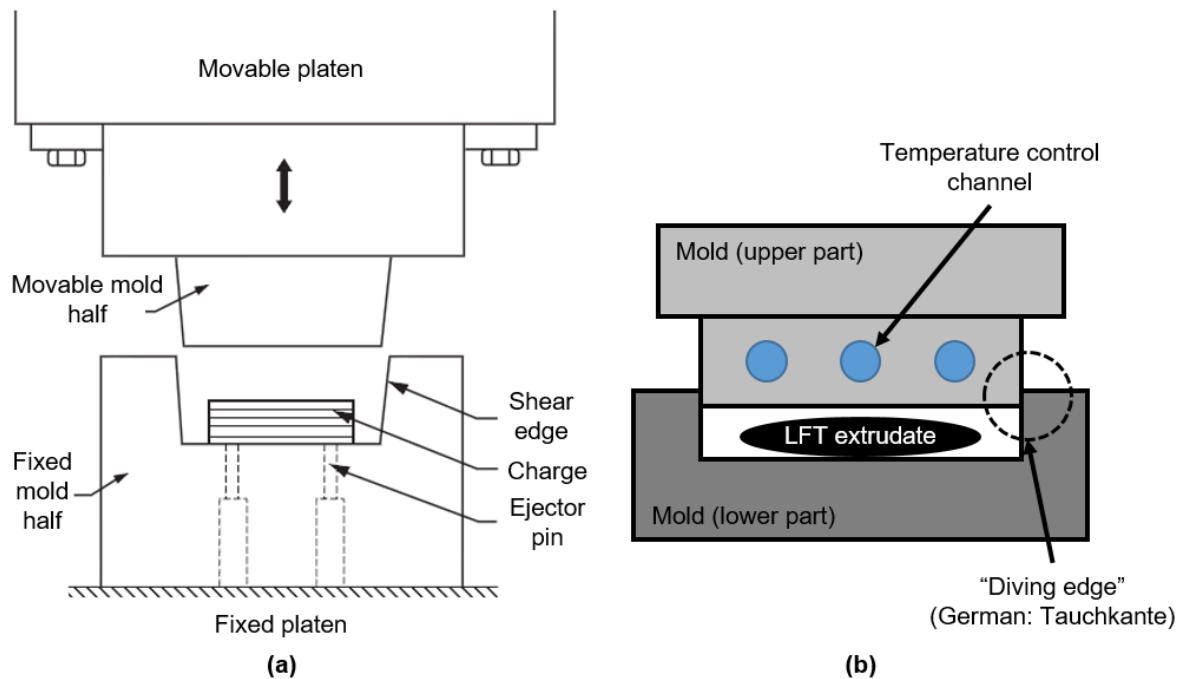


Figure 2-14 Schematic of a compression molding machine [13] (a) and its typical mold design (b)

Figure 2-14 shows a schematic of a compression molding machine and its typical mold design. At the beginning of the conventional compression molding process, the mold is opened and preheated semi-finished products (called "charge" or "extrudate"; e.g., LFT) are placed at the bottom of the fixed half of the mold. As the mold is closed, the charge fills the mold cavity. When the moveable half of the mold is completely closed, it will hold and maintain the pressure. The pressure can vary from 1.4 to 34.5 MPa, and the holding time can be as long as 45 s, depending on the part thickness. The part is then demolded with the help of ejection pins.

As shown in Figure 2-15, LFT direct compounding (LFT-D) is a process that allows high-volume production and avoids the need for the manufacture of semi-finished products by material suppliers. In this LFT-D process, two compounders are needed. The first is for the mixing of the polymer and additives and the second is for the mixing of the fibers and extrudate (charge). The hot polymer-impregnated fiber roving is cut to the desired length (25–50 mm) and directly compounded with the melted thermoplastic matrix as an extrudate in a mixing extruder (i.e., the second compounder). The extrudate is cut, based on the weight demand, at the end of the mixing extruder and automatically transferred directly into the mold by robots with needle grippers before it cools down.

Obviously, compared to conventional processes, this continuous LFT-D process skips the use of semi-finished products, thereby avoiding the reheating step and reducing material degradation to some extent. Since the melting of the polymer granules and the mixture of fiber are two separate steps in two compounders, the fiber percentage can be arbitrarily adjusted between 20% and 60%, providing considerable freedom in terms of the material choice and polymer modification [53]. By incorporating the direct compounding process into the normal compressing molding process, the highly automated and efficient LFT-D method has become

one of the most favorable manufacturing processes for automotive parts like underbody components and instrument panel carriers.

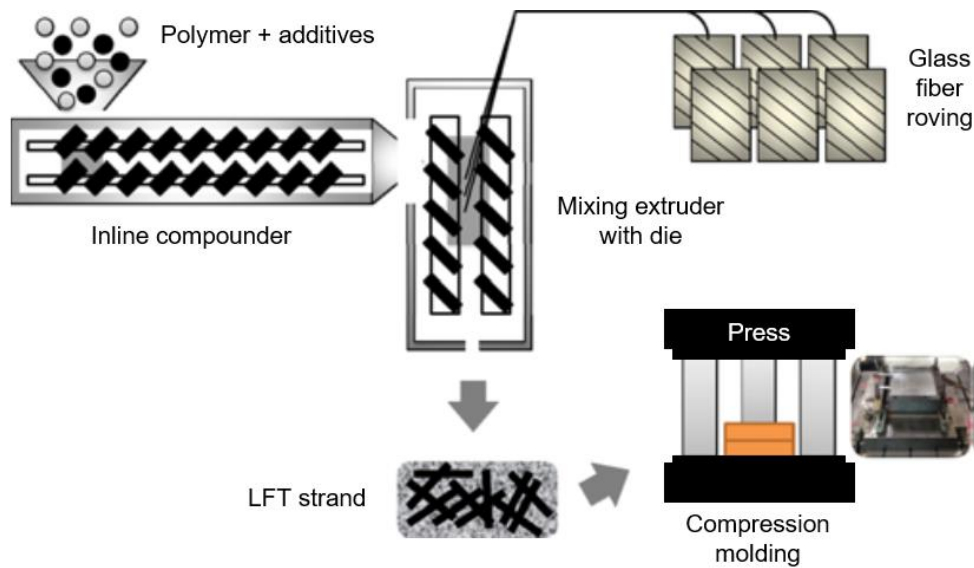


Figure 2-15 LFT-direct compounding [54]

The LFT-D process is combined with other manufacturing processes as well. The “Advanced LFT-D” process [55] is a combination of the LFT-D and the UD tape placement, which further expands the application scenarios of LFTs to structural and semi-structural components of the BIW. An automatic tape laying process is used to integrate the UD tapes into LFT-D components in the compression molding process, which helps to achieve a better strength and a higher energy absorption capability. A similar process can be found on the rear seat back, as shown in Figure 2-16 [23]. According to the specific loading situation, UD tapes are effectively applied in the major load directions of the component with the compression molding process. With this so-called E-LFT process [56], up to 30% weight reduction can be achieved compared to the reference, and the total number of sub-parts is reduced from 13 to 5 by the function integration.



Figure 2-16 E-LFT rear seat back [23]

Another innovative process combination related to compression molding is the “hybrid forming” process [57; 58; 59; 60; 61; 62]. It combines the forming of steel sheets with the compression molding of LFTs and realizes these two processes simultaneously. In this process, the LFT is

used as the medium to form the steel sheet, as with typical hydroforming, and is connected to the steel sheet with the help of an adhesion promoter. Figure 2-17 shows a front axle control arm manufactured with this process as a demonstrator with a 60 s cycle time. Compared to the steel reference, the part saves up to 20% weight by the thickness reduction of steel sheets and the use of LFT rib reinforcements.



Figure 2-17 Front axle control arm made of “hybrid forming” [57; 62]

Similar to the injection-molded parts, a strong fiber orientation can also be found on compression-molded FRTP components due to the flow of material during the forming process. Compared to injection molding, the fiber length degradation is reduced during the whole process; therefore, the average fiber length is significantly longer in compression-molded parts than in injection-molded parts, which means an increase in every aspect of the mechanical performance. The influence of fiber length is illustrated in section 2.1.1 (section LFT).

2.2 Lightweight construction methods for FRP BIW components and applications

There are four major lightweight construction methods [63]: 1) differential construction (Figure 2-18a); 2) integral construction (Figure 2-18b); 3) integrative construction (Figure 2-18c); 4) hybrid/multi-material construction (Figure 2-20). Typically, integral construction, integrative construction, and hybrid/multi-material construction can be readily found in FRP BIW applications. Differential construction is used more often for the traditional sheet-constructed components and is uncommon in the current applications of FRP BIW components (except for the life module from the BMW i3 and i8 [64]).

2.2.1 Integral and integrative construction

The principles of integral and integrative construction are similar, as both aim to minimize the total number of single components in one structure (Figure 2-18b and c). Specifically, the integral construction method attempts to achieve an ideal solution that combines all the functional elements, such as bolt holes and ribs, into a single component for one structure. The integrative construction method, by contrast, takes the necessities of repairing, exchanging, and recycling into consideration. Based on the analysis of structure usage and damage behavior, the structure integration area is limited and optimized. In this way, integrative construction can be seen as a practical version of integral construction, but it is more effective at constraining the influence of stress concentration, corrosion, and damage propagation.

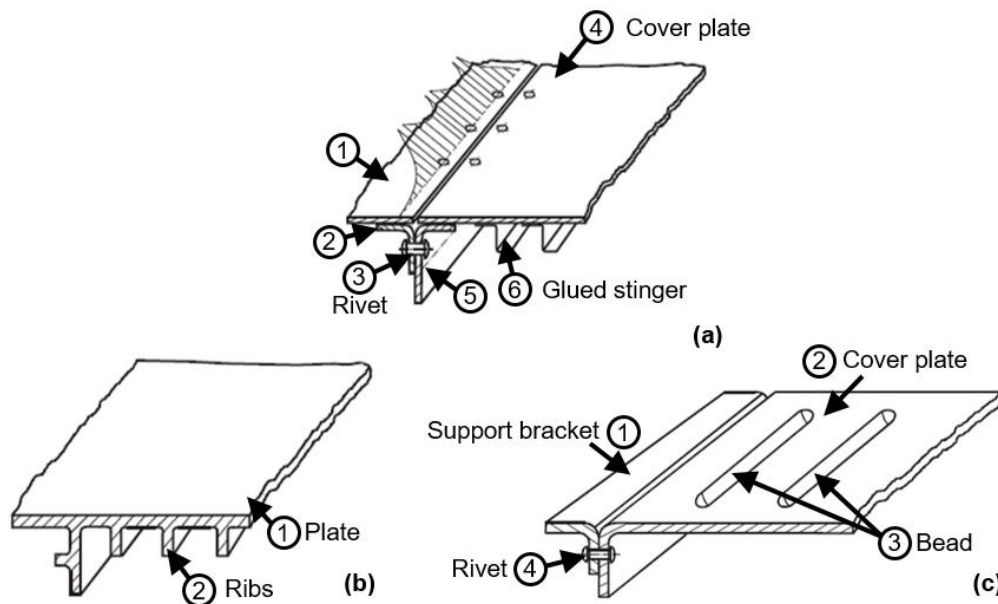


Figure 2-18 Schematic of the evolution from a differential construction (a) to integral construction (b) and integrative construction (c) [63]

Figure 2-19 illustrates two FRTP BIW semi-structural components with the integral construction from the Renault Espace [65]. Compared to conventional steel solutions with differential construction, the highly function-integrated front end carrier and the lift gate offer a 10% weight reduction.

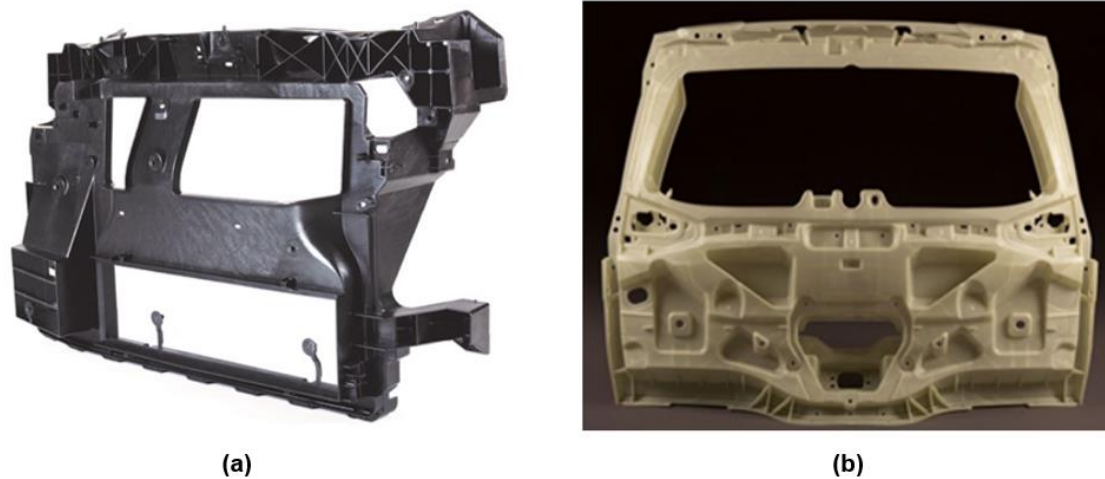


Figure 2-19 The front-end carrier (a) and lift gate (b) of the Renault Espace [65]

2.2.2 Multi-material construction

Due to the unrealistic additional material costs and the immature technology readiness, reaching complete FRP BIW in one step is very difficult. For this reason, multi-material construction (Figure 2-20) has become one of the hottest topics in the current automotive lightweight design area. The goal of this construction method is to reach the best compromise and optimization of material combinations. In other words: use the right material in the right position.

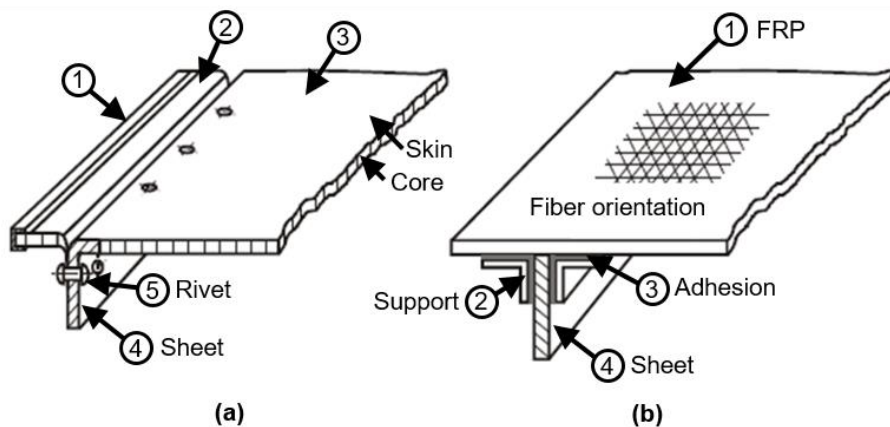


Figure 2-20 Basic principles of hybrid/multi-material construction: a) sandwich construction; b) FRP-metal hybrid construction [63]

Sandwich construction is a typical kind of multi-material construction (Figure 2-20a). Its principle is to increase the area moment of inertia of the structure without adding the amount of weight associated with solid materials. Typical sandwich-structured composites are fabricated by attaching two thin sheets to a lightweight but thick core. In this way, the sandwich material can achieve a high bending stiffness and weight savings with an overall low density. Figure 2-21a shows a schematic of a conventional sandwich material with a honeycomb core. (alternately: foam core (Figure 2-21b))

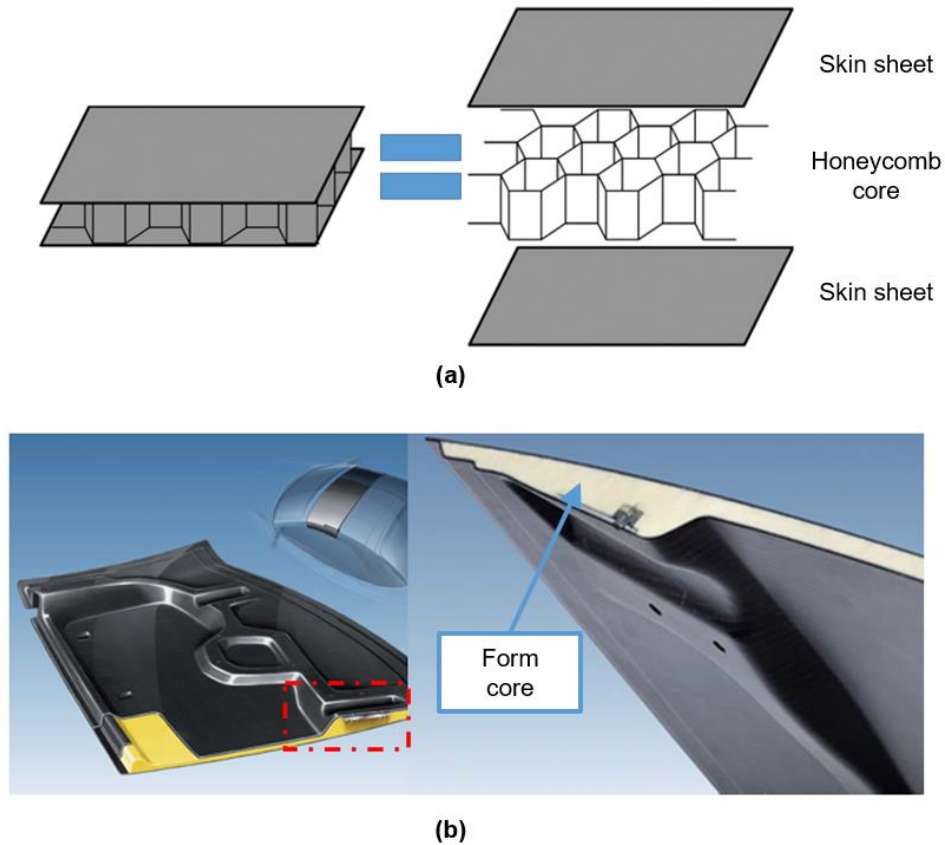


Figure 2-21 Schematic of a composite sandwich panel with a honeycomb core (a) [66] and foam core sandwich material on a convertible roof module (b) [67]

In recent decades, a new type of multi-material construction, “FRP-metal multi-material construction,” has developed rapidly. This construction has a significant feature, namely the use of FRPs to reinforce the thin sheet metal component, and this provides a substantial increase in bending and torsion stiffness. Several representative applications of FRP-metal multi-material construction on BIW components are illustrated in Figure 2-22 [68; 69; 70; 71].

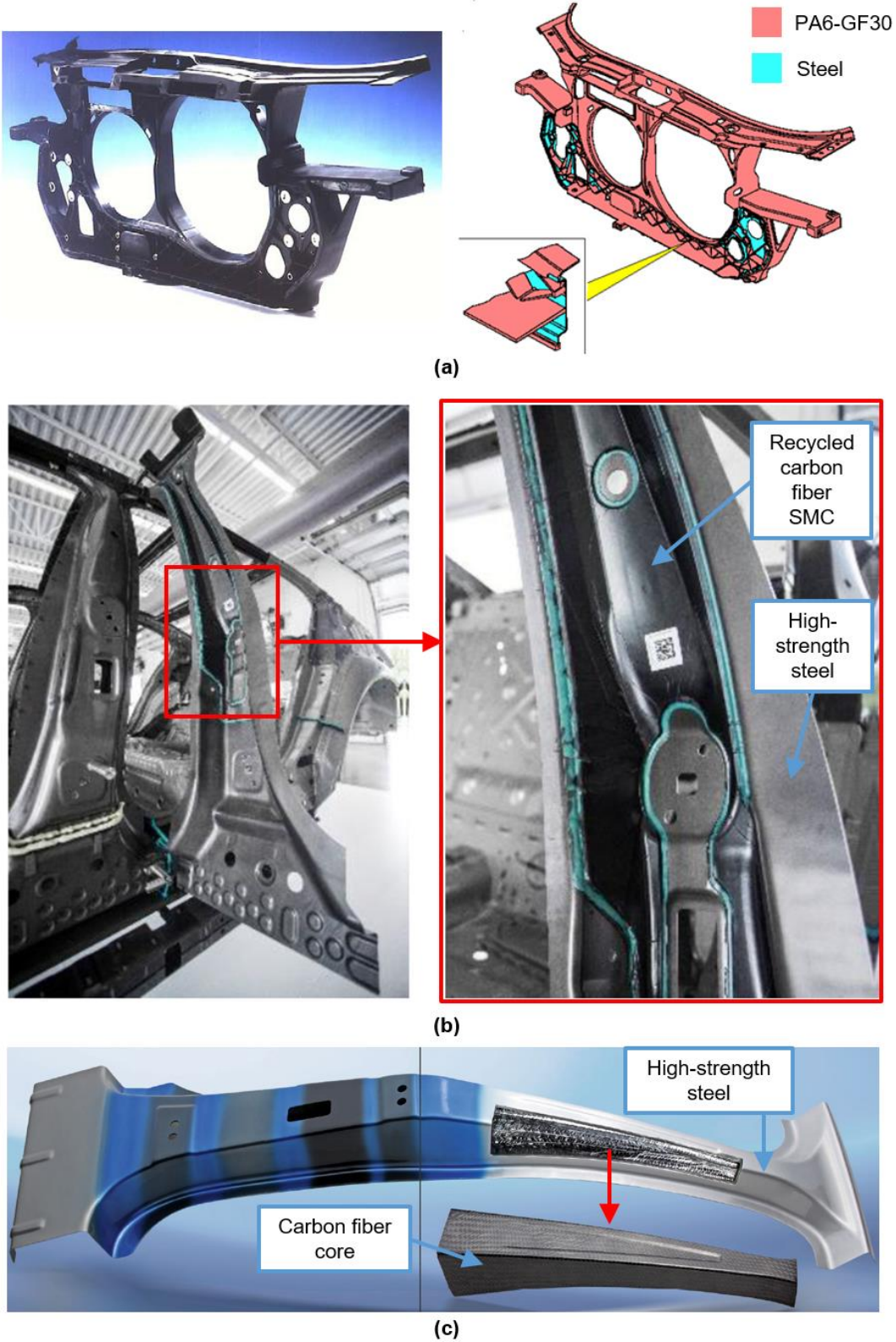


Figure 2-22 Front end carrier of the Audi A6 (1997) (a) [69]; B-pillar of the BMW 7 (2015) (b) [70]; Hybrid-B-pillar concept (c) [71]

The multi-material design approach with fiber-reinforced thermoplastics (abbreviated as “FRTP-metal multi-material design”) is one of the representative categories of FRP-metal multi-material construction. Generally, the basic form of the FRTP-metal multi-material design approach is to use FRTP ribs to reinforce metal sheet inserts. This design approach can be normally found on load-bearing multi-material structures. In the early phase of this technology, the connection between the metal sheet inserts and the FRTP ribs was only realized through discontinuous form-fitting connectors at the joining points.



Figure 2-23 Erlanger Träger: steel sheet with PA6-GF ribs joined by a bonding agent [72; 73]

The “Erlanger Träger” is one of the most famous testing specimens used to investigate the lightweight potential and the mechanical performance of the FRTP-metal multi-material design, which typically consists of an opened metal sheet insert and injection-molded FRTP ribs (Figure 2-23). The testing results in Figure 2-24 show that the “Erlanger Träger” can achieve a higher bending stiffness and comparable torsion stiffness compared to the typical closed sheet steel profile. The “Erlanger Träger” also shows the best “performance/weight” value in a standard comparison with the opened and closed sheet steel profile samples (Table 2-6).

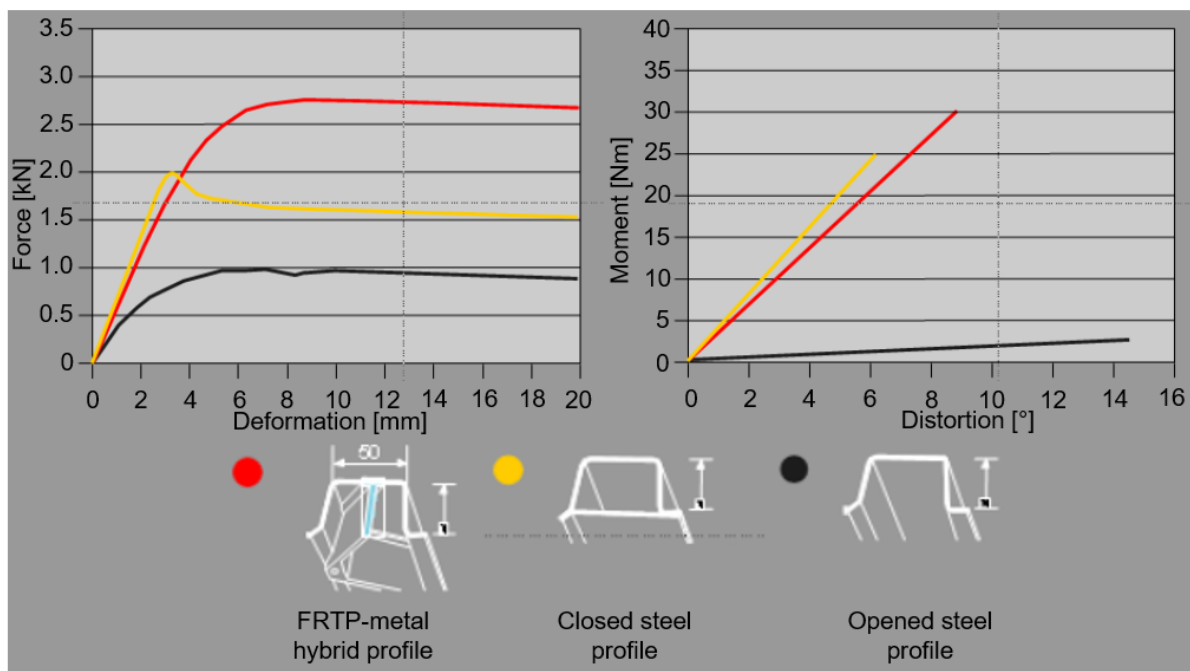


Figure 2-24 Bending and torsion test results among Erlanger Träger, opened and closed sheet steel profile samples [69]

Type	Bending	Compression	Torsion
Erlanger Träger	1.8	1.8	13
Closed sheet steel profile	1.1	1	8.5
Opened sheet steel profile	1	1	1

Table 2-6 “Performance/weight” value among Erlanger Träger, opened and closed sheet steel profile samples under different loading cases [74]

The most important achievement of the FRTP-metal multi-material design approach is that it shows the potential of using FRTPs on the BIW applications through the combination of the advantages of metal sheets (e.g., high stiffness/strength, ductile fracture behavior) and FRTPs (e.g., lightweight, high design freedom/function integration). Typical serial BIW applications can be found on front-end carriers, roof cross members, etc. The roof cross member of the Audi A6 (2004) (Figure 2-25) [75] is a representative serial product example with this design approach; it is made of steel sheets and reinforced with PA6-GF ribs. Compared to the steel reference, a 500 g weight saving is achieved. Meanwhile, under a quasi-static roof intrusion simulation according to the FMVSS 216 [76], this multi-material roof cross member achieves comparable mechanical performance (resistance force and energy absorption) [75]. According to Audi [75], the component cost (including tools, equipment, and logistics) is slightly lower than that of the steel reference with the calculation of a 1.5 million total production volume.

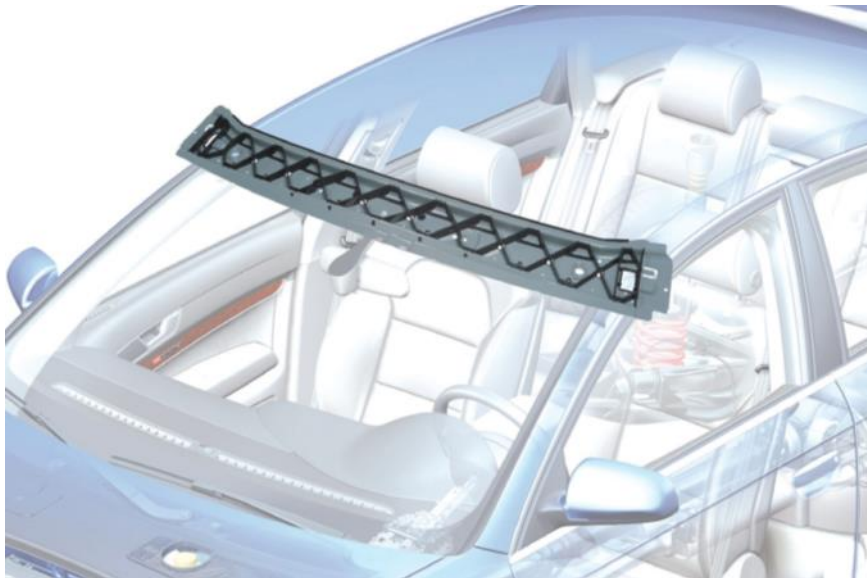


Figure 2-25 Hybrid roof cross member of the Audi A6 (2004) [75]

From the perspective of serial mass production, the FRTP-metal multi-material design approach is an economical lightweight method. Typically, its manufacturing process is based on the standard injection molding process, with one additional process of forming the metal sheet inserts (Figure 2-26).

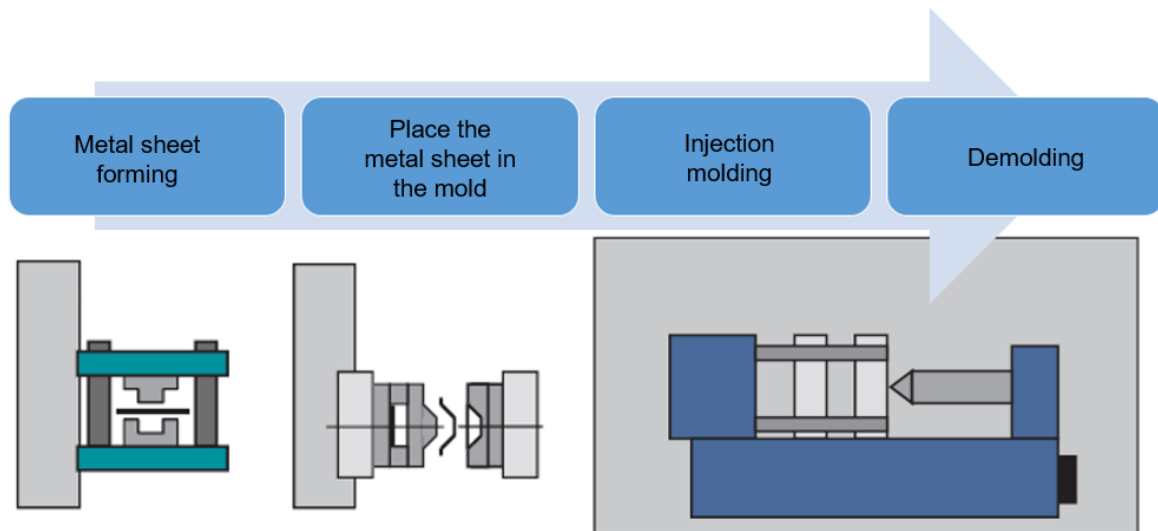


Figure 2-26 Typical manufacturing process for FRTP-metal multi-material components [75]

At present, the FRTP-metal multi-material design approach has undergone further development by the inclusion of new joining techniques and more material combinations [77]. The continuous area joining between metal sheets and FRTP ribs is realized simultaneously with the adhesion promoter (detailed in section 2.6.3) and the form-fitting connector. Material combinations have been expanded on inserts and ribs (e.g., insert: aluminum, PP/PA organo sheet; rib: PA66-GF and PP-GF). Tests with the “Erlanger Träger – plus” (Figure 2-27) show that the introduction of an organo sheet brings more lightweight potential and further increases the component stiffness (+56% bending and +206% torsion stiffness) compared to the original “Erlanger Träger” [74]. The front-end carrier of the Audi A8 (Figure 2-28) is a representative example that illustrates the latest development of the FRTP-metal multi-material design approach on a serial application. It uses the adhesion promoter to realize the joining between the aluminum sheet inserts and the PA6-GF60 ribs, and it applies a U-shape organo sheet insert on the lower belt for added stiffness and strength. Besides the developments, as illustrated in section 2.1, other process combinations, such as combining the injection molding and insert forming processes, have been investigated to further increase the manufacturing efficiency of the FRTP-metal multi-material components.

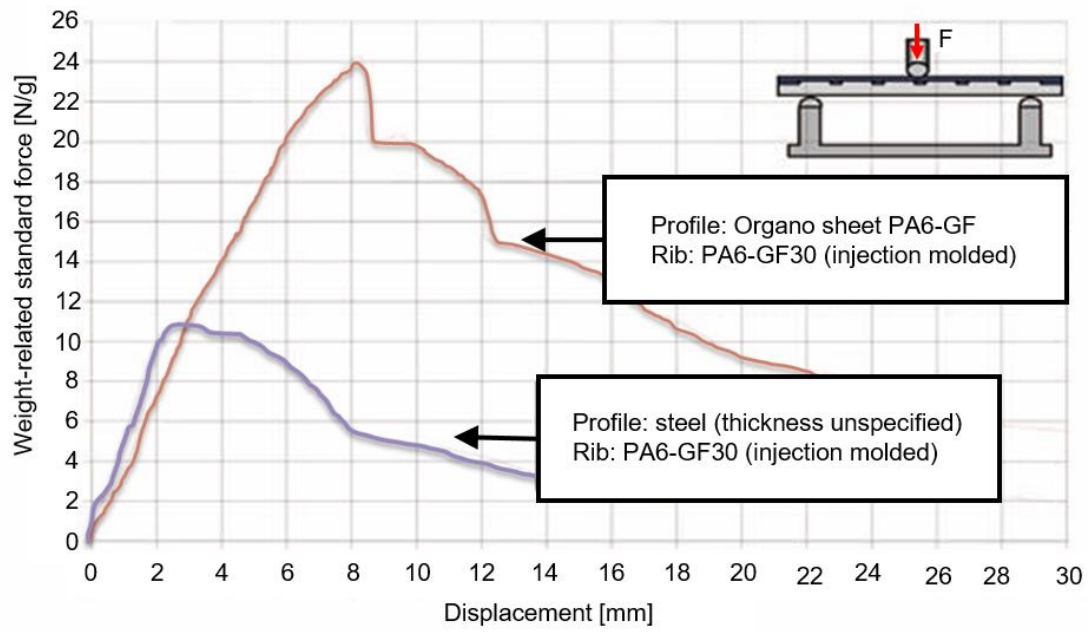


Figure 2-27 The 3-point bending comparison between the “Erlanger Träger” (purple) and “Erlanger Träger Plus” (red) [78]

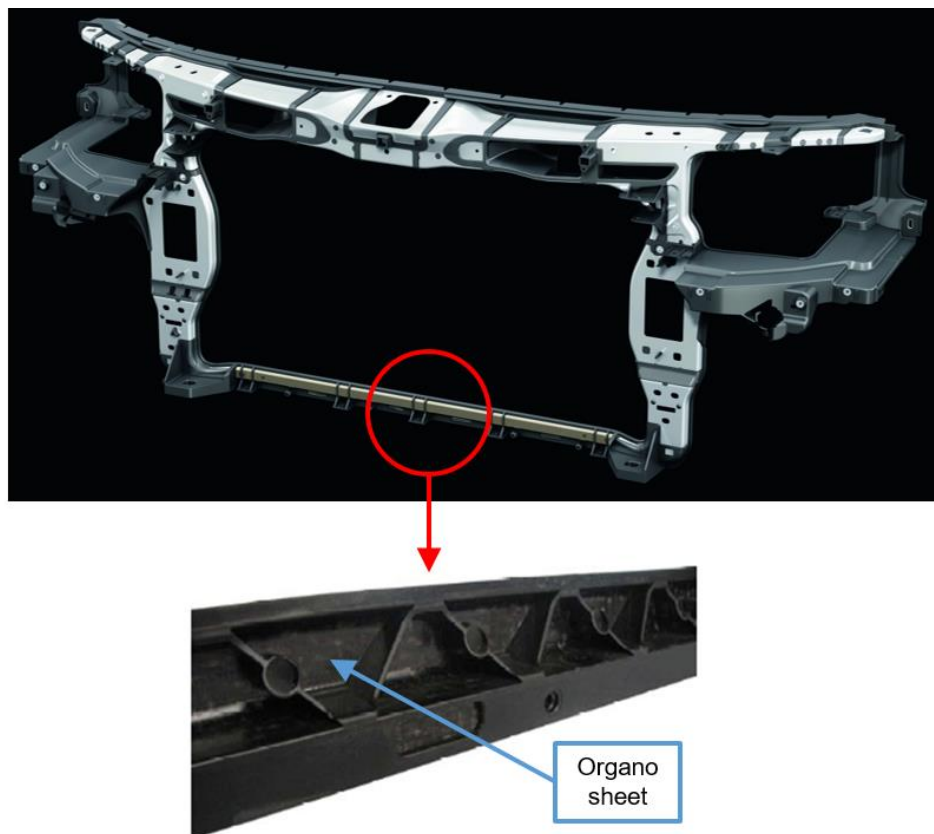


Figure 2-28 Front end carrier of the Audi A8 [78]

2.3 Typical construction of vehicle door

After the introduction of lightweight materials used in this work, as a research work related to the development of door structures, some necessary basics about this important vehicle component will be introduced in this section.

As can be seen on the street, vehicles typically have 2 or 4 side doors. Initially, the only function of those side doors was to let people in and out of the vehicle. Typically, the front of each door is connected with hinges to the A or B pillar. With the rapid development of the automotive industry, the vehicle doors now function as more than just an entrance. Today, the doors have more aesthetic and functional purposes and they distinguish the type of vehicle. People will always relate a falcon door to sportiness or to a high-end vehicle, such as Mercedes-Benz SLS AMG and Tesla Model X. The door now also provides indispensable functionalities in modern vehicles, such as side crash safety and NVH performance.

If we look at the appearance of vehicle doors, we can generally divide them into four main types:

- Regular turning door (mostly for daily-use vehicles) (Figure 2-29a)
- Scissor door (mostly for sports vehicles) (Figure 2-29b)
- Sliding door (mostly for vans and minivans) (Figure 2-29c)
- Falcon door (mostly for sports vehicles) (Figure 2-29d)



Figure 2-29 Typical appearances of vehicle doors. (a) regular turning door [79]; (b) scissor door [80]; (c) sliding door [81]; (d) falcon door [82].

2.3.1 Door classification based on load-bearing structures

From the perspective of load bearing, typical vehicle doors can be divided into two major classifications: 1) Sheet construction doors (Figure 2-30a); and 2) Frame construction doors (Figure 2-30b).

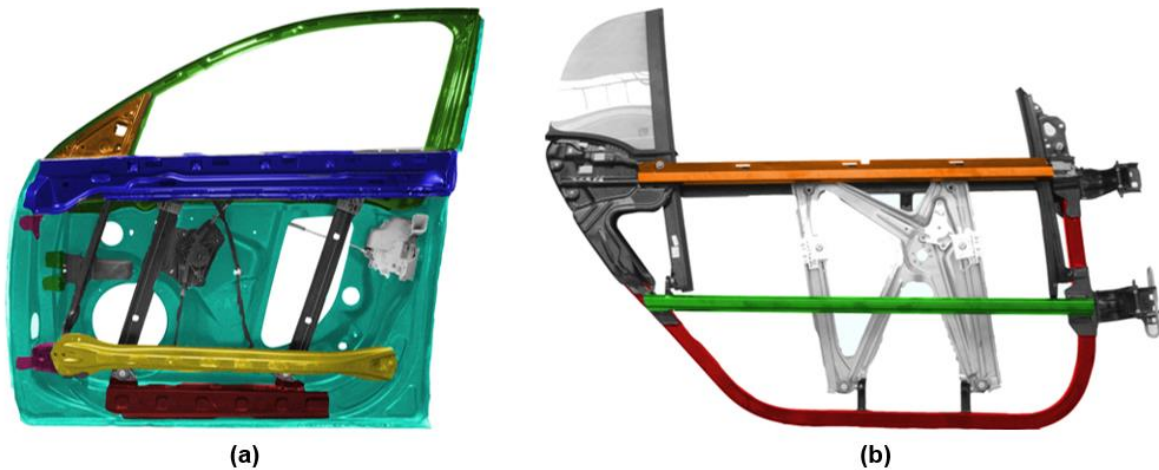


Figure 2-30 Sheet construction door: Audi A4 (a); Frame construction door: smart 4 two (b) [83]

On sheet construction doors, most structural components are made of metal sheets (e.g., doors from the Audi Q7 and BMW 7er in section 2.5.2). Typically, the inner panel is the major loading-bearing component. The final door assembly can be achieved after connecting different components by welding, adhesion, or bolts. A typical forming process for the components of sheet construction doors is stamping.

On frame construction doors (e.g., the ULSAC door in section 2.5.1), most structural components are made of closing aluminum or steel profiles. After the forming (bending) process, these components can be joined by welding, adhesion, and bolts, and they achieve an assembled frame, which is the major load-bearing structure. The inner panel, which in this case has little structural responsibility, is attached separately to this frame structure and can even be made of plastics. Obviously, high tooling costs can be eliminated with this construction. However, the additional cost of joining techniques and forming processes should not be overlooked.

Type	Advantages	Disadvantages
Sheet construction door	<ul style="list-style-type: none"> • Lower weight • Lower unit cost 	<ul style="list-style-type: none"> • Higher tooling cost
Frame construction door	<ul style="list-style-type: none"> • Lower tooling cost 	<ul style="list-style-type: none"> • Higher weight • Higher unit cost

Table 2-7 comparison between sheet construction door and frame construction door

A comparison of the weight and cost between these two door classifications is given in Table 2-7. Cost is an extremely sensitive factor in the automotive industry and is highly related to the total volume of production. Figure 2-31 shows a rough tendency on the total cost of sheet construction and frame construction doors. Due to the high tooling investment, sheet construction doors show more cost advantages when the production volume is sufficiently large (e.g., >100000 units per year). Below this value, frame construction doors are more economical.

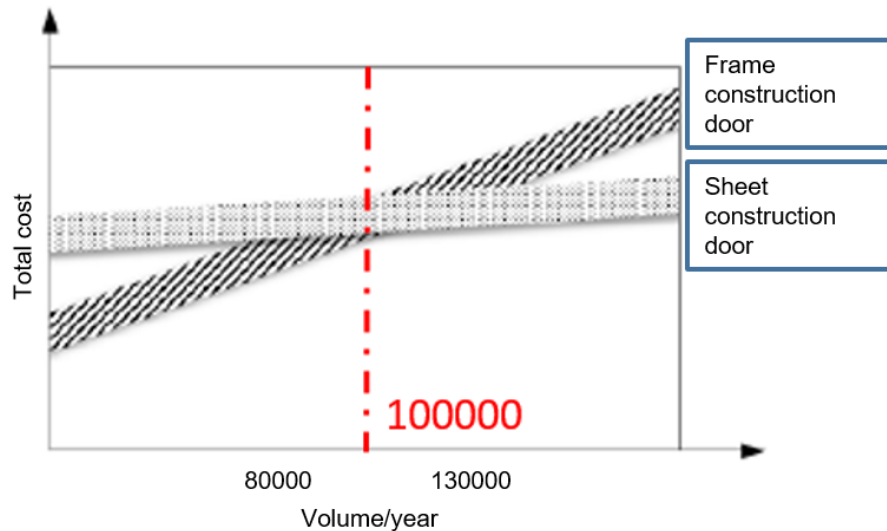


Figure 2-31 Total cost tendency of vehicle doors [84]

A comparison of sheet construction and frame construction doors indicates a middle point between them where both light weight and cost efficiency are achieved by choosing the proper construction principle in the right place, depending on the specific local loading situation. Obviously, this idea is hard to execute with traditional metal materials alone. However, the use of FRPs in this work provides the needed design freedom to realize this idea.

2.3.2 Door classification based on window frame structures

From the perspective of the window frame structure, typical vehicle doors can be divided into three major types: 1) Roof integrated door (Figure 2-32a); 2) Frame integrated door (Figure 2-32b); 3) Frameless door (Figure 2-32c). Among these, the frameless door is not the point of interest in the present work.

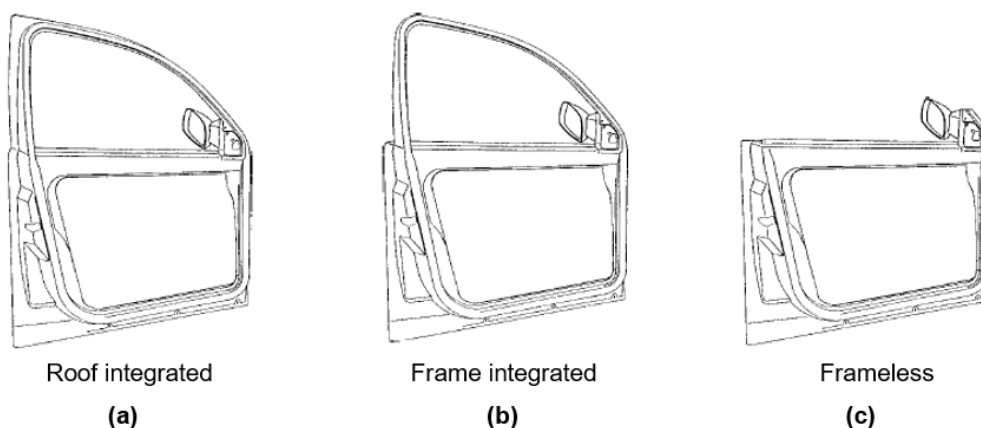


Figure 2-32 Door classification based on the window frame structure [85]

The roof integrated door is the most widely used type. The feature of this type is that the window frame and inner panel are “one piece.” Obviously, the advantage of this type of door structure is the avoidance of the joining complexity between the window frame and the inner panel. However, complex tool designs, higher tooling costs, and low material utilization rates (for metal sheets) are drawbacks that cannot be ignored.

Frame integrated doors have the window frame and door panel as two separate parts that are manufactured separately. The window frame is joined to the door panel during the door assembly. This type of door structure provides the possibility of adapting one concept to different vehicle variants by fitting the window frame design only. In this way, a lower cost of tooling and a high rate of material utilization can be expected. However, the use of more components leads to more assembly procedures and costs. Meanwhile, to achieve an ideal frame stiffness, additional reinforcements and joining techniques must be applied at the frame-to-panel transition areas.

Overall, the assembly cost could be slightly higher for frame integrated doors than for roof integrated doors. Other than that, no absolute winner emerges between these two types. For this reason, the concept design in the present work is aimed at achieving two door concepts following these two structural types.

2.4 Door requirements definition

2.4.1 General requirements

Since the core of the present work is the concept development of economical lightweight doors, the following two categories of door-related requirements have a major influence: 1) general mechanical requirements and 2) economic requirements. The important requirements under these two categories are summarized in Table 2-8.

Category	Important requirements
General mechanical requirements	<ul style="list-style-type: none"> • High torsion and bending stiffness • High frame bending stiffness under aerodynamic loading (especially at high speed) • No noise development through vibration • No permanent damage when opened beyond the door stopper range • Withstand vertical loadings at the open position without significant permanent damage • Sufficient strength in the areas of the door handle and mirror mounting • Fatigue strength over whole service life
Economic requirements	<ul style="list-style-type: none"> • Low pollution during manufacture and disposal • Materials easy to separate • Return of production waste to the manufacturing process • Use of recycling materials • Low energy consumption

Table 2-8 General mechanical and economic requirements for vehicle doors [5]

In modern vehicles, doors are also more responsible for the NVH performance and passenger safety in side crashes, rather than simply having aesthetic attributes. The typical structural stiffness and strength requirements of doors can be summarized in two categories: 1) static loading cases and 2) crash loading cases. The quantitative analysis of the performance of door concepts is performed in the present work using specifically chosen static and crash loading cases and will be introduced in the following sections.

2.4.2 Static loading cases

For static loading cases, every OEM has its own requirements, and no uniform industry or international standard has been established for door static testing. To ensure universality, six typical static loading cases are defined in the present work according to previous benchmarking [86; 87]: 1) frame stiffness b-pillar; 2) frame stiffness middle; 3) door sag; 4) over opening; 5) belt stiffness outer; and 6) belt stiffness inner (see Figure 2-33).

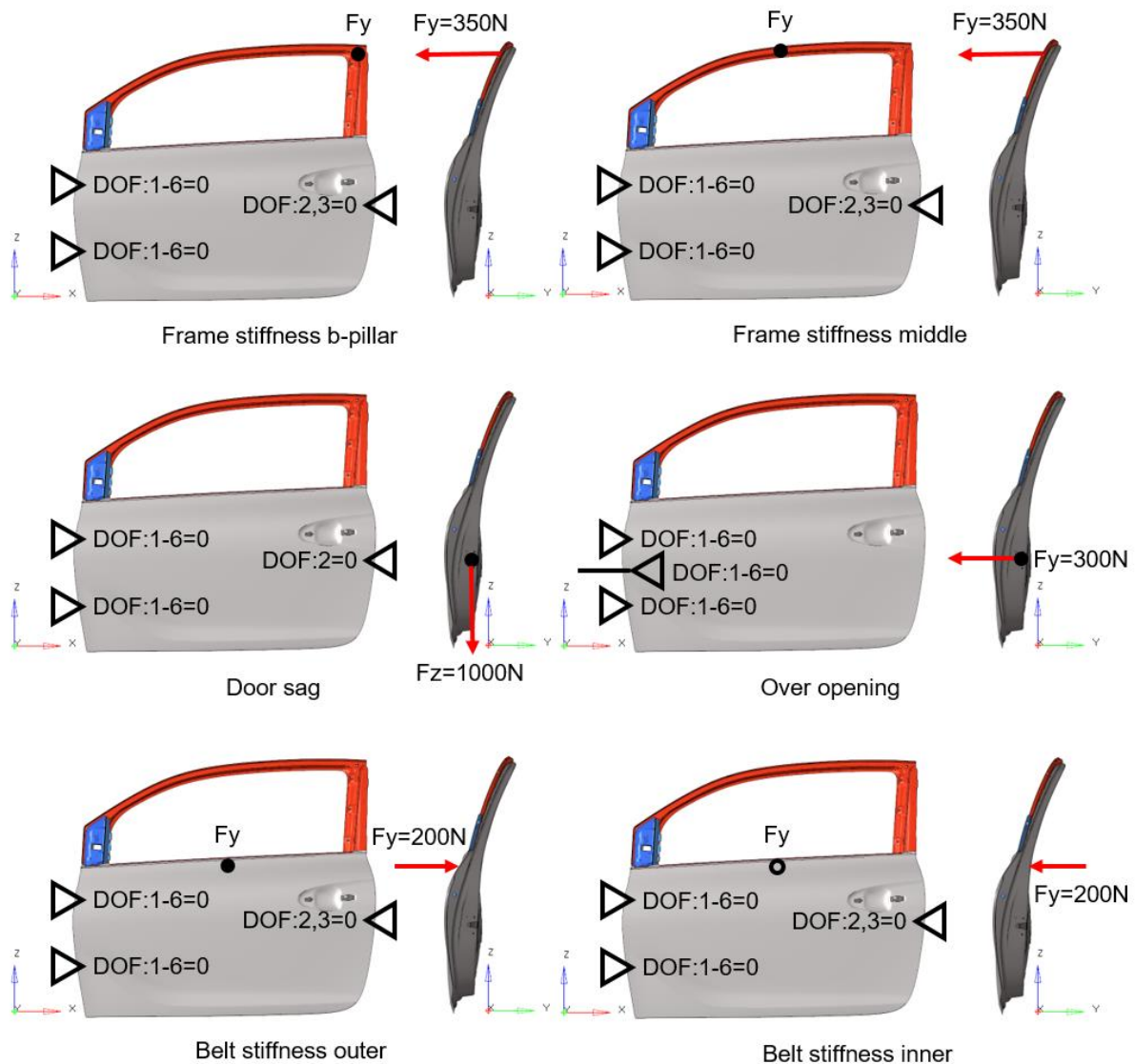


Figure 2-33 Six typical static loading cases with force levels and boundary conditions

These static loading cases are able to test all important areas, such as the window frame and hinge area, that require high stiffness. For example, two “frame stiffness” loading cases can test whether the frame structure is strong enough to withstand the “lift-off” effect caused by the aerodynamic force at a high driving speed, which is directly related to the level of wind noise. For the hinge area, two misuse loading cases, namely “door sag” and “over opening,” can simulate the typical “lean-on” and unintended opening over the door stopper limit situations, which are typical during daily usage. Clearly, no significant deformation or material failure is allowed in the hinge area under these two loading cases.

2.4.3 Crash loading cases

For crash loading cases, side impacts are the major crash scenarios related to the door structure. Different countries have different regulations and requirements, such as FMVSS 214 for the U.S.A. and the EuroNCAP side impact with moving deformable barrier (MDB) and rigid pole barrier for the European Union. Increasingly more OEMs use the door belt as an auxiliary loading path for a frontal crash. Especially under the offset frontal crash scenario, such as the EuroNCAP frontal crash test with offset-deformable barrier (ODB) and the IIHS small overlap

frontal test, this additional loading path can help to reduce the intrusion and deformation of the A-pillar.

According to the information from the OEM, the chosen reference vehicle in the present work has only been launched in the European market and has no responsible or special structural design for conducting the impact force under a frontal crash. For this reason, this work focuses on the EuroNCAP side impact tests. Among these, the more critical test, the EuroNCAP side impact with the rigid pole barrier (version 2001) [88], is used in this concept phase since its larger intrusion could be more vital to occupants than the side impact test with the MDB [89]. In this test, the test vehicle is placed on the sled and accelerated to reach the impact speed of 29 km/h right before the impact (Figure 2-34). The impact angle is 90°. The impact position between the vehicle and the rigid pole barrier is aligned with the center of gravity (COG) of the dummy's head.

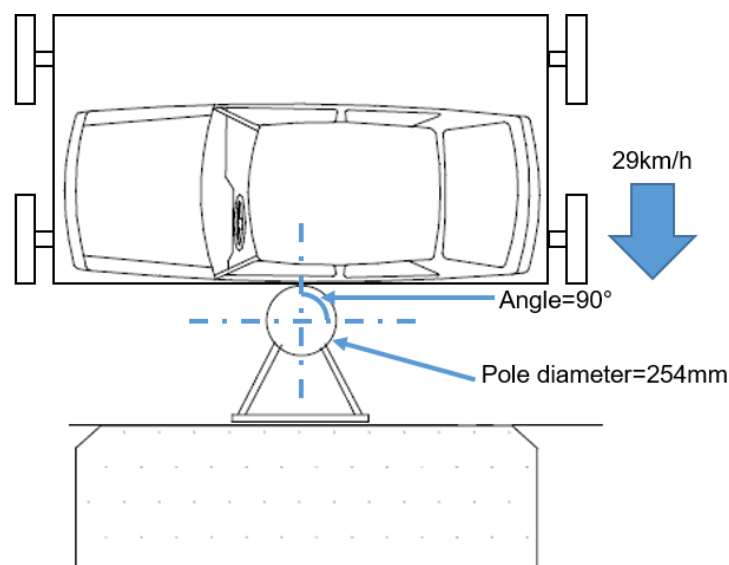


Figure 2-34 Euro NCAP side impact with rigid pole barrier (version 2001) [88]

2.5 Existing lightweight studies and applications on vehicle doors

Due to the trend of E-mobility and increasingly strict emission requirements, lightweight design has become one of the most effective methods in the automotive industry for helping electric vehicles reach a higher range or for reducing CO₂ emissions from traditional motor vehicles. The vehicle door, as a major steel-intensive closure component on a vehicle, has a certain amount of weight reduction potential through lightweight design. For this reason, much research has been done on weight reduction of vehicle doors, using different materials and constructions. For an overview, several representative examples of work/research in this area are summarized into three categories according to materials: (1) steel, (2) light alloys, and (3) fiber-reinforced plastics.

2.5.1 Lightweight door with steel

Any discussion of lightweight door design with steels must mention the “ULSAC” [87] and “InCar” [90; 91] projects. In this section, these two famous projects will be illustrated and discussed.

As the name of the project implies, the ULSAC project was focused on developing an Ultra-Light Steel Auto Closure [87]. This project developed and implemented a prototype for a frameless ultra-light steel vehicle door that simultaneously fulfills state-of-the-art performance requirements, incurs no additional costs, and provides a substantial weight reduction. In the concept phase of this project, lightweight concepts for all types of vehicle closures (door, hood, decklid, and hatch) were developed only with steel materials to reveal the considerable weight-saving potential available with those components. Compared to the benchmarked closures, up to a 32% weight reduction could be achieved without losing any structural performance. Meanwhile, a cost-neutral lightweight design was achieved by using standard steel materials and existing manufacturing and assembly processes. Because of the positive outcomes after the concept phase, the frameless lightweight steel door concept (ULSAC door) was selected for further development with the refined door-related packages based on the Porsche Boxster/911 and includes the window regulator, latch system, etc. To achieve high-level weight reduction, high-strength steel (yield strength $\geq 210\text{MPa}$) and ultra-high-strength steel (yield strength $\geq 550\text{MPa}$) are used. Stamping and hydroforming (tube) are the major manufacturing processes. Laser welding, resistance spot welding, metal arc welding, and adhesive bonding are the chosen joining technologies. Additional costs incurred by these processes and technologies can be recouped through the savings on material costs.

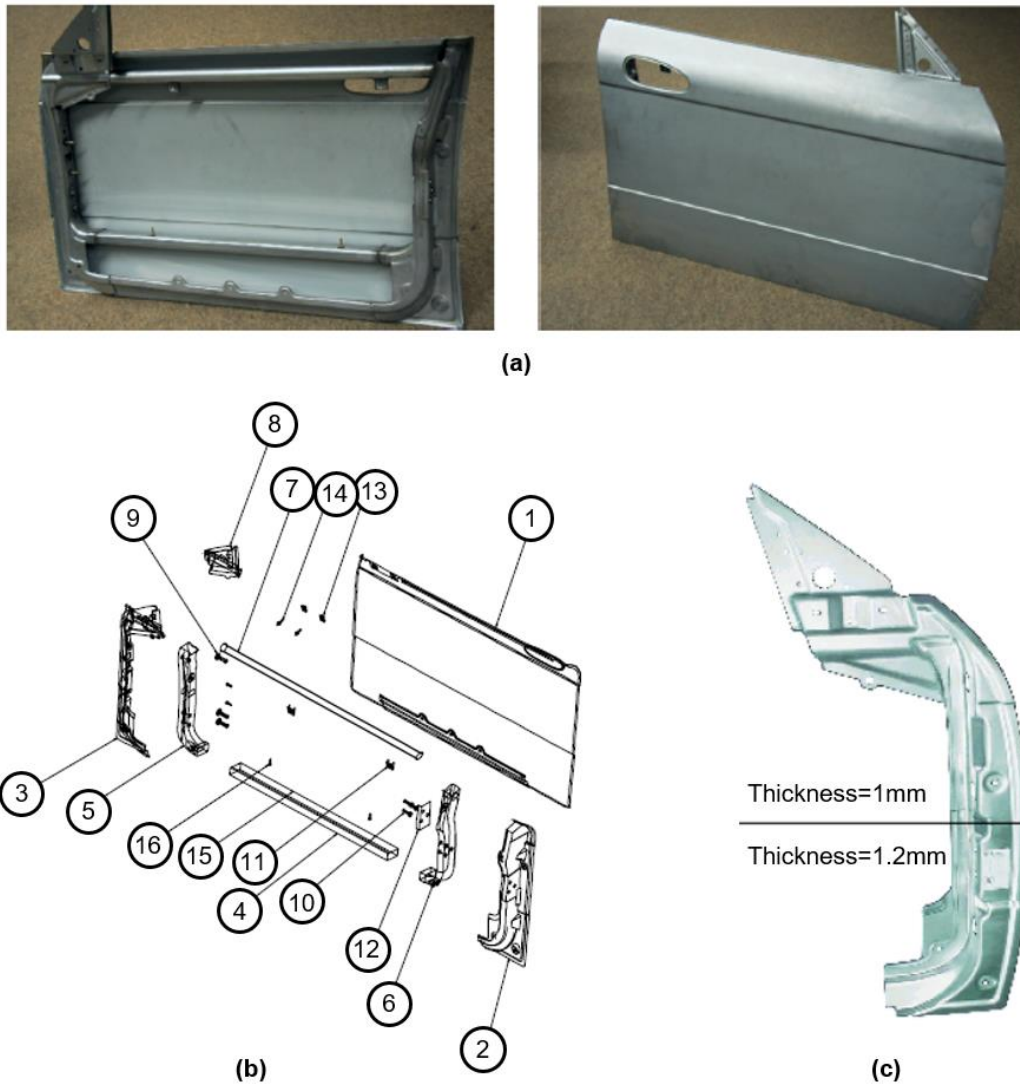


Figure 2-35 ULSAC door: hardware (a); explosion view (b); laser-welded tailored blank (c) [87]

The final assembly of the ULSAC door is illustrated in Figure 2-35a. As shown in Figure 2-35b, the ULSAC door features a load-bearing frame structure (part 4 to part 7), which plays an important role in the stiffness of the structure. Due to the different loading situations on the top and bottom hinges, a laser-welded tailored blank has been used for hinge reinforcement (part 3 in Figure 2-35b and c) to enable a further weight reduction.

To exclude the influence of different door sizes on the evaluation of weight reduction, the normalized weight (weight/area of the door) is used here. The final measurement of the prototype illustrates that the normalized mass of the ULSAC door (13.27kg/m^2) is significantly lower than that of the predefined target (15.5kg/m^2). Compared to the benchmarked doors (range: 19.74kg/m^2 to 23.02kg/m^2), ULSAC door achieved about a 30% to 42% weight reduction of the normalized weight. Even compared to the best-in-class door with frame, the ULSAC door still weighted 22% less (normalized). In the test phase, three static loading cases (vertical sag and upper and lower lateral stiffness) and FMVSS 214-QS (quasi-static side intrusion) were considered (Figure 2-36). Although the project-defined stiffness under the static loading case of “vertical sag” and the regulated crash resistance forces under FMVSS214-QS have not been fulfilled, the ULSAC door still achieved comparable structural performance to

that of other benchmarked doors (Table 2-9). Another point worth mentioning is that the low crash resistance force under FMVSS214-QS is due to the absence of surrounding BIW components. Chances are good that the ULSAC door can fulfill this requirement in the full vehicle testing scenario.

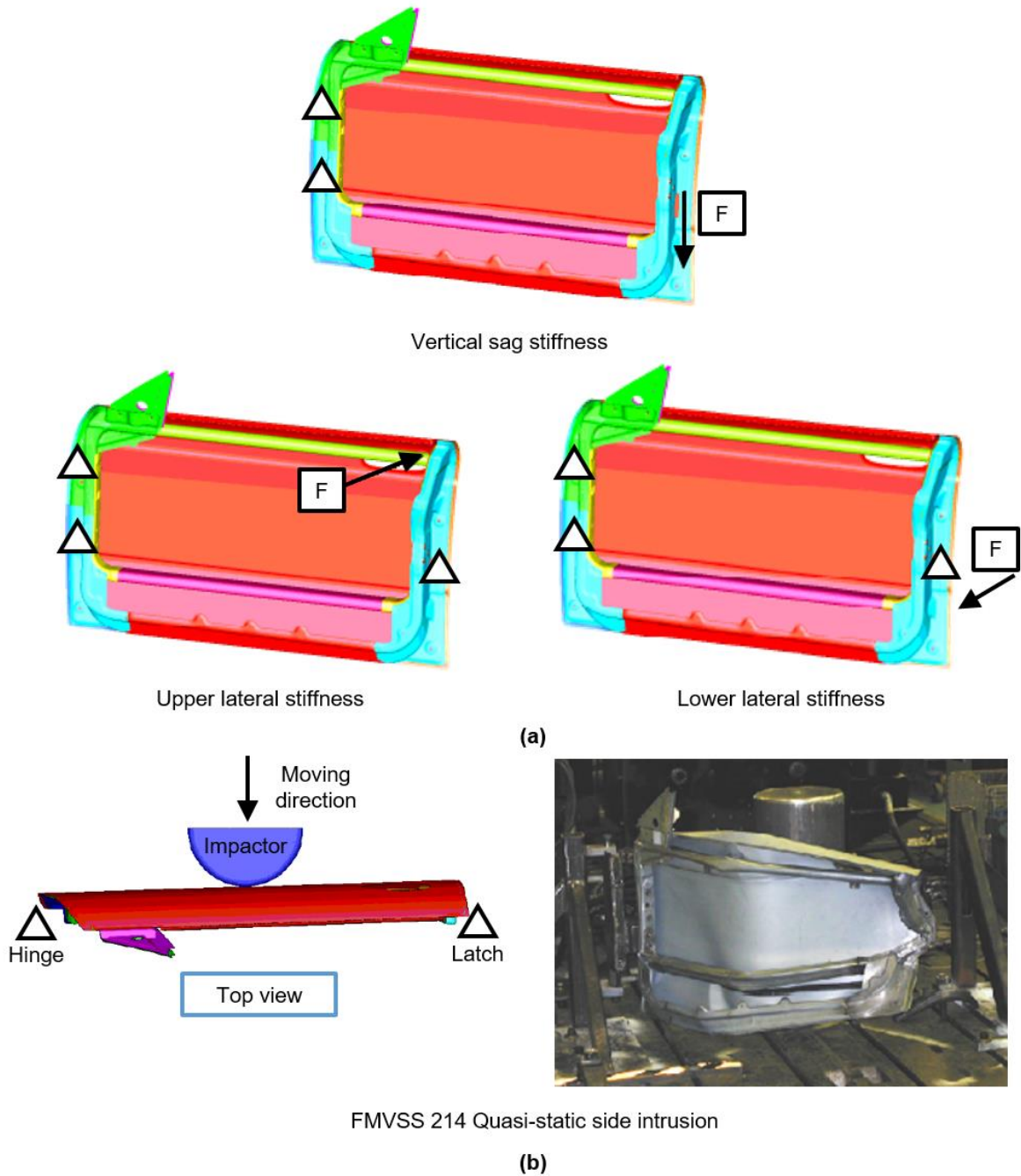


Figure 2-36 ULSAC: important loading cases in the testing phase [87]

Loading cases	Benchmarking frameless doors			ULSAC	
	Door A	Door B	Door C	Target	Prototype
Vertical door sag stiffness (N/mm)	109	194	497	287	157
Upper Lateral stiffness (Nm/deg)	352	197	188	127	259
Lower Lateral stiffness (Nm/deg)	467	309	188	127	261
FMVSS 214 Quasi-static side intrusion					
Average resistance force (kN): 0 to 6 inch intrusion	8.55	6.18	7.33	10.01	8.18
Average resistance force (kN): 0 to 12 inch intrusion	7.73	11.21	13.33	15.57	11.51
Peak force (kN)	15.17	25.56	24.59	31.14	38.90

Table 2-9 ULSAC door: structural performance of prototype under chosen loading cases

The InCar project [90; 91] developed two steel lightweight vehicle door concepts with the extensive use of FEA methods.

The first concept of a “steel lightweight door” (Figure 2-37b) is a good example of a steel lightweight door with a conventional design. It retains all the important components of a conventional sheet constructed door but uses advanced lightweight materials, such as a sandwich material (steel and PE/PA-compound) on the outer panel, a tailored blank on the inner panel, and ultra-high strength steel on the side impact beam (MBW1500). It achieves a 13% (2.31 kg/door) weight reduction in comparison to the reference, with an approximately 11% (6.34 €/door) cost increase, while fulfilling all pre-defined loading cases, including static loading cases (e.g., frame stiffness, door sag, over opening, similar to the loading cases mentioned in section 2.4.2), FMVSS214-QS, and IIHS (SUV). On a comparative basis, the reference door (Figure 2-37a) for the InCar project, also developed by ThyssenKrupp according to the state-of-the-art production standards, has a normalized mass of 20.69 kg/m² (mean value based on a door benchmark by ThyssenKrupp) and a leading structural performance among all benchmarked doors.

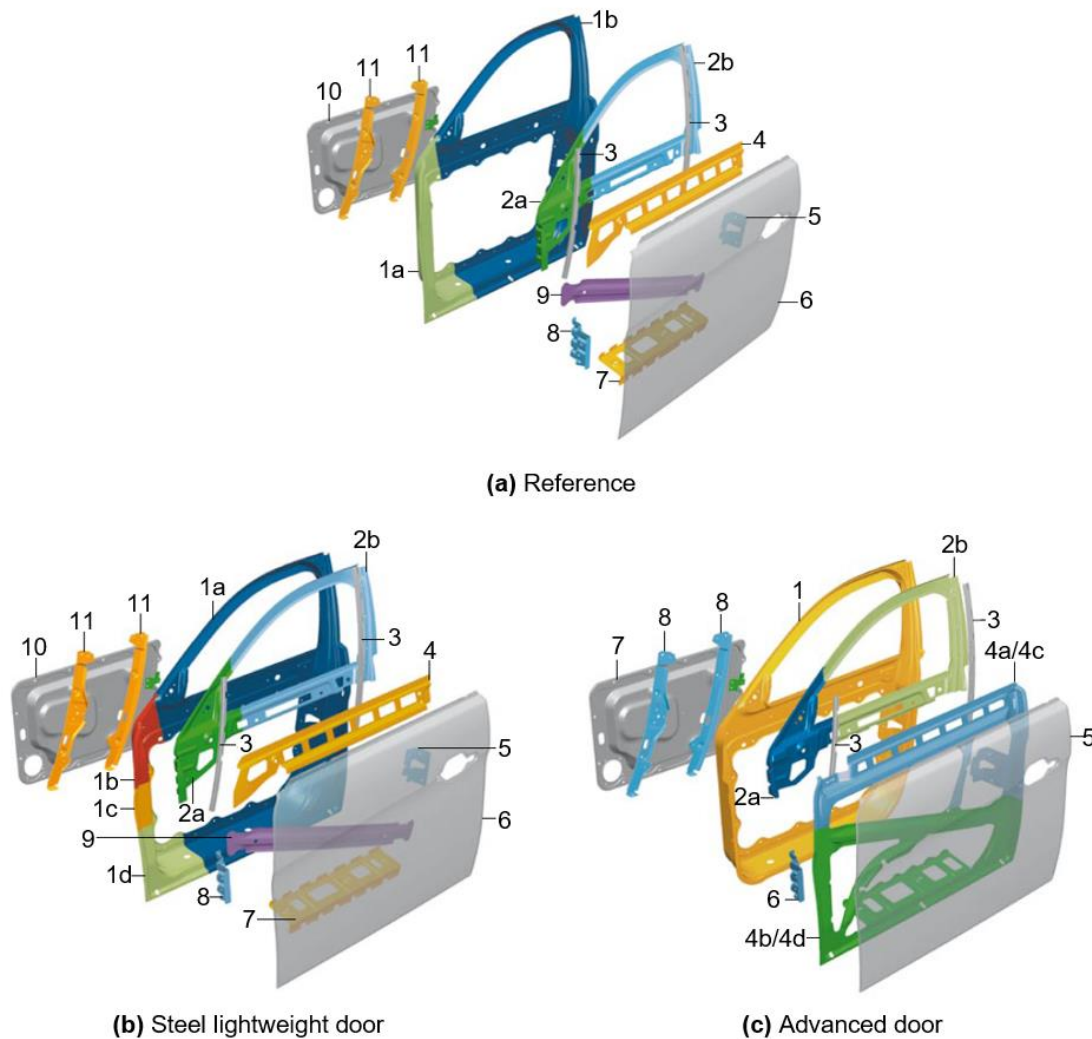


Figure 2-37 InCar project: reference (a) and door concepts (b) (c) [90]

The total number of parts and lightweight costs were reduced in the second concept “advanced door” (Figure 2-37c) using an innovative structural approach for both hot- and cold-stamping processes. It features a two-part inner panel: 1) inner panel outer (4a/4c and 4b/4d in Figure 2-37c); 2) inner panel inner (1 in Figure 2-37c). The innovative “inner panel outer,” which integrates many functional and reinforcement parts (e.g., the hinge and latch reinforcements and the side impact beams), is made of a high-strength tailored blank and can be realized by either hot or cold stamping, depending on the steel grade. This unique structure, together with the laser welding in the frame area, helps the “advanced door” achieve a ca. 11% (1.96 kg/door) weight reduction and a comparable structural performance to the reference under all loading cases. According to the cost analysis (including material cost, manufacturing cost, tooling investment, and BIW manufacturing cost), the “advanced door” has almost no additional lightweight cost.

The specific weight and cost information related to both concepts are listed in Table 2-10. The InCar project illustrates an important fact, namely that the weight reduction on steel doors can be achieved either by the use of conventional designs with advanced steels, semi-finished products, and manufacturing processes or by applying new design approaches.

	Reference	Concept 1: Steel lightweight door	Concept 2: Advanced door	
			hot stamping	cold stamping
Weight	17.17 kg	14.86 kg	15.21 kg	15.21 kg
Weight change		-13%	-11%	-11%
Cost change		+11%	0%	+1%

Table 2-10 InCar project: specific weight and cost information for both concepts [90]

2.5.2 Lightweight door with light alloy

Light alloys, such as aluminum and magnesium alloys, have been used for decades in the automotive industry as the lightweight materials on BIW [92; 93; 94; 95]. Due to the cost reason, the applications of aluminum alloys are more than that of magnesium alloys. Compared to traditional steel grades, however, low density aluminum alloys have a weight advantage. For this reason, many doors and closures achieve a substantial weight savings when made with aluminum.

Different aluminum alloys are extensively used on doors and closures of the 2015 Audi Q7 [96] (Figure 2-38). According to Audi, this door features a one-piece aluminum inner panel design with a roof integrated frame structure. This gives a weight savings of 24 kg per vehicle (6 kg per door) compared to its predecessor. This substantial weight savings is achieved by an "Ultra-Lightweight Design" approach. Specifically, on the door structure, all the steel sheet components that were on the predecessor are replaced with aluminum of different thicknesses. The side impact beam, which was made with aluminum extrusion profiles (the specific aluminum alloy types are not published) on the predecessor, is retained but with a different design. The use of a one-piece aluminum inner panel design reduces the cost of tooling and joining technologies and simplifies the quality control. However, one notable feature is the reduction in the depth of the aluminum door inner panel. Due to the one-piece design and the limit formability of aluminum alloys, the depth of door inner panel is decreased from 160–190 mm (steel predecessor) to 140–180 mm. Despite the reason for the door package change, it still reveals the important fact that the forming limitation of aluminum alloys might have some negative influence on the component dimension and could add additional constraints on the package definition for the surrounding components.



Figure 2-38 The Audi Q7 aluminum door (2015): Green components are made of aluminum sheets; blue components are made of aluminum extrusion profiles [96]

In 2015, BMW launched the new BMW 7er model, which features a large amount of lightweight innovations on the BIW structure, such as the famous “Carbon Core” [70]. The Door-In-White (DIW) of this generation BMW 7er [97] is simple and concise, and includes a total of only five aluminum sheet parts and one steel sheet part (side impact beam) (Figure 2-39). Except for the outer panel (AlSi0.6, Mg0.5), the rest of the aluminum sheet parts are made of standard EN-AW-5182 Aluminum (AlMg4.5, Mn0.4).

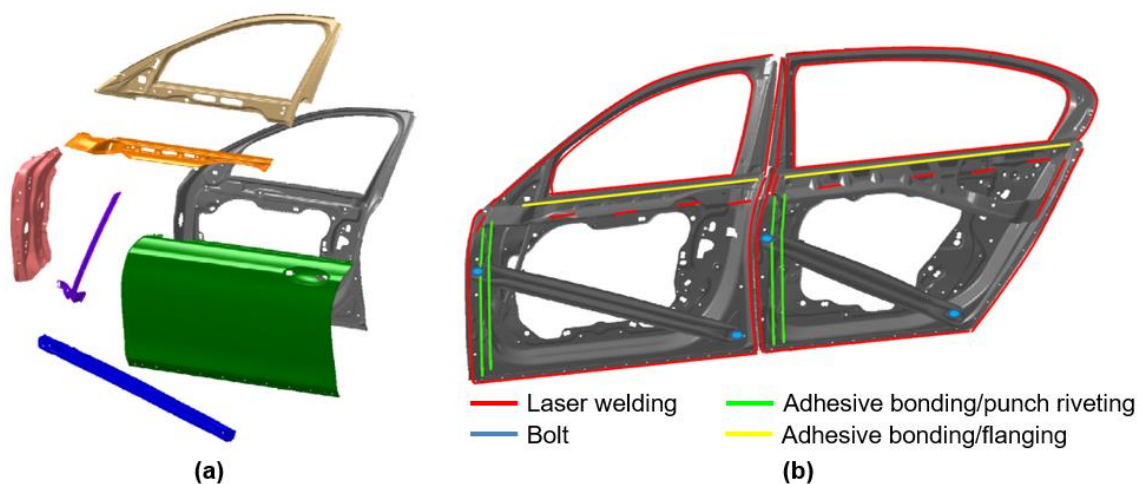


Figure 2-39 The BMW 7er (2015): Aluminum door (a) and applied joining techniques (b) [97]

According to BMW, the weight of door structure, including the hinge system, coating, and door stopper, is 42.8 kg per vehicle. Compared to its aluminum predecessor, a weight reduction of 6.5 kg per vehicle (ca. 1.6 kg per door) is achieved by the DIW. Considering the weight reduction due to the door carrier, hinges, and door stopper, the weight is reduced by 9.9 kg per vehicle (ca. 2.5 kg per door, ca. 19%). This weight savings is remarkable since the

predecessor is also made of aluminum. The major weight savings is achieved by: 1) component elimination; 2) thickness reduction (e.g., inner panel and hinge reinforcement); and 3) component downsizing (e.g., frame closing plate). The joining technique highlight of this door structure is the extensive use of laser welding: 1) a completely laser welded window frame (first in the market); and 2) a laser-welded outer panel flange, which greatly improves the aeroacoustics behavior and stiffness.

In contrast to the aluminum door approaches, the aluminum door from the 2016 Honda Clarity fuel cell (Figure 2-40) [98] has a frame-integrated construction and features a window frame made of aluminum extrusion profiles. The window frame is manufactured separately from the inner panel, thereby reducing the difficulty of aluminum stamping and enabling a deeper inner panel depth (the same as the steel reference). The inner panel is separated into several parts depending on the different stiffness requirements in different areas. A better crash performance under side impact tests is achieved by forming the side impact beam from 7000 series aluminum alloys. Compared to the steel reference (a door from a Honda medium-class vehicle), weight reductions of 38% and 32% are achieved on the front and rear DIW, respectively. Although a substantial weight savings is achieved on the frame area (40%), the loss of frame stiffness (ca. 30% lower than reference) on this aluminum door should be pointed out. The reason for this loss is that the insignificant expansion of the frame cross-section cannot compensate for the loss of bending stiffness caused by the material substitution from steel to aluminum.

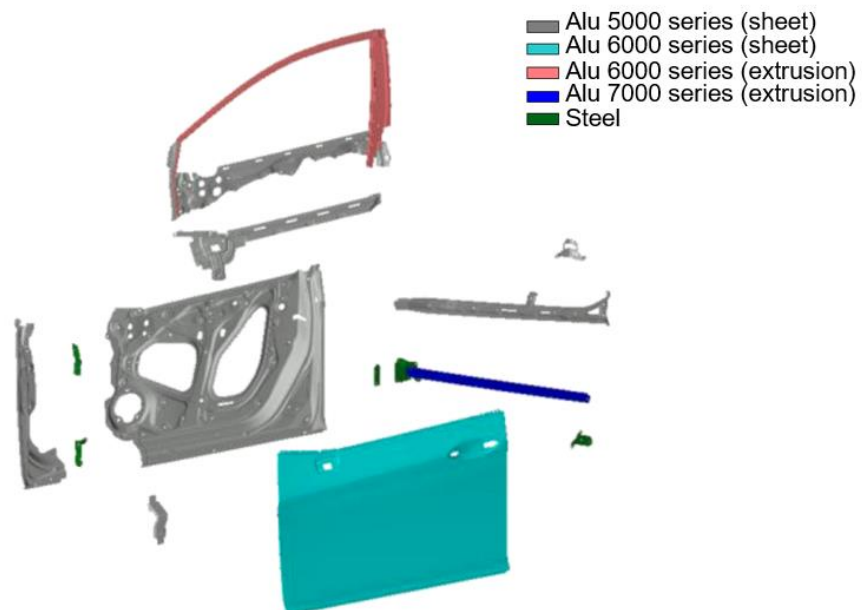


Figure 2-40 The Honda Clarity fuel cell (2016): aluminum door [98]

2.5.3 Lightweight door with fiber reinforced plastic (FRP)

In 2000, two FRP door concepts for commercial vehicles were introduced [5] (Table 2-11). The innovation point for both concepts is the unique load-carrying structure in the door belt area, which is called the “Tension-Compression-Unit” (German: Zugverbund-Druckelement-Einheit) (Figure 2-41). This unit not only provides the major stiffness to the door structure, but it also replaces the role of the side impact beam, which is able to conduct the force in side and frontal crashes appropriately to the A and B pillars. In these two concepts, both thermosetting and thermoplastic material system were investigated (Table 2-11). Only the door concept 1 with the thermosetting matrix material shows a comparable stiffness to that of the steel reference under static loading cases (frame stiffness and door sag). Under crash loading cases, such as side impact tests (FMVSS214 Quasi-static; side pole crash) and offset frontal crash tests (40% overlap), door concept 1 also achieves positive results. In the side pole crash test, the 10% intrusion is reduced with door concept 1. However, no specific weight savings information is given in this work. Although the “Tension-Compression-Unit” is a smart design, it is difficult to apply on passenger vehicles due to the significant difference in the hinge position (typically both hinges are below the belt area on passenger vehicles). The chosen manufacturing methods also limit the use of these door concepts to only small serial manufacturing due to the long cycle time and the high cost per part.

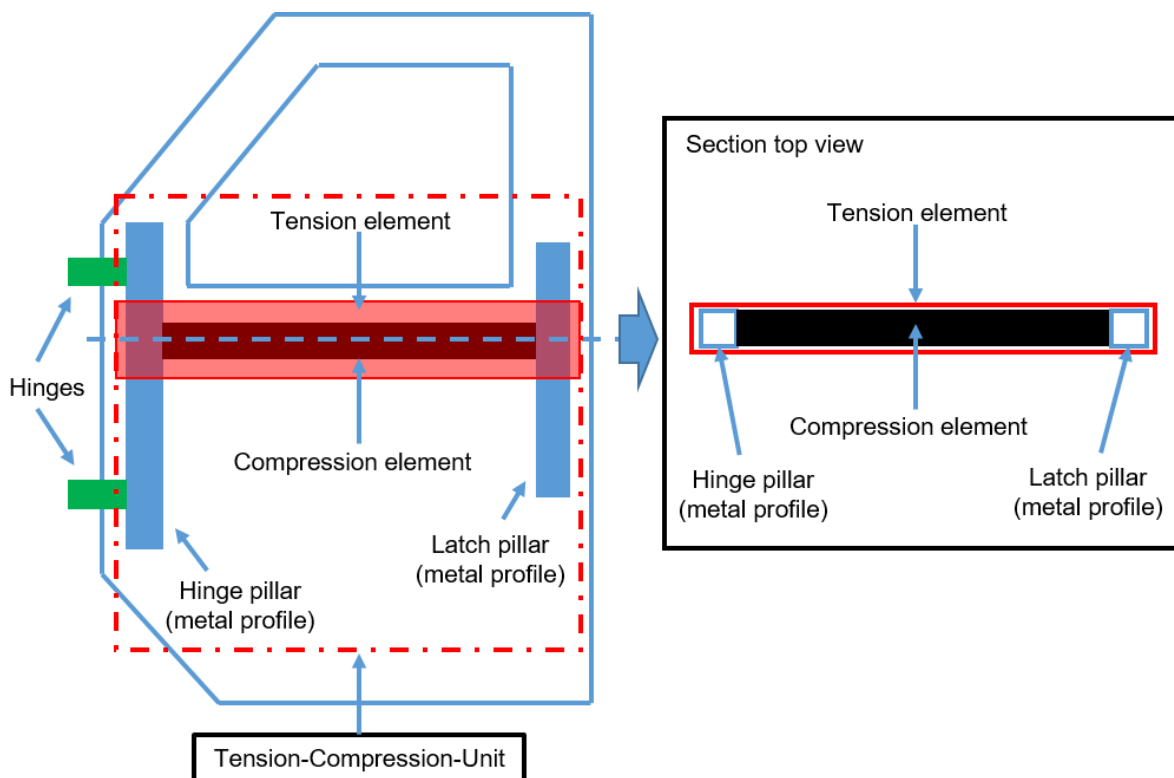


Figure 2-41 Schematic of the “Tension-Compression-Unit”

	Door concept 1	Door concept 2
Construction principle	Sandwich-sheet construction (reinforced with structural foam)	Sheet construction
Major material system	Thermosetting <u>Matrix:</u> Epoxy resin	Thermoplastic <u>Matrix:</u> Polypropylene (PP)
Sheet components (Inner and outer panel)	<u>Fiber:</u> Glass fiber (woven fabric) <u>Manufacturing:</u> Autoclave	<u>Fiber:</u> PP-Glass fiber (woven fabric with hybrid yarn) <u>Manufacturing:</u> Autoclave
Tension element (Figure 2-41)	<u>Fiber:</u> High-performance Polyethylene (HPPE) <u>Manufacturing:</u> Wrapping & vacuum process	<u>Fiber:</u> PP-Glass fiber (hybrid yarn) <u>Manufacturing:</u> Wrapping & press process
Compression element (Figure 2-41)	Pultruded Glass fiber-Polyester tubes	

Table 2-11 Important information for FRP commercial vehicle door concepts [5]

In 2008, a multi-material door concept was developed for a racing car (Audi-A4 based) [99] (Figure 2-42a). The idea underlying this concept can be summarized as: 1) substitute the steel used as material for the outer panel with CFRP; 2) remove non-structure-relevant components; 3) remove the side impact protection beam; 4) keep the original steel inner panel, belt reinforcement, and aluminum window frame. Based on the published results, the multi-material door achieved a 29% (3.16kg/door) weight reduction compared to the original Audi-A4 door, with a small sacrifice of structural stiffness. Obviously, due to the absence of the side impact protection beam, the crash performance of the concept door is taken over by another structure (e.g., a roll cage) on the racing car. The CFRP outer panel is manufactured by hand lamination and vacuum forming, so this door is only suitable for small-scale production. Based on this

racing car door, a full CFRP door concept was also virtually realized in this project [99]. With this concept, the inner panels are designed with integral construction—a so-called “shell-rib structure,” which is developed with the help of the structural optimization software (Optistruct) (Figure 2-42b). A 70% (7.6kg/door) weight reduction can be achieved compared to the original Audi-A4 door. Although no prototype is being built, the manufacturing methods (i.e., hand lamination and vacuum forming) for this concept door are clearly far from the requirements for serial production.



Figure 2-42 Multi-material door concept (a) and full CFRP door concept (b) from IKA [99]

In 2012, a mass-production-oriented CFRP door concept (Figure 2-43a) was developed and introduced by Brose Fahrzeugteile GmbH [100; 101]. This concept featured a CFRP roof-integrated inner panel and a metal outer panel. Unlike conventional doors, the highlight of this concept is the major load-bearing and highly function-integrated metal “outer panel module.” This module includes hinge, latch, and outer belt reinforcements, as well as the side impact beam. The complete DIW can be assembled simply by joining the metal outer panel to the CFRP inner panel (Figure 2-43b) with several bolts. The use of CFRP on this door concept achieves a substantial weight savings. Compared to conventional steel and aluminum references, weight reductions of 55% and 35%, respectively, can be reached. However, the additional lightweight costs also reach an unacceptably high value of 21 €/kg. For this reason, this concept has not been realized in any series application.



Figure 2-43 The CFRP-Door system from Brose Fahrzeugteile GmbH: assembled outer panel and inner panel (a); prototype (b) [100]

Since none of the CFRP door concepts so far are ready for mass production due to their high cost, suppliers have focused their efforts on the door carrier, which is a semi-structural component and has relatively lower performance requirements. In 2015, Brose Fahrzeugteile GmbH introduced a mass production-ready FRTP door carrier made of PP-LGF30 and reinforced locally with organo sheets [102]. The design concept, material distribution, and prototype are shown in Figure 2-44. The highlights of this door carrier are the significant thickness reduction by the extensive use of organo sheets and the mass production-ready one-shot-process.

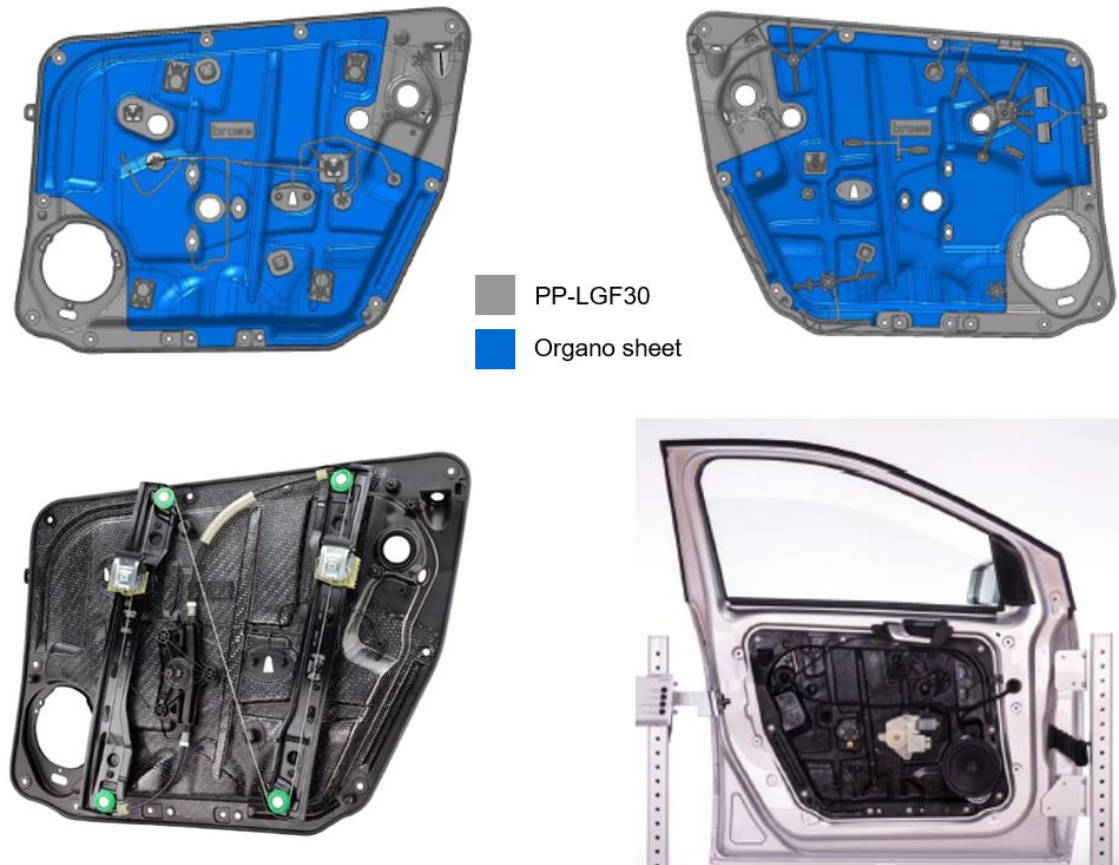


Figure 2-44 The FRTP door carrier with organo sheets from Brose Fahrzeugteile GmbH [102]

The one-shot process is a further development based on the standard injection molding process, and it achieves simultaneous organo sheet thermoforming and PP-LGF30 injection molding in one step. A schematic of the whole production process is illustrated in Figure 2-45. Compared to the conventional door carrier (typically 1.8 mm PP-LGF30 only), the implementation of organo sheets leads to a significant thickness reduction (0.5 mm total thickness on this carrier) and up to a 40% weight reduction. The use of this door carrier achieves a weight reduction of as much as 5 kg/vehicle compared to the conventional door (e.g., a 0.7 mm steel door with a window regulator and aluminum window rails). This innovative door carrier also shows better acoustical performance and higher energy absorption (factor 3 to 4 under the pendulum impact test) than the reference door. The thickness reduction and the one-shot-process create a cycle time for manufacturing this door carrier that is almost the same as the reference PP carrier. However, a point that should be noted is that the additional lightweight cost of this door carrier is not published. Although no change occurs on the cycle time, the extensive use of organo sheets will inevitably increase the material costs, and this could be a major concern for large series BIW applications when more organo sheets are required [103]. Other than that, the know-how for implementing FRTPs in combination with semi-finished prepreg reinforcements on a semi-structure component can eventually be transferred to structural components, e.g., doors. What remains to reach a balance between the cost and the structural performance is to find a way to use the organo sheet more efficiently [8; 104].

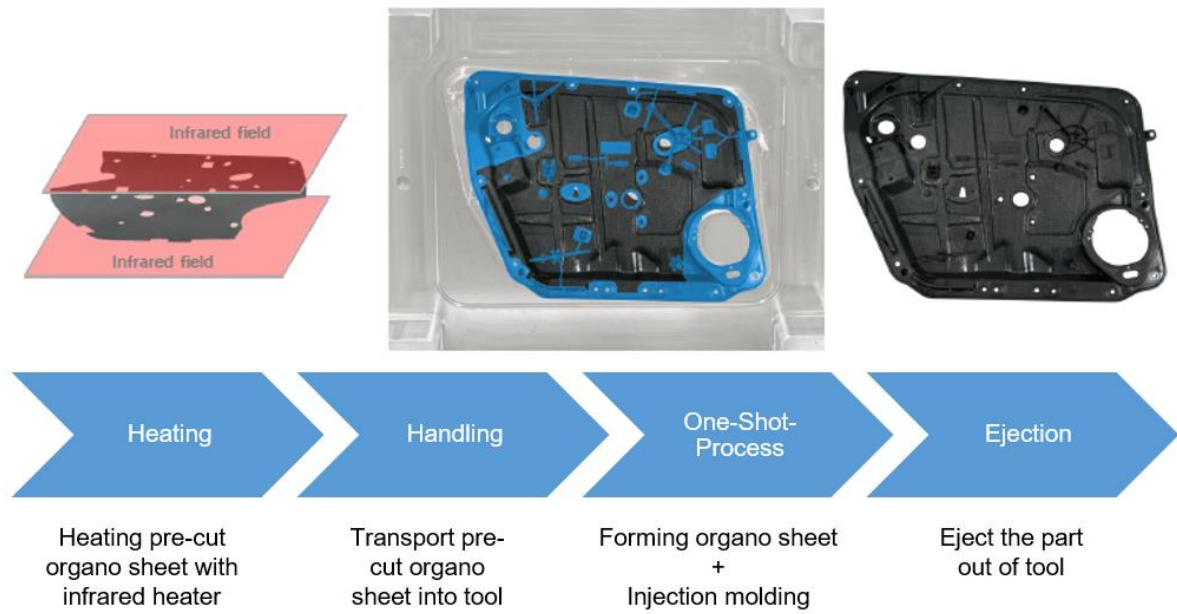
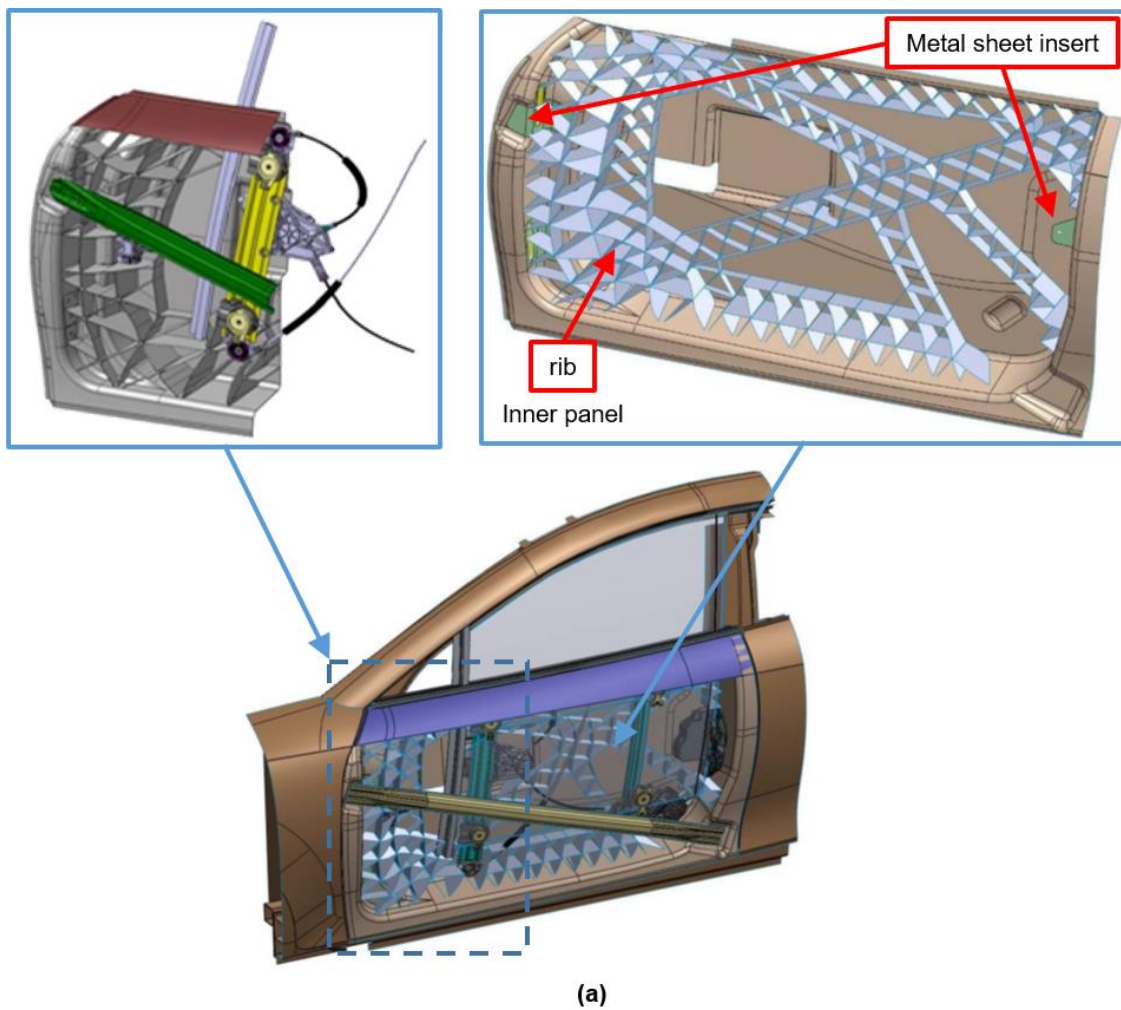


Figure 2-45 Production process for a FRTP door carrier with organo sheets [102]



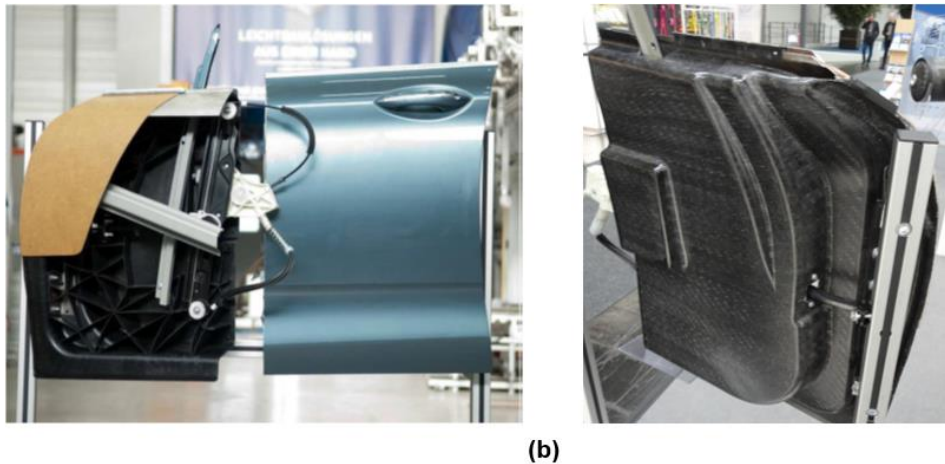


Figure 2-46 The Hybtuer: assembly and inner panel CAD (a); prototype (b) [105]

At present, very little research has been published on the use of FRTPs on vehicle door structures. One representative study is the introduction of the “Hybtuer” (Figure 2-46a) [105]. This multi-material door is a frameless door that uses organo sheets and rib reinforcements extensively in the major load-bearing inner panel area (shown in Figure 2-46b), while sharing the same design principle as typical metal doors. Wood fiber reinforced thermoplastics are used in the minor load-bearing components, such as the outer panel. Steel inserts (sheets) are used as major load-transferring elements and are placed in the hinge and latch areas.

The prototype of the Hybtuer (Figure 2-46b) was manufactured with a direct long fiber thermoplastic (D-LFT) compression molding process (see section 2.1.2), with a high level of automation (Figure 2-47). Organo sheets and pre-formed steel inserts are over-molded with LFT and assembled onto the inner panel during the compression molding process (In-Mold-Assembly). The cycle time is about 60 s. Based on a comparison with an unspecified reference, one of the most important research achievements is the 40% increase in the automation degree in this manufacturing process. Meanwhile, 15% weight reduction is achieved on the Hybtuer (the reference door is not given) and 25% of the assembly costs are saved through the use of production-integrated metal inserts and an assembly-efficient component design, such as the one-piece design of the inner panel.

Further information about the lightweight cost and structural performance of the Hybtuer are not given. Based on the amount of organo sheet usage (almost the complete inner panel), the Hybtuer is likely to have a good structural performance but with a relatively high lightweight cost. This organo sheet approach on the inner panel is more like a material substitution based on the typical design principle of metal doors, rather than a completely innovative multi-material design approach. For this reason, the lightweight potential of FRPs is not fully achieved with this door concept. The absence of a structural solution for the window frame on the Hybtuer further constrains the application of this concept to major economical vehicles.

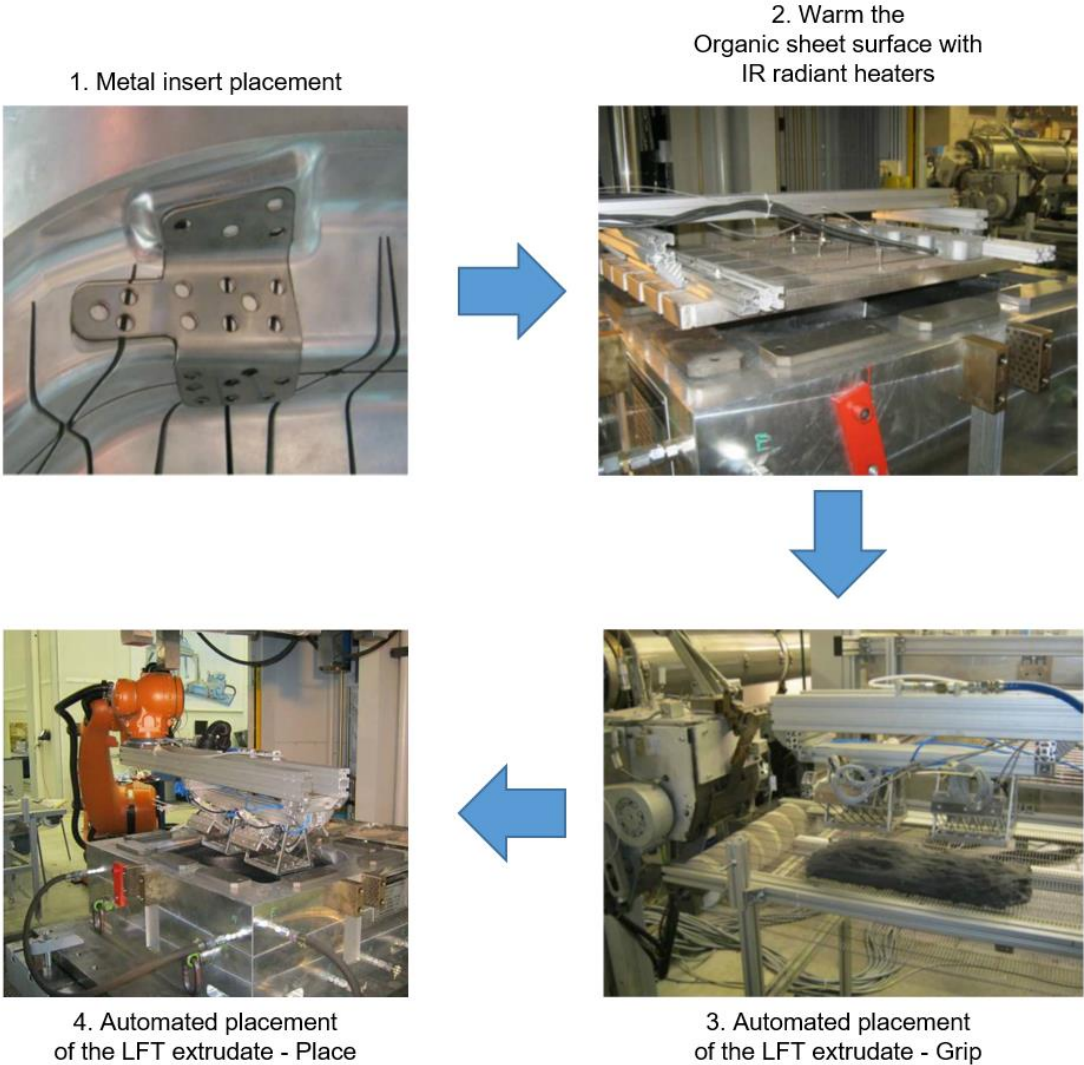


Figure 2-47 The manufacturing process of the Hybtuer [105]

2.6 Mass-production-oriented joining techniques for FRTPs and multi-material components

2.6.1 General

The joining techniques for FRTPs fall into three categories: mechanical joining, adhesive bonding, and welding or fusion bonding [106]. Table 2-12 summarizes the common FRTP joining techniques.

Generally, some mechanical joints have the advantage that they can be disassembled repeatedly, which is preferable for repairing, replacement, and recycling. Adhesive bonding of FRTPs is problematic due to the difficulty of bonding adhesive materials to thermoplastic polymers without performing a proper surface treatment. Welding can be used to join FRTPs with the same matrix material and, in some cases, with different but compatible blends. An important point to mention is that not all of the available joining techniques for FRTPs can be applied to all components and materials, which means an appropriate method must be selected for each application depending on the actual situation.

Mechanical joining	Adhesive Bonding	Welding / fusion bonding
1) Riveting 2) Clamping 3) Bolting	1) Solvent Bonding 2) Adhesive Agglutination	1) Vibration 2) Rotational 3) Ultrasonic 4) Heated tool 5) Laser Beam 6) High Frequency 7) Induction 8) Resistance

Table 2-12 Joining techniques for fiber reinforce thermoplastics [106]

Joining FRTPs to metals on multi-material components requires mechanical joining (i.e., form-fit joining (Figure 2-48a) or force-fit joining (Figure 2-48b)) and adhesive bonding (Figure 2-48c) as the major joining techniques. The application of these joining techniques can be found on serial components in the automotive industry today (for examples, see section 2.2.2).

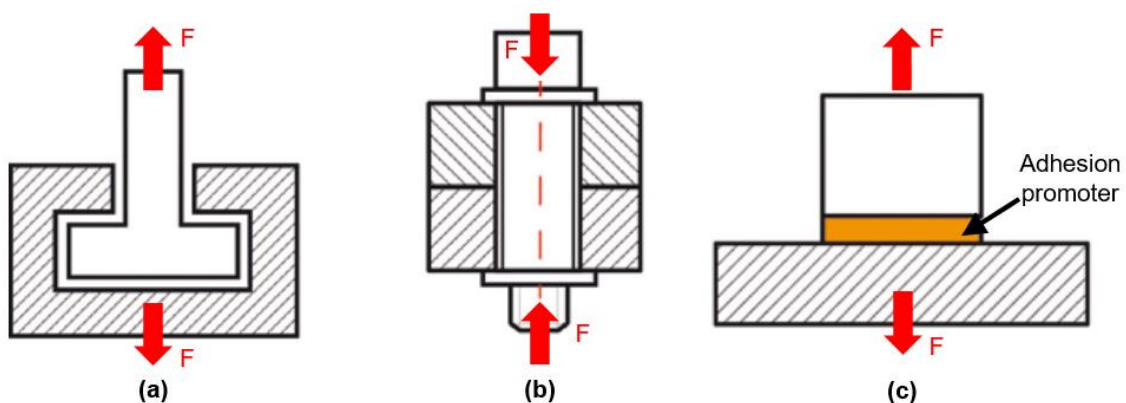


Figure 2-48 Joining between FRTPs to metals: form-fit joining (a); force-fit joining (b); adhesive bonding [107]

Form-fit joining is typically realized with undercuts on insert components, which can be deliberately constructed (e.g., beading or clinching) or generated by over-molding in the injection molding process. The disadvantage of this joining type is that the point force transmitted between inserts and connected components constrains the overall mechanical performance of components, and a high stress concentration is also easily produced at the joining areas [107]. For this reason, form-fitting joining has not been chosen in the present work.

Force-fit joining, by contrast, is realized by the compression force generated with additional fasteners, such as bolts and rivets. The detachability of force-fit joining guarantees a good recyclability of assemblies, which is one of the focuses of the present work. In door concepts, force-fit joining with metal inserts is used and will be introduced in detail in section 2.6.3.

Adhesive bonding on multi-material components is realized by: 1) the In-Mold-Assembly (IMA) process with or without adhesion promoters, or 2) the Post-Mold-Assembly (PMA) process with adhesives. This type of joining, and especially the IMA with adhesion promoters, is used extensively in the present work because of its ideal continuous force transmission through large surfaces between connected parts, as this is preferred in the crash-relevant areas on the concept doors. Moreover, parts with a complex connecting geometry can be joined in the In-Mold-Assembly process, thereby enabling high design freedom. Further technical details about adhesive joining with the In-Mold-Assembly process will be illustrated in section 2.6.3.

Due to the scope of this work, only the chosen joining techniques will be introduced in the following sections.

2.6.2 Joining between FRTPs

Joining techniques must fit the application scenario. To choose the proper joining techniques for a vehicle door, joining strength (short and long period), time and cost must be considered at first. Using the mechanical fastener to joining FTRP components directly could be inappropriate for vehicle doors since the presence of creep, moisture, and stress relaxation during use will lead to the loosening of fasteners. The use of adhesive bonding is possible from the perspective of the joining strength in this scenario only if an additional surface treatment (e.g., solvent cleaning, abrasive methods, or surface energy treatment) of the FTRP components can be done. However, the additional processing step increases the cost, so this is difficult to accept by OEMs. For these reasons, welding seems to be the better choice for this work. Taking a look at the welding techniques for FRTPs available in the automotive industry and considering the geometry of vehicle doors (free-form surface), two types of welding techniques are chosen.

Ultrasonic welding

Ultrasonic welding is one of the most common welding techniques used in the automotive industry for FRTPs [10]. The basic principle of this type of welding is that it uses high-frequency (20 to 50 kHz), low amplitude (15 to 60 μm) vibration motion, either normal to or parallel to the interface between the two parts, which are held together under pressure (typically 1–10 MPa), to cause localized FTRP melting that realizes the join. Line welding and spot welding are two typical joining forms of ultrasonic welding. Special geometry is required for the normal-to-interface vibration: one of the surfaces must have energy directors (Figure 2-49a). This special geometry with a triangle cross-section can help concentrate the ultrasonic vibration energy at

its top end, which facilitates the local heat accumulation. Eventually, these energy directors will melt and spread across the joining interface during the process.

Depending on the distance between the horn (vibration producer) and the joining position, ultrasonic welding can be categorized into near-field welding and far-field welding (Figure 2-49b) [106]. In the near-field welding, the distance between the horn and the joining position is less than 6 mm. Typically, excellent welding results can be obtained even with thin-walled components and low stiffness materials. In far-field welding, the distance is more than 6 mm (maximum 250 mm). Due to the long distance, far-field welding requires higher amplitudes and welding forces, as well as a longer weld time, to reach an ideal welding quality. Thicker walls or high stiffness are also required for the component materials.

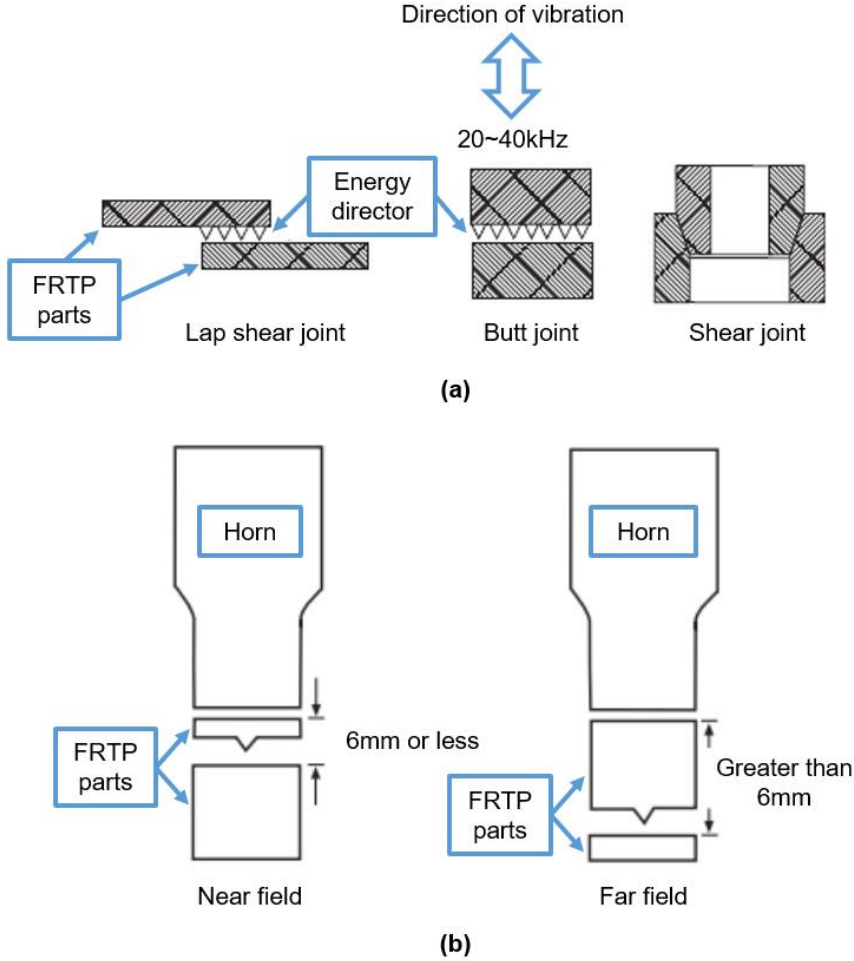


Figure 2-49 Different joining designs for ultrasonic welding (a) [108]; Ultrasonic welding: near-field and far-field welding (b) [109]

Advantages	Disadvantages
<ol style="list-style-type: none"> 1) Ease of assembly: requires only the alignment of the two parts; well suited to automated assembly. 2) Internal joining: even internal ribs can be ultrasonically welded with small, flat-surfaced parts 3) Contour freedom: parts of any surface contour can be welded (as long as the joining surface can be made within the required size and shape limitations) 4) Short cycle time: 20 to 60 parts per minute; actual welding time < 1s 	<ol style="list-style-type: none"> 1) Shape limitations: flat or nearly flat joining surface between the parts is preferred. 2) Process limitation: tight process control is required to create the necessary tolerance and flatness of joining details (such as energy directors) 3) Material limitation: limited to compatible thermoplastics

Table 2-13 Important advantages and disadvantages of ultrasonic welding [106]

The important advantages and disadvantages of ultrasonic welding are summarized in Table 2-13. Note that, for FRTPs, the presence of fibers could have both positive and negative influences on the quality of ultrasonic welding. Research shows that the addition of 10–20 wt% of glass fiber can considerably improve the weldability of crystalline thermoplastics since stiffer materials help to transmit mechanical vibrations. However, when the fiber content reaches 30–40 wt%, the ultrasonic welding parameters, such as welding time and welding pressure, must be carefully increased to realize an optimum welding strength [110]. The reason is that the higher fiber content can cause insufficient polymer at the joining interface and inhibit weldability.

The most common applications of ultrasonic welding in the automotive industry are lamp assemblies, instrument panels, air ducts, body components, and small engine components.

Infrared welding

Infrared welding is a non-contact welding technique (Figure 2-50a) with three major steps: 1) heating of the interface with infrared energy; 2) change-over; 3) joining and cooling under pressure [108]. During the process, the bonding surfaces are heated through exposure to intense infrared radiation, which is produced by high-intensity quartz lamps. Research [108; 111] shows that lap shear joining performed with the infrared welding can reach 40% of the strength of compression-molded lap shear joining, which confirms that the infrared welding process can realize a precise, repeatable, and consistent joining. Infrared welding can also achieve 100% gas tightness.

For industry use, infrared welding is a fast process with a high level of automation [112]. It is able to join components with complex geometries (flat, curved, and even 3D welding contours). A schematic of a typical infrared welding machine is illustrated in Figure 2-50b. Multiple welding positions can be realized simultaneously in one shot with controlled and monitored process parameters. For example, the temperature of both bonding surfaces can be measured using an on-line sensor installed on the reciprocating arm [108]. One caution is the possible deconsolidation and warpage of the bonding components during the heating process.

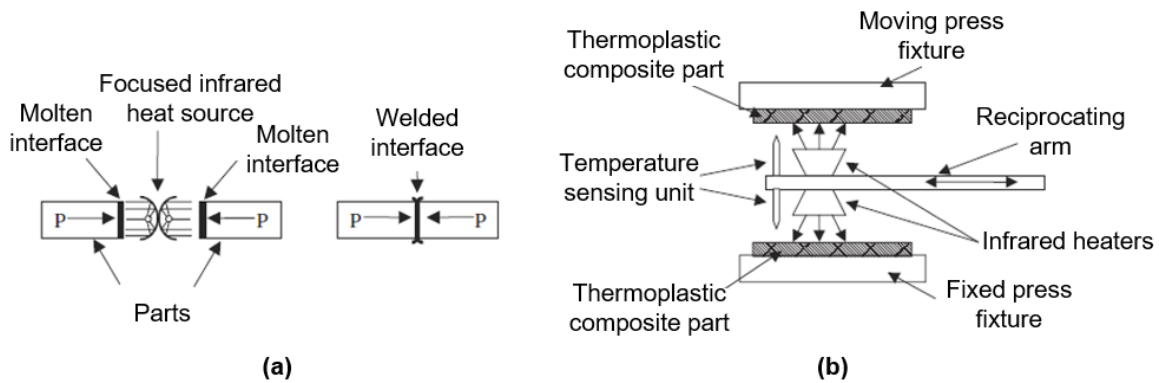


Figure 2-50 Schematic of the infrared welding technique (a); schematic of the infrared welding machine (b) [108]

The most common applications of infrared welding in the automotive industry are typically materials with a complex 3D geometry, such as instrumental panels, door modules, and center consoles. Due to its gas tightness, air ducts and fuel tank systems are also welded with this joining process.

2.6.3 Joining between FRTP and metal

Metal insert (MI)

Joining between the FRTP and metal with metal inserts (MIs) can be treated as a combination of the form-fit and the force-fit. MIs connect to FRTP components through form-fit joining with the help of the specially designed grain. When used together with fasteners (e.g., bolts), the force-fitting joining between FRTP and metal components can be achieved.

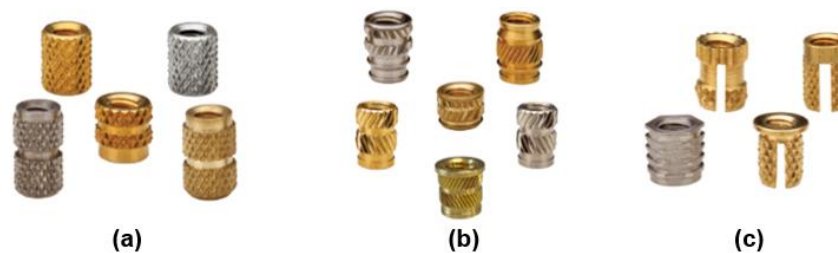


Figure 2-51 Typical threaded metal inserts: (a) ultrasonic/heated installed inserts; (b) molded-in inserts; (c) pressed-in inserts [113]

In applications in the automotive industry, MIs with internal threads are typically molded in during the molding process, either installed with ultrasonic/heat or simply cold pressed into a drilled hole after the molding process. These different MI installation methods are used for four types of inserts [106]: 1) the mold-in insert (Figure 2-51a); 2) the ultrasonic insert (Figure 2-51b); 3) the heat-installed insert (Figure 2-51b); and 4) the cold pressed-in insert (Figure 2-51c). The most common material for the MI with internal threads is brass, although aluminum inserts have become more popular, especially for lightweight applications, as aluminum is ca. 70% lighter than brass. Since the overall performance of cold press-in inserts cannot meet the joining requirements of BIW components in most circumstances, it was taken out of consideration in the present work. Only the first three types of inserts are considered in this

work and are used at different locations depending on the specific geometries around the MIs and the loadings situations on the MIs. A brief discussion about these three methods is given below.

Molded-in metal inserts are integrated into the host part using the insert molding process, which is a way of molding one or multiple additional parts directly into the host part during the molding process, thereby eliminating further assembly processes. The major advantages of using this method to install metal inserts are [106]: 1) molded-in metal inserts can provide almost the highest resistance to torsional and tensile loadings among most inserts, 2) molded-in metal insert use is a long-established technique and requires no highly complex molds and is suitable for high volume production. Of course, these inserts also have several major challenges [106]: 1) stress can concentrate around metal inserts due to inappropriate geometry; 2) the cost of disassembly and recycling might increase due to the additional process needed to separate the MIs; 3) special attention must be given to the cooling rates, especially when a large difference exists in the linear thermal expansion coefficient between the MI and plastic materials; 4) automatic insert placement is necessary for high volume production, 5) floating of the MI during the molding process might lead to serious mold damage. Molded-in threaded MIs are used with thermoplastics with glass fibers in the present work. In this situation, attention must be paid to the possibility of increasing weld line problems, especially around the MIs.

The challenges of molded-in MIs have led to MIs with ultrasonic insertion becoming a preferred alternative for thermoplastics. The principle of ultrasonic insertion is that a small area of plastic around the MI is melted during the process by the ultrasonic vibration. The MI can be inserted either by forcing it into the hole of the plastic part or by pushing the plastic onto the MI. The use of either of these two methods depends depending on which part is touching the horn (ultrasonic vibration transmitter) of the machine. After cooling, the plastic resolidifies around the MI, fixing it and generating a resistance to extraction [106]. With this process, the stress surrounding the MIs is largely reduced in comparison to the molded-in MIs. The ultrasonic insertion also requires a lower installation force and can achieve a typical cycle time of less than a second (but can up to 3.5 s for large inserts) [106]. The advantage of ultrasonic insertion is that it eliminates the molding problems of molded-in MIs, but with a slightly higher insert cost. As for geometries, the diameters of the holes for ultrasonic insertion can be smaller than those needed for molded-in MIs, which is valuable for design in tight regions. Note, however, that ultrasonic insertion is an additional post-molding assembly process, so it will definitely increase the assembly cost to some extent.

The principle of heat-installed inserts is quite similar to that of ultrasonic inserts, with the key difference being the generation of heat with a thermal installer rather than ultrasonic energy to melt the plastic surrounding the MIs. The insert shape and hole design for heat-installed and ultrasonic inserts are same. Compared to ultrasonic inserts, heat-installed inserts have a lower equipment cost (ca. 50%) and they work better with fiber-reinforced thermoplastics (less sensitive to voids in FRPs) [106]. However, the cycle time for heat-installed inserts is longer since the entire insert must be heated, and the “heat-effect zone” is also larger, which might lead to inaccurate positioning of inserts, as well as material degradation of the thermoplastics due to excessive heating.

A strength comparison between ultrasonic/heat-installed and molded-in inserts in thermoplastics under pull-out and torque-out tests is given in Table 2-14 [113]. As mentioned

earlier in this section, the molded-in insert has the best performance among the three chosen types. Another test result (Figure 2-52) shows that molded-in inserts with fiber-reinforced thermoplastics can provide even better performance [114] and can meet the joining requirements for crash-relevant components with the proper choices of insert size and material for the host components. For example, using an M6 insert size on a component of PA66-GF30 can achieve a pull-out force of more than 12kN, which could be suitable for some crash-relevant regions on vehicle doors.

Matrix material	Maximal pull-out force (N) /Jack-out torsion (Nm) (*Different M6 insert geometries with comparable length)		
	Ultrasonic / heat-installed inserts	Mold-in inserts	Cold press-in inserts
ABS	1664 / 7.3	4040 / 12.2	1045 / 3.16
Polycarbonate	2731 / 12.2	4120 / 12.5	1370 / 8.66

Table 2-14 Strength comparison between ultrasonic/heat-installed, molded-in and cold pressed-in inserts in thermoplastics under pull-out and torque-out tests [113]

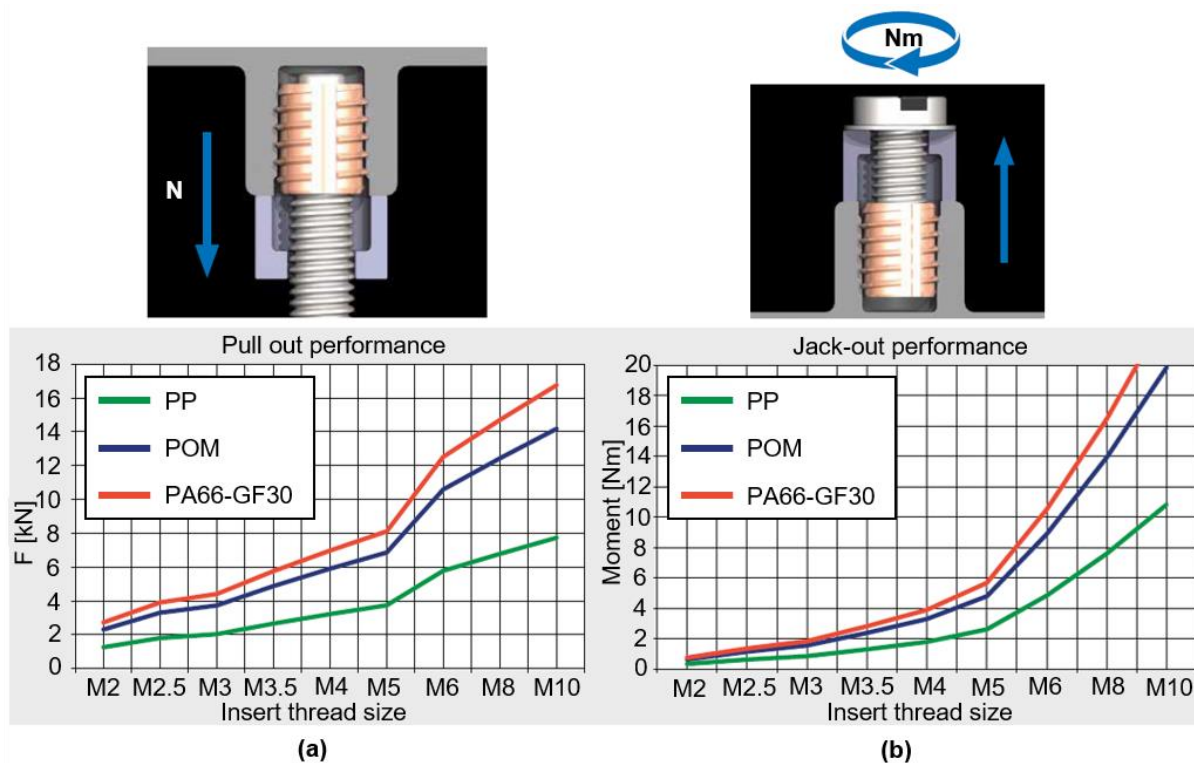


Figure 2-52 Molded-in inserts with fiber-reinforced thermoplastics: Pull-out test (a); Jack-out performance (b) [114]

Direct adhesion

As mentioned, joining thermoplastics with adhesives directly is problematic. For example, PP, as one of the common thermoplastics used in the automotive industry, is difficult to join using adhesives due to its low surface energy [10]. Joining thermoplastics to metal for multi-material components can lead to severe situations as well. For this reason, direct-adhesion methods with the In-Mold-Assembly process are preferred in the automotive industry. These methods can be summarized into three categories [115]: 1) micro-scale polymer-to-metal mechanical interlocking, 2) in-coil or stamped-part metal priming with adhesion promoters, and 3) chemical modifications of the thermoplastic material for enhanced adhesion to metal.

For the first approach, “micro-scale polymer-to-metal mechanical interlocking,” the joining is achieved by infiltration of the thermoplastic melt into the micro roughness features of the metal substrate. The mechanism of this approach differs from the over-molded form-fit joining, which is achieved by having the material shrink onto material with a specially designed undercut geometry on the macro level. Based on previous work [57; 115], this joining process includes three steps: 1) metal-surface pre-treatment for micron-sized rough metal surfaces (oil-free and clean is preferred, but not mandatory), 2) pre-heating the metal substrate to a sufficiently high temperature (minimum ca. 200°C), and 3) joining realized during in the injection-molding or compression-molding process. Based on previous studies [116; 117], the joining strength with this method between low-carbon steel or 6061 aluminum metal substrates and injection-molded poly-carbonate under optimal process conditions can reach 40 MPa, which is high enough for a load-bearing structure. However, a standard deviation of joining strength of up to 10 MPa is also found under the same process parameters, so the consistency of this joining technique can only be guaranteed with tight manufacturing process control. The cooling process should also be properly optimized to reduce the residual stress caused by the incompatibility of properties between the polymer and metal [116; 117].

For the potential application in BIW structure, the typical hybrid components made with this joining method consist of stamped metal sheets and thermoplastics/fiber-reinforced thermoplastics. Sufficient surface roughness of the metal substrate can be ensured by proper surface texture of the stamping dies [115]. Most of the unfavorable side effects of metal stamping caused by the additional pre-heating step (e.g., warping, additional costs, and strength changes) can be overcome by integrating the induction heating coil into the injection molding tool. Although this joining approach can be seamlessly integrated into standard manufacturing processes and can realize a decent joining strength with thermoplastics, a major drawback that must be dealt with before joining FRTPs to metals is the incomplete infiltration of the thermoplastic into the micro roughness features due to the presence of fibers. This leads to an insufficient joining strength between FRTP and the metal substrate. Based on previous work [118; 119], almost all the shear joining strength between FRTPs and metals are in the range of 7 to 12 MPa. An exception is one approach that uses a laser for pre-treatment of the metal surface, where a shear joining strength of more than 30 MPa can be achieved between steel and PA66-GF30 [120]. However, a minimum joining strength of 10 MPa (usually a shear strength) must be reached to provide enough load transfer between metal and fiber-reinforced thermoplastics [115]. Obviously, joining through micro-scale polymer-to-metal mechanical interlocking cannot provide sufficient joining strength for BIW practices at present, let alone for crash-relevant areas.

The second approach of “in-coil or stamped-part metal priming with adhesion promoters” creates an enhanced joining strength between metal substrate and thermoplastic by priming the metal surface with the so-called adhesion promoters. Silane is one of the most frequently used primers. According to a previous study [121], this joining process includes three steps: 1) cleaning and pre-treatment of the metal substrate surface (grinding, polishing, and rinsing), 2) priming with adhesion promoters, 3) joining realized in the injection-molding or compression-molding process. Depending on the form of the adhesion promoters, different priming methods can be used: 1) foil [122], 2) coil-coating [123], 3) electrostatic powder coating [124], and 4) thermal spray coating [125]. The joining strength is increased with this joining approach, even for fiber-reinforced thermoplastics. Based on previous studies [107; 124; 126], most shear joining strengths between metal (steel) and fiber-reinforced thermoplastics (PA6-GF30) lie in the range of 12.4 MPa to 22.5 MPa if the proper adhesion promoters are used. This is higher than the required shear joining strength (10 MPa) for BIW applications. For potential application in a BIW structure, the additional steps of cleaning and pre-treatment of the stamped metal parts surfaces and priming with adhesion promoters in this joining approach might be the only obstacles limiting its integration into current BIW manufacturing processes for economic reasons. The shortcoming of the long curing time (several minutes) needed by the adhesion promoters has been resolved using higher temperatures for the mold and thermoplastics. Recent work [122] has proven the potential of this joining approach in large-scale production and on crash-relevant BIW components in a 3D-hybrid B-pillar. This B-pillar is made of DP600 (with adhesion promoters), an organo sheet, and LFT with the compression molding process and realizes a 10% weight reduction while still providing static and dynamic performance (three-point- and four-point-bending tests) comparable to the steel reference.

The third approach, “chemical modifications of the injection-molding thermoplastic material for enhanced adhesion to metal,” employs various chemical modifications to the polymeric material or resin to realize an enhanced joining strength. Although a high joining strength can be achieved even in the presence of stamping oil, this approach has significant shortcomings, such as incompatibility with injection and compression molding processes due to part ejection difficulties, thermal instability of the modified thermoplastics caused by the chemical modifications, and sensitivity to moisture, high temperature, and fatigue, which make this joining approach unsuitable for BIW components [115]. For this reason, this third approach is not considered as an option for the door concept in the present work and no further details will be discussed in this thesis.

Based on the features of direct-adhesion joining techniques for FRTP-metal connections, the second approach, “In-coil or stamped-part metal priming with adhesion promoters,” is deemed the most promising for crash-related BIW components, such as doors, considering the joining strength, cost, and cycle time.

2.7 Component development method with limited BIW data

Due to the reduction in vehicle development time and cost constraints, increasing volumes of vehicle development work of vehicle BIW components and modules are being transferred from automotive manufacturers to suppliers. Theoretically, to deliver a good structural solution, suppliers need a large quantity of accurate vehicle data from OEMs. However, the reality is that suppliers are only able to access very limited quantities of highly simplified local vehicle data and have to develop their own concepts based on these data. After the delivery of the concepts, OEMs test and compare different concepts from multiple suppliers in a full vehicle (FV) environment. Only the suppliers that are able to deliver a concept that meets the cost and performance requirements of OEMs are given contracts and can put their concept into series production. For these reasons, developing crash-relevant components and modules, such as the A- and B-pillar and the door module, can be a significant challenge for suppliers. Finding a reliable method to overcome the obstacle of limited local vehicle data to deliver highly competitive and accurate products is therefore important for suppliers.

Many component development methods have been investigated and developed for vehicle side structures in the automotive industry in recent decades. The traditional three-point-bending test is one of the most widely used component development methods. This method does not take into account the effect of surrounding components. In this test, the force-displacement curve, local deformation, and material failure level are used as the evaluation criteria. Suppliers must typically develop and optimize their concepts according to their own experience because the OEM guidelines are most often not available to them. Correspondingly, the prototype must be manufactured and validated under the three-point-bending test [127]. Several components on the side structure, such as the B-pillar and door beam, can be developed by this method. Figure 2-53 shows a B-pillar under the three-point-bending test.

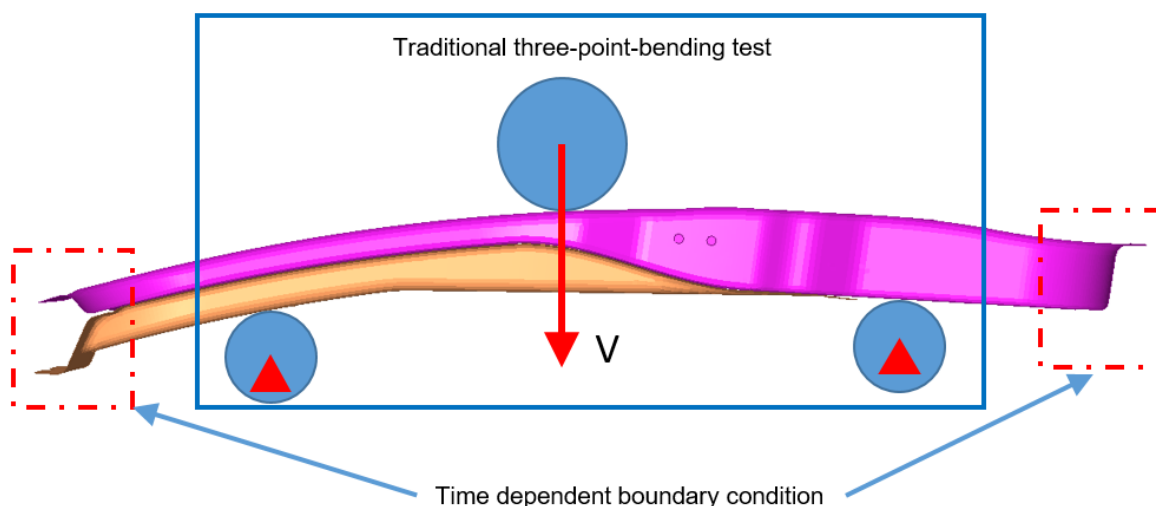


Figure 2-53 Schematic of the three-point-bending test on a B-pillar

After delivery to OEMs, concepts from suppliers are evaluated in a full vehicle (FV) crash simulation, which uses much more complicated boundary conditions than the three-point-bending test. For this reason, the three-point-bending test is highly limited. Because there is no consideration of the surrounding components in the three-point-bending test, it cannot

guarantee that the results of this simplified test are reproducible in the FV environment. Thus, suppliers can only achieve an “A to B” comparison with this method, which is obviously insufficient.

This limitation can create more problems in the development of component modules. In previous work [128], a door module with hinges and a latch was simulated under the side pole impact test without the surrounding components; this can be treated as a three-point-bending test for a door module. The results showed that only the deformation of the hinges correlated well with the FV simulation. The door module, however, showed a completely different deformation behavior, highlighting that the absence of the surrounding components can cause a substantial difference in the crash behavior of component modules.

In this work, only partial BIW components are provided by the OEM due to confidentiality clauses. To reproduce the crash behavior of the door and surrounding components close to a FV simulation, a self-developed component development method of Fang and Zhang [129], with the limited BIW data, is used in the present work. This method investigates the behavior of component sub-models and aims to reach a reasonably high level of component sub-model simplification. As shown in Figure 2-54, it also tries to find the proper universal time-dependent boundary conditions under different side impact scenarios for different vehicles. As illustrated in Figure 2-55, the FE model (named the “level-3 model” [L3M]) of this component development method includes 3 major parts: 1) a moveable fixture for the “component sub-model”; 2) a component sub-model; 3) a background as the floor or the sled.

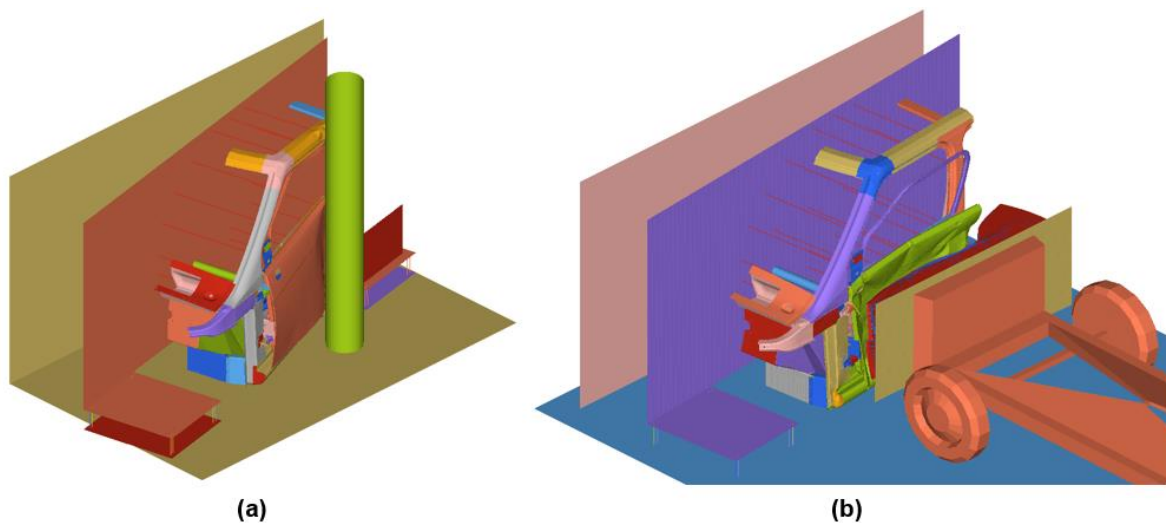


Figure 2-54 Component development method under different side impact scenarios: (a) Euro NCAP side pole test; (b) ECE-R95 test: side impact with MDB

The “component sub-model” (part 2 in Figure 2-55), also named the “level-3 sub-model” in the present work, is cut from the available BIW model, step by step, according to the method illustrated in Figure 2-56 [129]. It consists of the partial vehicle side structure with a 1/3 length of the cross components, such as the A- and B-pillars, rocker panel, door module, and part of the shotgun. Similar approaches can also be found in the work of Teibinger [130; 131] and Schmidt [132], but this method by Fang [129] is simpler (fewer components on the component sub-model).

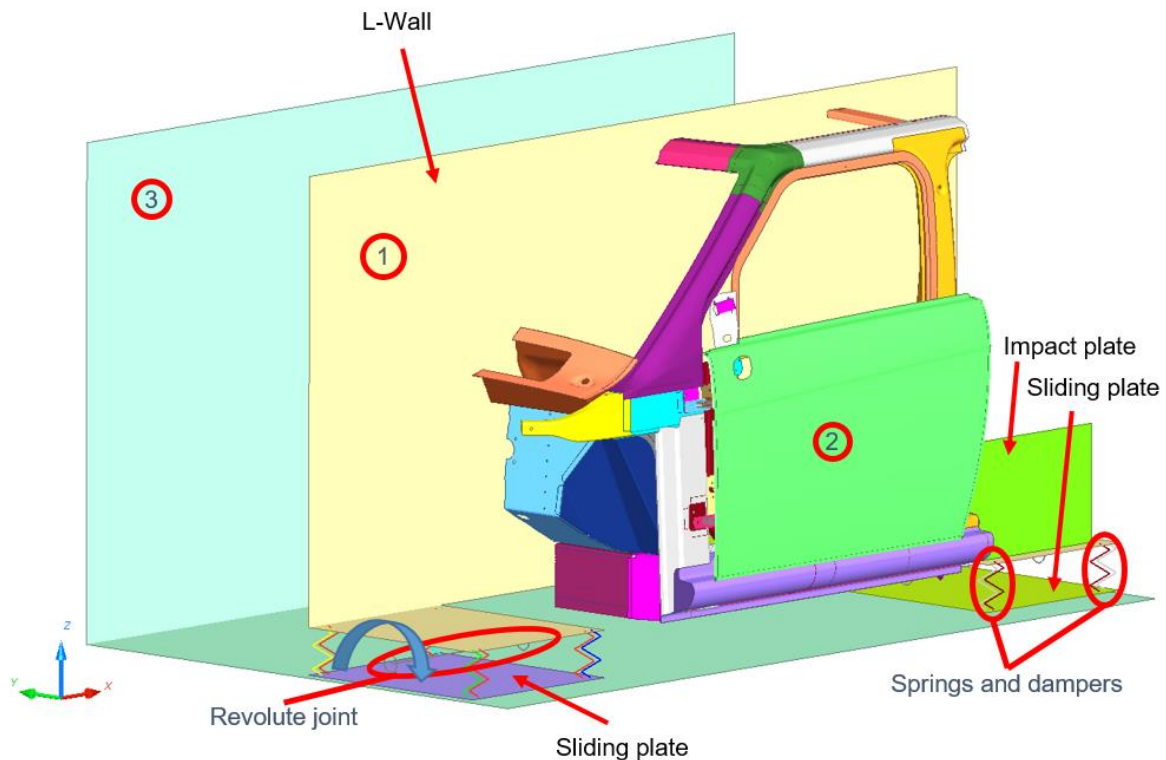


Figure 2-55 Component development method - Level-3 Model (L3M): (1) movable fixture; (2) component sub-model; (3) background

The movable fixture for the component sub-model (part 1 in Figure 2-55) is made of four rigid parts (L-Wall, two sliding plates, one impact plate) and two revolute joints (front and rear), as well as eight springs and dampers. It provides a platform for connecting the component sub-model and substitutes the missing BIW components. The connection between the component sub-model and the movable fixture is realized by connecting nodes on the edge of components (Figure 2-57) to the L-Wall with the keyword “*CONSTRAINED_EXTRA_NODES” in Ls-Dyna [133]. To compensate for the missing weights and to match the COG to the full vehicle model, artificial weights are added to the movable fixture using the keyword “ELEMENT_MASS” in Ls-Dyna [133]. Since the missing BIW components are replaced with non-deformable rigid parts on the movable fixture, the revolute joints, together with springs and dampers, generate a universal “spring-damper system,” which is specially designed to simulate the tilting behavior (blue arrow in Figure 2-55) of the vehicle during side impacts. Springs are defined with material model *MAT_S01 (*MAT_SPRING_ELASTIC) with an elastic stiffness of 2kN/mm. Dampers are defined with the material model *MAT_S02 (*MAT_DAMPER_VISCOUS) [134] with a damping constant of 29 kN·s/m. The impact plate is used to compensate for the absence of rear chassis components, which play a crucial role as a secondary load path during side impacts, especially for the side impact with an MDB. To reproduce the sliding movement of the vehicle under the side impact, only the Z-translation of sliding plates is constrained, and the remaining degrees of freedom are all free.

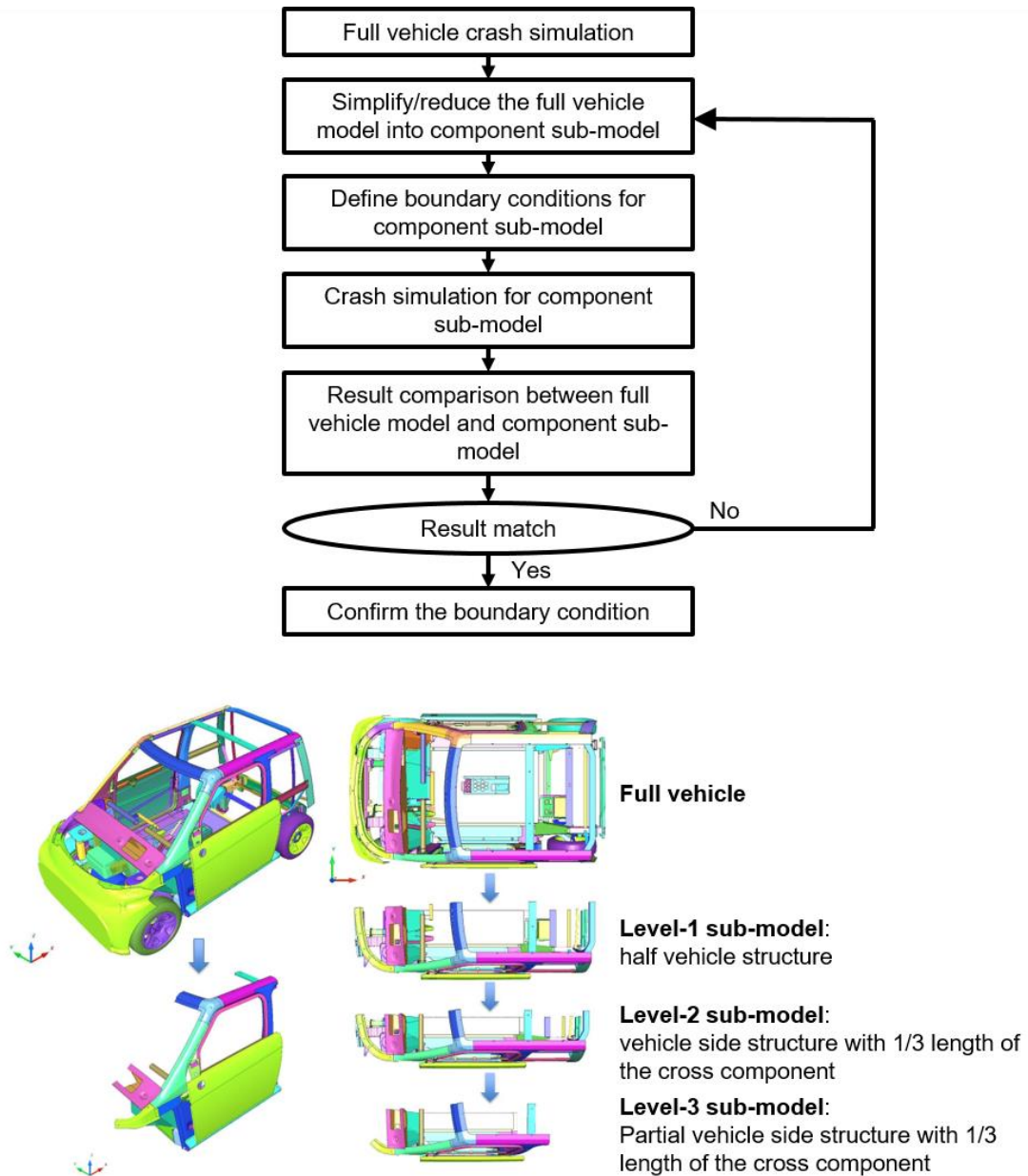


Figure 2-56 Schematic for determining the “component sub-model” from the available BIW information [129]

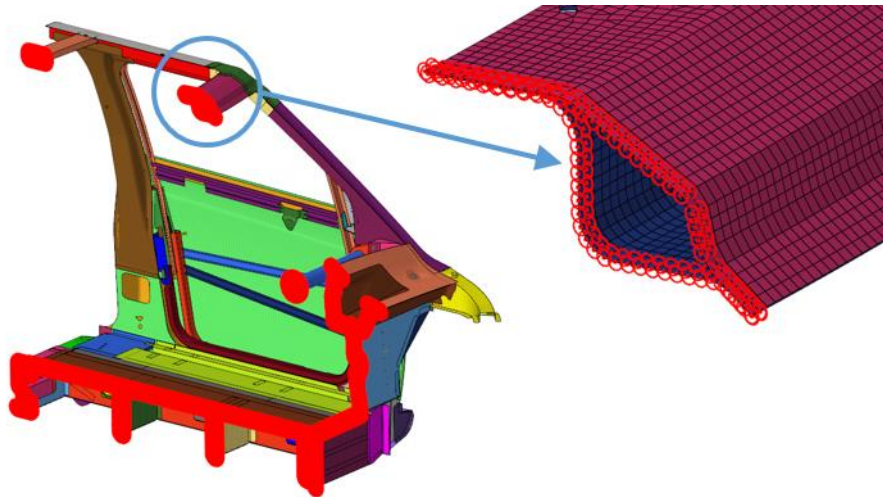


Figure 2-57 Connected nodes (red highlighted) on the cutting edge of the component sub-model to the L-Wall using “CONSTRAINED_EXTRA_NODES”

According to the simulation results in [129], this method is able to obtain accurate crash behavior on the side components of vehicles under typical side impact loading cases with the limited BIW component information. The deviation of intrusion between the FV and component simulation with L3M is marked on the structure of both tested vehicles (one small and one mid-size vehicle) in Figure 2-58. A good correlation with the intrusion is achieved in the occupant area on both vehicles, including the B-pillar, rocker panel, and door module (intrusion deviation is less than 20%). Meanwhile, for both vehicle models, a very good correlation of the intrusion velocity is also achieved in the occupant area between the FV and the component simulation with L3M. For brevity, only the curves of intrusion velocity at the measuring point “B-pillar-chest” are illustrated in Appendix 10.1 for the small and mid-size vehicles as representatives. Overall, these result comparisons provide strong evidence of the high reliability of this component development method with limited BIW data at a theoretical level. The small deviation in the door area with this method makes it suitable for the validation of door concepts under side impacts in the present work.

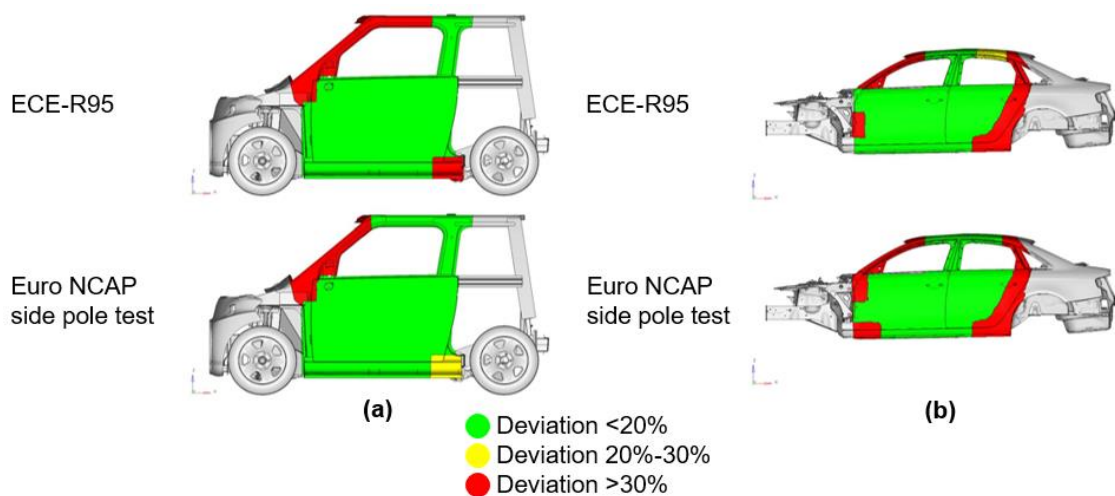


Figure 2-58 The deviation of intrusion between the FV simulation and the component simulation with L3M [129]: (a) small vehicle; (b) mid-size vehicle

2.8 Summary and cognition of the state-of-the-art technology

Based on the introduction of state-of-art technologies, it can be concluded that using a single material is a possible way to achieve a certain amount of weight reduction on door structures. However, this is not an optimum way to achieve a cost-neutral lightweight design door, especially with aluminum alloys and FRTPs. Major drawbacks are the dimension constraints caused by the material forming limitations and the appreciable lightweight costs caused by the increased material costs. For this reason, among the multiple methods for achieving a lightweight design, the multi-material design method has drawn more attention, especially for the application of structural and semi-structural BIW components. As the philosophy of lightweight design says: use the right material in the right place. Multi-material design is undoubtedly one of the best ways to fulfill this. Many existing serial BIW applications in the automotive industry, such as the front-end carrier [68; 135; 136; 137; 138], the roof cross component [75], and the instrument panel carrier [139], prove that the multi-material design method is able to achieve a certain amount of weight reduction without sacrificing performance and with an acceptable lightweight cost. The continuously developing material and process combinations and the In-Mold-Assembly (IMA) techniques (e.g., adhesive bonding with adhesion promoter, mechanical connection with optimized shapes) for manufacturing multi-material components continue to expand the application scenario of multi-material design at a fast pace [57; 59; 77].

Several important cognitions are also identified for the research work:

- Weight saving on vehicle doors can make significant contributions to the vehicle lightweight design.
- Instead of looking for innovative structural solutions, most research work on the lightweight design of vehicle doors does not step outside the convention design principle and focuses only on the uneconomical material substitution method.
- Very little research have been conducted on the vehicle doors with an FRTP-metal multi-material design approach, although this approach has the potential to solve the lightweight dilemma between weight savings and additional costs on vehicle doors.
- Injection molding and compression molding are flexible for process integration and are suitable for manufacturing mass-production FRTP components.
- LFT is a suitable FRTP material for complex door structures, considering the impact resistance, design freedom, and formability.
- Reaching a possibly high function-integral level on FRTP components is important for weight savings.
- Using an appropriate structural optimization method is an effective way to take full advantage of the lightweight potential of FRTPs
- According to the performance of semi-structural components, FRTP-metal multi-material construction has the potential to reach the ideal weight savings while still providing enough structural performance for crash-relevant door structures.
- Ultrasonic welding and infrared welding provide enough design flexibility for door structures and are also mass-production ready.
- IMA with MIs or adhesion promoters are promising methods for achieving sufficient joining strength and for providing local reinforcements to the door structure with an acceptable manufacturing cycle time for mass production.

3 Concept, development process, and requirements

3.1 The multi-material door concept

3.1.1 Preliminary FLB concept (starting point)

In 2014, a preliminary FRTP-metal multi-material door concept (named “FLB concept” in further text) was introduced by Fang [9]. The fundamental idea of the FLB concept is to separate the door structure into two regions: 1) a major load-bearing region, 2) a minor load-bearing but highly function-relevant region. The major load-bearing region is responsible for providing the most stiffness and strength to the whole door structure. The minor load-bearing but highly function-relevant region is specifically the door inner panel. It only needs to take very little load but should be able to integrate all the necessary functional components of vehicle doors, such as the latch, window regulation system, loudspeaker, and door stopper. For the construction of the load-bearing region, unlike traditional constructions of typical vehicle doors (section 2.3), a unique “two-ring structure” is developed with the FLB concept and is achieved by reusing many existing original components (Figure 3-1).

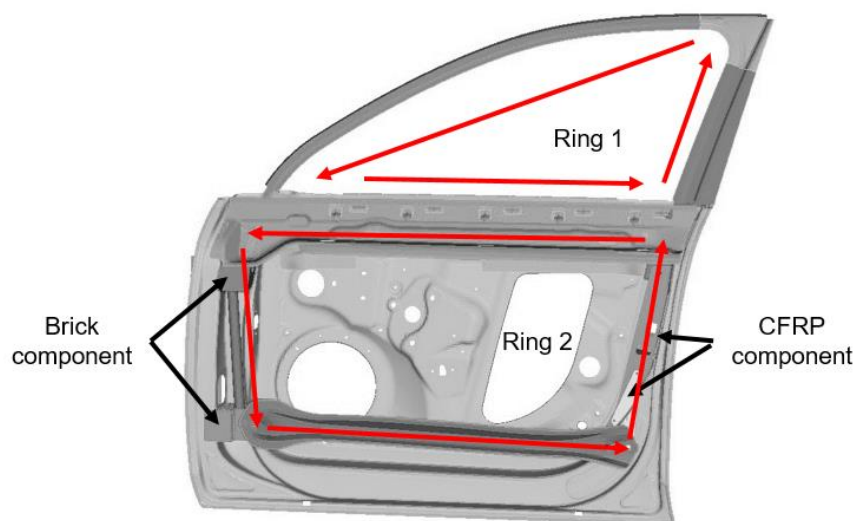


Figure 3-1 FLB concept: FRTP-metal multi-material door concept

The first ring structure includes the window frame and belt reinforcements. The second ring structure includes the hinge reinforcements, side impact beam, latch reinforcements, and belt reinforcements. As shown in Figure 3-1, using a serial middle-class vehicle door (steel reference door), the preliminary “two-ring structure” concept is tentatively realized. The bill of material (BOM) of the “FLB concept” can be found in Appendix 10.2 (Table 10-1). With this concept, almost all components are redesigned except for the side impact beam, considering its importance for side impact safety and the high possibility of reuse. Meanwhile, to make it comparable to the steel reference, the original door package of the design space is also kept untouched. According to the internal calculation, this FRTP-metal multi-material door concept shows an appreciable weight-saving potential of up to ca. 30% (compared to the steel reference). The additional lightweight material cost per saved kilogram of this concept is reduced by ca. 20% compared to lightweight door concepts made of aluminum. FEM simulations with Abaqus under two typical static loading cases (door sag and frame stiffness,

see section 2.4.2) show that this concept has a comparable stiffness under door sag but reaches only about 1/3 of the frame stiffness compared to the reference.

Although this FLB concept achieves a substantial weight savings, several shortcomings still need to be optimized: 1) the “brick” components made of PP-GF30 are too thick for manufacture with standard FRP manufacturing methods within an acceptable cycle time; 2) the components made of CFRPs should be optimized and replaced with glass-fiber-reinforced thermoplastics, considering the cost; 3) the low component integration level and large number of parts; 4) the unacceptably low frame stiffness. Another major obstacle for the further development of this FLB concept is the unavailability of CAD data for important function components, such as the loudspeaker, window regulation system, and latch. These function components highly influence the available design space, which is crucial for the effective construction of rib structures with FRTPs.

3.1.2 New concept ideas

Since developing new door concepts based on the FLB concept and pushing the technology readiness level (TRL) of this concept forward are the major motivations of this work, three questions need to be answered at the very beginning of the further development: 1) What is the goal? 2) What should be kept from the FLB concept? and 3) What are the future directions?

The goal can be summarized as further development of economical FRTP-metal multi-material door concepts based a market-available high-volume production door with a minimal change in the design package/space. The door concept should be virtually constructed with CAD software and validated by using the FEA method (CAE) under chosen critical loading cases. The overall mechanical performance of door concepts should be comparable to the reference door. The construction of door components should take into consideration the basic design guideline of common manufacturing methods for FRTPs. The outcome concept designs should be at least theoretically manufacturable and illustrated as a middle-surface model. Due to the constraints of the concept design, the fine features related to the final manufacturing model design, such as the minimal fillet radius, maximal rib height, and minimal rib distance, will be defined under ideal situations.

For the second question, the innovative “two-ring structure” apparently must be kept, as it is the core of the FLB concept and can be categorized as a mixture type of sheet and frame construction according to the door structure classifications (see section 2.3.1).

Further directions to solve existing problems include the choice of a new serial steel door as the reference (Figure 3-2a). Thanks to the courtesy of the cooperative automotive OEM, all important function components on this reference are available. According to the classification of the window frame structure (see section 2.3.2), two new concept ideas/directions are chosen and sketched: “Concept 1” (Figure 3-2b) is a frame integrated door design (following FLB concept) and “concept 2” (Figure 3-2c) is a roof integrated door design.

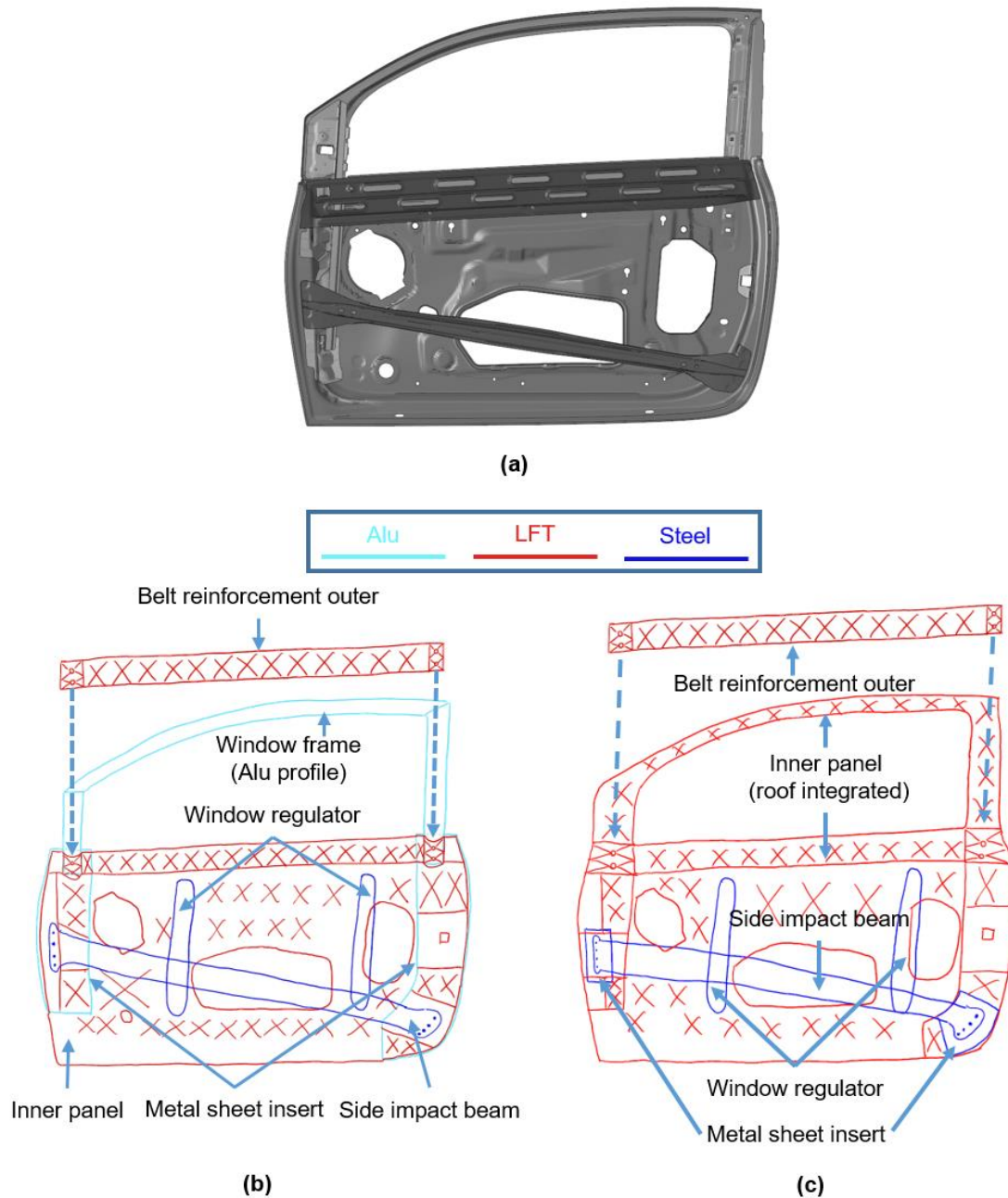


Figure 3-2 Door-in-white (DIW) of the reference door (outer panel is masked) (a); concept 1 sketch (b); concept 2 sketch (c)

Concept 1

Concept 1 (Figure 3-2b) features a highly function-integrated long-fiber thermoplastic (LFT) inner panel with metal sheet inserts in major load-bearing regions, a window frame made of aluminum extrusion profiles, and a LFT belt reinforcement outer. The outer panel (not shown in Figure 3-2b) is made of an aluminum sheet. As with the FLB concept, the original side impact beam from the reference door is kept. The major joining techniques are: 1) adhesion promoters between LFTs to metal sheet inserts, as well as LFTs to aluminum extrusion profiles; 2) flow drilling screws (FDS) [140; 141; 142; 143] between the aluminum profiles and aluminum sheet inserts; 3) spot welding between the side impact beam (steel) and metal sheet inserts; and 4) bolts between the belt reinforcement outer and inner panels. Since concept 1 is a frame-

integrated door design, the foreseeable major challenge is to find a good structural and joining solution in the connecting areas between the window frame and the inner panel to reach the aimed frame stiffness.

Concept 2

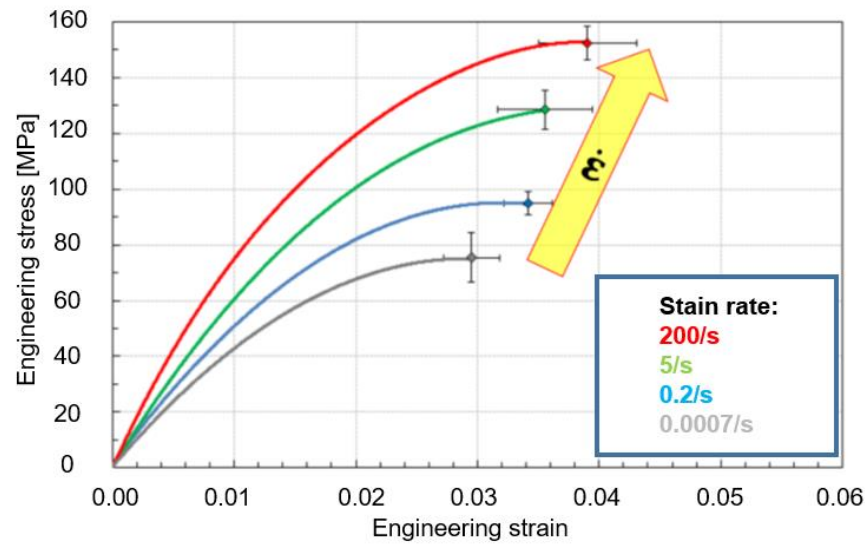
Basically, concept 2 (Figure 3-2c) can be treated as a forward-looking version of concept 1. The fundamental starting point of concept 2 is to exploit the capability of function integration of FRTPs on a vehicle door structure. For this reason, the concept 2 door features a highly function-integrated and roof-integrated inner panel made of LFTs with metal sheet inserts in major load-bearing regions and a LFT belt reinforcement outer. Obviously, by integrating the window frame to the inner panel, the integration level is much higher for concept 2 than for concept 1 and the joining difficulty in the connecting area between the window frame and the inner panel is eliminated. Correspondingly, the area of the metal sheet inserts is also reduced. Similar to concept 1, the outer panel (not shown in Figure 3-2c) is made of an aluminum sheet. The original side impact beam from the reference door is also kept. The major joining techniques are: 1) adhesion promoters between LFTs and metal sheet inserts; 2) spot welding between the side impact beam (steel) and metal sheet inserts; and 3) bolts between belt reinforcement outer and inner panels. Since LFTs are used in the window frame area, the major challenge on this concept 2 is to reach the aimed frame stiffness with LFTs under a constrained cross section (design space).

Other points worth mentioning are that the sketches of both concepts are only treated as a guideline for further development work and that the specific material usage and joining techniques can be adjusted based on the available design space and specific loading situations.

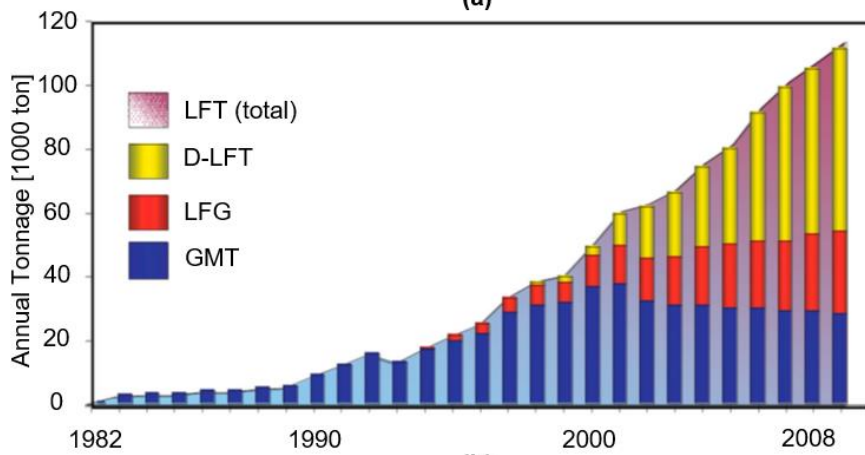
3.1.3 Material choice and property – LFT and UD Tape

The material choice in multi-material design influences not only the performance of the structure, but also the cost. For both economical multi-material door concepts, the LFTs are the major materials. In addition, to help the structure reach its performance goal with a reasonably low lightweight additional cost, aluminum sheets and UD tapes are only used as local reinforcements.

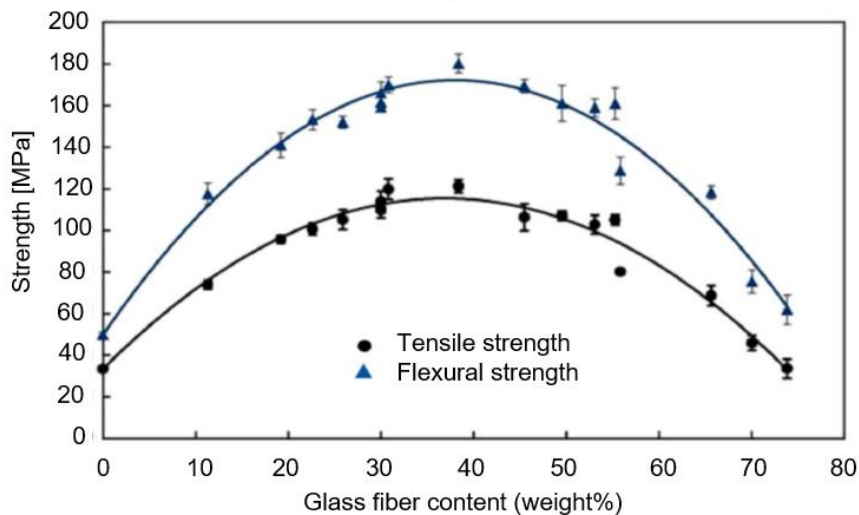
Choosing the major material is the first step in this door concept design. Generally, based on the common FRTP materials (section 2.1.1), SFTs, LFTs, and GMTs are the candidates for the major material of the door concepts. Due to the inadequate impact resistance, SFT is the first to be rejected from the competition. Between LFTs and GMTs, the reason for choosing LFTs rather than GMTs is that LFTs have the advantage of cost, design flexibility, and processing. These three points are all important for the design of door concepts.



(a)



(b)



(c)

Figure 3-3 Strain rate dependency of PP-LGF30: tensile tests in flow direction (a) [144]; Growth of total LFT market between 1999 and 2008 in the European Union (b) [11]; the effect of fiber content on the tensile and flexural strength of PP-LGF (c) [145; 146]

The higher design flexibility and the ease of processing provide not only a higher level of design freedom for the possibly complex rib structure, especially on the LFT inner panel, but they also reduce the uncertainties for manufacturing. From the perspective of the mechanical performance, as mentioned earlier in section 2.1.1, the relatively long fiber length of LFTs can provide good impact resistance, which is crucial for the crash-relevant door structure to achieve a reliable level of passive safety under crash loading [147; 148; 149; 150; 151]. LFTs, as a strain-rate-dependent material, show higher ultimate strength and failure strains under increased strain rates (Figure 3-3a) [144; 152], and this is also preferred for largely deformed BIW components, such as doors, under crash conditions. Last but not least, the rapidly increasing share of the LFT market (Figure 3-3b) [11] verifies the potential of this material and also draws attention to try LFTs on the vehicle door structure in the present work.

The most used LFT material is PP-LGF40 in this work, as it is one of the most widely used types of LFTs (ca. 65% of the LFT market is polypropylene-based [23]) and lays a good foundation for a cost-neutral lightweight design. The fiber weight percent (40%) is determined by considering both the mechanical performance and the manufacturability. As shown in Figure 3-3c, previous study shows that both the strength and impact resistance of PP-LGF reach their peak value around 40% [145; 146]. An even higher fiber content, such as larger than 50%, can lead to the decrease of the average fiber length, the average fiber orientation parameter and the fiber-matrix interfacial strength, and eventually, decrease the mechanical performance while also creating more problems during manufacturing (e.g., incomplete rib filling).

Since the PP-LGF40 shows significant anisotropy, as influenced by the fiber direction, several specimens are cut from a PP-LGF40 plate manufactured with a compression molding process to achieve the different E-moduli from flow and cross directions. Obtaining a stable and reliable test result requires that all specimens be taken from the area away from where the LFT extrudates are placed and way from the plate edge. Figure 3-4 illustrates a schematic of the PP-LGF40 plate, specimens in the flow and cross directions, and the average true stress-strain curves from quasi-static tensile tests. The E-moduli of PP-LGF40 in the flow and cross directions are ca. 9500 MPa and 4300 MPa, respectively.

Since the material model used for the topology optimization in Optistruct is only available in isotropic form, a proper E-modulus must be given to avoid overestimating the capability of PP-LGF40 and even leading to a far-from-reality optimum design. In this case, to guarantee a sufficiently high design safety factor, and E-modulus of 6500 MPa is defined for PP-LGF40 in the topology optimization with Optistruct; this value is slightly smaller than the average E-modulus of the flow and cross directions (6900MPa).

To avoid high material costs, the use of semi-finished prepregs on door concepts is precautionous. Due to the relatively higher cost of the organo sheets, only UD tape is chosen for use. This is PP-based with glass fiber reinforcements (E-modulus in fiber direction: 50 GPa). The mechanical properties provided by the manufacturer are directly used in the concept design without further tests.

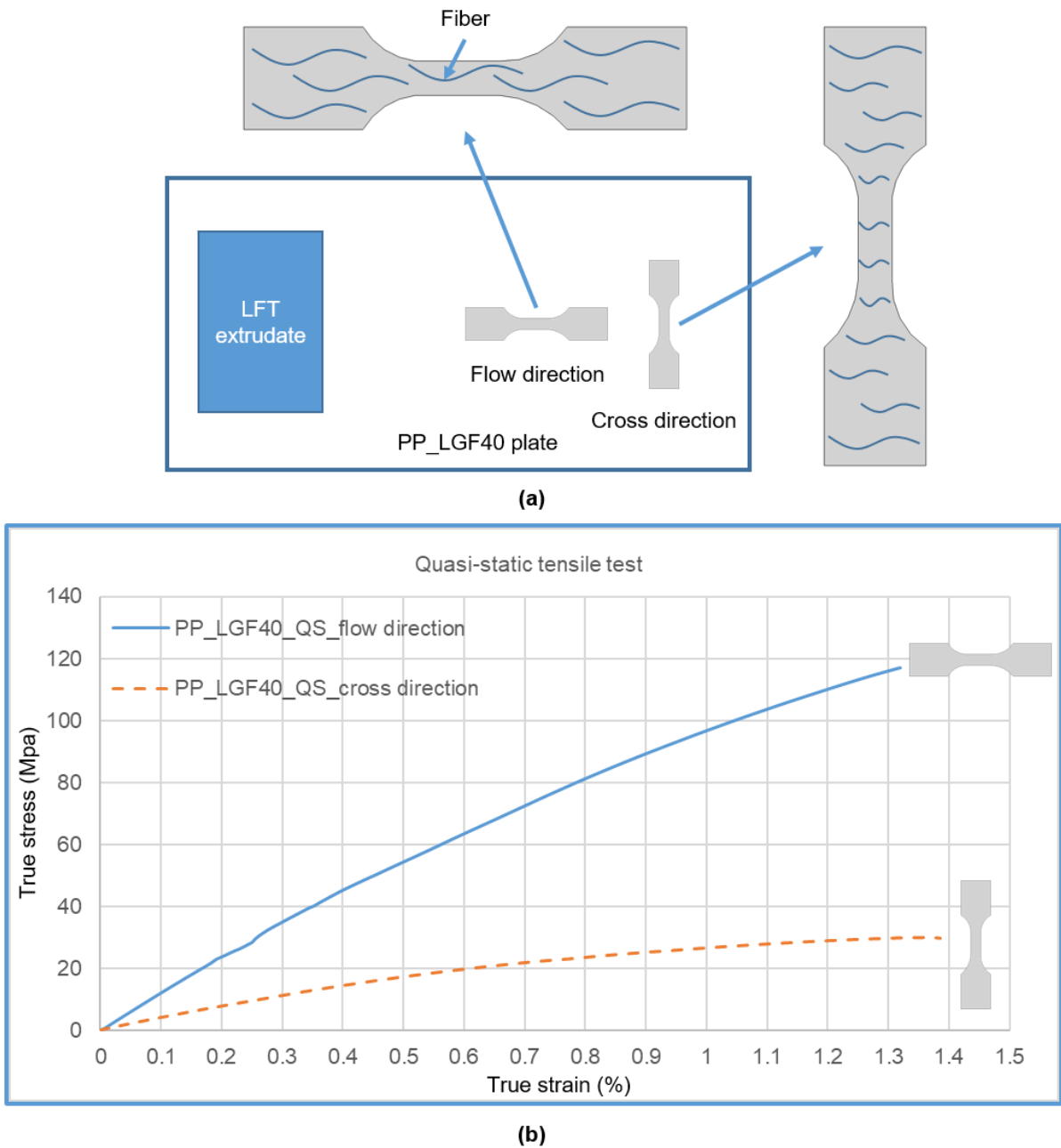


Figure 3-4 Schematic of the PP-LGF40 plate, specimens in the flow and cross directions (a) and the average true stress-strain curves from quasi-static tensile tests (b)

3.2 Development goal and process

The overview of the design and optimization process for the concept development is illustrated in Figure 3-5. The design goal is to reach a 20% weight reduction and still achieve a comparable structural performance in comparison to the reference door under defined static and crash loading cases (see section 2.4). The stiffness and strength requirements are defined by analyzing the reference door with the finite element analysis (FEA) method and are used as important inputs for the topology optimization, the parameter optimization, and performance validations.

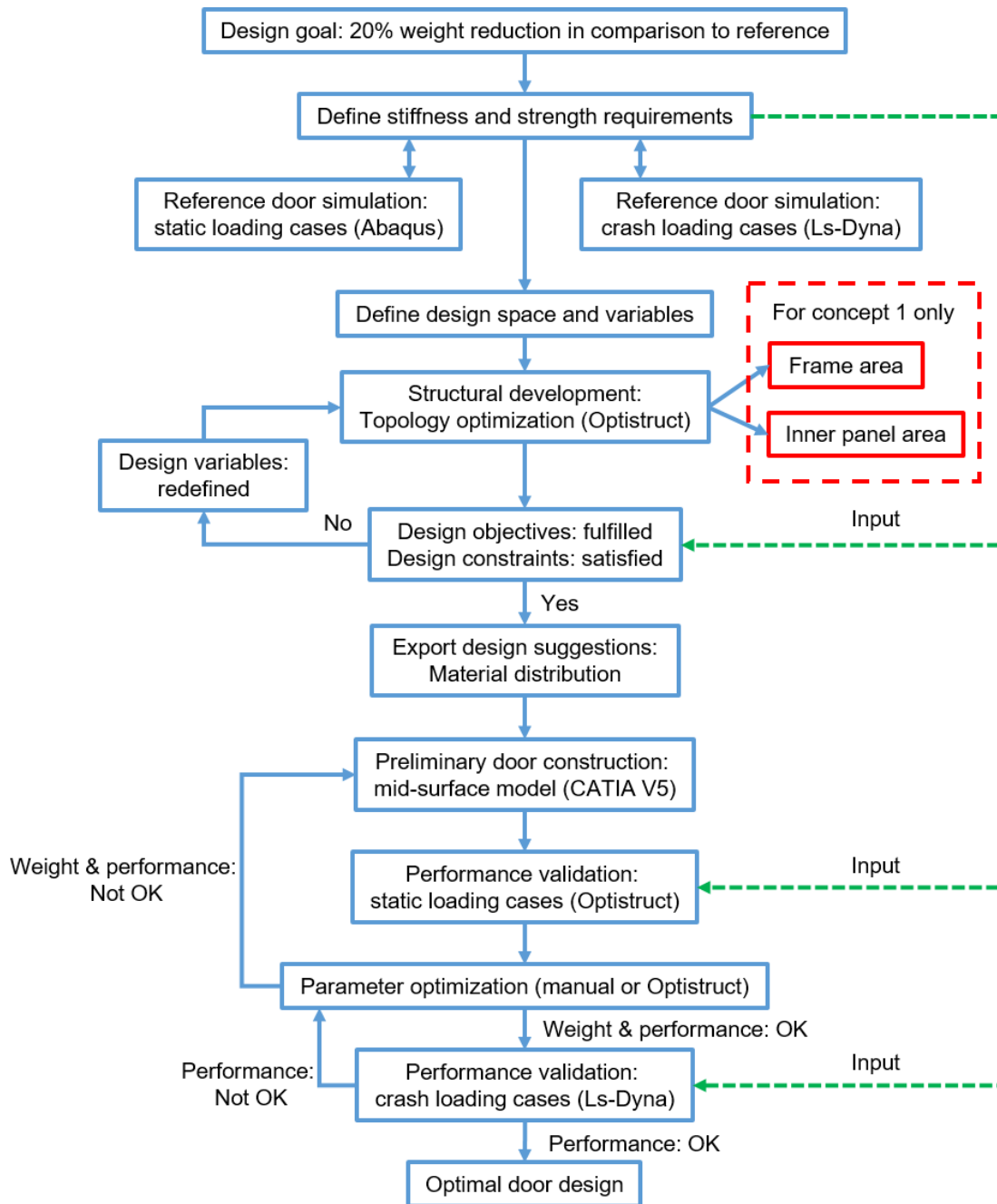


Figure 3-5 Overview of the design and optimization processes for door concepts

To properly use the topology optimization to accelerate this design process, the maximal allowable design space for the concept door should be carefully extracted from the reference

door and used first in topology optimization. The design suggestion or material distribution achieved from topology optimization is used as a guide for the construction of the preliminary door concept, especially for the rib construction. Considering the significantly different material usage between the frame and inner panel area, the structural development work of concept 1 in this step is separated into two parts and starts with the frame area. The preliminary door construction of concept 1 is then achieved by combining the frame and the inner panel structure.

For concept 2, the frame and inner panel areas are developed simultaneously. The thickness distribution of the preliminary door structure is further optimized by parameter optimization to reach the target light weight and performance goals. After the performance validation under both static and crash loading cases, the optimal door designs are achieved. In this process, several FEA solvers are used. Specifically, Abaqus 6.13 is used for the static simulation of the reference door. The topology optimization, parameter optimization, and performance validation under static loading cases for the concept doors are performed with Optistruct, while Ls-Dyna is used for all crash simulations.

3.3 Summary of general FEA modeling techniques

As mentioned in section 3.2, this concept development work relies highly on FE simulation and uses several solvers for different loading situations. For this reason, the important general FEA modeling techniques applied here need to be introduced at the beginning. According to the types of simulation, this section is separated into: (1) static simulation; (2) crash simulation; and (3) topology optimization.

3.3.1 Static simulation with Abaqus (reference door)

To illustrate the FEA modeling techniques in static simulations, the CAE model of the reference door (Figure 3-6) is used here as an example.

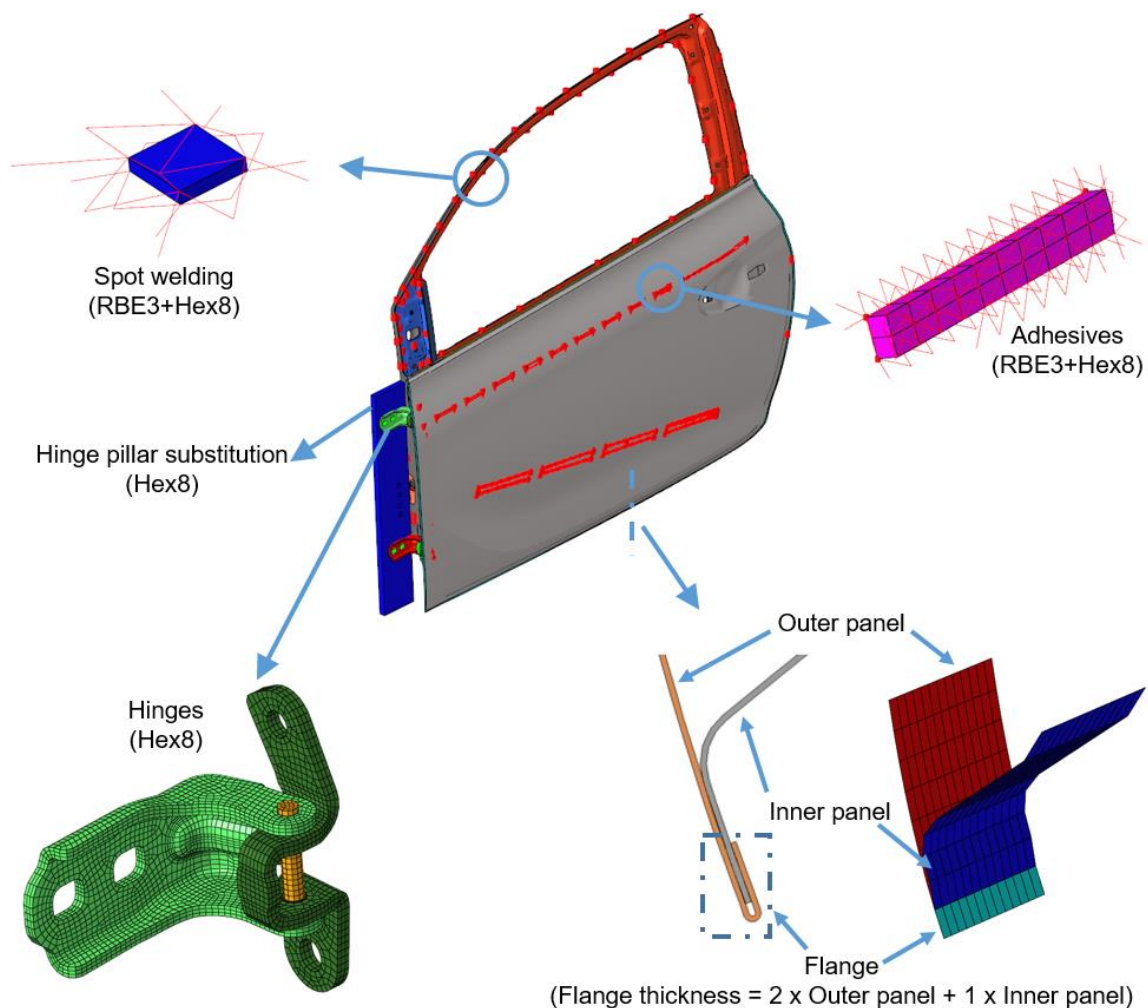


Figure 3-6 Important FEA modeling techniques in simulation models

Accurate simulation of the possible minor plastic deformation of steel components under certain static loading cases is achieved by defining the non-linear material data in the material cards according to steel types [153]. Since most of the FEA modeling techniques used in this FE model follow the state-of-art in the automotive industry, only important modeling features are illustrated in Figure 3-6. The CAE model is made of solid and shell elements. The average element length of the shell elements is 5 mm. Since hinges have a substantial influence on the door stiffness, they are included in the simulation and fully modeled with Hex8 solid elements

(the tetra4 solid element is too stiff). A steel plate is added in the simulation to substitute for the missing hinge pillar. Spot welding and adhesives are the only joining techniques in this model and are realized with standard “RBE3+Hex8” elements. In the flange area, the outer and inner panels are joined using “node equivalence”. The flange is simplified to one layer of elements with a thickness of “2× outerpanel + 1× inner panel”. All bolts and FDS connections are replaced by the “RBE2” element, which is also used on the boundary conditions (constrained areas and force points).

3.3.2 Topology-, parameter optimization, and static performance validation with OptiStruct (concept door)

In the FE model of topology optimization, both the metal and PP-LGF40 materials are defined with the isotropic and linear elastic material card (MAT1) in OptiStruct [154]. UD tapes are defined with an anisotropic material card (MAT8). A typical topology optimization model has two major component groups: “non-design” and “design space”. The “non-designs” (Figure 5-7), such as the base surface made of PP-LGF40 and local reinforcements (UD tapes, sheet/threaded metal inserts, etc.), will not be optimized in the topology optimization and are meshed with a 5 mm shell element (Quad4/Tria3) in this work. Meanwhile, the “design spaces” (Figure 5-7), which are the optimization space for rib structures, are meshed with 5 mm solid elements (Tetra4). The joining between “non-designs” to the corresponding “design spaces” are realized with the “node-to-node” connection (Figure 3-7). The rest of the modeling techniques are identical to the static simulation (section 3.3.1). Special modeling occasions are illustrated specifically in the corresponding section.

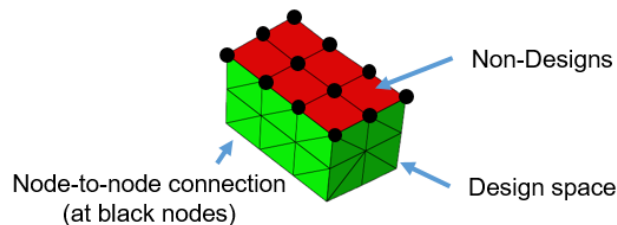


Figure 3-7 node-to-node connection between “non-designs” to “design spaces”

To achieve the maximal structural stiffness under different loading cases, all topology optimizations in this work use the “minimal weighted compliance” as the objective [155]. Depending on the weight saving goal, the volume fraction of the “design spaces” is constrained to a certain value (such as X%), which means that the use of the maximal X% of the defined “design spaces” is allowed to generate rib structures in the topology optimization. Considering the manufacturing method, design constraints, such as the draw direction, and the minimal and maximal dimensions of the PP-LGF40 components, are also given.

The modeling techniques of the parameter optimization and static performance validation are almost identical to the topology optimization, except that “design spaces” are replaced with real rib structures. Meanwhile, to reach further weight reduction through parameter optimization, the objective is set as “minimize mass,” and the constraints are defined with the maximal allowable displacements at force points under different static loading cases. Correspondingly, the material thickness (e.g., the PP-LGF40 and aluminum profiles) is set as the design variables and will be optimized in the given range.

3.3.3 Crash simulation with Ls-Dyna (reference and concept door)

To accelerate the concept development in this work, the crash simulation shares the same mesh of the door structure components (without the hinge-pillar substitution and solid hinges) as in the static simulation (including static performance validation). The FEA modeling techniques in the crash model of the concept door are the same as for the reference door (e.g., the position of the measuring springs, the element size/type, the joining modeling, etc.) and follows the state-of-the-art modeling requirements of FV crash simulations in the automotive industry (see Appendix 10.3.1). Besides the doors, most of the surrounding components are meshed with shell elements with an average element length of 5 mm. All the metal components use the Mat_24 (*MAT_PIECEWISE_LINEAR_PLASTICITY) in Ls-Dyna [134] with a strain rate dependency (further explanations see Appendix 10.3.2). Generally, these material cards include the flow curves which cover a strain rate range from $2e-4/s$ (quasi-static) to 500/s. Especially for the ultra-high-strength steel, this range is up to 1300/s.

One specific point is the material models used for FRPs. Since material modeling with high accuracy is beyond the scope of this concept phase, failure criteria for the FRTPs are not taken into consideration in the crash simulations. Moreover, because the filling simulation is not feasible with a middle-surface CAD model at present, the manufacture-dependent and anisotropic PP-LGF40 is also simplified to the isotropic material model Mat_24 in Ls-Dyna [134]. The Young's modulus and the flow curve of the PP-LFG40 are the average values from tensile tests of flow- and cross-direction specimens (see section 3.1.3). According to the work by Sun [144], the error of this modeling of PP-LGF40 with Mat_24 is acceptable for this type of concept validation usage. The UD tapes are modeled with Mat_54 (*MAT_ENHANCED_COMPOSITE_DAMAGE) in Ls-Dyna [134] (details see Appendix 10.3.3). Further specific modeling occasions for crash simulations are illustrated in the corresponding sections.

4 Reference door analysis

A market-available door from a compact vehicle is chosen as the reference for this work. Since the goal of this work is to achieve a 20% weight reduction and comparable mechanical performance based on the reference door, a complete analysis of this reference door is necessary to quantify the design goal. The mechanical performance evaluation of the reference and concept doors relies especially on the FEA method. Proving the reliability and accuracy of the applied modeling techniques in the FE model is important. This section illustrates the following analyses of the reference door: 1) structural analysis; 2) performance analysis.

4.1 Structural analysis

In this structural analysis, the components of the reference door are categorized into structural components and functional components, since the structural components define the mechanical performance to a large extent and the functional components determine the available design space in the narrow area between inner and outer panels.

As shown in Figure 4-1, the reference door is designed with sheet metal construction and weighs 16.39 kg. The assembly includes the following structural components: 1) inner panel; 2) outer panel; 3) frame reinforcement; 4) mirror and upper hinge reinforcement; 5) door stopper and lower hinge reinforcement; 6) belt reinforcement outer; 7) latch reinforcement; 8) side impact beam; and 9) window rail. The details of each structural component (BOM) are given in Appendix 10.4 (Table 10-4).

The functional components are also indispensable for a vehicle door. Passengers interact a lot with these functional components during daily use, and the passengers' first impressions of the vehicle are influenced, for example, by the door closing efforts/sounds and the wind noise during driving. Several important functional components will therefore be retained in this work and used further in the concept. The sizes and positions of these components have a significant influence on the available design space for LFT components in new door concepts. The change in material from steel to LFTs will decrease the E-modulus, so the typical rib construction on LFT components will definitely increase the demand on the design space in the new concepts. Important design-space related functional components of the reference door are the: 1) window glass; 2) latch system; 3) window regulator; 4) door stopper; 5) frame trim; and 6) door trim (see Figure 4-2). Considering the component sharing strategy in OEMs and the styling requirement from the design studio, the door stopper, latch system, window glass, and window regulator system are retained for the new concepts, which means that sufficient space must be reserved to install those functional components. However, the higher geometry design freedom of LFTs means that the unused available space between the frame/door trim and the steel inner panel can be partially used to expand the existing design space without any geometry conflicts.

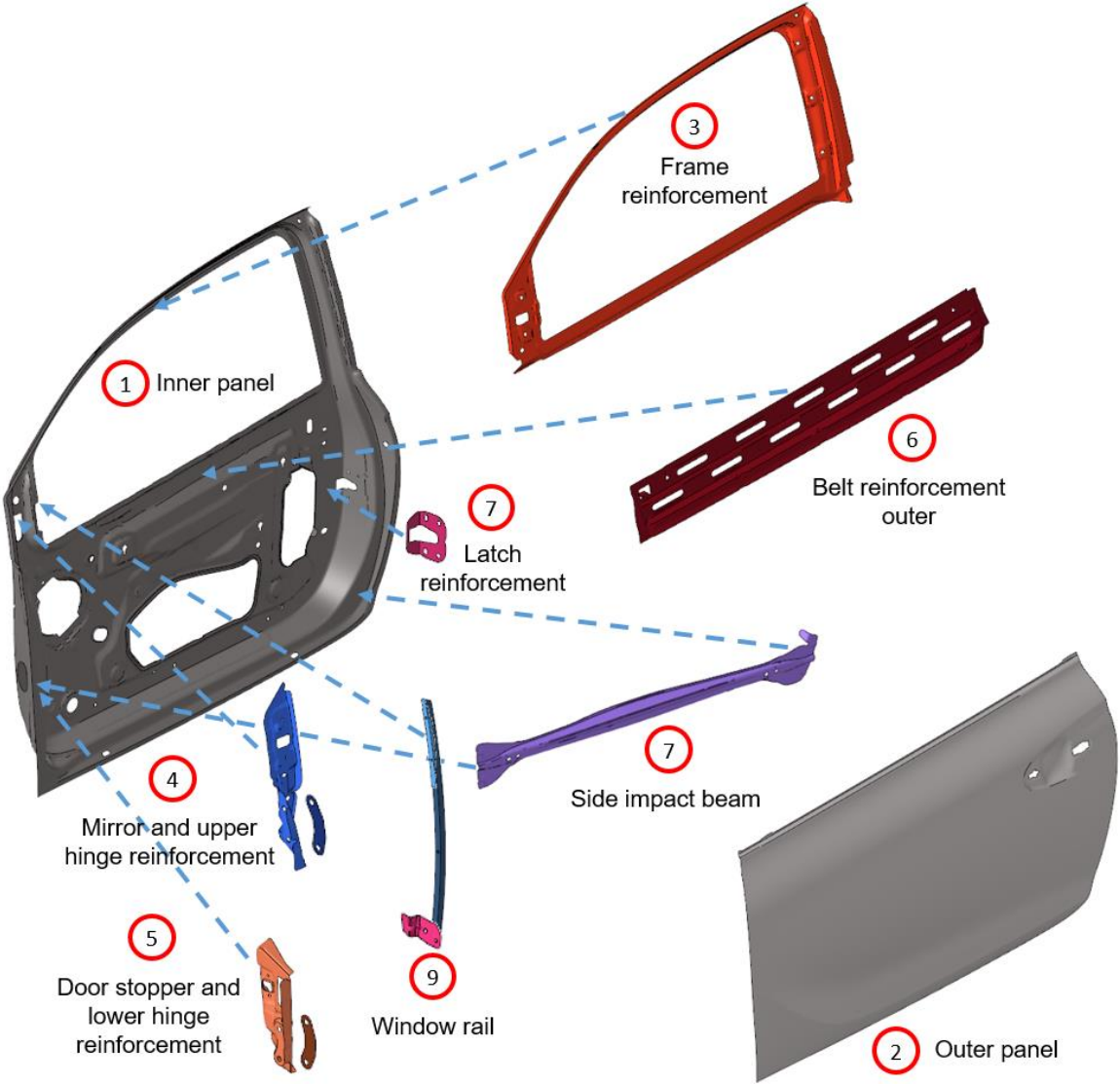


Figure 4-1 Reference door: structural components

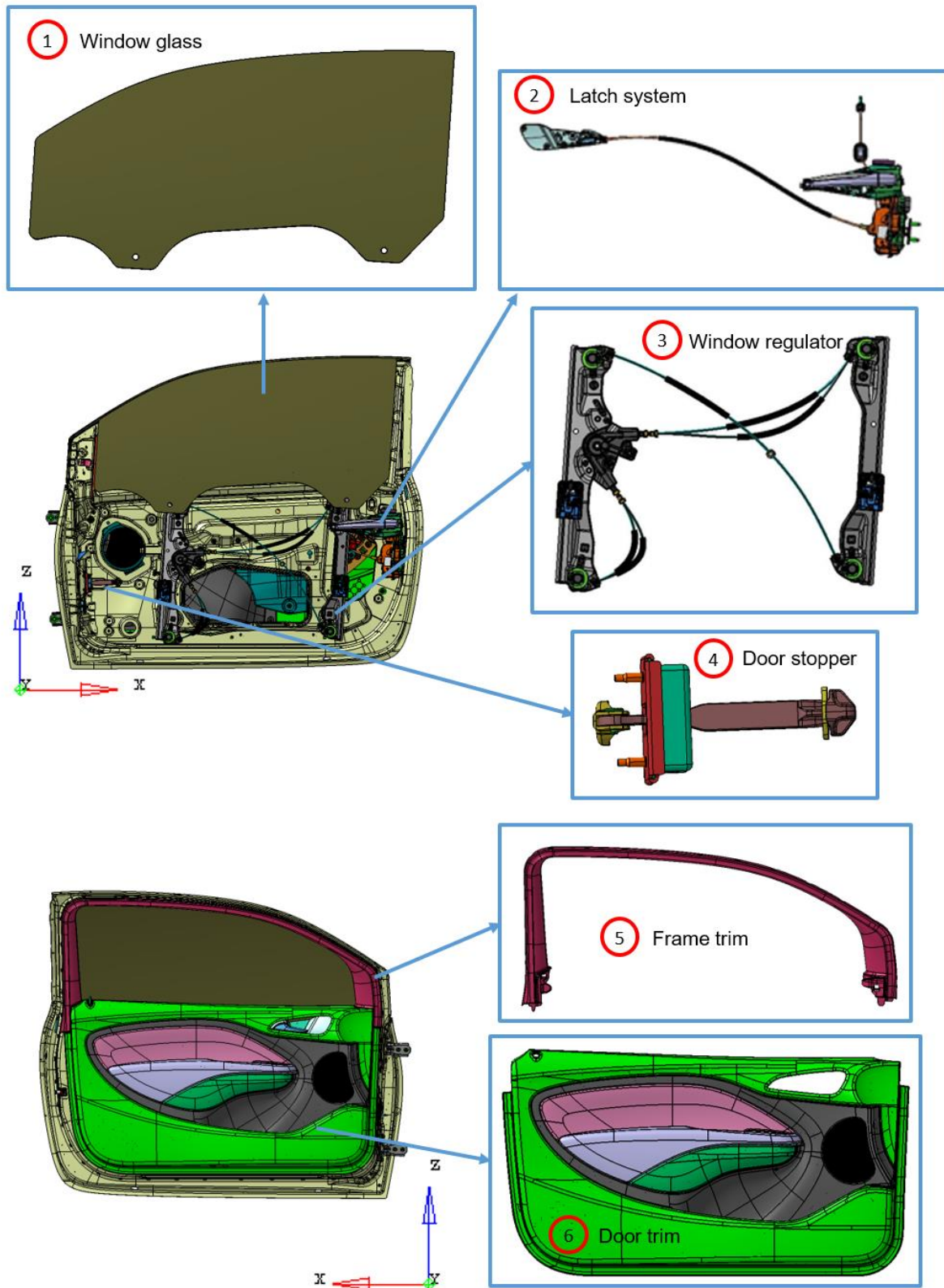


Figure 4-2 Reference door: design-space-related functional components

4.2 Performance analysis

4.2.1 Static loading cases and anisotropy analysis

Simulation results

To obtain a clear goal for further development, the chosen reference door is simulated under the six static loading cases (section 2.4.2). Displacements at force points following the force directions under each loading case are listed in Table 4-1 and are used as the design requirement for further concept development.

No.	Static loading case	Force (N) / Direction (Vehicle global coordinate)	Displacement at force point following force direction (mm)
1	Frame stiffness B-pillar	350 / -Y	12.48
2	Frame stiffness middle	350 / -Y	10.74
3	Door sag	1000 / -Z	8.49
4	Over opening	300 / -Y	19.84
5	Belt stiffness outer	200 / +Y	3.58
6	Belt stiffness inner	200 / -Y	2.09

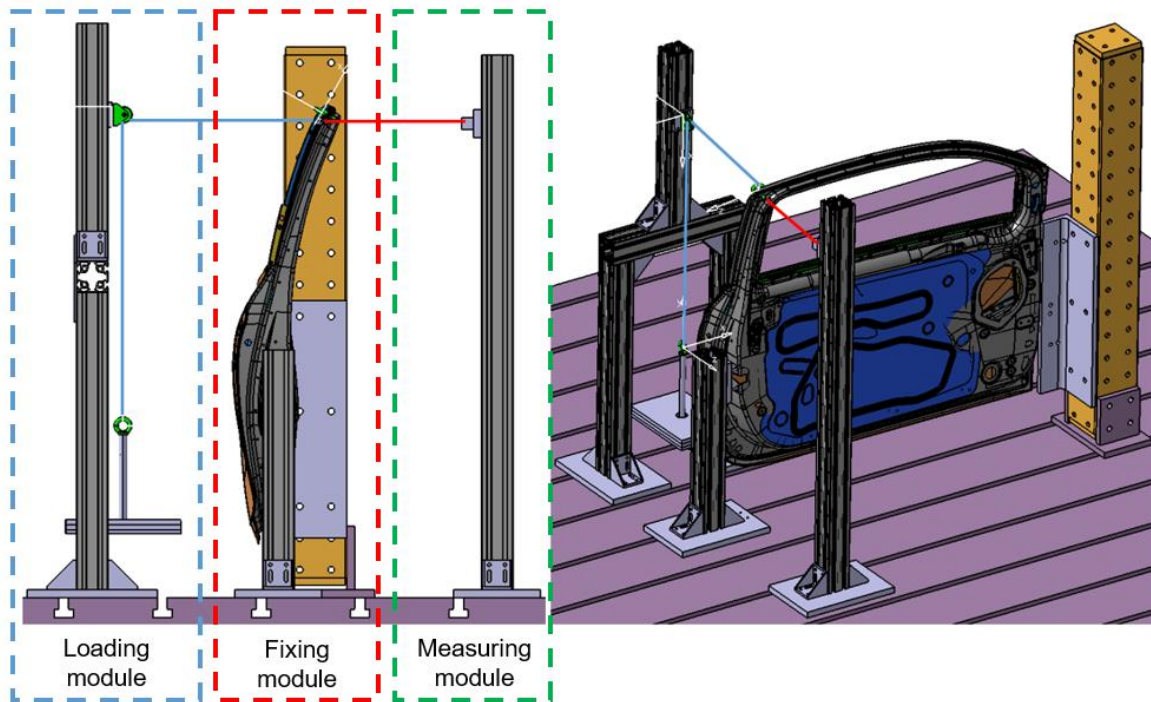
Table 4-1 Reference door: static simulation results

Testing results

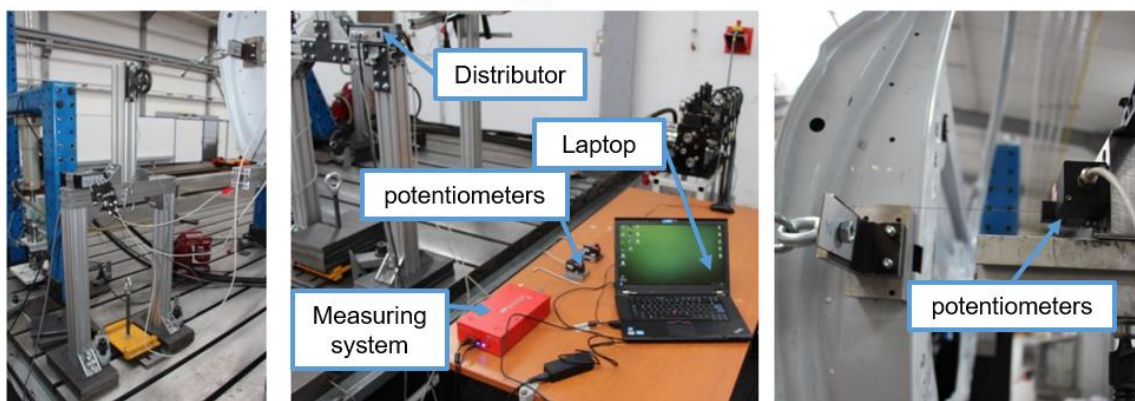
As mentioned earlier, all concept doors in this work will only be validated with the FEA method. For this reason, the accuracy of the simulations (static) with FEA modeling techniques (section 3.3.1) must be proven in the early phase. This can be achieved by testing the reference door hardware and comparing the results between the testing and simulation. According to the feasibility, 5 static loading cases are tested (see Table 4-2).

The static loading cases mentioned in section 2.4.2 are used to develop a door static test bench. The schematics of this test bench (CAD) under the static loading case “frame stiffness b-pillar” are shown in Figure 4-3a as an example (rest loading cases: see Appendix 10.5). The door static test bench has three major modules: 1) fixing module; 2) loading module; and 3) measuring module. According to the specific boundary conditions related to the static loading cases, the degrees of freedom (DOF) in the hinge and latch areas can be properly constrained by the fixing module. The corresponding forces are converted to weights and imposed on an

accurate position of the door structure by the “rope-pulley” system of the loading module (blue line in Figure 4-3a), following the defined loading direction. The measuring module measures the displacement at the loading point in the loading direction using calibrated cable potentiometers [156]. The principle of cable potentiometers is that they convert the change in electric potential to a change in the cable length since there is a linear relationship between these changes. In this way, displacements at the loading points can be measured with a high level of accuracy. The force conduction, the testing setup, and the positioning of the cable potentiometer in a practical test are illustrated in Figure 4-3b, as an example.



(a)



(b)

Figure 4-3 Schematics of test bench (CAD) “frame stiffness b-pillar” (a); testing setup in a practical static test (b)

Table 4-2 summarizes the chosen loading cases and the corresponding displacement deviation at force points between the static simulations and the tests. Note that the maximal deviation is less than 10%, which confirms the reliability of the FEA modeling techniques.

No.	Static loading case	Displacement deviation at force point (%) (+: Simulation > testing; - : Simulation < testing)
1	Frame stiffness b-pillar	+10%
2	Door sag	0%
3	Over opening	-5%
4	Belt stiffness outer	+3%
5	Belt stiffness inner	+10%

Table 4-2 Deviation between static simulation and testing

Anisotropy analysis

According to two concept ideas (section 3.1.2), the LFTs and UD tapes are the major materials that have a high level of anisotropy. Identifying the areas on a structure with a high level of load anisotropy at the beginning of the development is the most efficient way (cost and weight) to use the UD tapes, which are used as a local reinforcement.

For the door structure, the loading situation is complex even for static loading cases. For this reason, an anisotropy analysis with the reference door is made using the algorithm from the work of Fang and Grote [104; 157]. This algorithm uses a dimensionless “anisotropy value”, defined by [158], to describe the level of load anisotropy on components, where a higher value means a higher load anisotropy level. In this analysis, the six static loading cases are considered simultaneously. The load anisotropy values on every component, along with the calculated fiber directions, are shown in Figure 4-4. Based on the distribution of the anisotropy value, the areas with the highest anisotropy value (ca. > 0.7) are identified on the components “inner panel,” “frame reinforcement,” and “belt reinforcement outer” (red marked areas in Figure 4-4). This result is an important reference for the later determination of the areas of UD tapes.

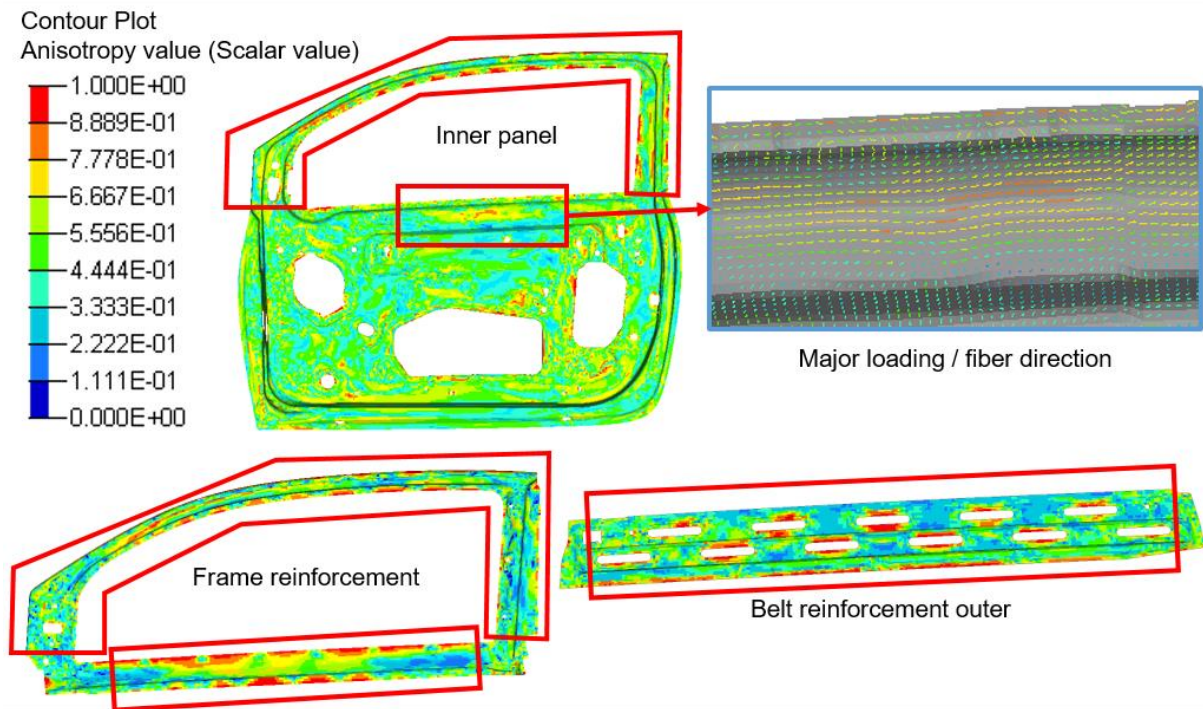


Figure 4-4 Reference door: anisotropy analysis result with static loading cases

4.2.2 Crash loading cases

The crash simulation is performed with the reference door under the Euro-NCAP side pole impact loading case (section 2.4.3). Based on the component development method (section 2.7), the L3M of the reference vehicle (Figure 4-5) underlying this loading case is built with the limited BIW data.

Typically, the intrusion and the intrusion velocity are the key values to evaluate the structural performance of doors under crash loading cases [159]. Accurate and quantitative comparison of the intrusion and the intrusion velocity are attained by defining several measuring points on the door and surrounding BIW side wall components at the occupant's side (Figure 4-6). In this way, no matter how large the rotation on the BIW during the side pole impact, an accurate intrusion value is easily measured on every measuring point by the length change of specially defined intrusion measurers (springs with extremely low elastic stiffness) (Figure 4-5). These predefined measuring points are able to cover almost all areas that can be influenced by the door structural performance. Obviously, relatively more measuring points are defined in the impact areas, where the maximal intrusion happens, and they are also crucial for occupant safety.

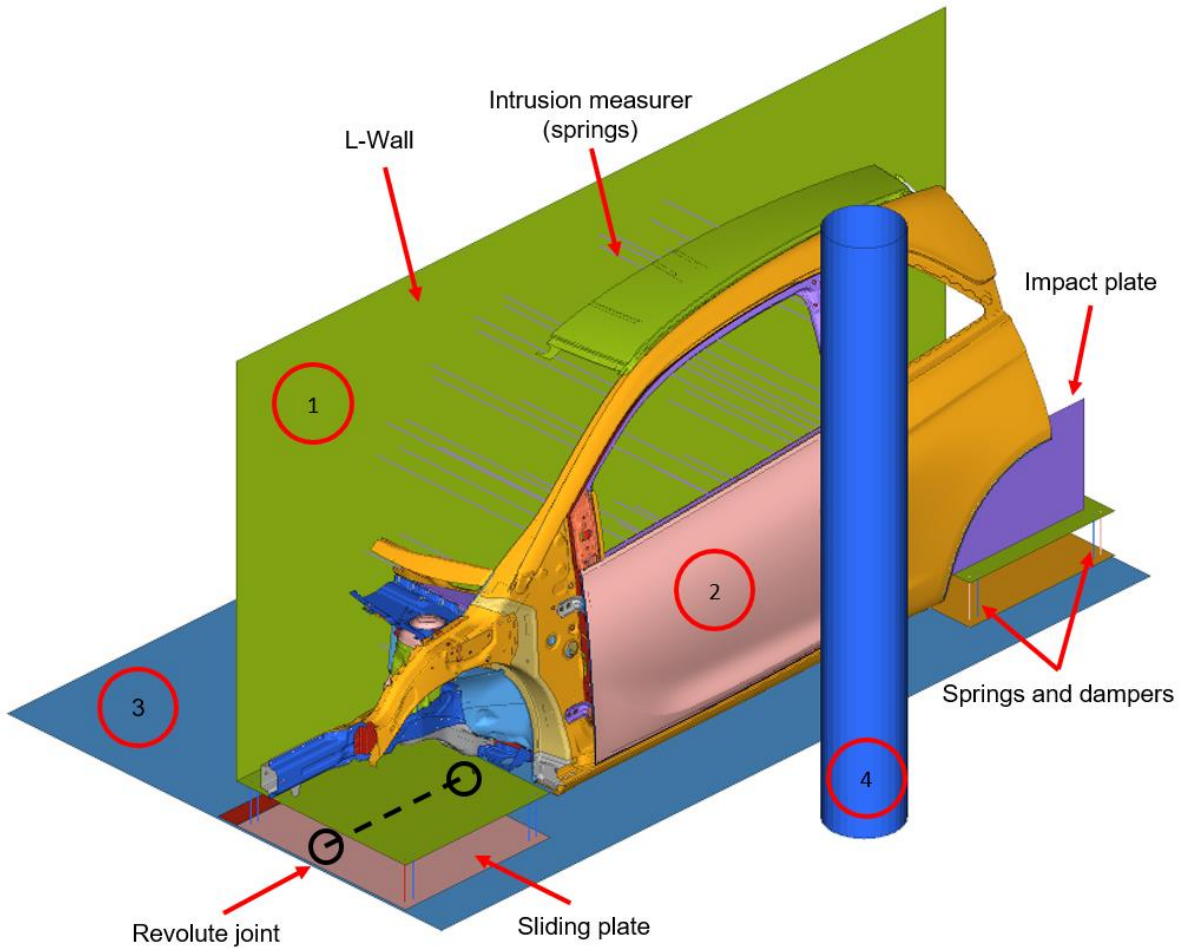


Figure 4-5 L3M of reference vehicle under Euro-NCAP side pole impact test

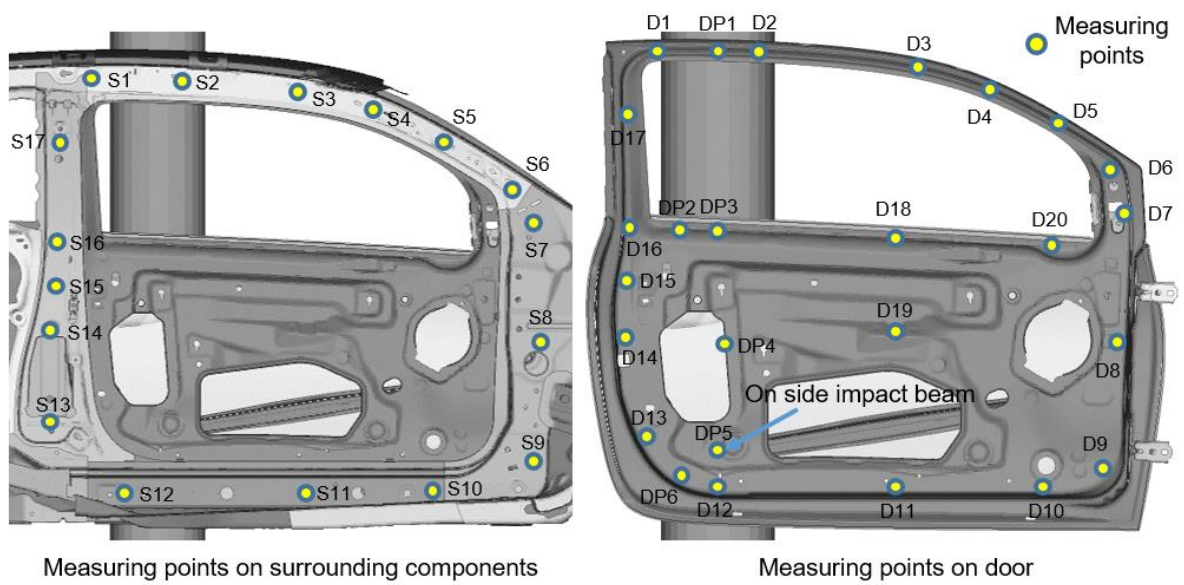


Figure 4-6 Measuring points on the door and surrounding BIW components (unnecessary components are masked)

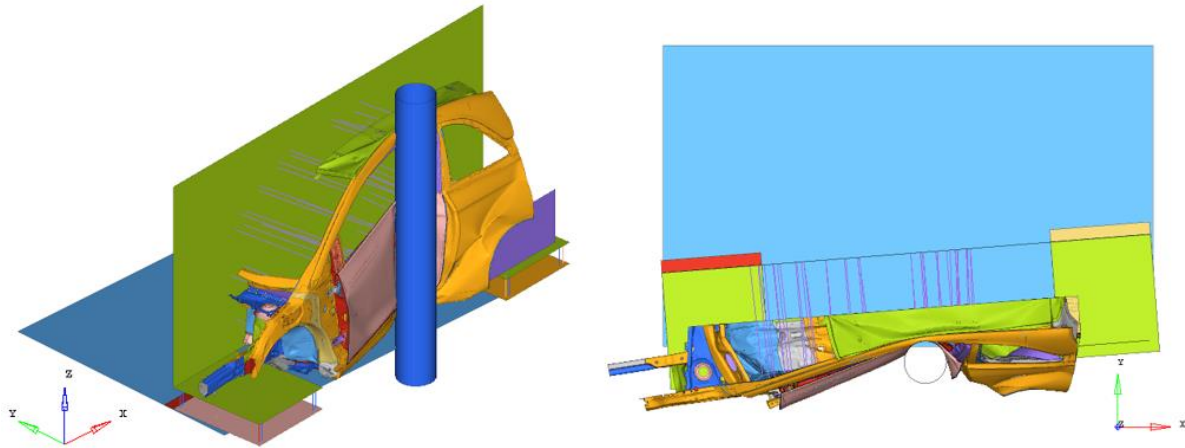


Figure 4-7 Reference door model under the side pole impact: maximal intrusion at 70 ms

Figure 4-7 illustrates the deformation plot of the reference door and the surrounding components at 70 ms, when the “bounce back” starts and maximal intrusion happens. The corresponding maximal intrusions on measuring points at 70 ms of the reference door are listed in Appendix 10.6 and 10.7 in the column “reference door”. The intrusion velocity in the passenger-related area (measuring points: DP1, DP3, DP4, and D12) can be found in Figure 6-4 and Figure 6-8. Both figures are used as the comparison criteria for the further validation of the concepts.

4.2.3 Implementable test bench design for a component development method

Although the component development method can provide sufficiently accurate crash results, a major problem remains regarding how to realize the ideal virtual boundary conditions of the L3M (e.g., the right L-wall, the “spring-damper system,” and the connection between the component sub-model to the L-wall) on an implementable test bench. Since this method is used extensively to validate door concepts, solving this major problem and developing an implementable test bench model (ITB) is crucial for this work. Due to the absence of the full vehicle BIW information on the reference vehicle in this work, another vehicle, the “Streetscooter” [159], was chosen as it has full vehicle information (Figure 2-56) and therefore allows the necessary comparison of crash results between the FV, L3M, and ITB models. To achieve a comparable ITB structure and crash behavior, the chosen Streetscooter and the reference vehicle in this work belong to the same small vehicle class.

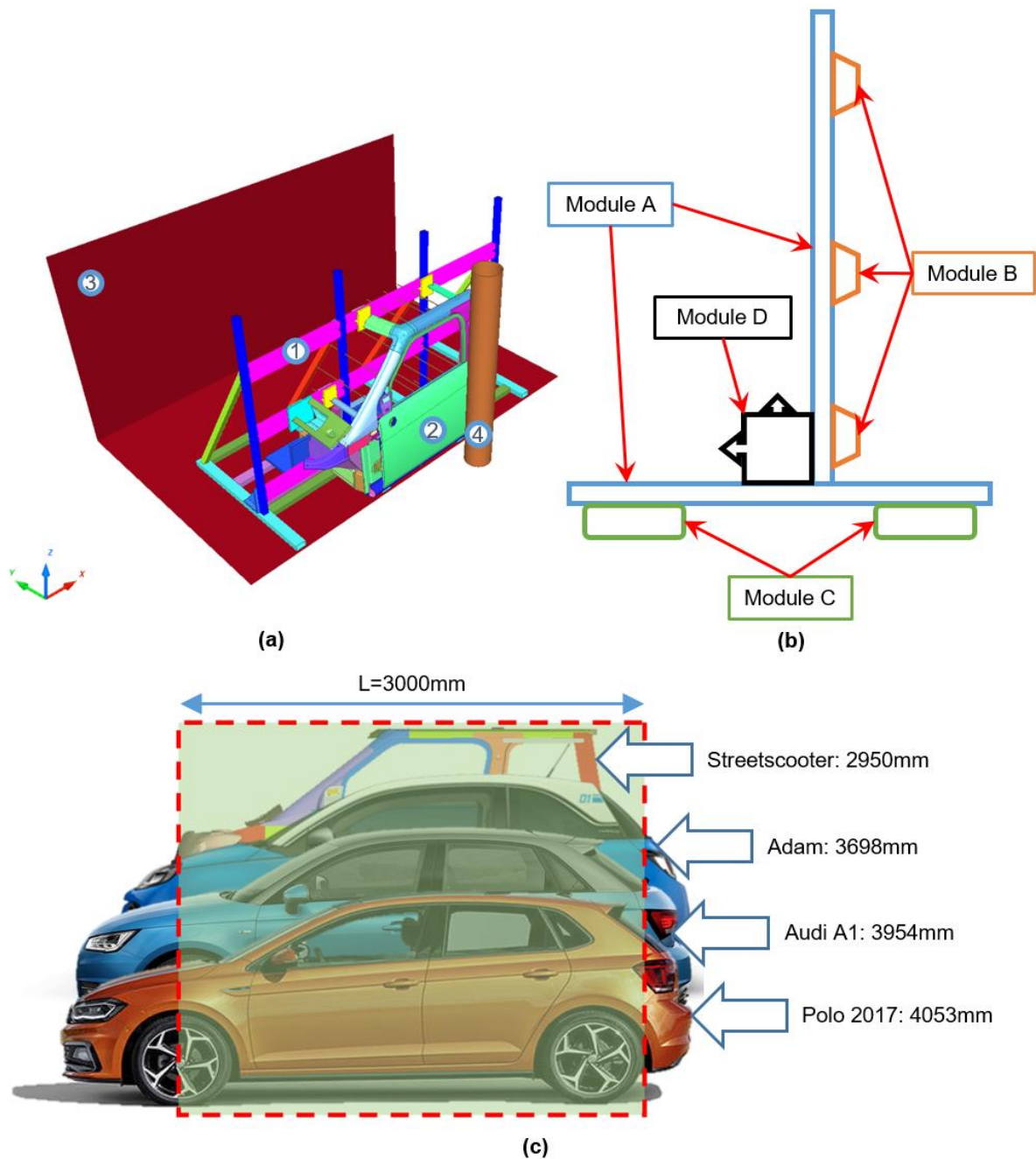


Figure 4-8 ITB model of the Streetscooter under a side pole impact (a); Modular structure of the test bench (b); Module A length and the typical length of compact vehicles (c)

As Figure 4-8a illustrates, the ITB model under the side pole impact, realized with the Streetscooter, includes four major parts: 1) a moveable test bench; 2) the component sub-model; 3) the floor as the sled; and 4) a fixed rigid pole barrier. Unlike the L3M, the moveable fixture is replaced with the moveable test bench. The total weight of this moveable test bench is 515 kg (without added weights). This test bench is made applicable to similar compact vehicles, possibly lightweight and with high strength, by developing a frame construction with a modular structure (Figure 4-8b). The function of the different modules is summarized in Table 4-3.

Module	Function
Module A	<ul style="list-style-type: none"> • Main body of the test bench • Provides sufficient strength and support for the impact energy absorption • Versatile connection area to modules B and D
Module B	<ul style="list-style-type: none"> • Connector between the component sub-model and module A • Detachable and exchangeable during the change of vehicle models
Module C	<ul style="list-style-type: none"> • “Spring-damper system” to reproduce the tilting behavior of vehicles • Stable sliding platform
Module D	<ul style="list-style-type: none"> • Weight and COG adjustment • Easy and flexible mounting on module A

Table 4-3 Functions of different modules

For module A specifically, considering the cost, weight, loading, and reliability, a standard S355JR steel profile with a hollow square cross section is extensively used. Since the compact vehicle class is the focus of this work, the length of module A is set as 3000 mm (Figure 4-8c), which is able to cover the typical length range of compact vehicles.

For module B, the connection concept realizes the joining between the component sub-model and module A (Figure 4-9a). Module B features an exchangeable fitting part for different cross sections of components and a universal fixing part that connects to module A. This concept can carry the component sub-model firmly and conduct the force to module A, while also facilitating exchangeability between different vehicle models by being adjustable. Specifically, two types of typical connections can be made between the component sub-model and module A: 1) cross components to module A; and 2) rear suspension mounting to module A. For the first one, a core insert is designed (Figure 4-9b) that will be pushed into the hollow of the cross components and helps to avoid the local buckling of thin-walled sheet metal parts. Adhesives are also applied to the overlapped area to provide enough strength for a reliable connection. For the second type, a connector is added to connect the mounting of the rear suspension on the BIW to module A (Figure 4-9c), which replaces the load path function of the rear suspension in side impact tests. This connector can be built without knowing the vehicle-specific suspension data.

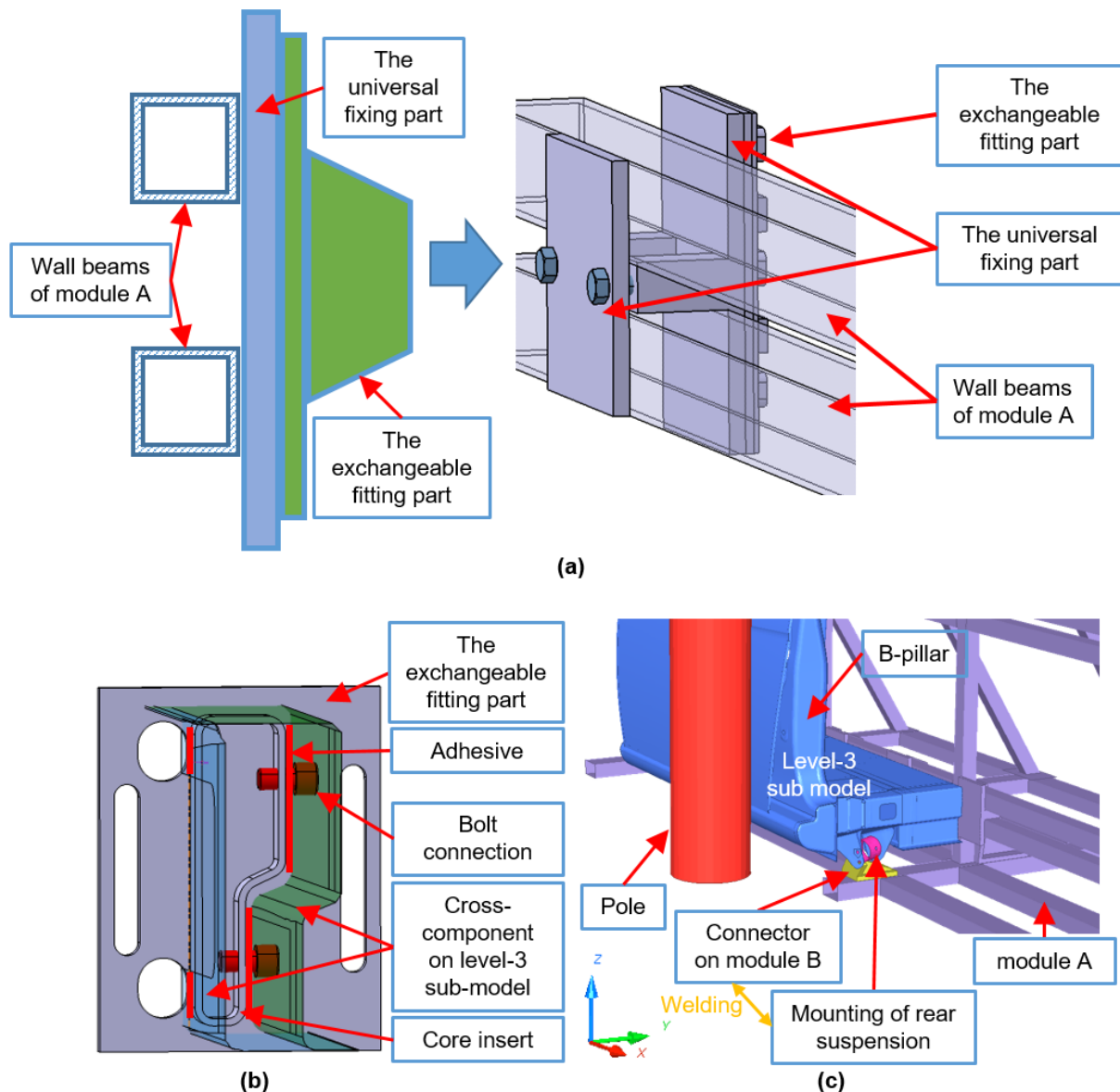


Figure 4-9 The concept of module B (a); the connection solutions for cross components (b); the mounting of the rear suspension (c)

Module C is a spring-damper system in L3M. As defined in Figure 2-55, three major challenges limit the realization of module C on the ITB: (1) the substantial damping constant of the damper and the appreciable elastic stiffness of the spring; (2) implementation of reliable revolute joints; and (3) the constraint of the Z-translation of the sliding plates. For these reasons, a significant difference exists between L3M and ITB for module C.

According to the parameters and setups in L3M, the spring and damper used here must have an elastic stiffness of $k=2 \text{ kN/mm}$ and a damping constant of $d=29 \text{ kN}\cdot\text{s/m}$, respectively. A thorough search for market-available spring and damper systems with this high elastic stiffness and damping constant has been conducted. For springs, only a disc spring can meet the stiffness requirement. However, a disc spring can only hold a compressive force, whereas the spring in module C must be able to hold tensile force as well. For dampers, neither an oil-hydraulic damper [160] nor a pneumatic damper [161] is suitable for the heavy impact loads on module C. Only a rubber-metal buffer can work with heavy loads [162; 163]. However, the

damping constant of the rubber-metal buffer cannot be quantized, so it is not acceptable in this case. In other words, neither proper springs nor dampers have been found on the market.

Since no spring or damper can meet the requirements, an alternative structural solution is the only way forward. For this reason, the tilting behavior of the L3M has been investigated under two side impact tests. As shown in Figure 4-10, a Z-displacement of only around 10 mm can be found at measuring point 1 for both tests. This small tilting behavior on L3M (ca. 1.6 degrees) could be reproduced by the structural elastic deformation of the movable test bench in ITB, to some extent. Based on this observation, a structural simplification is made: no specific “spring-damper system” is designed for the ITB.

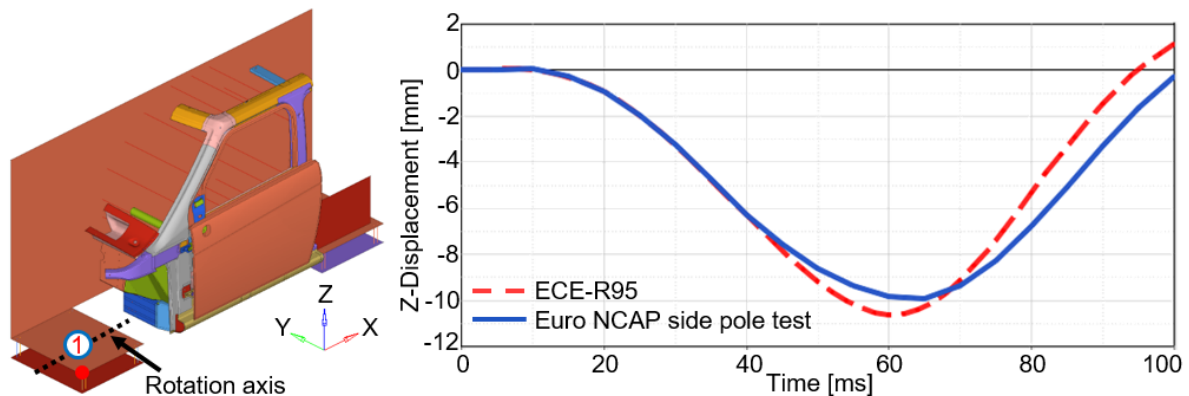


Figure 4-10 The Z-displacement curves of measuring point 1 under ECE-R95 [164] and Euro NCAP side pole test

Due to the elimination of the “spring-damper system,” the constraint of the Z-translation on the sliding plate has been correspondingly canceled. Theoretically, the long beams on the base of module A are sufficient to guarantee a stable and smooth sliding motion with a natural and subtle tilting behavior of the ITB. For this reason, no extra constraints are needed here. The following validation result of the ITB proves the feasibility and accuracy of this solution.

Module D is designed for weight matching, which helps to achieve the same weight and COG between the FV and the “movable test bench + component sub-model”. The concept of module D is shown in Figure 4-11a. Part 1 connects to module A, which works as the platform for added weights. Parts 2 and 3 are added weights. By changing parts 2 and 3, the COG and weight can be adjusted. As shown in the side view of the movable test bench in ITB (Figure 4-11b), a geometry conflict between the added weight and the suspended component sub-model is avoided using an unsymmetrical design.

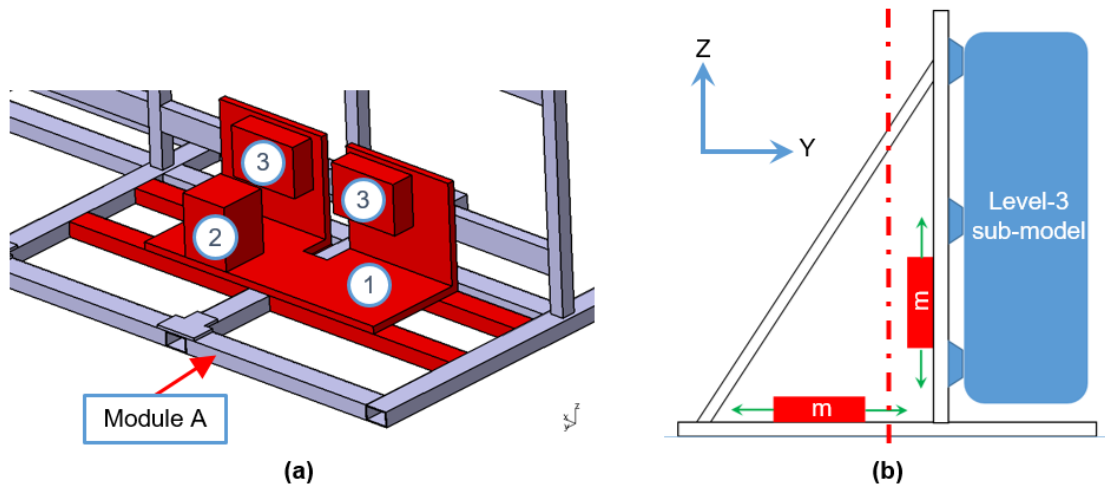


Figure 4-11 The schematic of module D (a) and the side view of ITB (with added weights) (b)

Besides the strength, the ITB model must be able to reproduce the result of the L3M within a reasonable percentage of error as a key criterion for evaluating its performance. For this reason, the ITB is validated with the FE method under the loading case of the Euro NCAP side pole test (version 2001) [88].

The crash simulation results reveal no noticeable deformation on the movable test bench of the ITB. The maximal von Mises stress also never exceeds the yield stress of the S355JR (355 MPa). So far, the ITB fulfills the strength requirements.

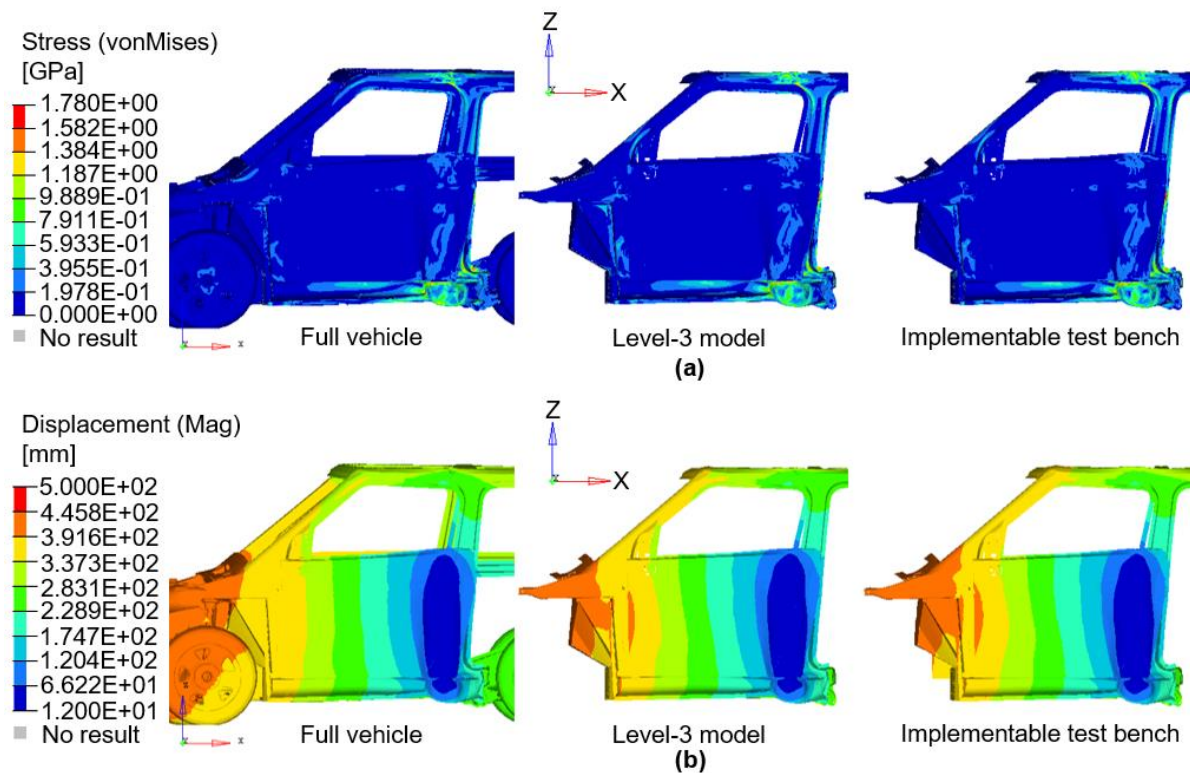
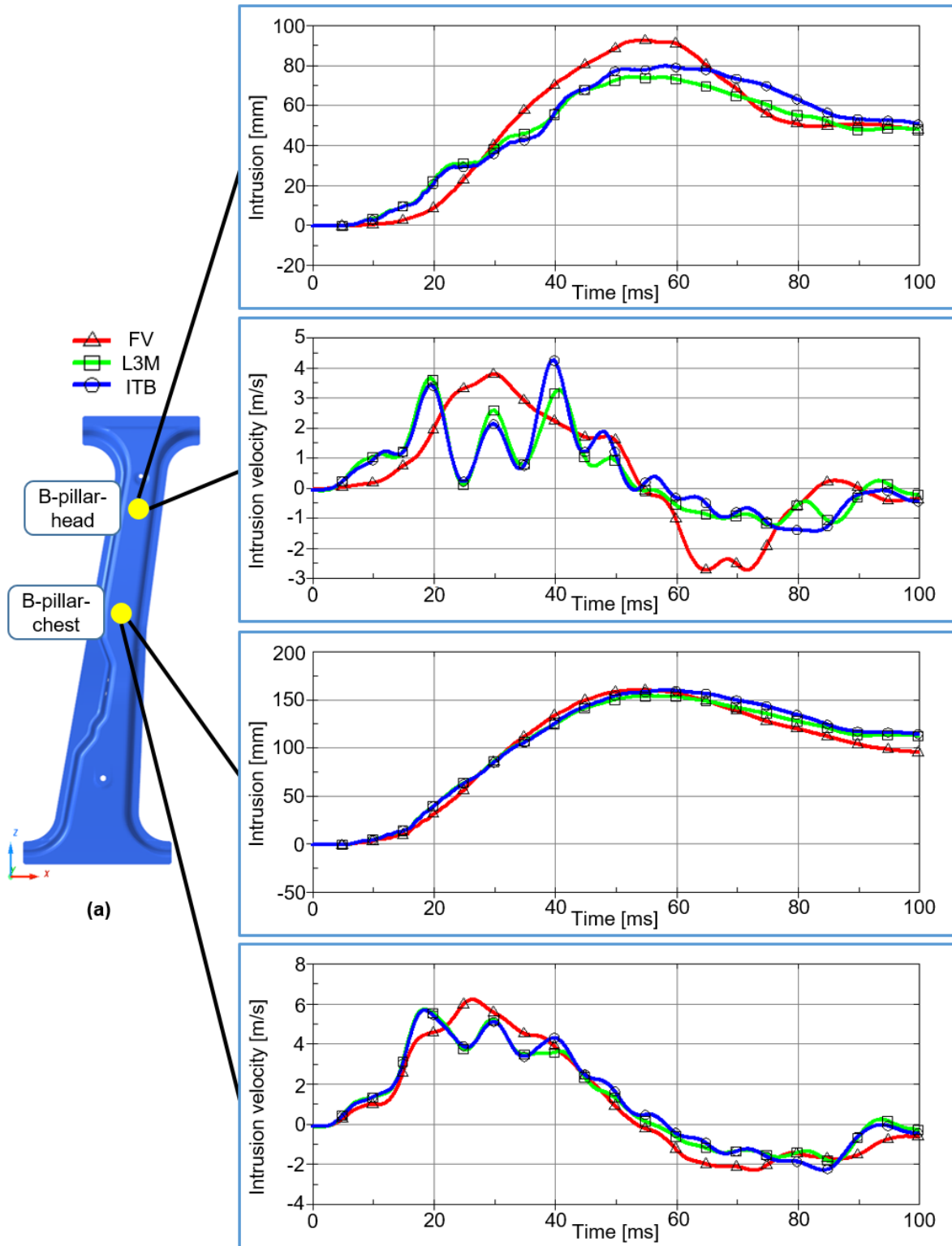


Figure 4-12 The stress (a) and displacement (b) plots at 60 ms

Figure 4-12 shows the stress distribution and displacement plot at 60 ms in all simulations when the maximal intrusion occurs. A good correlation is achieved between the L3M and the ITB model for both stress and displacement. However, the stress values are slightly higher here than in the FV simulation in the upper part of the component sub-model (roof frame and B-pillar upper). This difference is caused by the reduction in BIW components and the low level of elastic deformation of the test bench.

An accurate comparison of the intrusion and intrusion speed is obtained, as shown in the corresponding data for the occupant relevant areas shown in Figure 4-13. On the B-pillar (Figure 4-13a), the curves of the measuring points "B-pillar-head" and "B-pillar-chest" are chosen as representatives of the results for all the measuring points. For both the intrusion and intrusion velocity on the B-pillar, a good correlation between the ITB model and the L3M has been achieved. Compared even to the FV results, the intrusion and intrusion velocity of measuring points "B-pillar-chest," "B-pillar-abdomen," and "B-pillar-pelvis" on the ITB model show a high level of accuracy (see Table 4-4). However, a deviation is evident at the "B-pillar-head" measuring point, where the intrusions on the ITB are smaller than on the FV, and the intrusion velocity shows a certain amount of oscillation.



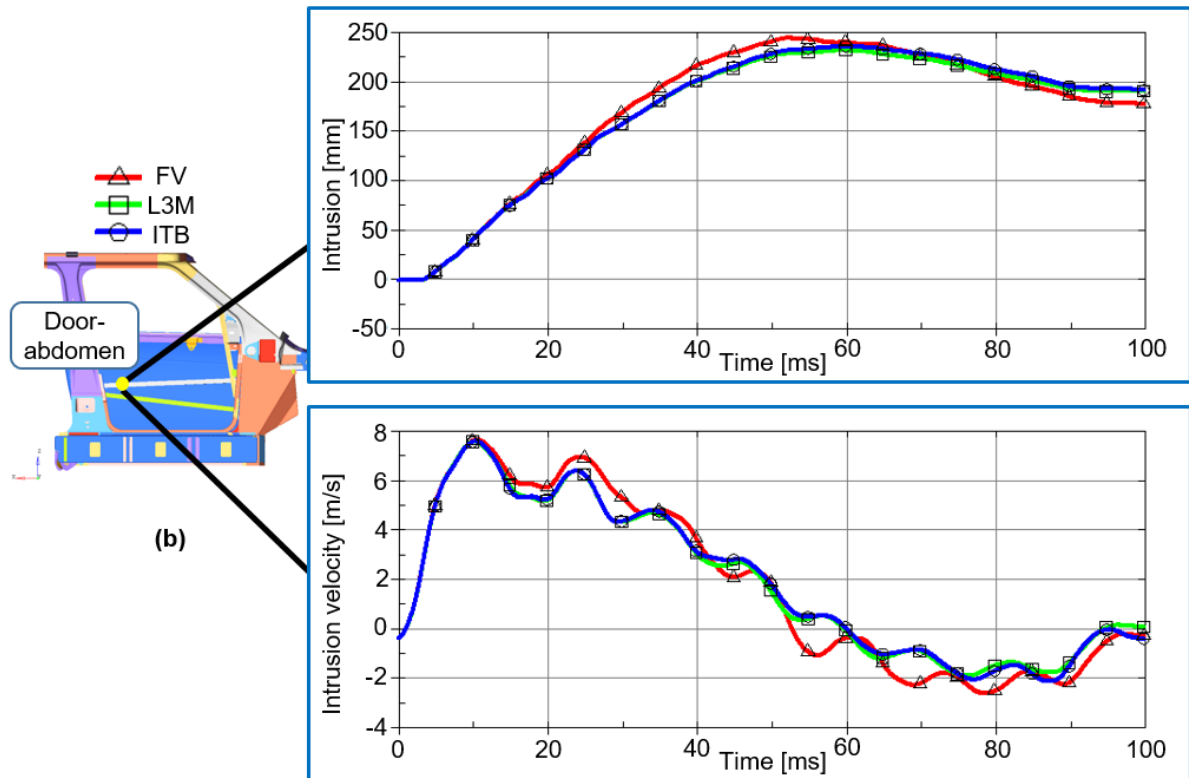


Figure 4-13 Comparison of the intrusion and intrusion velocity among the FV, the L3M, and the ITB model simulation (Euro NCAP side pole test (version 2001)): a) B-pillar; b) door area

The results for the door area are shown in Figure 4-13b. The curves of the measuring point “Door-abdomen” are chosen as representative of the remaining measuring points. A good correlation of the intrusion and intrusion velocity between the L3M and the ITB model has been achieved. Compared to the FV results, only a very small deviation of intrusion and intrusion velocity can be found in the door area (see Table 4-4).

Test	Measuring points	Max. intrusion (mm)			Max. intrusion velocity (m/s)		
		L3M	ITB	Deviation	L3M	ITB	Deviation
Euro-NCAP side pole test	B-pillar-head	75	80	6.7%	3.7	4.3	16.2%
	B-pillar-chest	155	161	3.9%	5.8	5.7	1.7%
	B-pillar-abdomen	177	181	2.3%	6.5	6.5	0.0%
	B-pillar-pelvis	188	192	2.1%	7.6	7.6	0.0%
	Door-abdomen	233	237	1.7%	7.6	7.6	0.0%
	Door-pelvis	224	227	1.3%	7.1	7.1	0.0%

Table 4-4 B-pillar and door area: the comparison of maximal intrusion and intrusion velocity between the L3M and the ITB model on measuring points

The distribution of the intrusion deviation according to the measuring points between the L3M and the ITB model is illustrated in Figure 4-14. A deviation of less than 10% is evident in area A, which includes the major components related to occupant safety in a side impact, such as the B-pillar, door module, and sill.

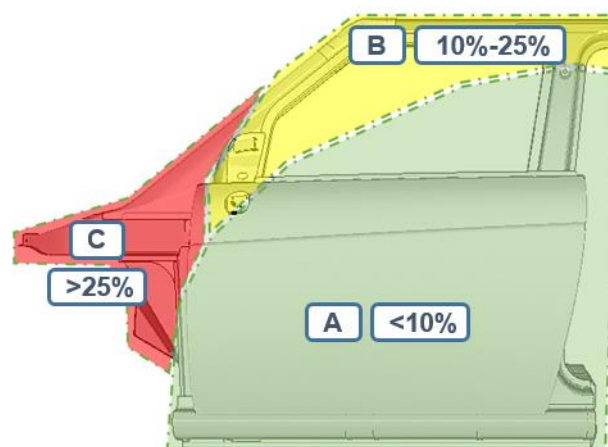


Figure 4-14 The deviation distribution of intrusion between the L3M and the ITB model

The deviations on the roof frame (area B) are between 10% and 25% and are caused by the relatively large elastic deformation in the upper part of the ITB. The resulting periodic vibration

force acts on the component sub-model and creates the intrusion deviation on the upper part of the component sub-model.

Area C (A-pillar and hinge pillar) shows a relatively large deviation of intrusion of more than 25%. Due to the small absolute value of intrusions in this area (considerably smaller than 10 mm), a small change in intrusion can lead to a large deviation percentage-wise. This can be seen in Figure 4-15. As shown on the representative measuring point “Hinge-2” in Figure 4-15, the absolute deviation at this point, and in area C, is very small.

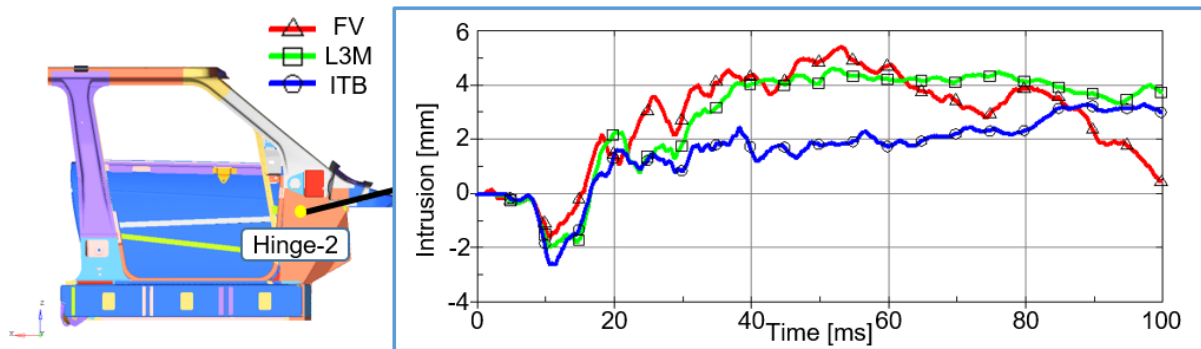


Figure 4-15 Hinge-2: the comparison of intrusion among the FV, the L3M, and the ITB model simulations (Euro NCAP side pole test (version 2001))

Overall, based on the comparison of intrusion and intrusion velocity and deviation analysis, it can be concluded that, under the loading case of the Euro NCAP side pole test (version 2001), the ITB model is able to provide a proper reproduction of the boundary conditions of the L3M and to deliver a sufficiently accurate crash result for the development of vehicle side components. Real test bench hardware can therefore be built, based on the construction of the moveable test bench in the ITB model.

5 Structural development with topology optimization

This section will illustrate the structural development for two door concepts separately.

5.1 Concept 1

As mentioned in section 3.2, the structural development work of concept 1 is separated according to: 1) the frame area; and 2) the inner panel area. The reason, as mentioned by Fang [104], is that the optimization solver is quite often not able to deliver the best possible results if too many or too ambiguous design variables/inputs are given. The best solution for avoiding this problem is to reduce the number of design variables or to provide a clear input for the optimization. For this reason, the total topology optimization work for concept 1 is split into the frame area optimization and the inner panel area optimization, according to the material types. Details about this topology optimization process are illustrated in Figure 5-1. Since the frame geometry can have a substantial influence on the design space definition of the inner panel, especially at joining areas, the frame area is designed first and used as the input for the design of the inner panel area.

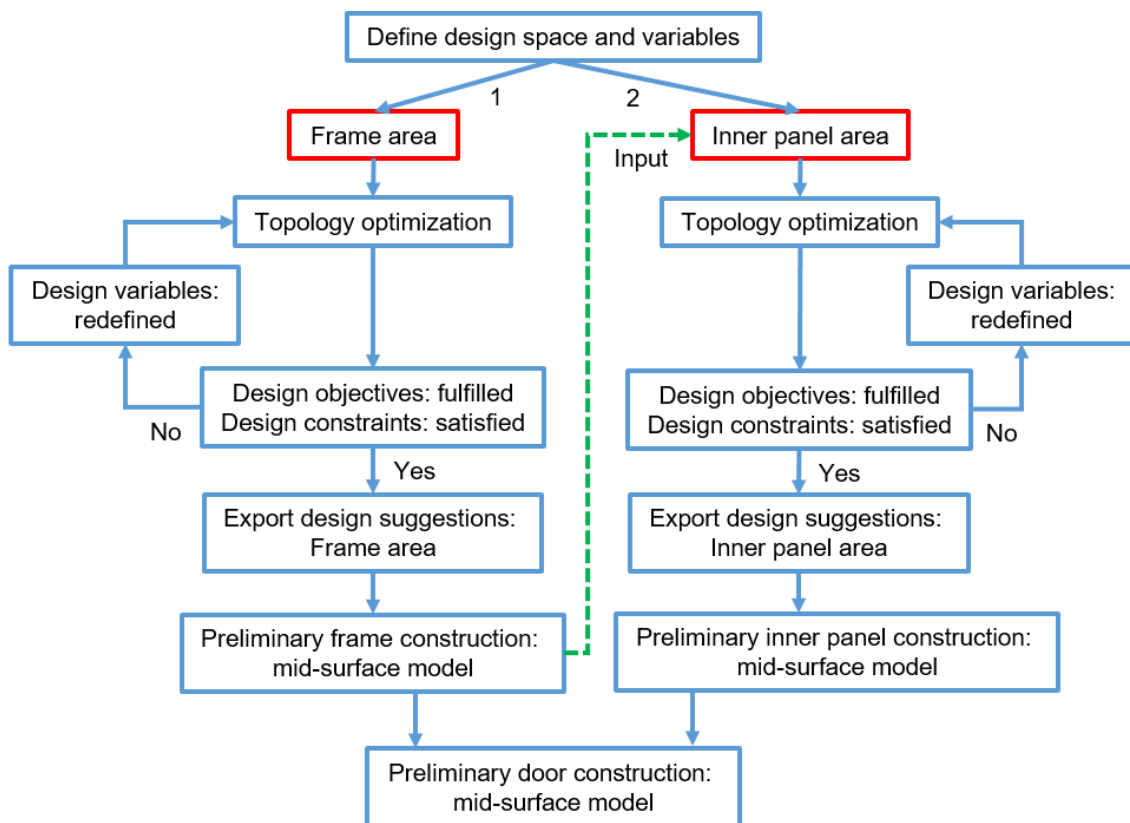
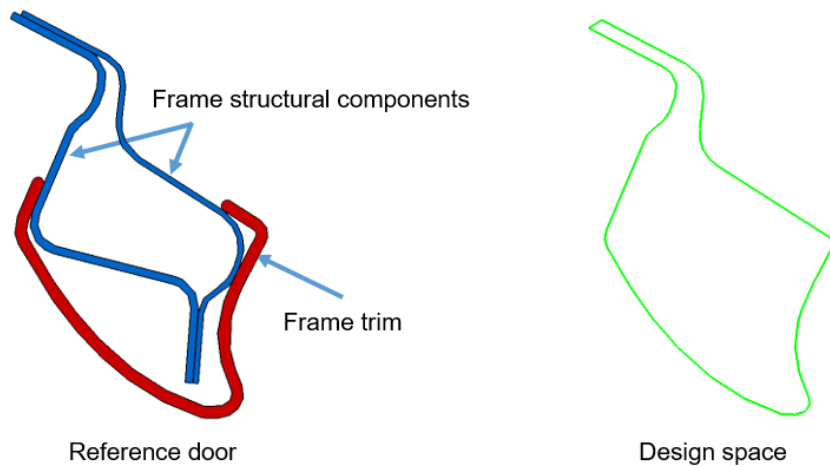
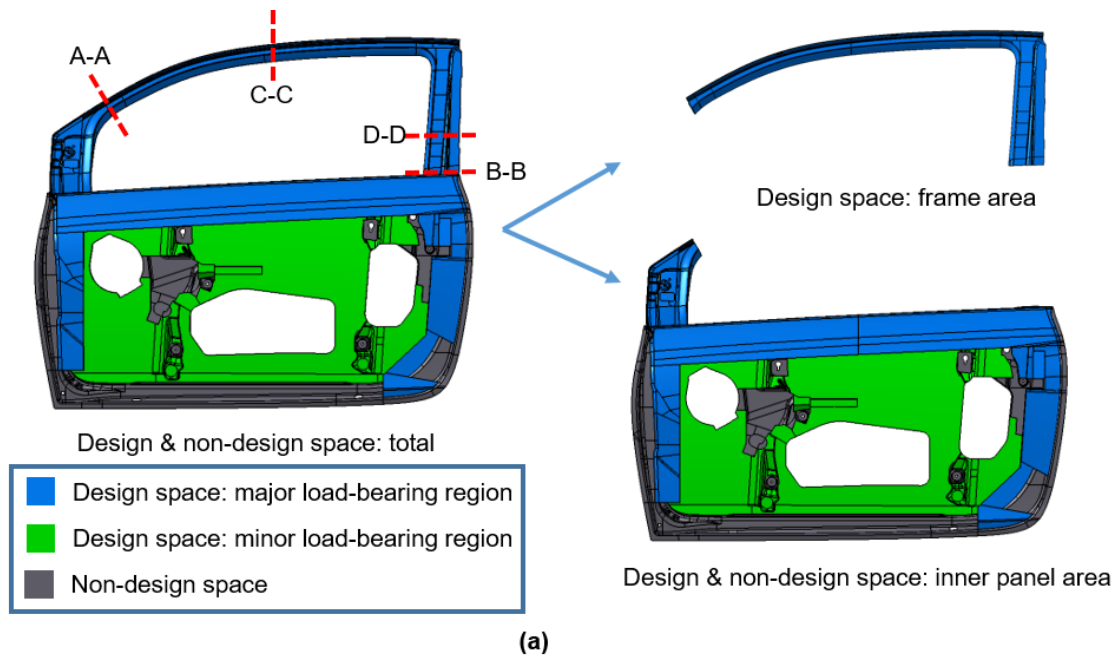


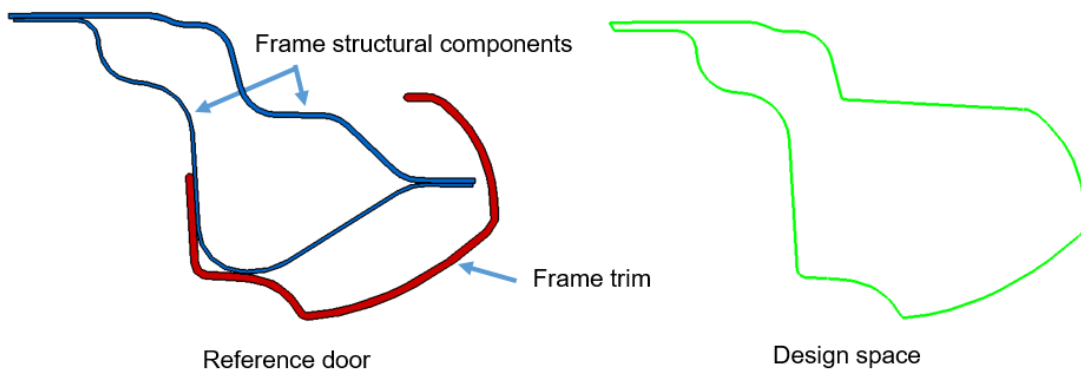
Figure 5-1 Concept 1: topology optimization process for the frame and inner panel area

5.1.1 Design space definition

Based on the CAD data (sheet metal components and function components) of the reference door, the maximal allowable design space and non-design space are defined in Figure 5-2a.



(b) Cross section: C-C



(c) Cross section: D-D

Figure 5-2 Design space definition (a); Cross section definition of the design space in the frame area (b)(c)

Almost all the contour of the design space matches the sheet metal parts of the reference door, except for the frame area. As illustrated in Figure 5-2b and c, compared to the reference door, the cross section is expanded to the inside surface of the frame trim for the new concept. This is reasonable, since the aluminum extrusion profiles have no welding flange (see Figure 3-2 in section 3.1.2), and the rubber sealing concept can be easily adapted. This has two obvious advantages: 1) the surface moment of inertia can be increased due to the enlarged cross section of aluminum profiles, which compensates for the lower E-modulus of aluminum in comparison to steel; 2) the same visual block area is kept at the upper A-pillar.

Following the new design principle shown in Figure 3-1, the total design space is categorized into a major load-bearing region and a minor load-bearing region (Figure 5-2a). During the definition of the design space, the original side impact beam and all important door functional components (e.g., loudspeaker, window regulation system, and latch) were taken into consideration. The mounting points/areas of those function components were defined as non-design space. As mentioned earlier, the total design space was separated at the section “A-A” and “B-B” into the frame area and the inner panel area (Figure 5-2a). Section “A-A” and “B-B” were defined in the position where the geometry of the frame cross section starts to change drastically. In this way, the design space of frame area has a relatively constant cross-section, which is important for further frame designs with aluminum extrusion profiles.

5.1.2 Frame area design

Since the frame area is only a part of the whole design space, the mechanical performance requirements (section 4.2) for the complete door cannot be directly applied here. These should be redefined specifically for the frame area with simplified boundary conditions. This is achieved by cutting a partial frame model from the reference door. The cutting position corresponds to the frame area design space (A-A and B-B in Figure 5-2a).

As illustrated in Figure 5-3, the simplified boundary conditions are defined at the cutting areas: DOF 1–6 are constrained on sections A-A and B-B. Two frame-related loading cases were chosen: frame stiffness B-pillar and middle (as described in Figure 2-33). The displacements following the loading direction at the force points under these two loading cases (see Table 5-1) are used as the mechanical requirement for further development of the frame area. The weight of the aluminum frame should be lower than the partial steel frame of the reference door.

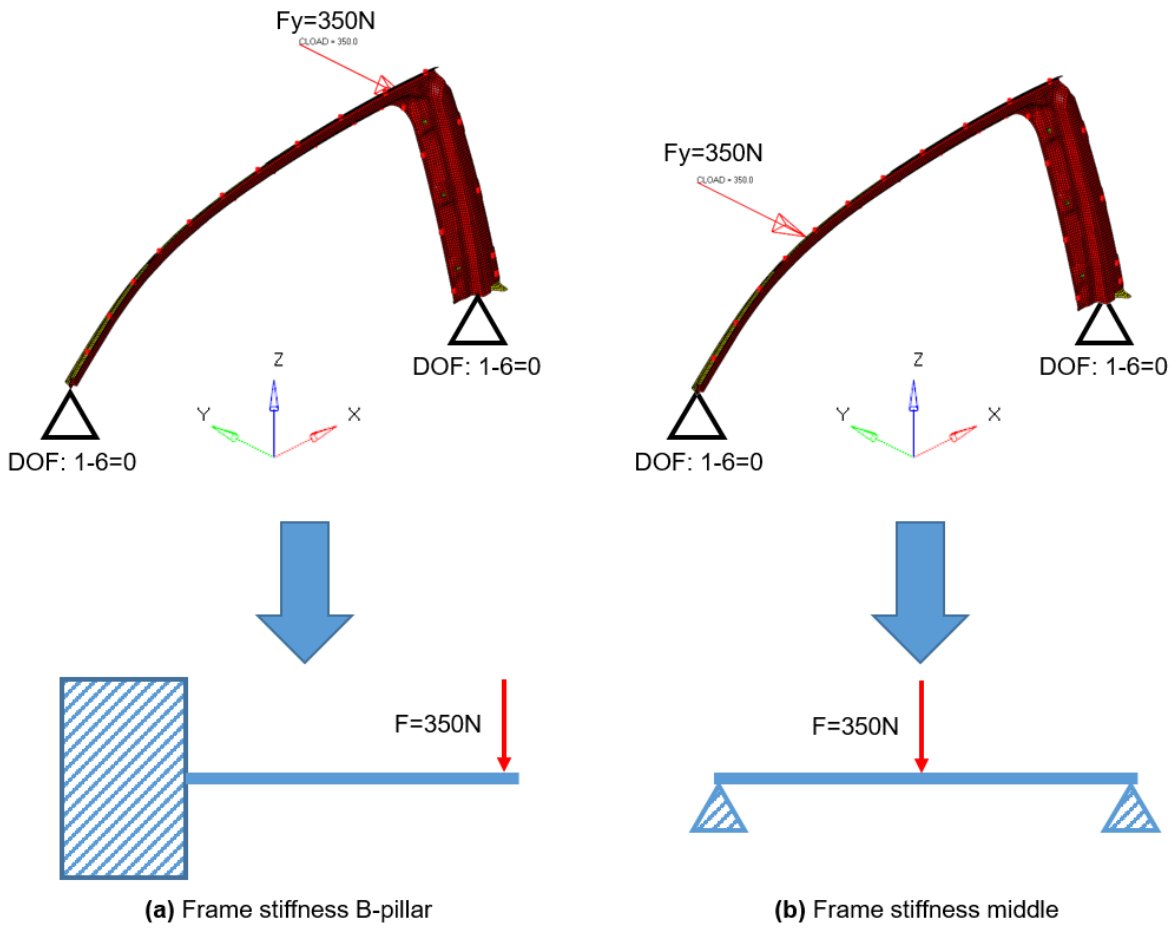


Figure 5-3 Partial frame of the reference door with simplified boundary conditions

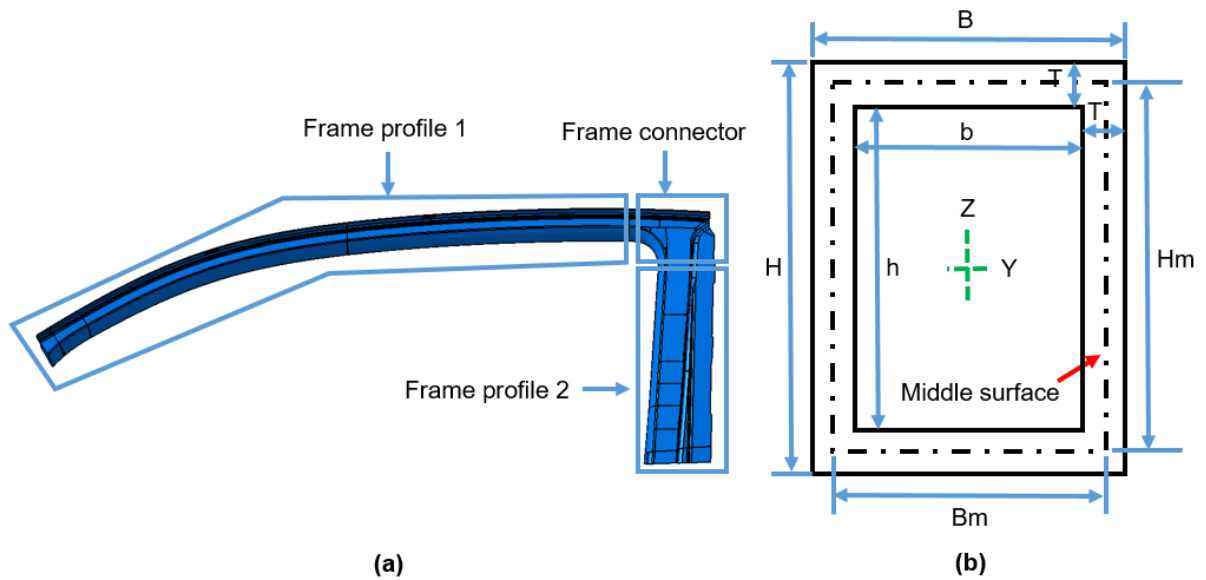


Figure 5-4 Frame sub design spaces (a) and a schematic of the “calculation rectangles” of the frame profile (b)

According to the consistency of the cross sections, the design space of the frame area is further divided into three sub design spaces (Figure 5-4a): 1) frame profile 1; 2) frame profile 2; and 3) frame connector. The design of the frame area starts with two profiles. The frame connector is only necessary if the two profiles cannot be welded together directly due to a substantial difference in the cross sections.

Several profile contours are sketched for the profile design. Trying to achieve the best possible thickness range of aluminum profiles by building the complete frame CAD and FEM model for every contour is inefficient; therefore, a simplified calculation method is used here by using the cross section of frame profiles. This is realized by simplifying the loading cases on the frame area to a cantilever and a 3-point-bending beam problem (Figure 5-3). Frame profile 1 is used here as an example to illustrate the calculation. Before the start of calculation, the middle surface contour of the reference steel frame and the aluminum profile is defined as a sketch in CAD (Figure 5-5). The “middle surface contours” of the reference and frame profile 1 are then converted into different “calculation rectangles” (Figure 5-5) according to the direction of the force. One important factor is to ensure that the areas of the “calculation rectangles” (Figure 5-5) are equal to its original “middle surface contour” (Figure 5-5). Subsequently, the moment of inertia I_z of the “calculation cross section” can be easily determined by inputting a specific thickness (T) (Figure 5-4b):

$$I_z = \frac{1}{12} * (B^3 * H - b^3 * h)$$

$$= \frac{1}{12} * ((B_m + T)^3 * (H_m + T) - (B_m - T)^3 * (H_m - T)) \quad \text{Formula 5-1}$$

The frame of the reference door is made of two steel sheet parts, which have a thickness of 0.7 mm and 1 mm. The average value of 0.85 mm is used here as the thickness (T) for the “calculation cross section” of the reference door. To make sure the performance of aluminum variation is the same or even better than that of the steel reference, the deflections on the aluminum variation should be equal or smaller than:

$$|W''_{\text{Steel}}| \geq |W''_{\text{Alu}}| \quad \text{Formula 5-2}$$

$$\frac{M_{\text{Steel}}}{E_{\text{Steel}} * I_{\text{Steel}}} \geq \frac{M_{\text{Alu}}}{E_{\text{Alu}} * I_{\text{Alu}}} \quad \text{Formula 5-3}$$

Since the loadings on both variations are the same, the moments are the same:

$$M_{\text{Steel}} = M_{\text{Alu}} \quad \text{Formula 5-4}$$

The E-modulus of steel is about three times that of aluminum:

$$E_{\text{Steel}} \approx 3E_{\text{Alu}} \tag{Formula 5-5}$$

$$3 * I_{z,\text{Steel}} \leq I_{z,\text{Alu}} \tag{Formula 5-6}$$

Therefore, the lower thickness limit of “frame profile 1” is:

$$T_{\text{Frame profile 1}} \geq 2.3\text{mm} \tag{Formula 5-7}$$

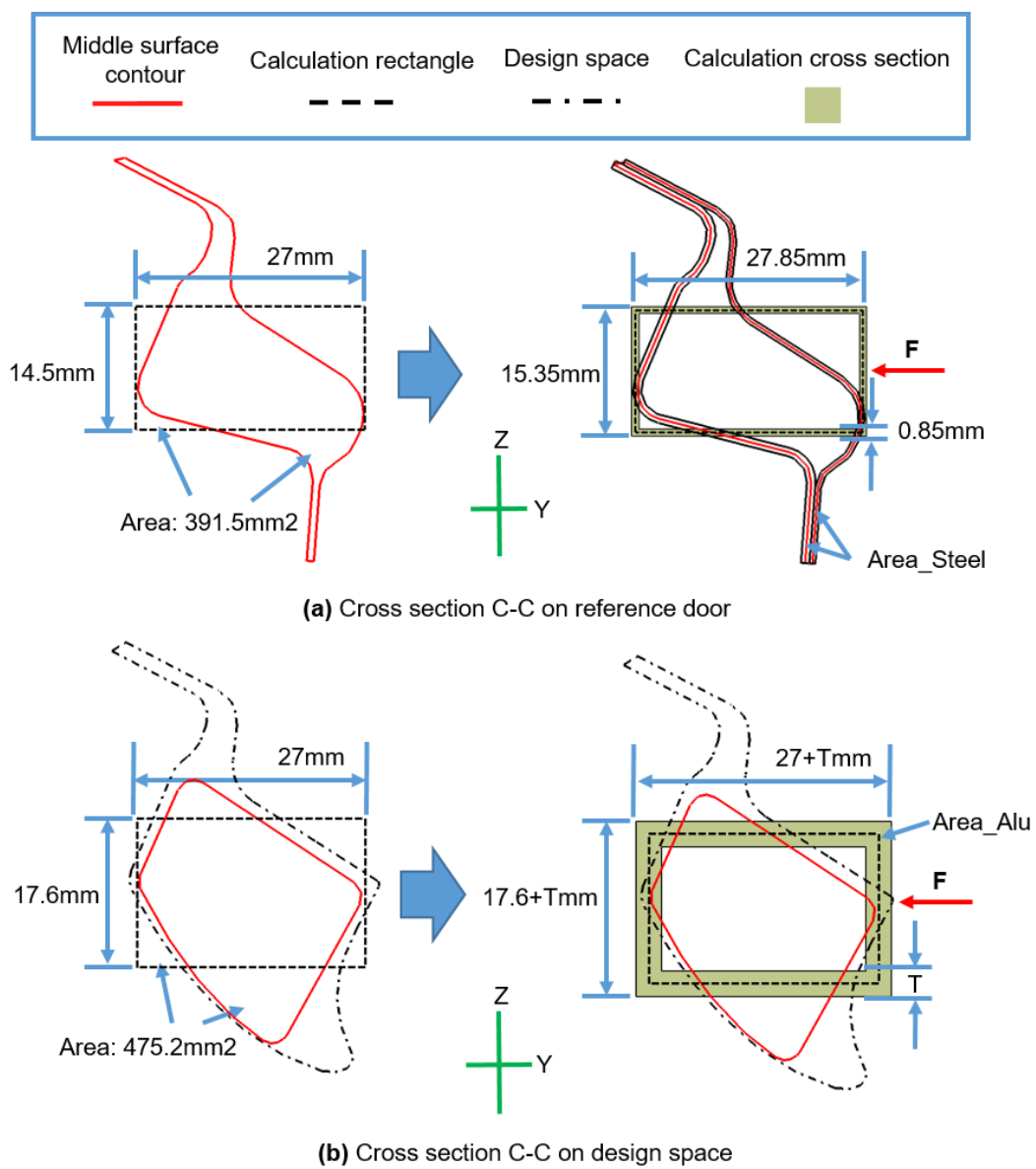


Figure 5-5 Simplified frame cross section calculation for the reference door and frame profile

Since the weight of the aluminum profiles should weigh less than steel reference:

$$m_{area_steel} \geq m_{area_alu} \quad \text{Formula 5-8}$$

$$\rho_{steel} * Area_Steel \geq \rho_{alu} * Area_Alu \quad \text{Formula 5-9}$$

$$\rho_{Steel} \approx 3 * \rho_{Alu} \quad \text{Formula 5-10}$$

The area relationship between the steel reference and the aluminum profiles (Figure 5-5):

$$3 * Area_Steel \geq Area_Alu \quad \text{Formula 5-11}$$

$$Area_Steel = 113mm^2 \quad \text{Formula 5-12}$$

The upper thickness limit of the “frame profile 1”:

$$T_{frame\ profile\ 1} \leq 3.8mm \quad \text{Formula 5-13}$$

According to the calculation, the thickness of frame profile 1 ranges from 2.3 to 3.8 mm. Using the same method, the middle surface contour and the thickness range of frame profile 2 are also determined; the thickness ranges from 2.3 to 4.4 mm. The final middle surface contour and the cross section of frame profiles 1 and 2 are illustrated in Figure 5-6a. Considering the feasibility of manufacturing (extrusion and forming) and the space for the joining areas, not all design space is occupied and the contour is possibly optimized. A significant difference in the frame cross sections also exists between the steel reference and the aluminum frames due to the omission of welding flanges.

Due to the constraint of the design space and a substantial contour difference in the frame profiles, the two profiles are difficult to join together directly by MIG-welding. To solve this problem, a frame connector made from the aluminum casting is designed as a platform to connect frame profiles 1 and 2. The design space for this frame connector is extracted from the available frame area design space (Figure 5-6b).

Since the frame connector is made of aluminum casting, the most efficient way to determine its geometry is to use topology optimization. The model, loading cases and boundary conditions in the topology optimization for the frame connector are the same as the partial frame from the reference (Figure 5-6b).

In the topology optimization of the frame connector, the previously determined thickness ranges of two frame profiles were used. Considering the possible loss of stiffness during the optimization and the uncertainties in the further joining area between the frame and the inner panel, the preliminary thicknesses of frame profiles 1 and 2 are determined conservatively with a sufficient safety factor (Table 5-1) and are set as 3 mm and 4.4 mm, respectively.

Unlike the standard setup (section 3.3.2), the mesh size of this topology optimization was 1 mm for both the shell and the solid elements. The volume fraction for the design space “frame connector” was defined as the constraint and should be lower than 0.54 to ensure a 10% weight reduction on the aluminum frame concept compared to the steel reference frame.

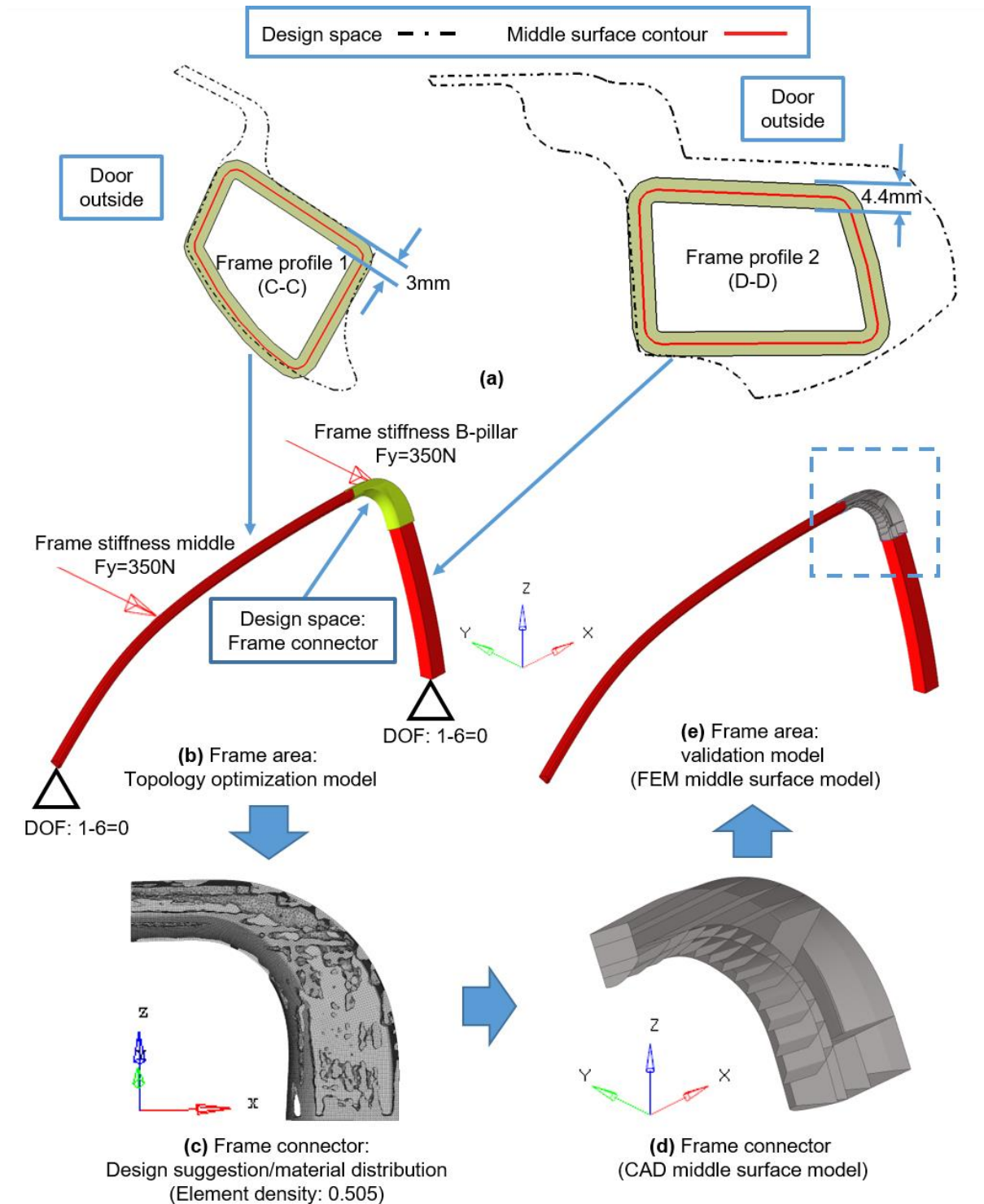


Figure 5-6 Frames 1 and 2: final middle surfaces with preliminary thickness (a); Frame connector: topology optimization model and static loading cases (b), material distribution (c), preliminary design (d); FEM validation model of the frame area (e)

The displacement results of the topology optimization (Table 5-1) indicate that the design is feasible. Based on the design suggestion/material distribution (Figure 5-6c) from the topology optimization, a preliminary middle surface CAD model of the frame connector was built (Figure 5-6d). The thickness range for the aluminum casting on this component is between 2.5 and 3.5 mm, and this range was placed in the FE model of the frame area to validate the performance of the complete concept frame (Figure 5-6e). Aluminum MIG welding was used to connect the frame connector to the profiles.

The validation result (Table 5-1) shows that the performance of the aluminum concept frame is better than that of the reference. The aluminum concept frame achieves a 12.2% weight reduction. To illustrate the geometries of the frame profiles intuitively, the cross sections with the thicknesses of both profiles are shown in Figure 5-6a. Note that the cross sections are only slightly larger than the design space (<1.5 mm), which is absolutely acceptable for a concept design. Based on this positive result, the aluminum concept frame with these parameters is used for further development of the structure of the inner panel area.

Model	Reference frame	Concept frame			
		Prior topology optimization	After topology optimization	Validation	
Loading cases	Y-Displacement (force point) (mm)	Y-Displacement (force point) (mm)	Y-Displacement (force point) (mm)	Y-Displacement (force point) (mm)	Difference to reference (%)
Frame stiffness B-pillar	0.738	0.695	0.720	0.735	-0.4%
Frame stiffness middle	1.722	1.306	1.441	1.507	-12%

Table 5-1 Mechanical performance of the aluminum frame concept from topology optimization and validation

5.1.3 Inner panel area design

After the successful determination of the concept in the frame area, the design space of the inner panel area can be further defined in detail. This is achieved by considering two important aspects: 1) splitting the sub design spaces - different components; 2) joining refinement – geometry and technique.

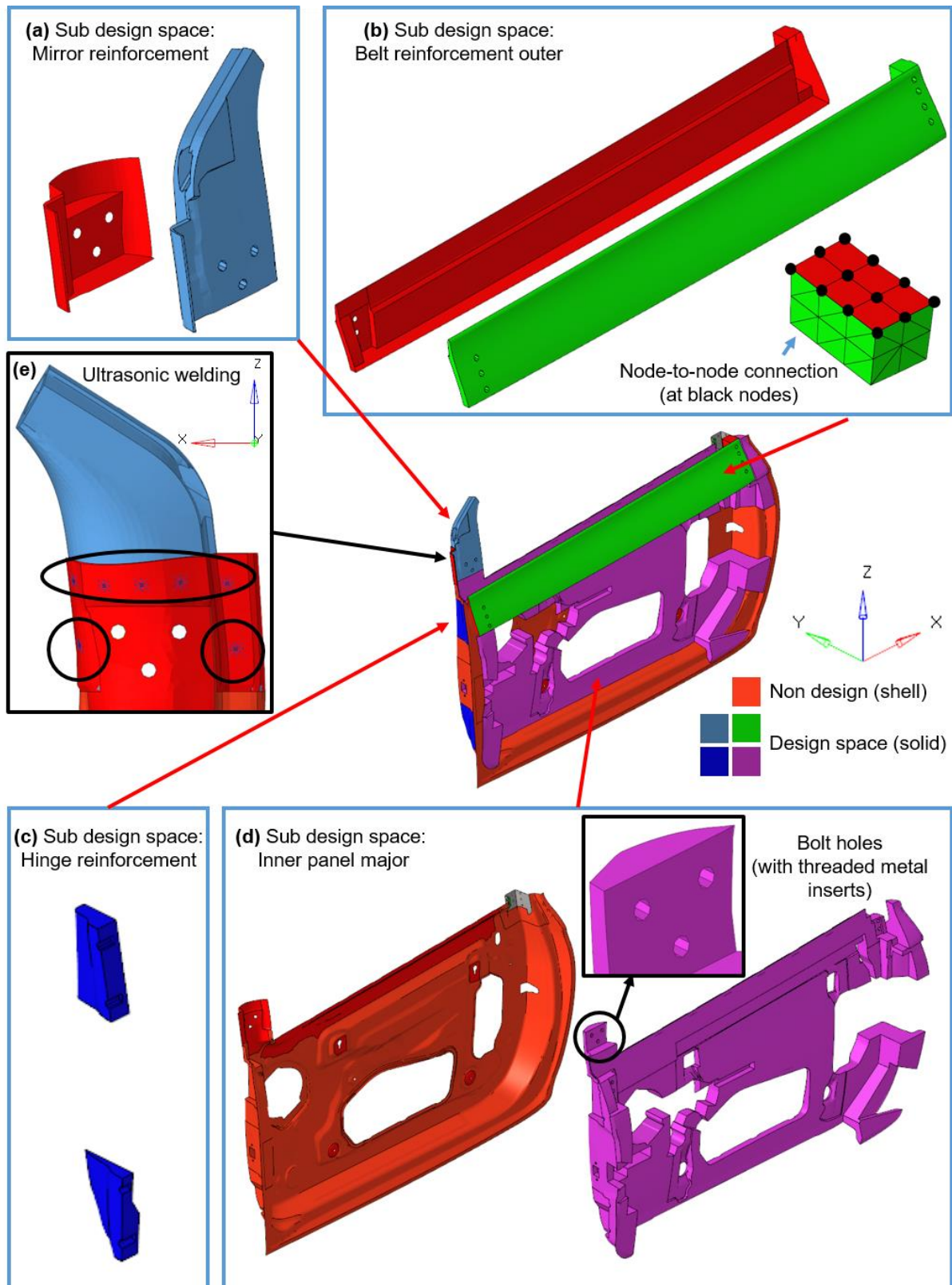


Figure 5-7 Concept 1: sub-design spaces in the inner panel area and the joining techniques

The sub design spaces are formed by separating the design space of the inner panel area into four different “sub-design spaces” (SDS): SDS-mirror reinforcement (Figure 5-7a), SDS-belt reinforcement outer (Figure 5-7b), SDS-hinge reinforcement (Figure 5-7c), and SDS-inner panel major (Figure 5-7d). A better material distribution from the topology optimization is achieved by adding a non-design shell layer to the volume design space. The -Y direction of

the vehicle global coordinate is set as the demolding direction for most SDSs, except for the SDS-hinge reinforcement. To ensure the In-Mold-Assembly (IMA) of threaded metal inserts in the hinge holes and an optimal rib construction, the demolding direction of the SDS-hinge reinforcement is set as the -X direction.

For joining refinement, two major problems need to be solved: 1) joining between the sub design spaces; 2) joining between the frame profiles and the sub design spaces. Bolts and threaded metal inserts were used to join the SDS-mirror reinforcement and SDS-belt reinforcement outer to the SDS-inner panel major. The threaded metal inserts were installed into the PP-LGF40 component during the compression molding process (IMA). The size (diameter=10 mm) and position of the bolt holes were defined in the design space. The required frame stiffness was achieved by additional ultrasonic welding to connect the SDS-mirror reinforcement and the SDS-inner panel major (Figure 5-7e). No joining is needed between the SDS-hinge reinforcement and the SDS-inner panel major since they belong to the same component.

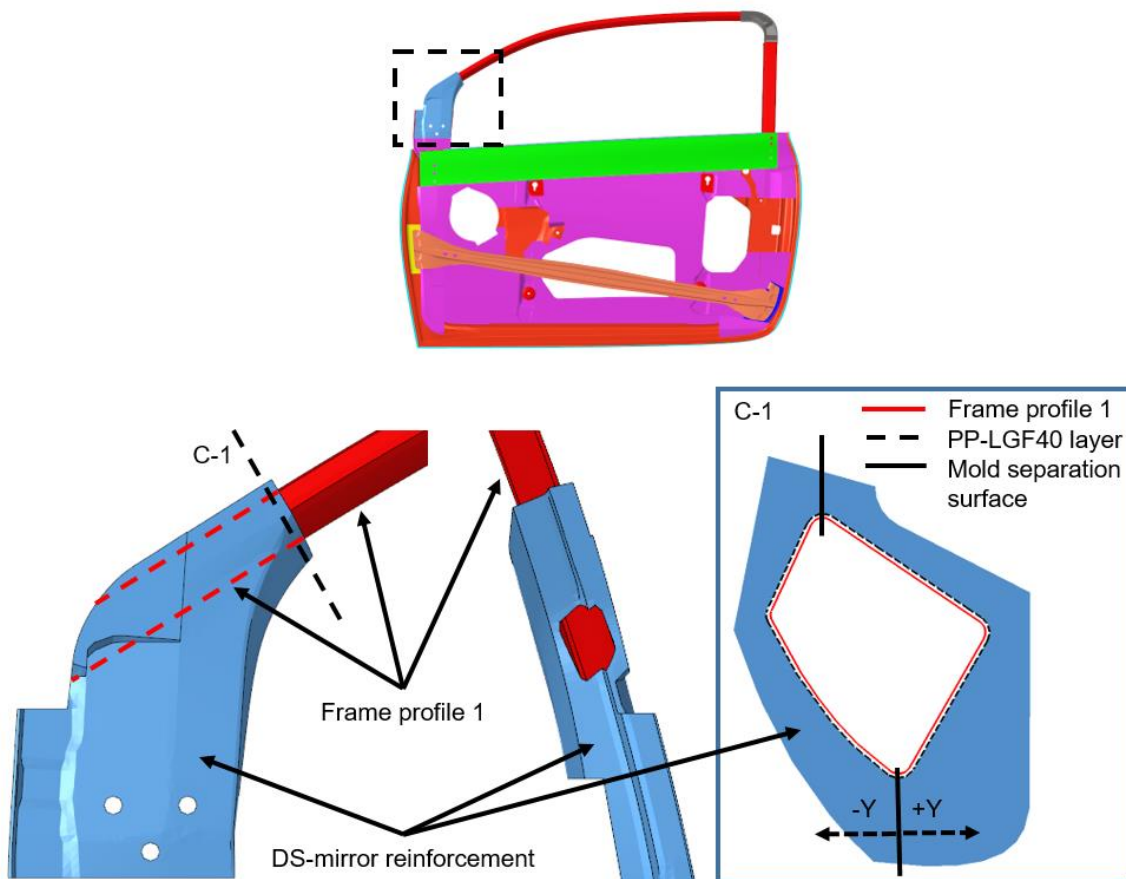


Figure 5-8 Concept 1: joining between frame profile 1 and the SDS-mirror reinforcement: over-molding with an adhesion promoter

Different joining techniques were used to connect the window frame profiles to the sub design spaces, as this joining is one of the major challenges and focuses of this work. The joining between frame profile 1 (aluminum) and the SDS-mirror reinforcement (PP-LGF40) is achieved using the adhesion promoter in the injection molding process, as this is currently an effective and reliable surface joining method in multi-material design [57; 77]. As shown in Figure 5-8, the SDS-mirror reinforcement is specially designed to ensure that frame profile 1 can go

through it and still leave enough design space for the rib construction. In this way, the mirror reinforcement can be directly over-molded onto frame profile 1.

Theoretically, two challenges limit this over-molding process: 1) aluminum profile sealing, which can be achieved by direct contact and geometry fitting between the end of profile and the wall of the mold; and 2) aluminum profiles can be deformed due to the high hydraulic pressure of fluid PP-LGF40. Depending on the stiffness of the aluminum profile, this can be solved by either adjusting the injection molding process parameters or using an insert to support the aluminum profiles (this is possible if the over-molded area of aluminum profiles is straight or has a constant bending radius).

The joining between frame profile 2 and the SDS-inner panel major was achieved with FDSs and bolts with threaded metal inserts and with the help of SDS-belt reinforcement outer (Figure 5-9). Estimation of the performance of joining before the topology optimization is difficult; therefore, a 360 degree joining concept was developed.

In this concept, the smart design involved trimming frame profile 2 in the joining area and extending it into the bolt connecting area between the SDS-inner panel major and the SDS-belt reinforcement outer, which not only shares the pre-defined bolt connections but also brings more stiffness into this complex joining area. An additional frame reinforcement is also added and joined to frame profile 2 with MIG welding. This then plays a role as a platform for the FDS installation and ensures the fixation of frame profile 2 in every direction with every surrounding component. The surrounding components should be able to provide enough support forces to frame profile 2; therefore, the geometries of the surrounding components were adjusted accordingly (Figure 5-9a). The section view (Figure 5-9b), shows that two over-molded aluminum sheet inserts are specially designed on SDS-inner panel major and SDS-belt reinforcement outer to guarantee a reliable FDS connection. The joining between the aluminum sheet inserts and PP-LGF40 is also achieved with the adhesion promoter. In this way, the aluminum profile and sheets can be connected directly with FDSs without any PP-LGF40 interlayer, thereby avoiding the possibility of losing joining strength due to the creep of PP-LGF40. The same design principle can also be found in the bolt connection areas. Overall, 11 FDSs and 2 bolts, together with surrounding components, builds two major load paths that provide a sufficient joining strength in this area.

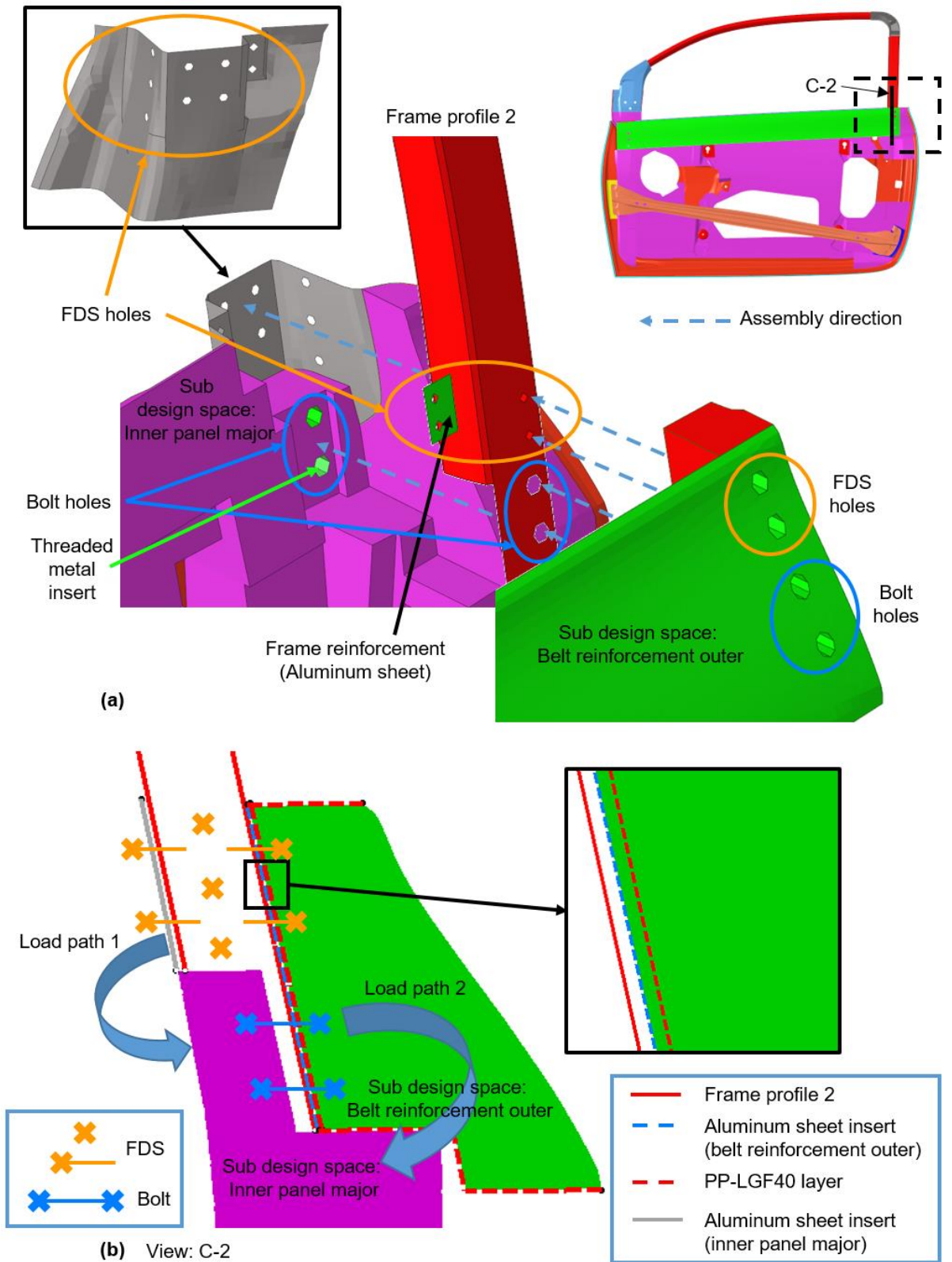


Figure 5-9 Concept 1: joining of frame profile 2, the SDS-inner panel major, and the SDS-belt reinforcement outer: exploded view (a) and section C-2 view (b)

In the topology optimization model for concept 1, the position and dimension of the UD tapes are determined according to the areas with a high load anisotropy state from the anisotropy analysis (see section 4.2.1). Based on the distribution of the anisotropy values (Figure 5-10a), three areas with UD tapes are defined, together with suggested fiber directions (Figure 5-10b): 1) UD frame; 2) UD belt inner; and 3) UD belt outer.

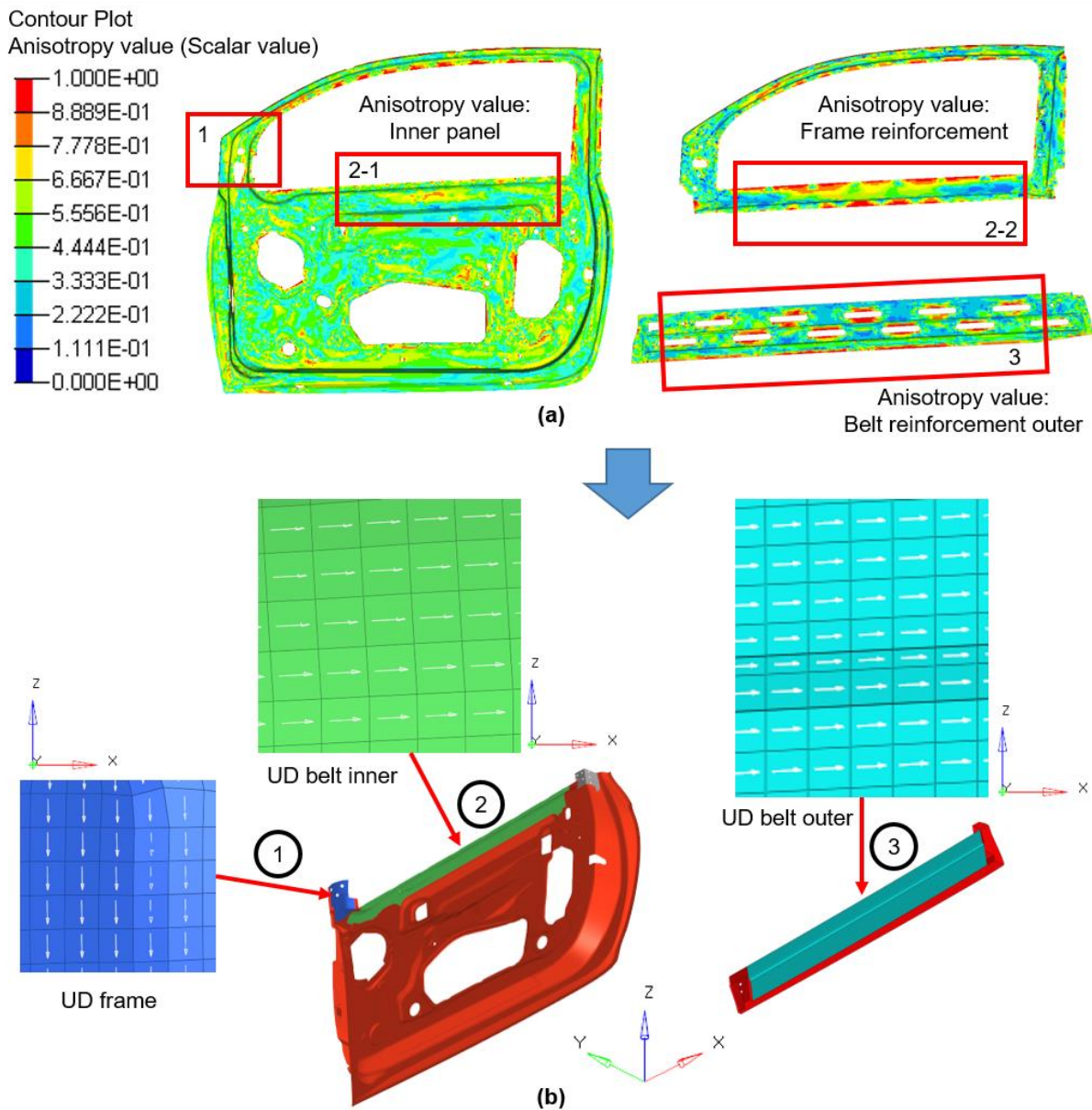


Figure 5-10 Concept 1: anisotropy analysis with the reference door (a); areas with UD tapes on the topology optimization model and the fiber direction (b)

To consider the pole crash loading case in the topology optimization of the door inner panel, besides the six static loading cases (see section 2.4.2), a substituted crash loading case was derived from the side pole crash simulation with the reference door (see section 4.2.2). Two sections were specially defined on the side impact beam (Figure 5-11a) in the area near the joining position to the inner panel. The peak section forces in the X and Y directions on these two sections from the crash simulation were defined as static forces in the topology optimization (Figure 5-11a). To join the steel side impact beam to the PP-LGF40 inner panel

by spot welding, two steel sheet inserts (coated with adhesion promoter) are designed on the inner panel in the joining areas (Figure 5-11b) and are pre-formed and joined to the inner panel by overmolding during the compression molding. The adhesion promoter enables bonding between the steel inserts and the LFTs. Besides the joining function for the crash beam, these steel sheet inserts also help to conducting the crash loading to the inner panel and the major load-bearing structure.

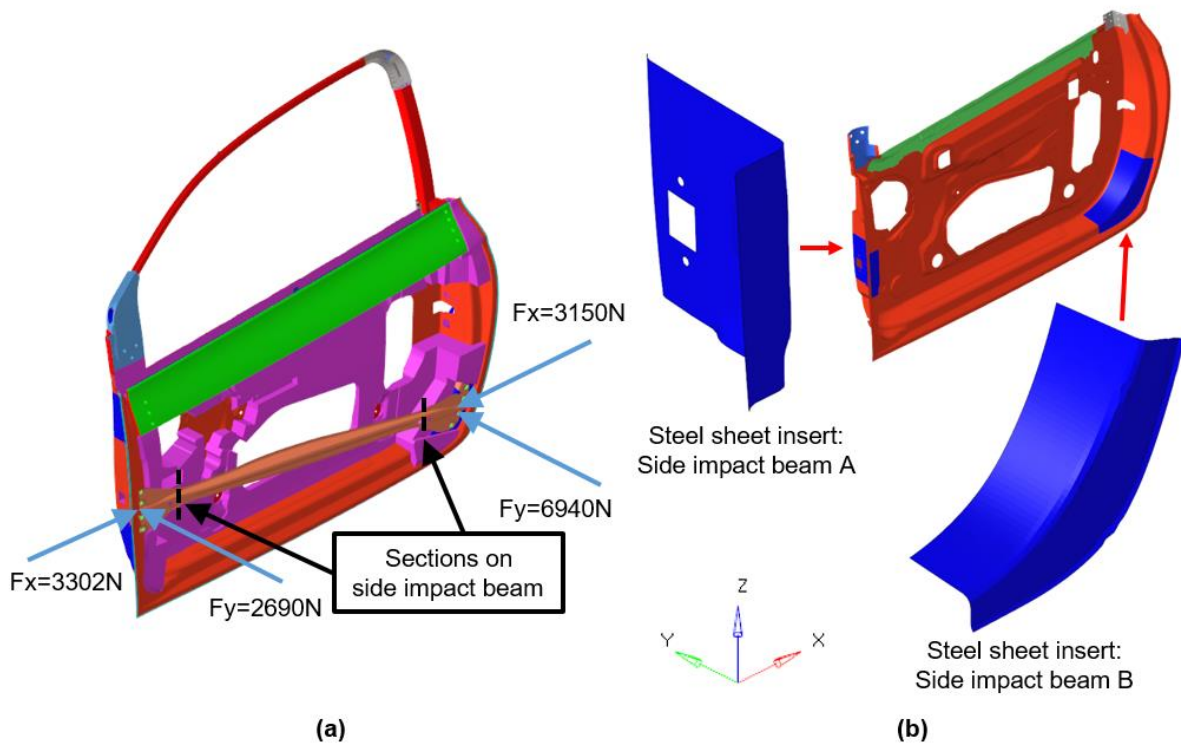


Figure 5-11 Concept 1: substituted crash loading case (a) and steel sheet inserts (b)

The topology optimization of the inner panel area was done after the definition of all the necessary parameters in the simulations (section 3.3.2). To achieve a 20% weight reduction, the maximal volume fraction of the PP-LGF40 was constrained to ca. 12%. Figure 5-12, Figure 5-13, and Figure 5-14 illustrate the achieved design suggestions/material distributions and the preliminary construction for the components “mirror reinforcement,” “belt reinforcement outer,” and “inner panel major.” Besides the standard topology optimization with all loading cases (a in Figure 5-12 to Figure 5-14), one additional optimization is done with the substituted crash loading case only (b in Figure 5-12 to Figure 5-14). This is done to achieve a clearer material distribution in the crash relevant areas, such as the joining area between the side impact beam and the “inner panel major.” Accordingly, the preliminary designs of the “mirror reinforcement” (Figure 5-12c), “belt reinforcement outer” (Figure 5-13c), and “inner panel major” (Figure 5-14c) were achieved by combining the material distributions from both topology optimizations. All UD tapes and metal inserts (threaded metal inserts and metal sheet inserts) are transferred directly from the topology optimization model to the preliminary design without major changes.

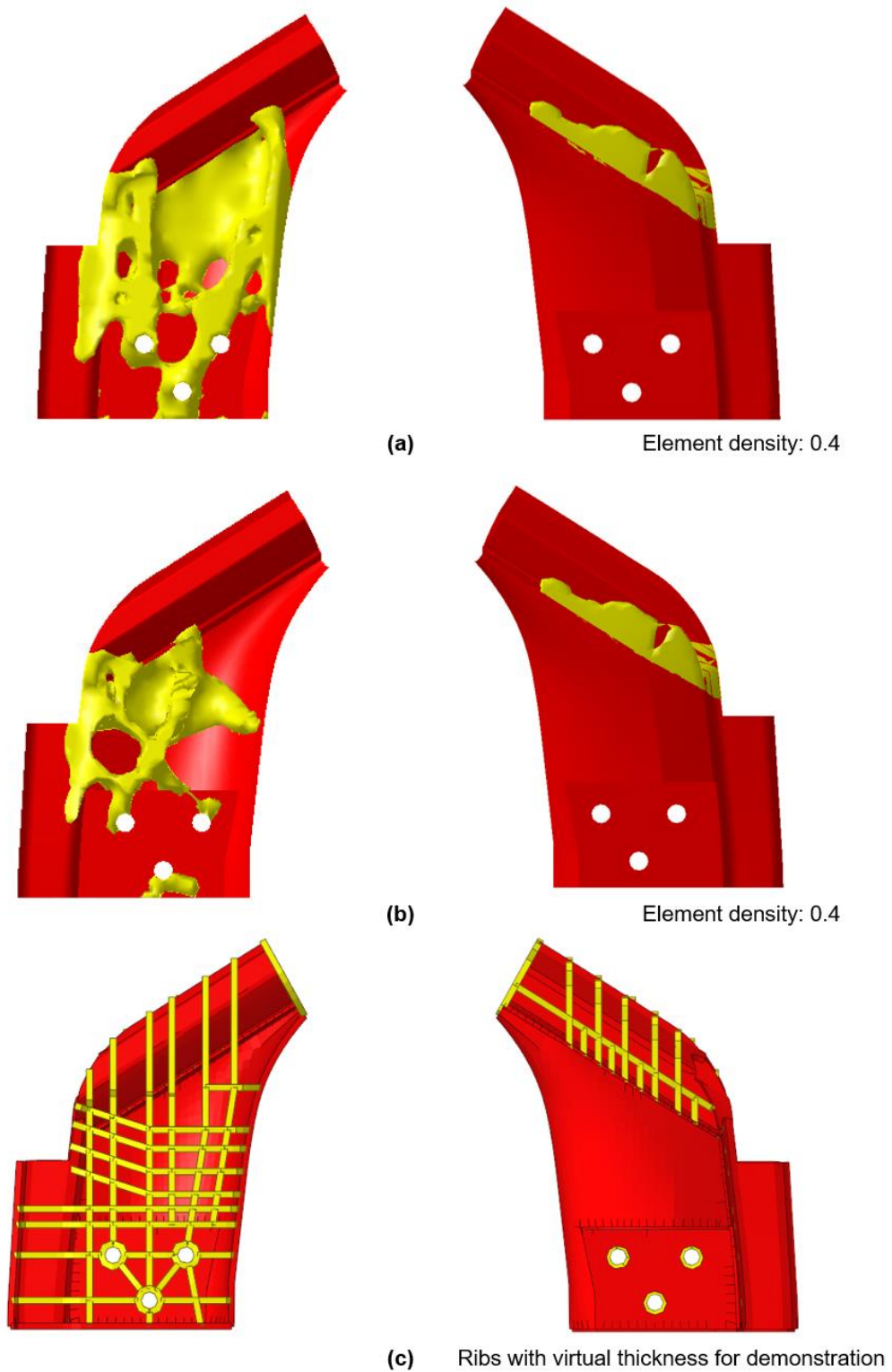


Figure 5-12 Concept 1: mirror reinforcement - material distribution (topology optimization) and component structure (middle surface): (a) static + substituted crash loading; (b) substituted crash loading case only; (c) Surface and rib construction with virtual thickness

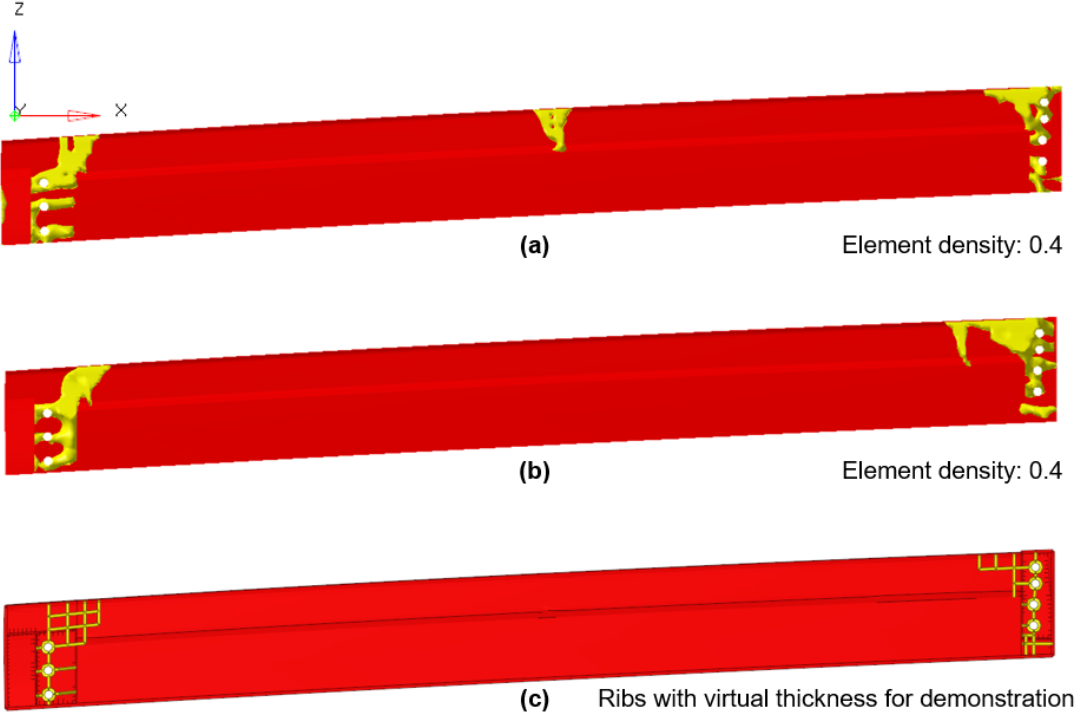


Figure 5-13 Concept 1: belt reinforcement outer - material distribution (topology optimization) and component structure (middle surface): (a) static + substituted crash loading; (b) substituted crash loading case only; (c) surface and rib construction with virtual thickness

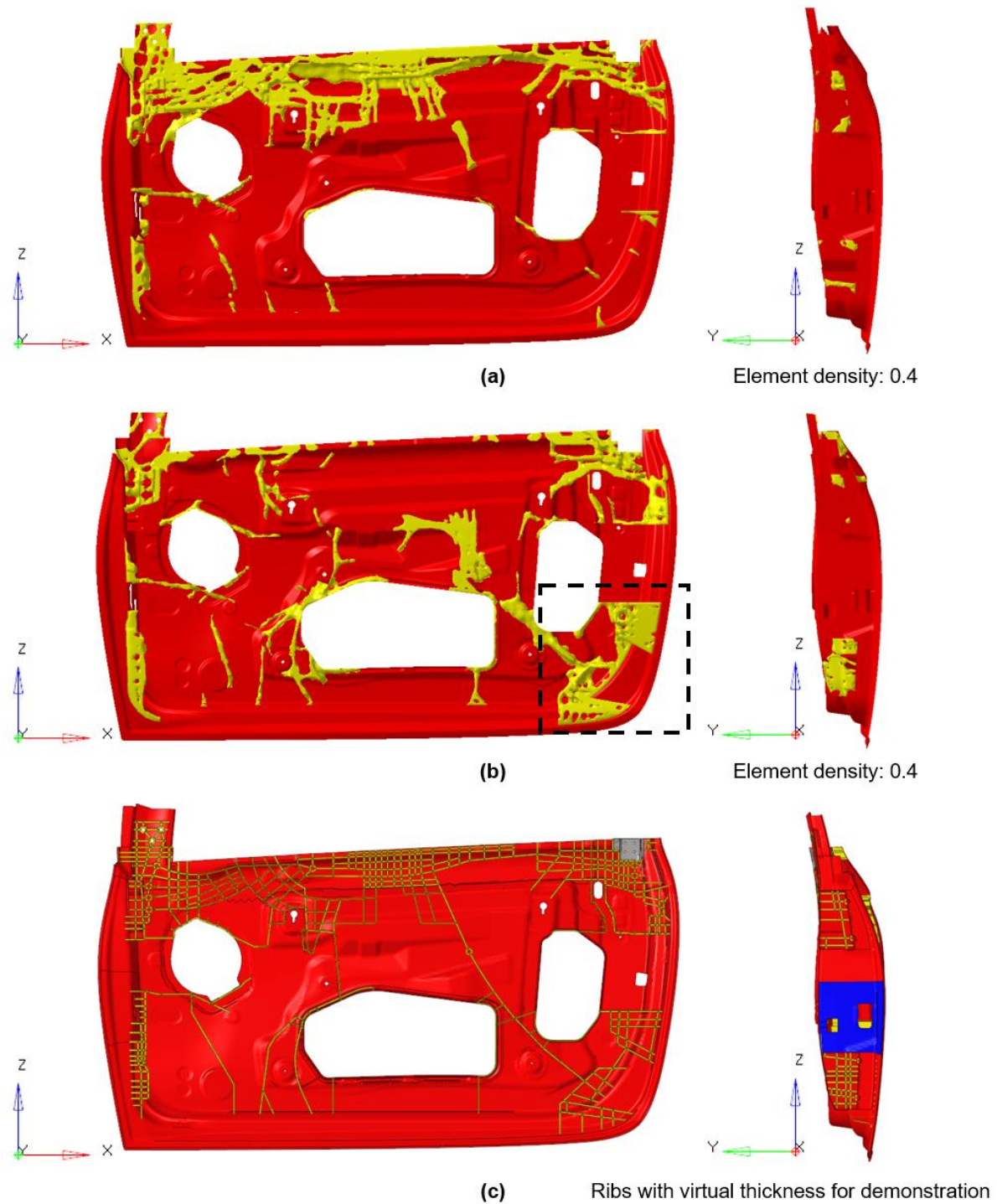


Figure 5-14 Concept 1: inner panel major - material distribution (topology optimization) and component structure (middle surface): (a) static + substituted crash loading; (b) substituted crash loading case only; (c) surface and rib construction with virtual thickness

5.2 Concept 2

The principal of the structural development with topology optimization for concept 2 is identical to that for concept 1. To avoid unnecessary repetition, the description in this section will focus on the important design differences and innovations on concept 2.

5.2.1 Design space definition

The total design space for concept 2 is the same as for concept 1 (see section 5.1.1). Since door concept 2 has a roof-integrated construction (i.e., the window frame belongs to the inner panel), no further separation of the design spaces for the frame area was needed.

5.2.2 Frame and inner panel area design

The total design space of concept 2 is separated into sub-design spaces for different components, while considering the joining technique (method and geometry). Three different sub-design spaces (SDS) are defined: SDS-belt reinforcement outer (Figure 5-15a), SDS-hinge reinforcement (Figure 5-15b), and SDS-inner panel major (Figure 5-15c). Similar to concept 1, the -Y direction of the vehicle global coordinate is set as the demolding direction for most SDSs, except for SDS-hinge reinforcement. The In-Mold-Assembly (IMA) of the threaded metal inserts in the hinge holes and an optimal rib construction are ensured by setting the demolding direction of the SDS-hinge reinforcement as the -X direction.

Besides the sub design spaces, the reinforcing closing plate (Figure 5-15d) for the window frame is specially designed to increase the frame stiffness, based on a preliminary performance investigation in the frame area. As illustrated in Figure 5-15 (section A-A), due to the demolding direction constraint of the SDS-inner panel major, only the opening profile can be achieved in the frame area with the surface on the inner panel, making it very inefficient for holding bending moment even with the rib reinforcements. To solve this problem without adding too much extra weight, the reinforcing closing plate is added to achieve a closing cross section together with existing frame surfaces on the inner panel.

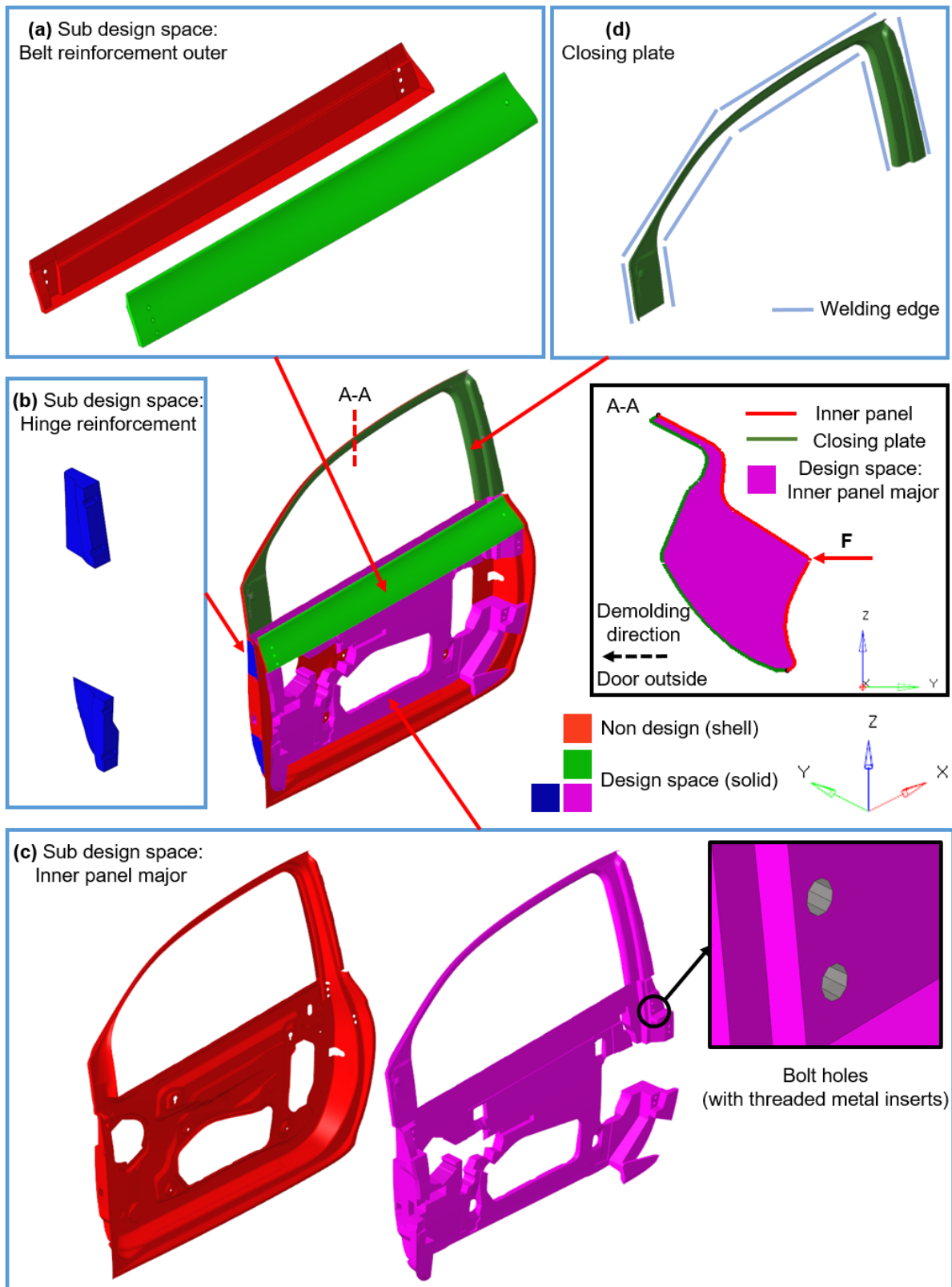


Figure 5-15 Concept 2: sub-design spaces and joining techniques

Further investigation in the frame area is also made on the material usage with a simplified calculation method. As mentioned in the concept 1 development, the cross sections of the reference door and the design space are simplified as rectangles and calculated with two simplified frame-related loading cases (Figure 5-16a and b). Since no concrete component is constructed at this moment, estimating the effect of the rib structures on the frame stiffness is difficult. For this reason, the possible stiffness provided by rib structures on the frame of the concept door is neglected in this simplified calculation.

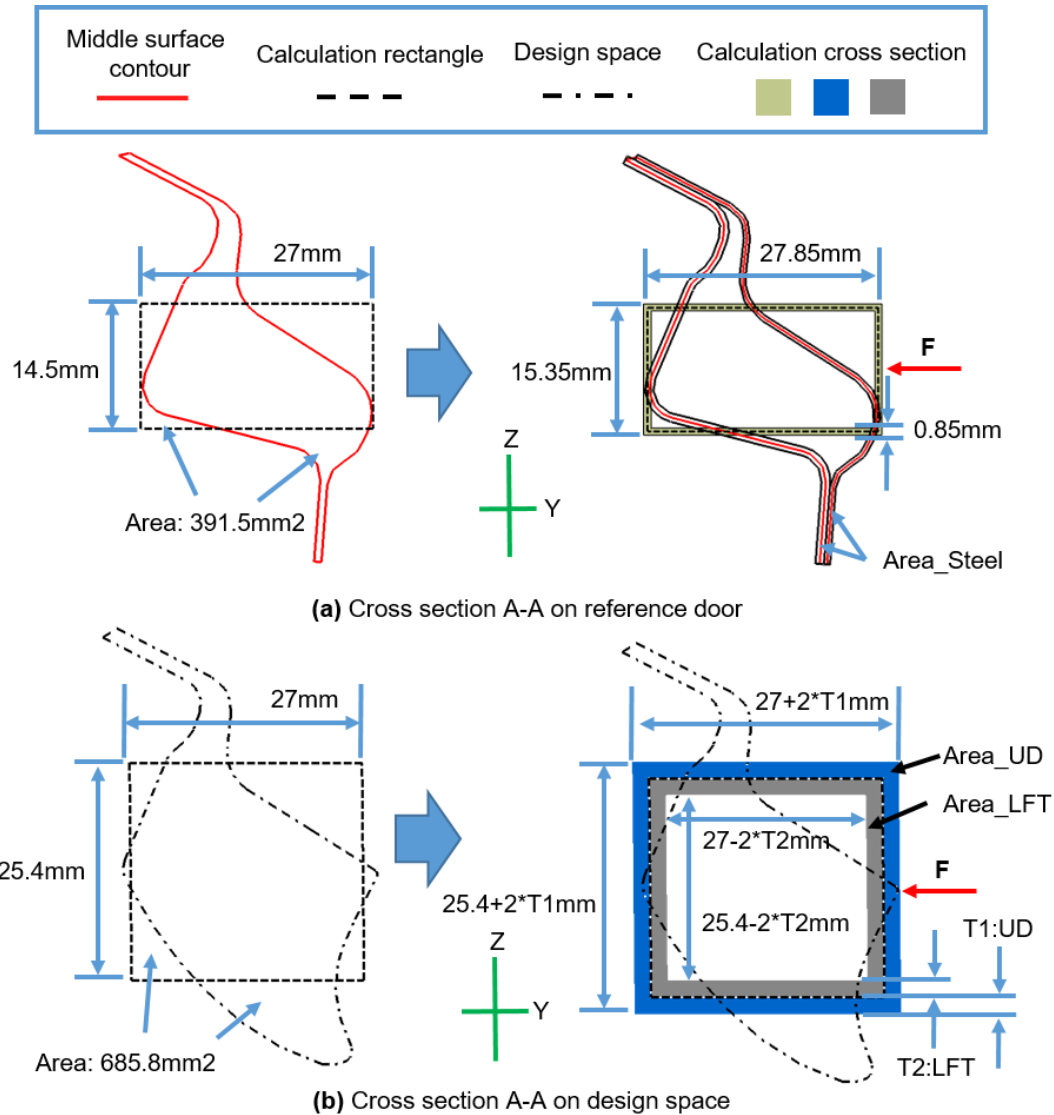


Figure 5-16 Concept 2: simplified frame cross-section calculation (reference door and frame concept)

With this simplified calculation method, the thickness range/combination is tested by using the parameters given in Figure 5-16 and the relationship between the deflections, E-modulus, and the moment of inertia. To reach the same or an even higher performance level, the frame deflection on concept 2 should be smaller than or at least the same as that of the reference. The area mass on the cross section must be lower to ensure the weight reduction. Based on these requirements and the calculation results, the following conclusions can be made: (1) A frame made of pure PP-LGF40 cannot reach the aimed stiffness in a manufacturable thickness range (typically 2 to 4 mm); and (2) The “UD tapes + PP-LGF40” combination is a promising

and practical solution for the frame area and can reach the aimed stiffness and still achieve a certain amount of weight savings (Figure 5-16b). For example, according to the calculation result, using 1.85 mm UD tapes and 2 mm PP-LGF40 on cross section A-A can achieve a comparable frame stiffness to the reference with ca. 26% weight savings (Figure 5-16b). Since the influence of possible rib structures cannot be considered in the simplified calculation, an accurate thickness and region of the UD tapes and LFT can only be achieved by further topology optimizations.

For the joining technique, bolts and threaded metal inserts are used to join the SDS-belt reinforcement outer and SDS-inner panel major. The threaded metal inserts are installed into the PP-LGF40 component during the compression molding process (IMA). The size (diameter=10 mm) and position of the bolt holes are defined in the design space (Figure 5-15c). No joining is needed between the SDS-hinge reinforcement and the SDS-inner panel major since they belong to the same component. The closing plate can be joined to the inner panel on the edge (Figure 5-15d) using either ultrasonic welding or infra-red welding, depending on the final geometry on the manufactured door model.

In the topology optimization model for concept 2, four areas with UD tapes are derived from the anisotropy analysis (Figure 5-17a) and defined with suggested fiber directions (Figure 5-17b): 1) the UD frame; 2) the UD belt inner; 3) the UD belt outer; and 4) the UD closing plate.

The substituted crash loading case in concept 1 is also used in the topology optimization of concept 2 (Figure 5-18a). The joining solution between the steel side impact beam and the PP-LGF40 inner panel (steel sheet inserts + spot welding) is also retained (Figure 5-18b).

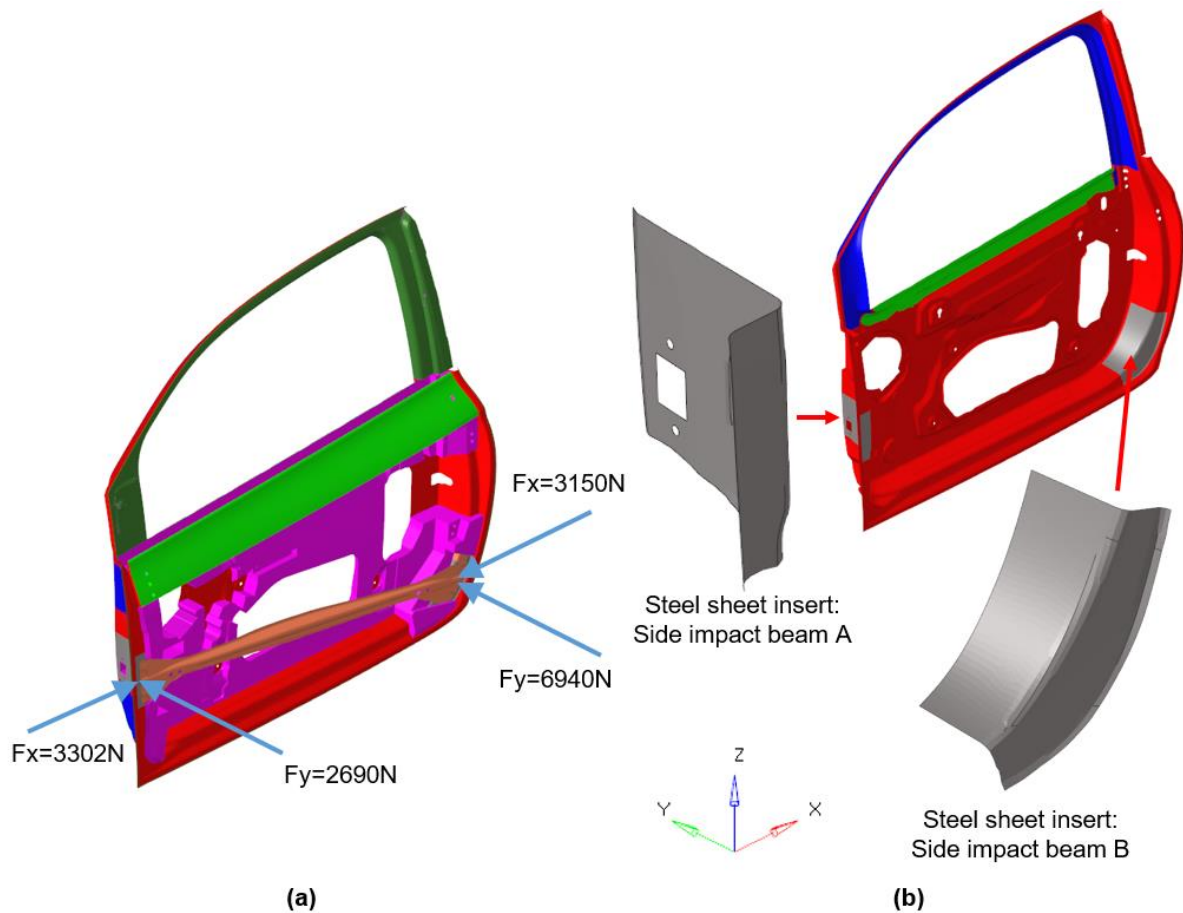


Figure 5-18 Concept 2: substituted crash loading case (a); steel sheet inserts on the inner panel (b)

Specifically, for the topology optimization of concept 2, the maximal volume fraction of PP-LGF40 is constrained as ca. 10% to achieve a 20% weight reduction. Figure 5-19 and Figure 5-20 illustrate the achieved design suggestions/material distributions and the preliminary construction for components “belt reinforcement outer” and “inner panel major”. Optimization results with the substituted crash loading case only are also given in Figure 5-19b and Figure 5-20b. As with concept 1, the preliminary constructions are achieved by combining the material distributions from both topology optimizations. All UD tapes and metal inserts (threaded metal inserts and metal sheet inserts) are transferred directly from the topology optimization model to the preliminary construction without major changes.

So far, a comparison on the preliminary CAD constructions between concept 1 and 2 can be made. As for the similarities, except for the frame areas, the base surface geometries of the core component “inner panel major” are almost identical on both concepts. Meanwhile, rib structures in hinge, belt and crash beam joining areas are also closely resembled on both concepts. It is not hard to explain this situation since these areas belong to the major load-bearing structure and are majorly responsible to crash loading cases. Similar dominated

loading cases leads to similar rib structures in these regions. The steel sheet inserts in the crash beam joining areas are also identical on both concepts.

Clear differences on both concepts can be found on the frame structures. Due to the different material usage on the window frame and different required joining techniques accordingly, a large difference of the rib construction can be majorly found in the frame-to-inner-panel transition areas. Rib structures in these transition areas on two concepts are very intensive but complete different. For the same reason, UD Tapes are applied in different local areas on two concepts, especially for the frame areas.

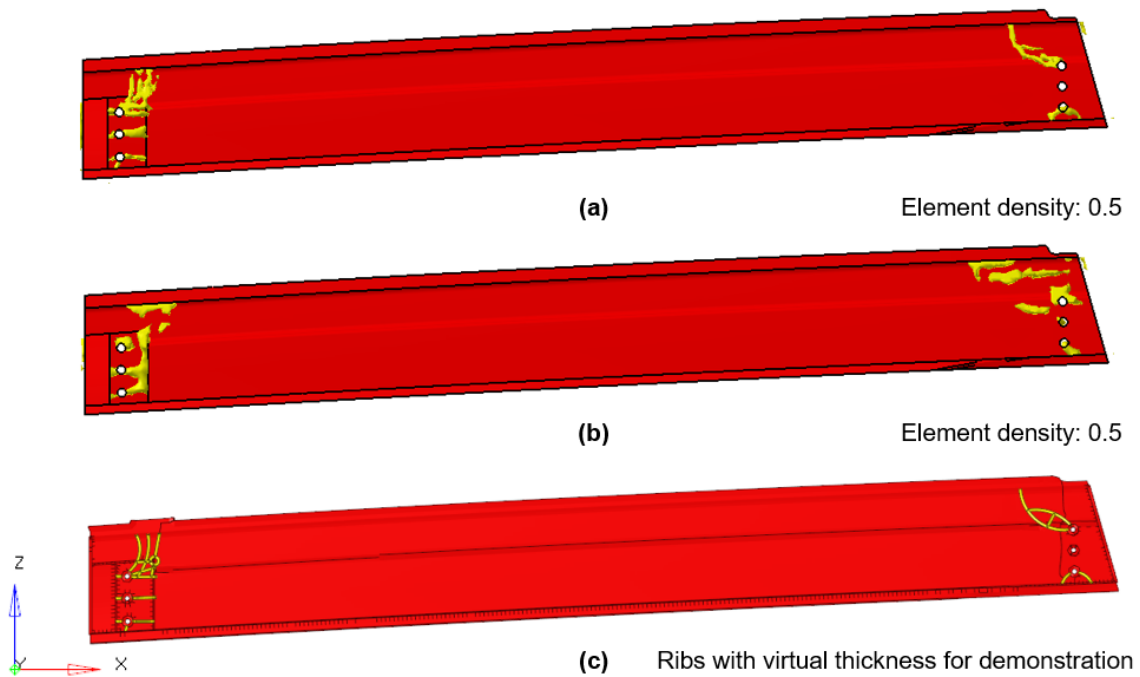


Figure 5-19 Concept 2: belt reinforcement outer - material distribution (topology optimization) and component structure (middle surface): (a) static + substituted crash loading; (b) substituted crash loading case only; (c) surface and rib construction with virtual thickness

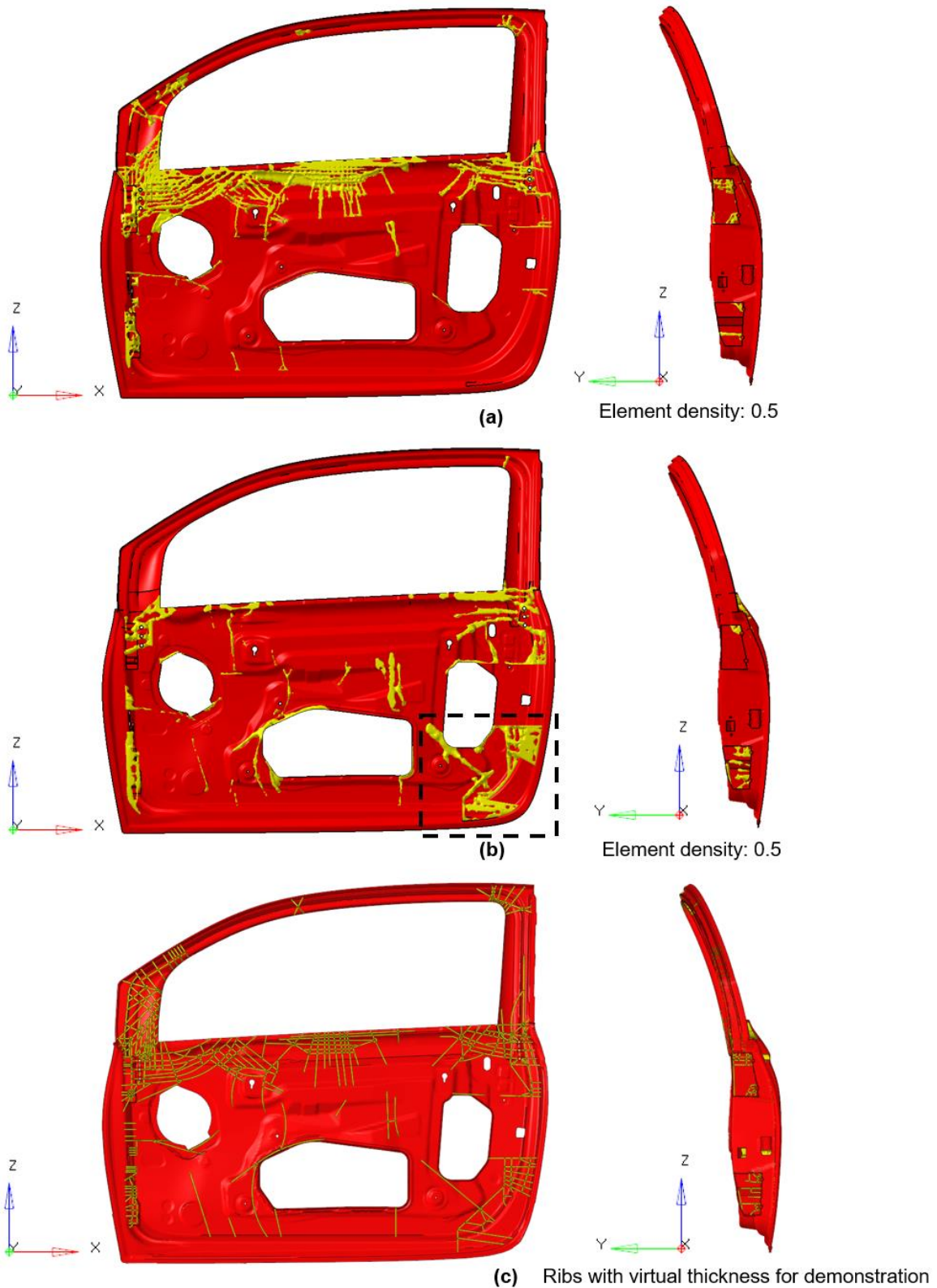


Figure 5-20 Concept 2: inner panel major - material distribution (topology optimization) and component structure (middle surface): (a) static + substituted crash loading; (b) substituted crash loading case only; (c) surface and rib construction with virtual thickness

6 Door concept, structural validation, and parameter optimization

6.1 Concept 1

After structural development of the frame area and the inner panel area, the newly developed components were assembled as the preliminary door concept 1. The static simulation of this preliminary door concept 1 was done with the same hinge and hinge-pillar setups and loading cases used in the reference door simulation (see section 2.4.2 and section 3.3.1). As illustrated in Table 6-2, the static performance and weight of the preliminary door concept 1 are close to the pre-defined design goal. However, the deficiencies on the loading cases “frame stiffness middle,” “over opening,” “belt stiffness inner,” and weight reduction are not negligible, but they can be optimized through parameter optimization.

The following parameters on the preliminary door concept 1 are changed manually or optimized with the parameter optimization using Optistruct:

- Frame profiles 1 and 2: The thickness of the aluminum profiles for frames 1 and 2 was optimized in the range of 2.3 to 3.8 mm and 2.3 to 4.4 mm, respectively (defined in section 5.1.2). Slight thickness changes can be seen in Figure 6-1 compared to Figure 5-6.
- Frame connector: The ribs were reduced due to manufacturing difficulties. The rib thickness was optimized in a range from 2 to 4 mm.
- Mirror reinforcement: The base surface and the rib thickness were increased to 3.5 mm
- Belt reinforcement outer: The base surface thickness was reduced to 2.75 mm.
- Inner panel major: The local base surface thickness was increased to 3.5 mm, in such regions as the mirror reinforcement, the door stopper, and the belt on the inner panel, which have a direct and substantial influence on the unsatisfied loading cases. The rib thickness was further optimized in a range from 2 mm to 3.5 mm.

The optimized door concept 1 (Figure 6-1) is achieved after parameter optimization. The important design parameters and manufacturing methods for this optimized door are summarized in Table 6-1.

For the manufacturing processes, compression molding is preferred for the components “belt reinforcement outer” and “inner panel major” as these require a longer average fiber length for a better crash performance [18]. The injection molding is chosen for the overmolding of the “mirror reinforcement” onto “frame profile 1”. Considering its molding difficulty with such complex part geometry, it is not feasible for the compression molding process.

For this optimized door concept 1, manufacturing restrictions were also taken into account. Since the rib distance and the rib height are key factors for the feasibility of manufacturing, the following general restrictions were applied to both manufacturing methods: 1) average rib distance 10 mm; and 2) average rib height 40 mm. The average rib distance and rib height of the optimized door 1 (Table 6-1) proves its manufacturability to a large extent.

Nevertheless, a very small number of ribs in this design violate the manufacturing restrictions on the rib height due to the package constraint defined in this work. An investigation of high ribs shows that the fixation of the inner panel depth and the fixed position of the door stopper are two major reasons for this violation. For example, some of the top surfaces of the high ribs

are the joining surface for the “belt reinforcement outer” to “inner panel major”. Reducing the height of these ribs is difficult without a local depth change on the door inner panel. Some high ribs on the side wall of door inner panel are also built to provide a surface for installing the door stopper at its original position. For these necessary high ribs, a theoretically feasible design is used in this work to define the extreme situation where the ribs are 129 mm high, with a 3.5 mm bottom thickness and a 0.5° draft angle [165; 166].

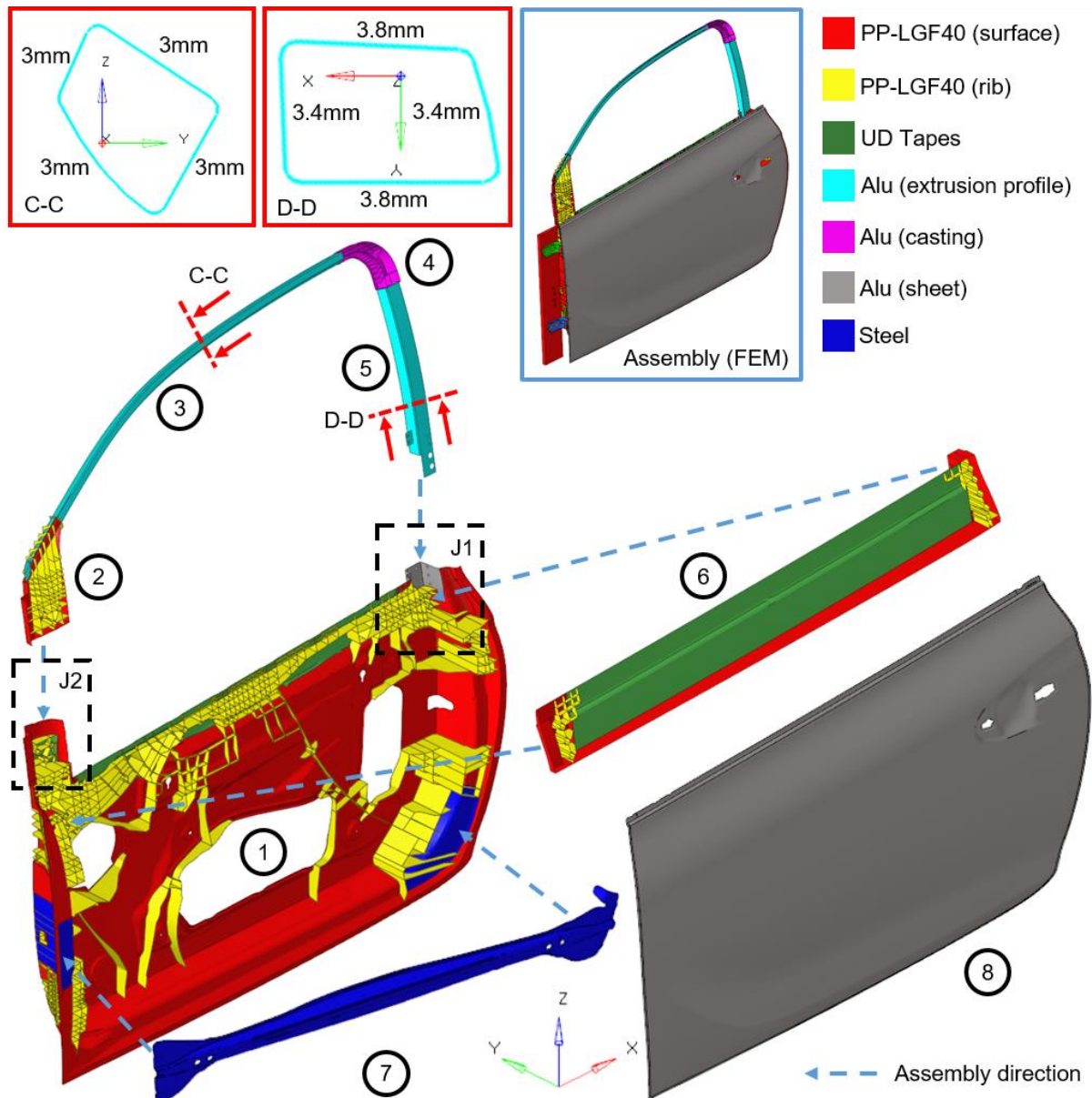


Figure 6-1 Concept 1 - Optimized door concept and the FEM model: (1) Inner panel major, (2) mirror reinforcement, (3) Frame profile 1, (4) Frame connector, (5) Frame profile 2, (6) belt reinforcement outer, (7) Side impact beam, (8) Outer panel

This “rib height” problem can also be solved easily during typical product development when these constraints are removed. For example, shifting the inner panel surface in the high rib area to the middle of the rib height and building ribs on both sides of the surfaces could be one possible way to reduce the maximal rib height with only a minimal structural performance sacrifice.

The few ribs with a minimal 5.5 mm rib distance on this design could also be challenging for manufacturing with standard FRTP processes. Another point is that the allowable minimal rib distance varies from case to case in practice and depends largely on the geometry, manufacturing process, and material. In this case, an experience value was used here. According to the work by Kloska [57], a LFT component with a 5 mm rib distance can be manufactured with the compression molding process. The same criteria should be applied to the long-established injection molding process.

So far, for this concept design phase, the design of all the components on the optimized door are accepted without further change, and all the mentioned parameters in Table 6-1 are used further in this work.

Component	Mirror reinforcement	Belt reinforcement outer	Inner panel major
Manufacturing method	Injection molding	Compression molding	
Surface thickness (Ts)	3.5 mm	2.75 mm	3–3.5 mm
Rib thickness (Tr)	3.5 mm	3.1–3.2 mm	2–3.5 mm
Average rib distance* (Dr-avg)	12 mm	15 mm	13 mm
Minimal rib distance* (Dr)	5.5 mm	5.5 mm	5.5 mm
Average rib height (Hr-avg)	36 mm	40 mm	43 mm
Maximal rib height (Hr)	43mm (Tr=3.5 mm)	76mm (Tr=3.1 mm)	129mm (Tr=3.5 mm)
UD tape thickness (Tu)	None	UD belt outer: 1 mm	UD frame: 1 mm UD belt inner: 1.5 mm

*Rib virtual thickness is considered.

Table 6-1 Concept 1: important design parameters of components with the two different dedicated manufacturing methods

The joining areas J1 and J2 (highlighted in Figure 6-1 with black boxes) are illustrated in detail in Figure 6-2. In joining area J1 (Figure 6-2a), by fitting the geometry of frame profile 2 and combining the bolt and FDS connections, an ideal joining stiffness is achieved among components “frame profile 2,” “belt reinforcement outer,” and “inner panel major.”

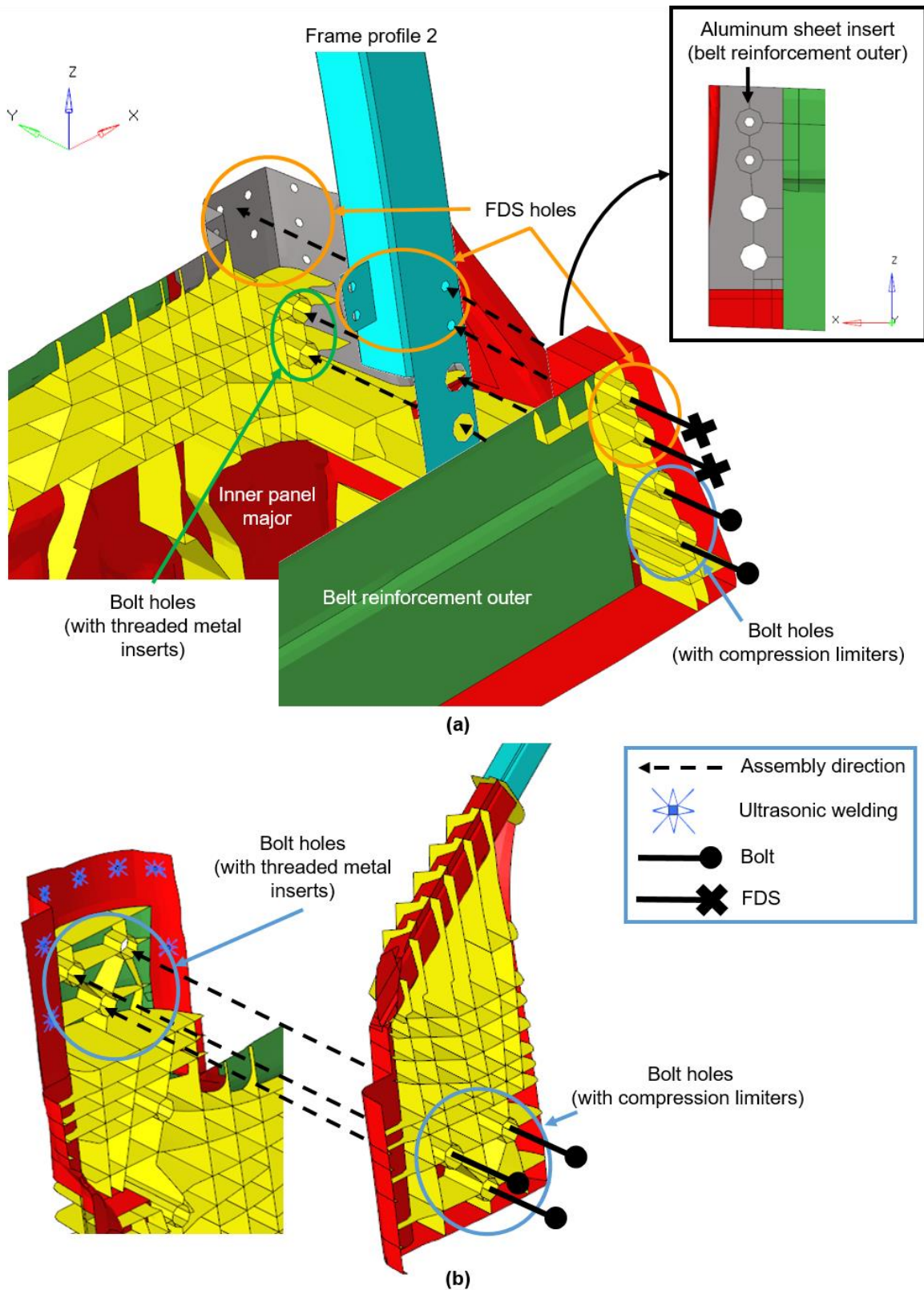


Figure 6-2 Concept 1 – joining concept in area J1 (a) and J2 (b) (in Figure 6-1)

	Reference door	Topology optimization: Static + substituted crash loading	Door concept 1: Preliminary	Door concept 1: Optimized
	Displacement following force direction at force point / Displacement difference to reference door			
Frame stiffness b-pillar	12.4 mm	10.31 mm / -17%	11.07 mm / -11%	11.35 mm / -9%
Frame stiffness middle	10.74 mm	10.45 mm / -3%	11.04 mm / +3%	10.63 mm / -1%
Door sag	8.49 mm	6.78 mm / -20%	6.60 mm / -22%	6.46 mm / -24%
Over opening	19.84 mm	17.85 mm / -10%	20.87 mm / +5%	19.84 mm / 0%
Belt stiffness outer	3.58 mm	2.45 mm / -32%	2.69 mm / -24%	3.05 mm / -15%
Belt stiffness inner	2.09 mm	1.69 mm / -19%	2.17 mm / +4%	2.09 mm / 0%
	Weight / Weight reduction			
	16.39 kg	20% (Objective)	13.33 kg / -18.67%	13.11kg / -20.01%

Table 6-2 Concept 1: mechanical performance and weight of the reference, topology optimization, and preliminary and optimized door concept

For the joining area J2 (Figure 6-2b), the combination of the bolt and the ultrasonic welding also achieves a good joining stiffness between component “mirror reinforcement” and “inner panel major.” Obviously, the joining number, position, and geometry for both joining areas can be further optimized, but this is beyond the scope of this concept development work.

As shown in Table 6-2, the static performance and weight of the optimized door concept 1 fulfills the design goal. Note also that the final weight of the optimized door concept 1 includes all the UD tapes, sheets, and threaded metal inserts, but not the bolts and FDSs.

The static simulation results show that the stress level on all components is under the yield strength. (The stress concentrations caused by the RBE2 elements are excluded by choosing one element away.) For the anisotropic PP-LGF40, the middle value of the ultimate tensile strength (70 MPa) in the flow and cross section is defined as the yield strength since no clear yield point for this material can be found.

The FE pole crash simulation of the optimized door 1 (Euro NCAP side pole impact test version 2001) is done with the component development method (section 2.7). Since the failure criteria cannot be deactivated in the material card Mat_54 of LS-DYNA (see section 3.3.3) [134], the parameters related to the failure criteria are specially defined (large failure strength and strain were given, details see Appendix 10.3.3) to achieve a minimal/no failure situation on the UD tapes under the side pole impact loading case. Overall, with the applied material models of the FRTPs (detail see section 3.3.3), their behavior in the “linear region” (before reaching the failure strain or strength of PP-LGF40 and UD tapes) in this crash simulation is reliable.

Figure 6-3a illustrates the deformation of door concept 1 and the surrounding components at 70 ms, when the “bounce back” starts and the maximal intrusion occurs. By comparing the intrusion at every measuring point/spring between “door concept 1” and the reference (see Appendix 10.6), the door and surrounding components are separated into different areas following the criteria based on intrusion difference as a percentage (given in Figure 6-3b): “ $\leq 0\%$ ” means that the intrusion on “concept door” is smaller than the reference, whereas “ $0\% \sim 10\%$ ” and “ $\geq 10\%$ ” means the intrusion is larger and at different levels. Clearly, concept 1 shows a positive crash performance, since most areas are either in “good (green)” or “ok (yellow)” areas. The overlap area between the pole barrier and concept 1, which has a substantial influence on the passive safety of the passenger, is almost all “good.”

Apart from the intrusion, the intrusion velocity is another important criterion for passenger safety [159]. As shown in Figure 6-4, the concept door 1 also shows a comparable intrusion velocity on measuring points corresponding to the position of different body parts (head, chest, and abdomen). All these values are below 7.5 m/s and thus are acceptable (for criteria, see [159]). Based on the crash simulation results, concept door 1 can achieve a high degree of passive safety with the original BIW side structure.

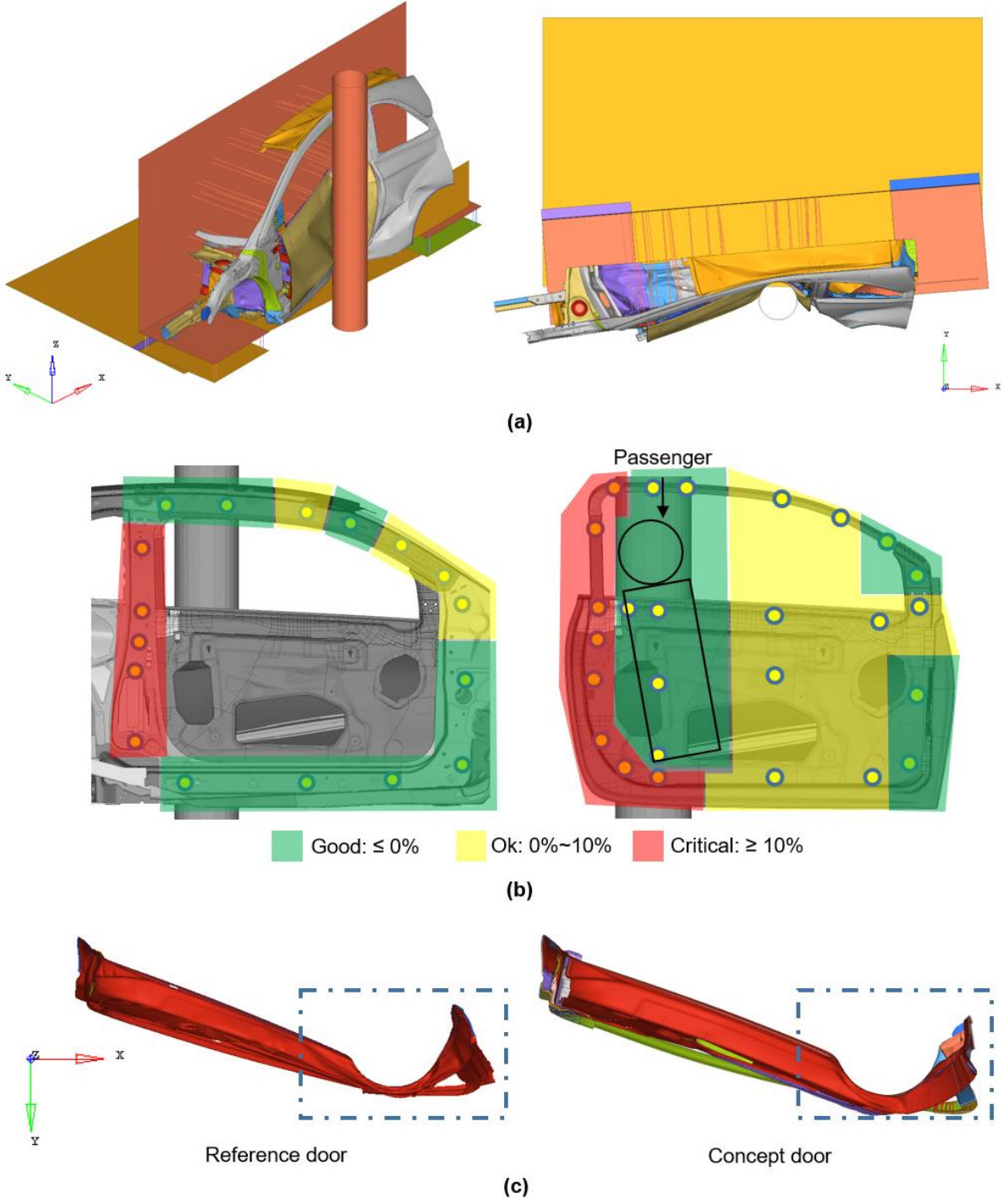


Figure 6-3 Concept 1: deformation plot at 70 ms (a); Intrusion comparison between optimized door concept 1 and the reference (b); Deformation mode comparison on inner panel (c)

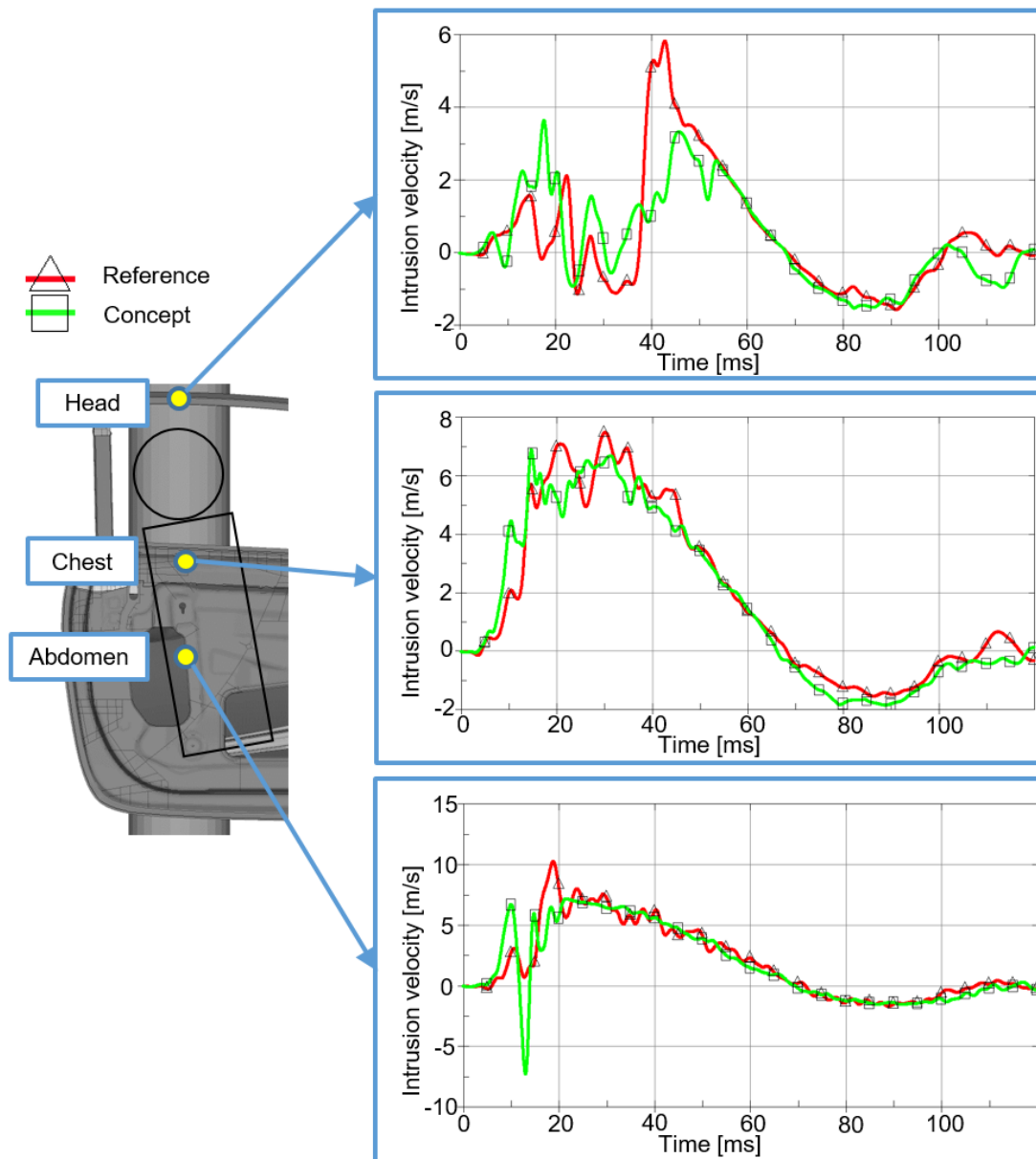


Figure 6-4 Concept 1: intrusion velocity of reference and concept door at different measuring points related to passenger safety

Further investigation is also made of the “critical” areas: the B-pillar area and neighboring areas on the door inner panel (Figure 6-3b). As shown in Figure 6-3c, compared to the reference, the intensive rib structure changes the deformation mode on the inner panel of the concept door. The panel is hard to fold tightly and behaves more rigidly than the steel inner panel of the reference door, which leads to a smaller local deformation on the area close to or in contact with the B-pillar. Due to this relatively rigid behavior, a larger force is conducted further onto the B-pillar and causes an increase in the intrusion. This situation might be relieved in the simulation if the failure criteria are defined for the PP-LGF40 components and UD tapes. This should be further investigated in future work when the material properties related to the failure are obtained from specimen tests.

6.2 Concept 2

The newly developed components “inner panel major,” “closing plate,” and “belt reinforcement outer,” together with the original side impact beam and the aluminum door outer panel, are assembled as the preliminary door concept 2. The static simulation of this preliminary door concept is done with the same hinge and A-pillar setups and loading cases as in the reference door simulation. As illustrated in Table 6-4, the static performance and weight of the preliminary door concept 2 fulfills all the pre-defined static stiffness requirements, and some of them, such as loading cases “frame stiffness b-pillar,” “door sag,” “over opening,” and “belt stiffness outer,” are even “over-engineered.” However, the deficiencies in the weight reduction are not negligible, but this can be optimized through parameter optimization.

The following parameters on the preliminary door concept 2 are changed manually or optimized with the parameter optimization using Optistruct:

- Rib number reduction on components “belt reinforcement outer” and “inner panel major” due to manufacturing difficulties (small rib distance).
- Rib thickness optimization on components “belt reinforcement outer” and “inner panel major” to achieve a greater weight reduction and to relieve the over-engineered situation. The optimization range is from 2 mm to 3.5 mm.
- Local base surface thickness reduction on components “belt reinforcement outer” (light blue area in Figure 6-5) and “inner panel major” (dark blue areas in Figure 6-5). The chosen areas are either related to over-engineering loading cases or to a minor stress state. The thickness is reduced from 3.5 mm to 2.6 mm (belt reinforcement outer) and 3 mm (inner panel major).

The optimized door concept 2 (Figure 6-5) is achieved after the parameter optimization. The important design parameters and manufacturing methods for this optimized door are summarized in Table 6-3.

For the manufacturing processes, compression molding is preferred for the components “belt reinforcement outer” and “inner panel major”, which require a longer average fiber length for a better crash performance.

Similar to concept 1, the same manufacturing restrictions mentioned in section 6.1 were applied. As shown in Table 6-3, the average rib distance and height of the optimized door concept 2 proves its manufacturability to a large extent. The reason and solution for the very few individual ribs on concept 2 with either large height (125 mm) or small distance (6 mm) are the same as for concept 1 (see section 6.1), so there is no need to reiterate these here.

Besides the rib distance and height, the frame structure could also be another challenge for the LFT compression molding due to the slim geometry and the possible long material filling/flowing distance. To achieve a reliable component, the location and number of LFT extrudates must be optimized in practice by “trial and error”.

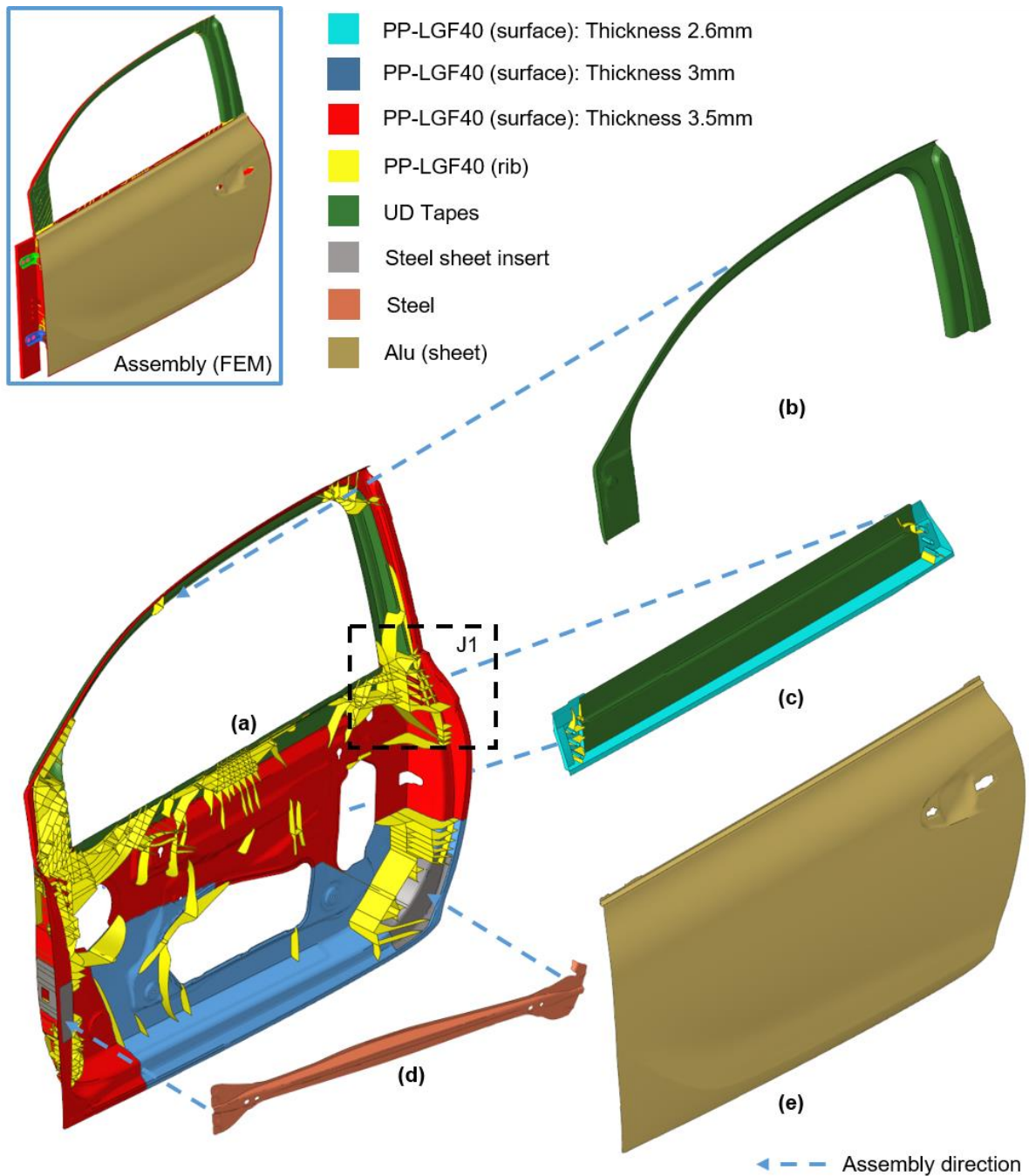


Figure 6-5 Concept 2: optimized door concept and FEM model: (a) inner panel major, (b) closing plate, (c) belt reinforcement outer, (d) side impact beam, (e) outer panel

So far, for this concept design phase, the construction of all the components on the optimized door concept 2 are accepted without further change, and all mentioned parameters in Table 6-3 are used further in this work.

Component	Closing plate	Belt reinforcement outer	Inner panel major
Manufacturing method	Injection molding	Compression molding	
Surface thickness (Ts)	3.5 mm	2.6 mm	3.5 / 3 mm
Rib thickness (Tr)	No ribs	3.5 mm	Frame area: 3.5 mm Bottom area: 2–3.5 mm
Average rib distance* (Dr-avg)	/	18.7 mm	12.2 mm
Minimal Rib distance* (Dr)	/	13.5 mm	6 mm
Average rib height (Hr-avg)	/	27 mm	40.5 mm
Maximal rib height (Hr)	/	40mm (Tr=3.5 mm)	125mm (Tr=3.5 mm)
UD tape thickness (Tu)	UD closing plate: 1.5 mm	UD belt outer: 1 mm	UD frame: 1.5 mm UD belt inner: 1.5 mm UD closing plate: 1.5 mm

*Rib virtual thickness is considered.

Table 6-3 Concept 2: important design parameters of components with the two different dedicated manufacturing methods

As mentioned in section 5.2.2, the components “belt reinforcement outer” and “inner panel major” are joined using bolts and IMA threaded metal inserts. Joining area J1 (highlighted in Figure 6-5 with a black box) is illustrated in detail in Figure 6-6, as an example. The closing plate (Figure 6-5b) is joined to the frame area (inner panel) on the edge by ultrasonic or infrared welding.

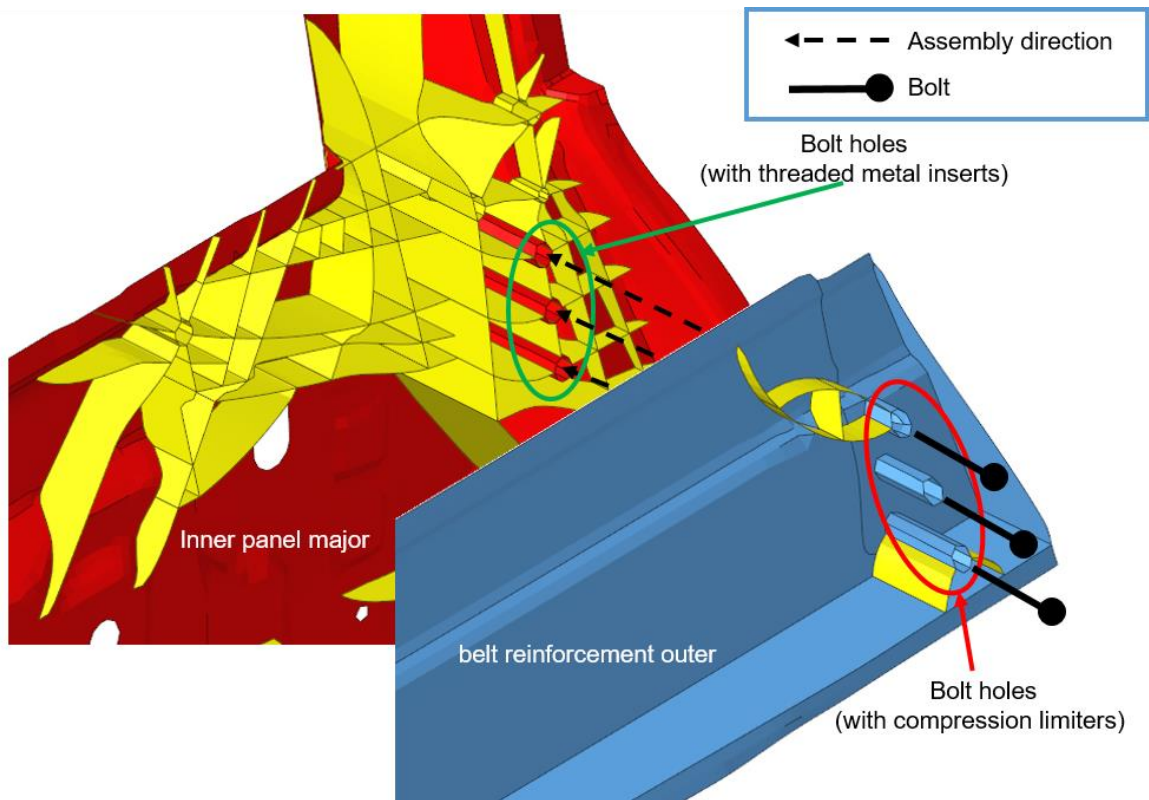


Figure 6-6 Concept 2: Joining concept in area J1 (in Figure 6-5)

As shown in Table 6-4, the static performance and weight of the optimized door concept 2 fulfills the design goal. Note also that the final weight of the optimized door concept 2 includes all the UD tapes, sheets, and threaded metal inserts, but not the bolts.

The static simulation results indicate that the stress level on all components is under the yield strength. Further details for determining the yield strength of PP-LGF40 (70 MPa) are provided for concept 1 (see section 6.1).

	Reference door	Topology optimization: Static + substituted crash loading	Door concept 2: Preliminary	Door concept 2: Optimized
	Displacement following force direction at force point / Displacement difference to reference door			
Frame stiffness b-pillar	12.48 mm	11.39 mm / -9%	11.08 mm / -11%	11.56 mm / -7%
Frame stiffness middle	10.74 mm	10.43 mm / -3%	10.63 mm / -1%	10.77 mm / +0.3%*
Door sag	8.49 mm	6.31 mm / -26%	6.04 mm / -29%	6.15 mm / -28%
Over opening	19.84 mm	16.53 mm / -17%	17.02 mm / -14%	18.71 mm / -6%
Belt stiffness outer	3.58 mm	2.55 mm / -29%	2.64 mm / -27%	3.31 mm / -8%
Belt stiffness inner	2.09 mm	1.70 mm / -19%	2.05 mm / -2%	2.10 mm / +0.5%*
	Weight / Weight reduction			
	16.39 kg	20% (Objective)	13.71 kg / -16.35%	13.11 kg / -20.01%

*Due to the combination of manual and computer-aided (Optistruct) parameter optimization, +1% is set as the acceptable tolerance range.

Table 6-4 Concept 2: mechanical performance and weight of the reference, topology optimization, and preliminary and optimized door concept

In the FE pole crash simulation for concept 2, the method and FE setups (e.g., loading case, material model, and boundary conditions) are the same as for concept 1, except for the substitution of the door model.

Figure 6-7a illustrates the deformation of door concept 2 and the surrounding components at 70 ms, when the “bounce back” starts and maximal intrusion occurs. The same criteria used for concept 1 are used to evaluate the intrusion of concept 2 (for detailed data, see Appendix 10.7).

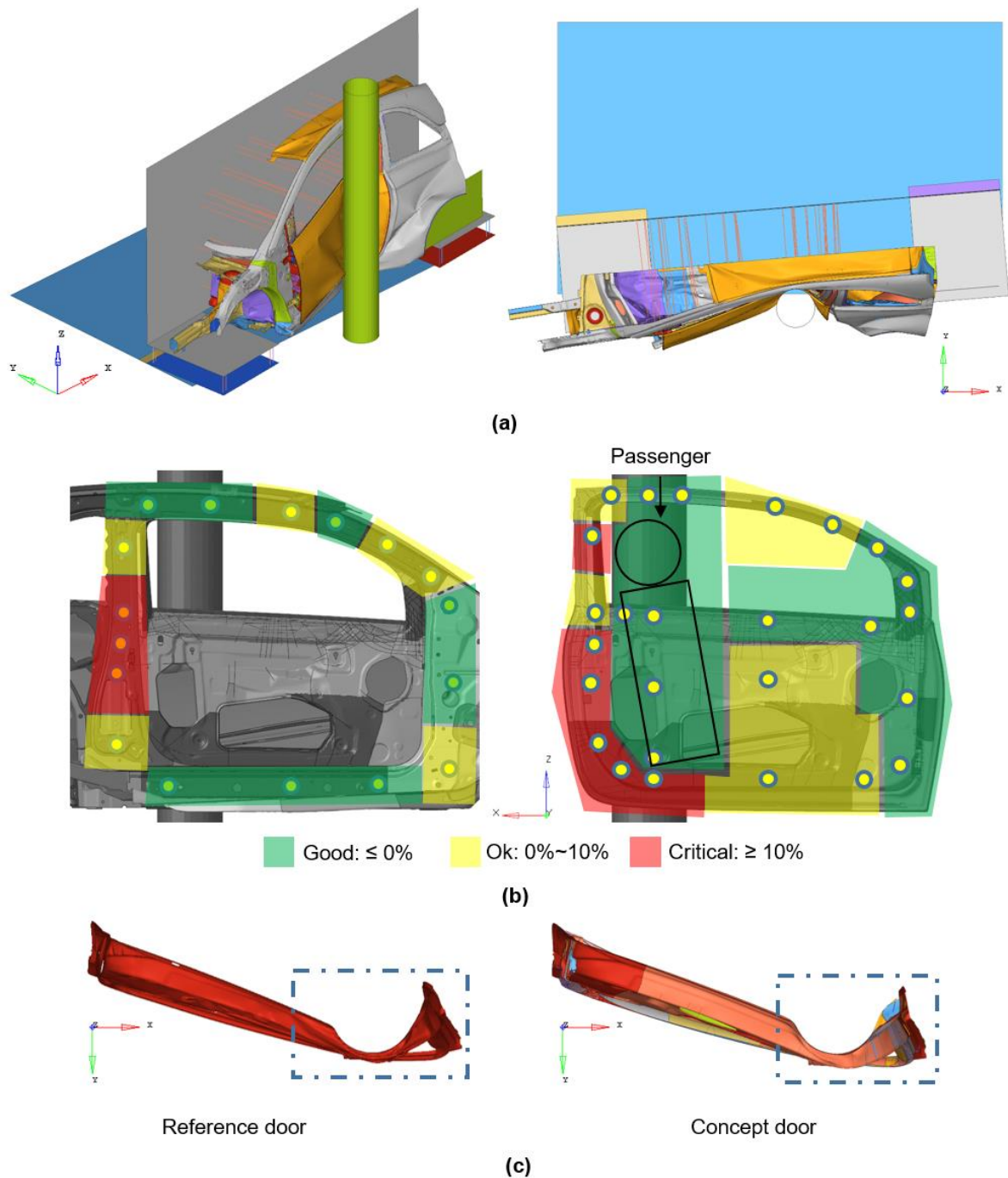


Figure 6-7 Concept 2: deformation plot at 70 ms (a); intrusion comparison between the optimized door concept 2 and the reference (b); deformation mode comparison on the inner panel (c)

As expected, concept 2 shows a positive intrusion behavior (Figure 6-7b) (most areas are in the “good (green)” or “ok (yellow)” areas), and the overlap area between the pole barrier and concept 2 (passenger area) is “good (green).” The intrusion velocity on concept 2 (Figure 6-8) is also comparable to the reference at measuring points corresponding to different body parts (head, chest, and abdomen). All these values are below 8.7 m/s (maximal at the measuring point “abdomen”) and are thus acceptable (for criteria, see [159]). Based on the crash simulation results, concept door 2 can achieve a high degree of passive safety with the original BIW side structure.

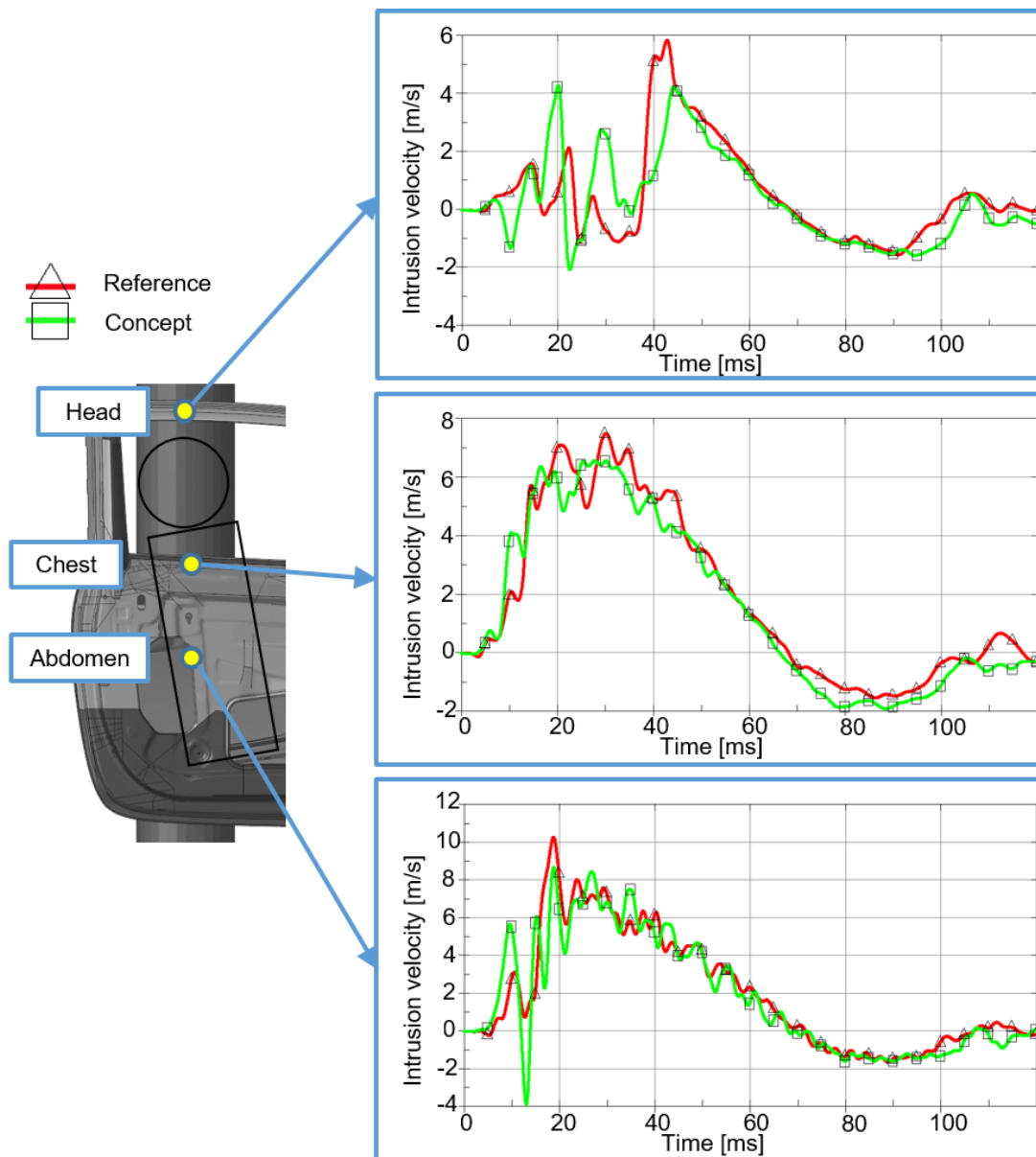


Figure 6-8 Concept 2: intrusion velocity of the reference and concept door at different measuring points related to passenger safety

For the intrusion “critical” areas on concept 2 (Figure 6-7b), the same “rigid behavior” on the inner panel is found in this area due to the intensive rib structures (Figure 6-7c). Since the structure in this area on concept 2 is comparable to that of concept 1, details of its explanation and possible solution can be found in section 6.1.

6.3 Comparison and evaluation of different door concepts

In this section, the optimized doors from both concepts are compared and evaluated from the perspective of weight, mechanical performance, and cost.

6.3.1 Weight and mechanical performance

The weight of the optimized doors from both concept directions are identical (concept 1: 13.11 kg; concept 2: 13.11 kg). They both fulfill the pre-defined 20% weight reduction goal.

Although the final weights of two concepts are identical, the difficulties to reach the save level of weight saving on them are totally different. For example, as shown in Figure 6-1, the thickness of the base surface on the inner panel of the concept 1 is almost uniform. Very few areas need the additional local thickness optimization after the global parameter optimization. However, as for the concept 2 (see Figure 6-5), to reach the same weight reduction goal, local thickness optimizations / reductions on the inner panel are required in more areas. Overall, in this “design fine-tuning” process, comparing to the concept 1, more iterations of “trial and error” were made on the concept 2 and longer time was invested accordingly. From other perspective, it can also be assumed that there might still be some further lightweight potential available on the concept 1. The 20% weight saving goal might constrain it in some way.

For the static performance, both concepts, in general, reach the same level of structural stiffness as the reference door (see Table 6-2 and Table 6-4). After a close comparison, one important fact is that concept 2 with the “PP-LGF40 + UD tape (PP-GF based)” frame structure is not as efficient as concept 1 with closing aluminum profiles in terms of reaching the target frame stiffness with a good weight reduction. The preliminary topology optimization of concept 2 (not illustrated in the text) resulted in severe material aggregation in the frame area, which is why the frame closing plate was added. In this way, a closing profile with PP-LGF40 and UD tapes is realized on the concept 2 frame, which is the preferred structure for bending load cases. However, even in this circumstance, the UD tape thickness is still 1.5 mm, which is relatively thicker than in typical applications and brings a certain amount of weight to the door structure. As mentioned in section 3.1.3, the chosen UD tape already has superior mechanical properties of the PP-GF-based sort, which means that a type of UD tape with even better mechanical performance, such as the PP-CF based type, might be required to reach both the stiffness and lightweight goals within the given constrained design space of the window frame. In this case, the aluminum extrusion profile on concept 1 is undoubtedly the better choice in the frame area from the perspective of the mechanical performance and weight savings.

For the crash performance, the difference between concept 1 and concept 2 is negligible, since the structures of the major crash-load bearing areas (area under the door belt + side impact beam) on both concepts are similar. The crash performance for both concepts and the reference is also comparable, especially in the passenger area.

6.3.2 Manufacturability and cost

Since manufacturability is considered at the early phase of this concept development work, both concepts can be manufactured with the standard processes already in use on existing serial components, except for the flange process for the aluminum outer panel and the PP-LGF40 inner panel. This needs to be developed based on the long-established standard flange

process for metals. Other than that, some further manufacturing challenges remain with both concepts. As mentioned in section 6.1, for concept 1, the IMA between the frame profile 1 and the mirror reinforcement and the multiple joining techniques (bolts with MIs and FDSs) are two major difficulties. For concept 2 (see section 6.2), the long flow distance for the PP-LGF40 and the slim window frame structure remain challenging. However, concept 2 clearly has much fewer required joining positions and techniques, which reduces the complexity of assembly. From this point of view, the overall manufacturing difficulty is lower for concept 2 than for concept 1.

Material price estimation for mass production (€/kg)			
PP-LGF40	Steel	Aluminum	UD tape (PP-GF)
1.26	0.7	2.5	12
Door material cost (€/door) (inclusive material waste)			
*Raw material usage rate: 1) PP-LGF40 = 90% 2) Aluminum & Steel sheet = 55% 3) Aluminum profile & casting = 90% 4) UD tape = 90%			
Concept 1	Concept 2	Aluminum reference (sheet constructed)	Steel reference (sheet constructed)
34.7	40.8	59.6	20.9

Table 6-5 The estimation of material price and material cost of the door concepts

In terms of cost, the major material cost for concept 1 comes from the PP-LGF40, UD tapes, and aluminum extrusion profiles. For concept 2, the cost arises from the PP-LGF40 and UD tapes. Since the price of the raw material can depend strongly on the order quantity, only a rough material price estimation can be made here (see Table 6-5). According to the specific material usage, the material cost of both concepts is given in Table 6-5 and includes the waste aluminum and steel material accumulated during the manufacturing (specific calculation see Appendix 10.8). Obviously, the use of lightweight material leads to a material cost increase compared to the steel reference. The extensive use of UD tape on the frame structure also gives concept 2 a significantly higher material cost (+16%) than concept 1. However, keeping the material cost of both concepts under the aluminum reference is more important and is the

crucial “game changer” for OEMs when determining whether a lightweight concept can be adopted for serial products [167]. From this point of view, both concept 1 and concept 2 are promising.

The major manufacturing cost of door concepts comes from the tooling and process costs (e.g., joining, forming). The mold costs for concept 1 are extrusion tools for aluminum profiles and molds for compression and injection molding. For concept 2, the costs are molds for compression and injection molding. Generally, due to the complex compression mold needed for the inner panel, the tooling cost is higher for concept 2 than for concept 1. However, the process cost is obviously higher for concept 1 due to the requirement for multiple joining techniques and the forming of the aluminum profiles. The addition of joining techniques will lead to additional steps in the DIW-manufacturing cell and an accordingly longer cycle time. Meanwhile, the bending process of the frame aluminum profiles can be costly due to the high tolerance requirements. Compared to the aluminum or steel reference, the molds for either compression or injection molding are much cheaper than conventional deep drawing tools. However, the process cost of both door concepts could be higher due to the longer cycle time. In addition, the new joining techniques for FRTPs (e.g., ultrasonic welding, infra-red welding) are more expensive than the steel or aluminum welding processes. At this point, due to the limitation on the available cost information, only a qualitative comparison can be made on the manufacturing cost. Further detailed costs must be calculated by the industry partner of this work in the future.

Overall, the final DIW costs for both concepts could be similar and lie between the costs of steel and aluminum doors.

6.4 Rapid prototyping with additive manufacturing

After achieving the door concepts, the next work in the future is prototyping. In the research project related to this work, expensive injection and compression molding molds are being designed and manufactured since testing and presenting the manufacturing process and prototype close to the final serial product are defined as project goals. However, this prototyping method puts some constraints on the design. For example, the final door design and optimization must be finished in a very limited time. After the start of molding manufacturing, due to the complexity of the door design, further design changes either cannot be implemented on the prototype or can only be achieved with an unacceptable cost increase.

Clearly, additive manufacturing (AM) is still far away from the mass production of serial automotive components due to its high cost, long building time, and low accuracy. However, AM can be a powerful tool for rapid prototyping of door concepts in this work, since the low production volumes, high design complexity, and frequent design changes are required [168]. The characteristics of the door concepts in this work could be helpful in the area “high performance prototyping”.

High performance prototyping

A high performance prototype is required in this work since the prototype will be tested under both static and highly demanding crash loading cases. To conserve efforts and costs on tools, a 3D-printable material with roughly approximate mechanical properties to the material chosen for door concepts could be used to build door prototypes.

As shown in Table 6-6, according to the available mechanical properties, the 3D-printable material “FDM Nylon12-CF” could be a possible alternative for the door concept material PP-LGF40 on prototypes. Figure 6-9 illustrates two structural applications with this material. The structural performance of these two parts can also fulfill the requirements of serial production parts. The additive manufacturing process of fused deposition modeling (FDM) is able to integrate the metal inserts into the part. For all these reasons, the components “printed” with this material on the door prototype could have a higher chance of achieving similar mechanical performance to that of the components made of PP-LGF40.

Property	FDM Nylon12-CF	PP-LGF40
Manufacturing methods	Fused Deposition Modeling (FDM)	Compression molding
Fiber type	Carbon fiber (chopped)	Glass fiber (long)
Fiber weight (%)	35	40
Density (g/cm ³)	/	1.22
Tensile modulus (GPa) (0°; 90°)	7.5; 2.3	9.5; 4.3
Tensile strength (MPa) (0°; 90°)	75.6; 34.4	118; 30
Strain-to-failure (%) (0°; 90°)	1.9; 1.2	1.32; 1.39

Table 6-6 Material comparison between PP-LGF40 and FDM Nylon12-CF [169]



Figure 6-9 Example of a part made from FDM Nylon 12CF: a) fixture; 2) brake pedal [170]

The “UD tape + rib” structure on the door concepts (shown in Figure 6-1 and Figure 6-5) could also be realized with a process combination of In-situ Automated Tape Placement (ATP) and Fused filament fabrication (FFF) [171]. As shown in Figure 6-10, a honeycomb structure with many fine rib geometries are 3D-printed (FFF) onto an existing laminate with a rough surface. The laminate is prepared with the ATP process. According to the results of shear tests, a decent joining strength can be achieved between 3D-printed ribs and the laminate.

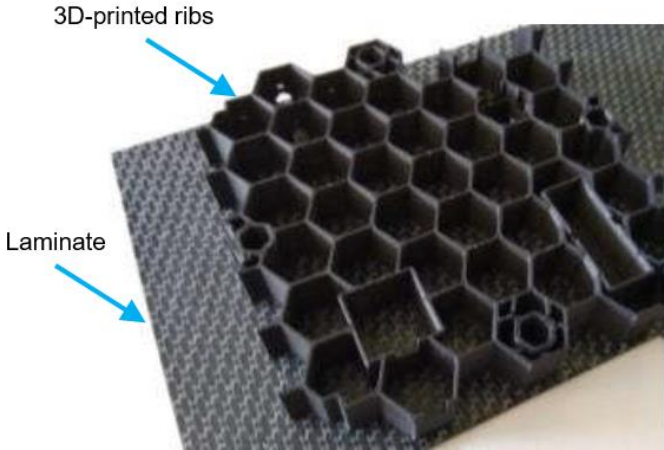


Figure 6-10 Ribs 3D-printed onto an existing laminate [171]

Overall, these methods appear very promising for building prototypes of door concepts with a comparable mechanical performance to that attained with additive manufacturing.

7 FRTP-metal multi-material door – opportunity and challenge in mass manufacturing

When talking about mass manufacturing, the multi-material door concepts must be treated as an industrial product and evaluated against the criteria related to manufacturers and customers. The major requirements for a vehicle door, from the perspective of manufacturers and customers [5], are summarized in Table 7-1.

Category	Important requirements
Manufacturer requirement	<ul style="list-style-type: none"> • low investment costs (manufacturers and car repair shops) • low material costs, use of recycled material, good utilization of raw materials • low energy costs, high level of automation • short cycle times through parallel production and assembly of component groups • short changeover times for product modifications • low maintenance • damaged components can be easily replaced after an accident • good accessibility for maintenance and repair work
Customer requirement	<ul style="list-style-type: none"> • easy entry and exit through the wide-opened angle • No rattling noises when opening, closing, and while driving • impermeability to wind and moisture • no dirtying when entering and exiting the vehicle • reliable function in a wide variety of weather conditions • good visual impression • no reachable component protruding into the interior • use of non-toxic materials

Table 7-1 Manufacturer and customer requirements for vehicle doors [5]

According to the mentioned requirements in Table 7-1, “cost” and “reliable-to-use” are the key words for manufacturers and customers, respectively. The following analysis on the opportunity and challenge of FRTP-metal multi-material doors will concentrate on these two facts, as well as the environmental effects.

7.1 Cost for manufacturer

Typically, the manufacturing of a vehicle door structure involves not only OEMs but also multiple suppliers. Clearly, among these actors, the OEMs are more sensitive to the cost since they need to bring a competitive and cost-effective final product to the end customer. For this reason, the following cost analysis is done largely from the point of view of the OEMs.

7.1.1 Investment cost

Due to the major change in material from steel to LFTs on the door concepts (especially on the inner panel), new manufacturing methods must be used, including injection molding and compression molding. This also means that investment should be made in new facilities or equipment. For serial manufacturing of LFT components, investments can include a D-LFT facility, the injection molding machine, and the equipment for joining LFTs, and the amount of money is usually substantial. Clearly, the facility investment for OEMs is a sizeable and difficult decision to make and is largely related to the number of productions per year. OEMs will normally launch a vehicle with this type of multi-material door in a model-by-model manner, which means that production will go through several years before reaching large-scale production. For small and middle scale production, the cost-effective solution would be to purchase the FRTP parts directly from suppliers, which is also state-of-art in OEMs, or even purchasing the whole door (for reasons, see section 7.1.3). For large scale production, to further reduce the cost per part, a sensible move for OEMs is to invest in those facilities and manufacture the parts “in house.” Since large-scale production happens several years after a product is first launched in the market, it also provides OEMs enough time to finish the rearrangement of manufacturing and logistics for the whole assembly process. Above all, the investment cost for OEMs can be relatively small for FRTP-metal multi-material doors in the short and middle terms. The possible large investment cost in the long term can be shared with each component and compensated for by the high production volume.

7.1.2 Material cost

The relatively high material cost is always a major obstacle for implementation of lightweight materials into a serial BIW structure. Previous work [172] has shown that more than 50% of the total production cost of the BIW component is the material cost, which means a small increase in the cost of the chosen raw material can have a substantial influence on the total production cost (Figure 7-1). This is the reason why steel dominates the BIW of large-volume production vehicles, not only because of its excellent material property, but also because of its relatively low price.

To make the FRTP-metal multi-material door concept competitive, PP-LGF40 is chosen as the major material. Since the E-glass fiber can be seen as the standard fiber material in the automotive industry, the matrix material largely determines the material cost of LFTs. As shown in Figure 7-2, PP, as a common type of standard plastic, has a substantial price advantage. Examples given in section 2 prove the feasibility of this material in the automotive industry from the perspective of costs.

DISTRIBUTION OF CAR MANUFACTURING COSTS
(COMPONENT LEVEL)

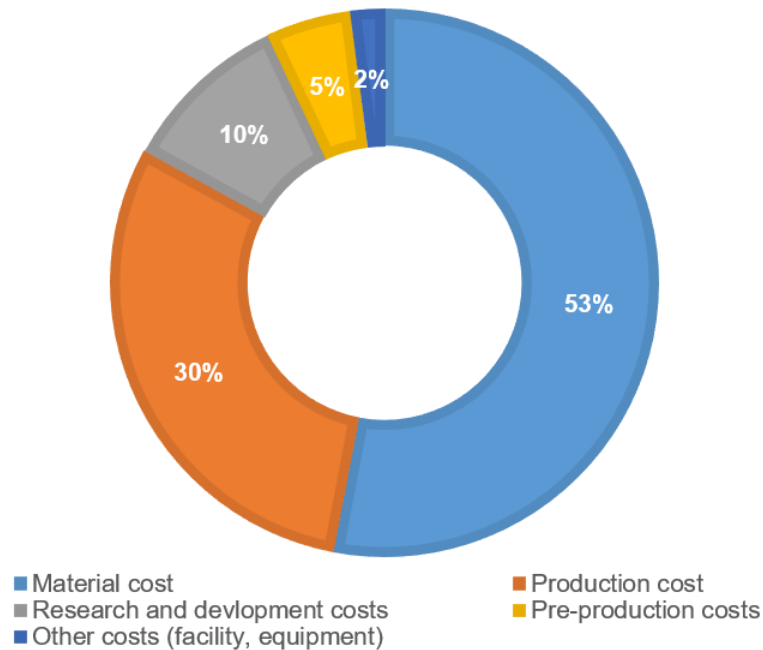


Figure 7-1 Distribution of manufacturing costs (component level) [172]

Nevertheless, the lightweight design always comes with a cost increase. The application of lightweight materials is possible if the vehicle selling price stays within a competitive range or if the extra cost can be compensated by reductions in other costs, such as the manufacturing cost and fuel consumption. Specifically, the competitive price range of an economical door structure should be lower than that of an aluminum door, based on the fact that very little aluminum can be found on a BIW of economical vehicles. According to an internal calculation, in comparison to aluminum doors, the door concepts with PP-LGF40 in this work can achieve up to ca. 40% in material cost savings if the material waste during the manufacturing is considered. The thermoplasticity of LFTs means that almost no manufacturing waste is generated since waste material can be recycled directly in the manufacturing process. In most cases, the manufacturing scraps (e.g., runners, rejected parts) are granulated and blended with virgin thermoplastic material in many injection molding processes [166]. The same type of recycling process is presumably applicable for the preparation of LFT extrudates in the compression molding process as well. A high degree of raw material usage (LFT) during manufacturing can profoundly reduce the material cost. The weight reduction due to the use of LFTs also helps to reduce fuel consumption, which is a special type of material cost reduction that is often easily neglected.

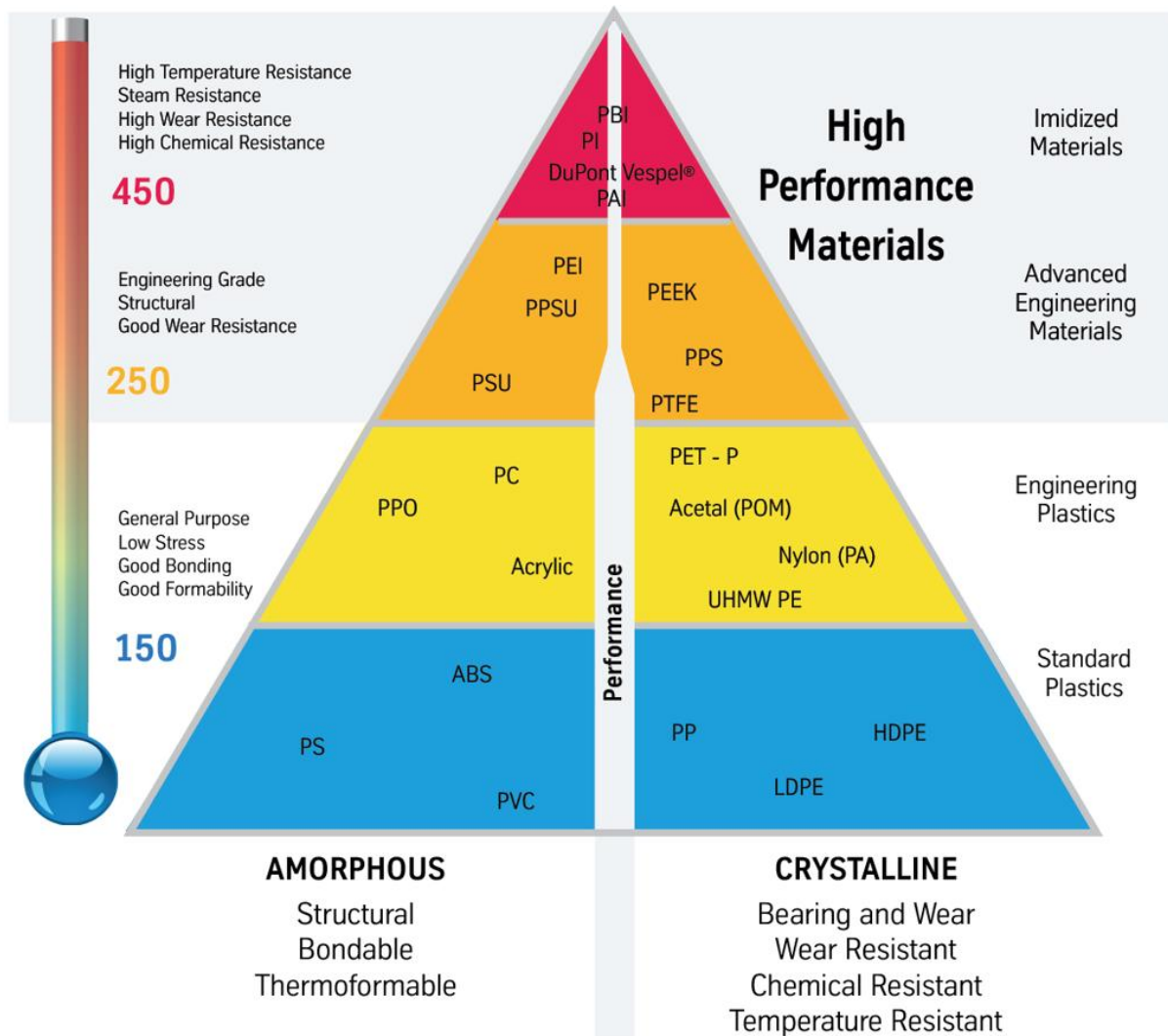


Figure 7-2 plastic material categories [173]

7.1.3 Manufacturing cost

The manufacturing cost of this multi-material door should be discussed by separating it into the Door-In-White (DIW) cost and the complete door cost.

The manufacturing cost of DIW is determined by the: 1) component cycle time; 2) joining time; 3) number of components; 4) joining techniques and positions; and 5) mold/tool costs. Clearly, the typical manufacturing methods for LFTs have longer cycle times (up to 1 minute) than the deep drawing process for common sheet-construction doors, due largely to the relatively long cooling time. However, the high integration level of LFT components on the door concepts greatly reduces the total number of components, and this compensates for the long cycle time of LFT components to some extent. The warming and placement of metal inserts and UD tapes [43] by fully automated robots is the state of art in manufacturing LFT components, and will not have any large negative influence on the cycle time. For joining techniques, the extensive use of adhesive promoters on the door concepts reduces the complexity of joining between different materials (IMA: LFT to steel or aluminum). Even on concept 1 door with unoptimized joining positions, the total number of joining positions is significantly lower than the number of optimized spot weldings on the reference door. The new flange technique under development for joining the metal outer panel to the LFT inner panel is comparable to the existing flange

process, so it will eventually cause no significant change in the cycle time. Based on these facts, estimates of the joining time of concept DIWs might be less than the reference. Besides the lower mold costs mentioned in section 6.3.2 (compared to deep drawing tools), the manufacturing cost of concept multi-material DIWs can also be, to a great extent, less than that of the market-available sheet-constructed vehicle door.

The complexity of integrating the FRTP-metal multi-material doors into the existing assembly process has a substantial influence on the complete door cost. Among the typical processes after the assembled BIW leaves the body shop, painting is the most challenging process for the door concepts since the PP-LGF40 is negatively affected by the high temperature occurring especially during the cathaphoretic immersion priming (E-coating) process. Typically, depending on the specific requirements from OEMs, the maximal temperature during the E-coating process can be up to 200°C [74; 174], which is above the melting temperature of PP (between 130 and 170°C). However, the presence of metal parts on the multi-material door concepts means that the E-coating process is absolutely necessary.

Considering the three major painting processes in the automotive industry (online, inline, and offline processes) [174], the best solution could be the offline process, which means the DIW would need to go through a separate painting process at a lower temperature and then be assembled with the rest of the vehicle at the final assembly line. The offline process is the standard painting process today for components like bumper covers [174], which are typically made of PP as well, and this step is commonly executed by the suppliers. This is also the reason why purchasing the whole door (with paint) is a cost-effective solution for OEMs (mentioned in section 7.1.1). In this way, OEMs save substantial effort on building a new painting line and rearranging the on-site logistics, while, at the same time, reducing the risk of a large investment at the phase of small and middle scale production. Overall, the offline process solves the painting problem for FRTP-metal multi-material door concepts, but the subsequent challenges, such as the painting cost increases and color matching, have to be overcome in any case.

7.2 Reliability for customer use

Since the FRTP-metal multi-material doors do not change the fundamental function of a vehicle door and are able to fulfill the important mechanical requirements, most customer requirements can also be satisfied. The exceptions are: 1) reliable function in a wide variety of weather conditions; and 2) no reachable component protruding into the interior. For the first point, the operation temperature of a BIW component (between -40 to 80°C [174]) is challenging for all components with LFTs. Unlike metallic materials, the mechanical properties of LFT materials are temperature dependent and might undergo substantial performance changes in multi-material doors in extreme environments (Figure 7-3). To ensure good reliability and safety for customers no matter where they use their vehicles, additional attention should be paid to the performance of multi-material doors under low and high temperatures. Regarding the second point, due to the nature of LFTs, they might undergo material failure (material split failure) under crash loading cases. On the one hand, this might dissipate a certain amount of the crash energy, but on the other hand, it could lead to high protrusion potential into the space occupied by the passengers. This might be one of the major obstacles that will limit the acceptance of multi-material doors by OEMs if the protrusion risk cannot be further reduced.

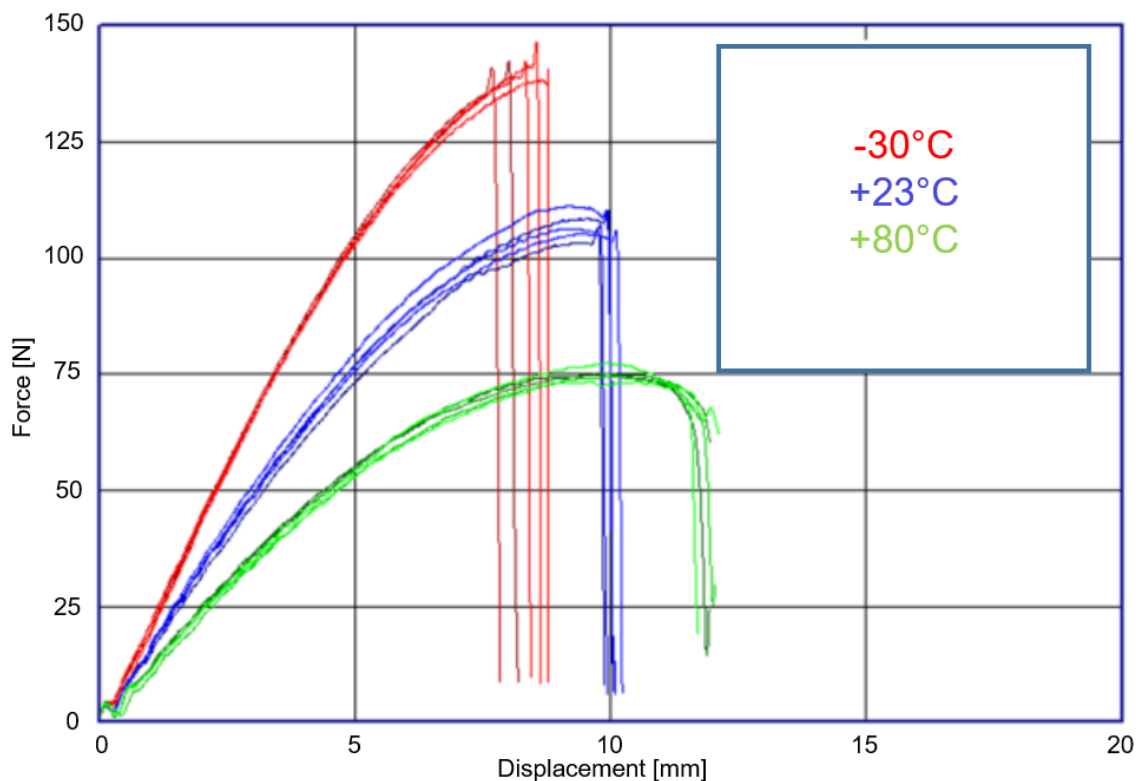


Figure 7-3 Temperature Influence on PP-GF40 (3-point-bending test at a velocity of 1 mps) [175]

7.3 Environment effect

7.3.1 Recycling

Recycling is always a major problem for multi-material BIW components. Compared to traditional metallic BIW components, which uses existing recycling methods, the recycling of multi-material components, especially FRTPs, can only occur at a low rate and is typically unfriendly to the environment. Actually, for components made of LFTs, because of their thermoplasticity, the preferred environmental-friendly recycling methods are reuse and remanufacturing [176]. However, this requires a labor-intensive “collecting and dismantling” process before shredding, which leads to additional recycling costs. The high complexity of dismantling existing multi-material components makes the recycling methods impracticable from an economical perspective. Making the multi-material doors proposed in this work recycling friendly will require careful choices of joining techniques and material combinations. The use of detachable bolts and flanges will decrease the complexity of disassembly. For the components joined with undetectable joining techniques (e.g., the closing plates and inner panels with ultrasonic welds in concept 2), the same material should be used. In the two concepts presented in this work, only one type of matrix material PP and one type of glass fiber are used, which further reduces the recycling cost. The metal inserts (with or without adhesive promoter) can be easily separated from the LFT materials with the standard recycling process of thermoplastics [177], since the LFTs will be heated up to the molten state. One point to note is that a mechanical property degradation occurs with recycled LFTs [178], which means they might not be suitable for demanding BIW applications. Clearly, if further multi-material BIW applications are introduced in the market, new recycling methods are required.

7.3.2 Life cycle analysis

Thanks to the significant weight reduction, multi-material doors illustrate their strength in reducing the CO₂ footprint as well. Compared to the traditional steel-intensive BIW, the use of FRTPs shows a substantial environmental benefit from the perspective of life-cycle assessment (LCA). As one of the most widely used criteria for material selection in the automotive industry, LCA determines the environmental impact of products at each stage from cradle to grave [179] and typically includes manufacturing, use, and recycling phases.

A LCA-based study (Table 7-2) [180] showed that simply switching the vehicle door outer panel from steel to PP-GF significantly reduced the cumulative energy demand (CED) in both the manufacturing and use phases. The detailed information on this study, such as the defined LCA system boundary, considered impact categories and characteristics of chosen door outer panels are given in Figure 10-5 and Table 10-9 in Appendix 10.9. Considering that the normal lifetime of one vehicle is about 15000 km, the environment benefits in the use stage will compensate for the negative impacts of FRTPs in the manufacturing and recycling phases by reducing greenhouse gas (GHG) emissions (e.g., CO₂).

Product	Vehicle door		
FRP Type	PP-GF		
Replaced traditional material	Steel		
Phase	LCA		
Manufacturing phase	Weight change (%)	CED change (%)	GHG change (%)
	-31 %	-59 %	+2 %
Use phase	Lifetime (km)	CED change (GJ/piece)	GHG change (kg of CO2/piece)
	150.000	-2.0	-150

Table 7-2 LCA-study of a FRTP vehicle door in the manufacturing and use phases [181]

8 Summary and outlook

8.1 Summary

This work proposes an approach for the design of an economical lightweight multi-material door concept with FRTPs based on a steel reference door. The lightweight design approach is the core innovation of this work, which includes not only the typical weight savings with the substitution of lightweight materials, such as aluminum and LFTs, but also the more important new structural design principle and methods, which fully exploits the lightweight potential of FRTPs on the multi-material-design vehicle door structure.

To reach the development goal, the principle of the innovative “two-ring structure” is adapted in the new development work as the foundation to provide a universal solution to convert the conventional door into a multi-material door structure without changing the original crash-relevant side impact beam. However, instead of directly copying all the features, the “FLB-concept” based on the original two-ring structure is investigated in depth, and the pros and cons are summarized. The innovative separation of major and minor load-bearing regions is fully maintained. However, to reach the goals of light weight and economy at the same time, thorough changes are made to new concepts to achieve cost-efficient material usage and the possibly high component integration levels, while taking into consideration the corresponding manufacturing methods as well. Specifically, the exclusion of carbon fibers and the choice of glass-fiber-reinforced PP-based FRTPs (LFTs and UD tapes) on the new concepts, together with the corresponding mass production-oriented manufacturing methods, guarantee the economy to a great extent.

The bold “LFT+UD Tape” solution for the window frame area on concept 2 in this work is a good example of the exploration of the potential of using LFTs to reach a high component integration level from the perspective of structural design. The extensive use of the IMA of MIs in the compression or injection molding process (e.g., threaded metal inserts with form-fit joining to LFTs and metal sheet inserts with the adhesion promoters) helps to achieve high component integration level with minimal addition of process steps and cost.

In this work, the whole structural development relies heavily on the FEA method, which is used to evaluate the mechanical performance and to develop, optimize, and validate the structure. The stiffness analysis results (displacement) under predefined loading cases on the steel reference door are used as the criteria for further optimization and validation of the door concepts. Since the same FE model is used for different FE solvers under different loading cases, the accuracy of the FEA modeling technique used in this work is confirmed by static door tests. The crash behavior of the door structure under side impacts is rebuilt close to the full-vehicle scenario with limited surrounding components using an innovative component development method and a corresponding test bench concept is further developed and realized virtually.

The structural design and optimization of door concepts with the FEA method is the major part of this work. The weight reduction due to the optimal material usage/distribution of LFT, UD tape, and aluminum, as well as the loading-considered construction, is realized by integrating the topology optimization with anisotropy analysis. Unnecessary iteration of topology optimization is reduced and the development process accelerated by establishing a simplified window frame calculation model that estimates the possible performance of new materials (or

material combinations) and provides a reasonable thickness range as the input for the time-consuming topology optimization.

Besides the weight reduction, six typical static loading cases, one critical crash loading case, and further manufacturing constraints (e.g., demolding direction, minimal and maximal dimensions) are considered simultaneously in the topology optimization. Complex rib structures are constructed on the preliminary concepts by properly translating the design suggestion from the topology optimization and are then further optimized by parameter optimization (e.g., rib thickness) to reach the target goal of weight reduction and mechanical performance.

With these methods, two innovative FRTP-metal multi-material door concepts are successfully developed. Both final door concepts reach a high level of component integration and achieve the target 20% weight reduction with a comparable mechanical performance under defined static and crash loading cases compared to the reference door. The variable of LFT thickness on a single component enables the local thickness optimization on ribs and base surfaces as an effective way to achieve a balance between weight and stiffness, especially for static loading cases. For the structural behavior under crash loading cases, simulations with the existing material model without defined failure criteria show good results (intrusion and intrusion velocity) under the challenging side pole impact test. However, for further development, special attention must be paid on the areas with a high risk of material failure, such as the belt area on the inner panel, which could be fatal to the passenger in a side crash accident.

The manufacturability of both door concepts, such as the optimum LFT thickness range and the feasibility of deforming, are considered during the development. However, since almost no existing LFT structural applications in similar dimensions or with such intensive rib reinforcements can be found as a manufacturing reference, only a conservative conclusion can be made that the LFT inner panel on both door concepts can be manufactured theoretically according to the standard FRTP design guideline [165] and other similar but small applications. For this reason, further optimization can be made to increase the manufacturability of LFT components, and especially rib construction. Possible methods include increasing the minimal rib distance while reducing the maximal rib height.

8.2 Outlook

The positive results from this concept design show the lightweight potential of the FRTP-metal multi-material design on vehicle doors and lay the foundation for future development related to the topics of “design for manufacturing”, prototyping, and testing.

To fully remove any doubt about the manufacturability of large LFT components with extensive rib construction (e.g., the LFT inner panel), process simulation (mold filling simulation) is the best solution. Besides proving the feasibility of the component manufacturing and suggesting mold designs, process simulation can also provide important information about the fiber orientation and distribution on the final LFT component, as this has a profound influence on the mechanical performance. Mapping the fiber information onto corresponding FE models also allows consideration of the relatively accurate anisotropic material behavior and the non-linear behavior of LFTs in structural simulations, as a prerequisite for accurate calculations of material failure behavior in simulations and of close-to-reality LFT mechanical behaviors. Future investigation should also examine the fine material modeling of LFTs, especially for crash simulations. Further specimen testing should be performed on LFTs to generate failure models that have greater accuracy, as this is crucial for correcting the unrealistic material behavior in crash simulations, such as the “rigid behavior” of rib-intensive areas observed on both concept doors.

Because of its minimal structural limitations, this FRTP-metal multi-material lightweight design approach with the two-ring load-bearing structure can be easily applied to other vehicle door models, even those with more or greater mechanical requirements (e.g., doors work as an additional load path for frontal crashes). With minor adjustments, the lightweight principle can definitely be translated to other automotive components, especially closures (e.g., engine hood, trunk lid) and other crash-related BIW components. Depending on the specific operating environment and loading situations, engineering plastics, advanced engineering plastics, and even plastic blends that have relatively better heat resistance and mechanical properties can be used as the matrix material of LFTs if the additional cost is accepted.

Looking back on the history of the material revolution in the automotive industry, the multi-material design approach could serve as the major economical lightweight method in the automotive industry for probably another several decades. However, for vehicle door structures, much research is now starting to focus on FRTP side impact beams and thermoplastic outer panels. The ongoing research, together with the work presented here, suggests that a “fully plastic” vehicle door can be expected in the near future.

9 Reference

- [1] C. Koffler & K. Rohde-Brandenburger: On the calculation of fuel savings through lightweight design in automotive life cycle assessments, In: The International Journal of Life Cycle Assessment, Vol. 15, P. 128–135, 2010
- [2] European Union: Reducing CO₂ emissions from passenger cars - before 2020, Internet Document: https://ec.europa.eu/clima/policies/transport/vehicles/cars_en#tab-0-0 (Access date 03.02.2021)
- [3] European Union: Setting CO₂ emission performance standards for new passenger cars and for new light commercial vehicles, and repealing Regulations (EC) No 443/2009 and (EU) No 510/2011, In: Official Journal of the European Union, Vol. 111, P. 13–53, 2019
- [4] R. Heuss, N. Müller, W. van Sintern, A. Starke & A. Tschiesner: Lightweight, heavy impact, McKinsey & Company, 2012
- [5] L. Patberg: Entwicklung von Karosseriestrukturen aus Faserverbundkunststoffen am Beispiel einer Nutzfahrzeug Seitentür, Dissertation, RWTH Aachen University, Aachen 2000
- [6] A. Brecher: A Safety Roadmap for Future Plastics and Composites Intensive Vehicles, NHTSA, November 2007
- [7] C.-K. Park, C.-D. Kan, W. Hollowell & S. I. Hill: Investigation of Opportunities for Lightweight Vehicles Using Advanced Plastics and Composites, NHTSA, December 2012
- [8] L. Ickert, D. Thomas, L. Eckstein & T. Tröster: Beitrag zum Fortschritt im Automobileichtbau durch belastungsgerechte Gestaltung und innovative Lösungen für lokale Verstärkungen von Fahrzeugstrukturen in Mischbauweise, FAT (Forschungsvereinigung Automobiltechnik e.V.) 2012
- [9] X. F. Fang: Fahrzeugtür in Hybridbauweise, Deutsches Patent DE 10 2021 114 962.2, 2021
- [10] P. K. Mallick (Eds.): Materials, design and manufacturing for lightweight vehicles, CRC Press, Boca Raton, Fla, Oxford 2011
- [11] M. Schemme: LFT – development status and perspectives, In: Reinforced Plastics, Vol. 52, P. 32–39, 2008
- [12] H. Schürmann: Konstruieren mit Faser-Kunststoff-Verbunden, 2., bearbeitete und erw. Aufl., Springer-Verlag Berlin Heidelberg, Berlin, Heidelberg 2007
- [13] P. K. Mallick: Fiber-reinforced composites, 3rd ed., CRC Press, Boca Raton 2008
- [14] W. Korte, S. Pazour & M. Stojek: A simple method for an appropriate simulation of short-fiber-reinforced injection molded plastics, In: LS-DYNA Forum, In: Conference Proceedings, Bamberg, October 6-8, 2014
- [15] KraussMaffei Group GmbH: Für anspruchsvolle Leichtbauteile: Faserverbundlösungen, Internet Document: <https://www.kraussmaffei.com/media/datastore/cms/media/rpm/downloads/km-br-faserverbund-de.pdf> (Access date 03.02.2021)

-
- [16] K. K. Chawla: Composite Materials, 3rd ed. 2012, Springer New York, New York, NY 2012
- [17] H. Ning, N. Lu, A. Arabi Hassen, K. Chawla, M. Selim & S. Pillay: A review of Long fibre thermoplastic (LFT) composites, In: International Materials Reviews, Vol. 65, P. 164–188, 2020
- [18] E. Bürkle, M. Sieverding & J. Mitzler: Spritzgießverarbeitung von langglasfaserverstärktem PP, In: Kunststoffe, Vol. 3, P. 47–50, 2003
- [19] Y. Kim & O. Ok Park: Effect of Fiber Length on Mechanical Properties of Injection Molded Long-Fiber-Reinforced Thermoplastics, In: Macromolecular Research, Vol. 28, P. 433–444, 2020
- [20] J. L. Thomason & M. A. Vluc: Influence of fibre length and concentration on the properties of glass fibre-reinforced polypropylene: 1. Tensile and flexural modulus, In: Composites Part A: Applied Science and Manufacturing, Vol. 27, P. 477–484, 1996
- [21] U. Vaidya: Composites for Automotive, Truck and Mass Transit, DEStech Publications, Lancaster 2010
- [22] AVK – Industrievereinigung Verstärkte Kunststoffe e.V. (Hrsg.): Handbuch Faserverbundkunststoffe, Vieweg+Teubner 2013
- [23] J. Markarian: Long fibre reinforcement drives automotive market forward, In: Plastics, Additives and Compounding, Vol. 7, P. 24–29, 2005
- [24] K. Friedrich & A. A. Almajid: Manufacturing Aspects of Advanced Polymer Composites for Automotive Applications, In: Applied Composite Materials, Vol. 20, P. 107–128, 2013
- [25] R. Leaversuch: In-Line compounding of long-glass/PP gains strength in automotive molding, Vol. 9, P. 39–40, 2001
- [26] J. Kim, S. Kim, C. Choi, T. Hwang, I. Lee & S. Park: Development of Plastic Rear Seat Cushion Frame Using PP-LFT, 2007
- [27] M. Steffens, N. Himmel & M. Maier: Design and Analysis of Discontinuous Long Fiber Reinforced Thermoplastic Structures for Car Seat Applications, Vol. 21, 1998
- [28] J. Markarian: Long fibre reinforced thermoplastics continue growth in automotive, In: Plastics, Additives and Compounding, Vol. 9, P. 20–24, 2007
- [29] W.-J. Noh, M.-H. Choi, C.-H. Choi & T.-W. Hwang: Development of Door Module Plate with Long-fiber-reinforced Thermoplastic Polypropylene, 2006
- [30] S. Vinay Seeba, S. Srikari & V. K. Banthia: Design and analysis of a plastic door module for car body application, Vol. 9, P. 1–8, 2010
- [31] K. Friedrich: Carbon fiber reinforced thermoplastic composites for future automotive applications, In: VIII International Conference on "Times of Polymers and Composites", In: Conference proceedings, Naples, Italy, June 19-23, 2016
- [32] S. Kulkarni & W. Schijve: Glass-Reinforced Thermoplastic Composites for Front End Module Applications, 2011

-
- [33] F. van Hattum & S. van Breugel: LFT: the future of reinforced thermoplastics?, In: Reinforced Plastics, Vol. 45, P. 42–44, 2001
- [34] S. Jeyanthi & J. J. Rani: Development of natural long fiber thermoplastic composites for automotive frontal beams, In: Indian Journal of Engineering & Materials Sciences, Vol. 21, P. 580–584, 2014
- [35] M. Ding, J. Liu, B. Liu, X. Wang, T. Li & D. Cao: On the Development of Automotive Composite Material Rear Bumper Beam, In: SAE-China Congress, In: Conference Proceedings: Selected Papers, 2015
- [36] L. Ramyasree, D. Venkataramanah & G. Naveen Kumar: Impact Analysis of Frontal Car Bumper using Long Fibre Reinforced Thermoplastics, In: International Journal of Current Engineering and Technology, Vol. 5, P. 1861–1865, 2015
- [37] P. Malnati: Reinforced Thermoplastics: LFRT vs. GMT, Internet Document: <https://www.compositesworld.com/articles/reinforced-thermoplastics-lfirt-vs-gmt> (Access date 04.02.2021)
- [38] C. Kuhn, I. Walter, O. Taeger & T. Osswald: Experimental and Numerical Analysis of Fiber Matrix Separation during Compression Molding of Long Fiber Reinforced Thermoplastics, In: Journal of Composites Science, Vol. 1, P. 2, 2017
- [39] N.A.: BLIC Frontverkleidung VW Golf III, Internet Document: <https://www.pkwteile.de/blic/7180137> (Access date 28.04.2021)
- [40] X. F. Fang: Faserverbundkunststoffe im Fahrzeugbau, Vorlesungsumdruck Kapitel 4 - Faser-Matrix-Halbzeuge, Siegen 2020
- [41] M. Kropka, M. Muehlbacher, T. Neumeyer & V. Altstaedt: From UD-tape to Final Part – A Comprehensive Approach Towards Thermoplastic Composites, In: Procedia CIRP, Vol. 66, P. 96–100, 2017
- [42] Dieffenbacher GmbH: Fiberforge - Tapegelege schneller fertigen, Internet Document: <https://dieffenbacher.com/de/composites/produkte/fiberforge> (Access date 05.02.2021)
- [43] I. Martin, D. Saenz del Castillo, A. Fernandez & A. Güemes: Advanced Thermoplastic Composite Manufacturing by In-Situ Consolidation: A Review, In: Journal of Composites Science, Vol. 4, P. 149, 2020
- [44] S. Baumgärtner, J. John, F. Henning, T. Huber & B. Hangs: The efficient route to tailored Organo Sheets -Producing CFRP efficiently in a vacuum using infrared radiation, In: Kunststoffe international, Vol. 10, P. 123–127, 2016
- [45] S. Schlerl, M. Cetin, C. Herrmann & M. Würtele: Continuous-fiber-reinforced parts safely in sight, In: Kunststoffe international, Vol. 3, P. 44–47, 2019
- [46] D. Bonefeld, S. Giehl, J. Haspel, A. Jäschke, R. Lahr, C. Obermann, S. Schmeer, M. Schuck & M. Würtele: Gemeinsamer Schlussbericht zum BMBF - Verbundprojekt: Kombination von Thermoplast-Spritzguss und Thermoformen kontinuierlich faserverstärkter Thermoplaste für Crashelemente (Spriform), 2011
- [47] D. Bonefeld & C. Obermann: SPRIFORM: A hybrid technique for serial production of 3D parts of continuous fiber reinforced thermoplastics, In: 15th European conference on composite materials, In: Conference Proceedings, Venice, Italy, 24-28 June 2012

-
- [48] H. Lee, M. Huh, S. Kang & S. Il Yun: Compressive behavior of automotive side impact beam with continuous glass fiber reinforced thermoplastics incorporating long fiber thermoplastics ribs, In: *Fibers and Polymers*, Vol. 18, P. 1609–1613, 2017
- [49] X. F. Fang: *Faserverbundkunststoffe im Fahrzeugbau, Vorlesungsumdruck Kapitel 8 - Fertigungsverfahren*, Siegen 2020
- [50] J. Rowe: *Advanced materials in automotive engineering*, Woodhead Publishing Ltd, Cambridge 2012
- [51] KraussMaffei Group GmbH: FiberForm - Perfekte Kombination aus Thermoformen und Spritzgießen, Internet Document: <https://www.google.com/url?sa=t&rct=j&q=&esrc=s&source=web&cd=&cad=rja&uact=8&ved=2ahUKEwiGld6HyM7uAhVDwKQKHbtXC9gQFjAAegQIBRAC&url=https%3A%2F%2Fwww.kraussmaffei.com%2Fmedia%2Fdownload%2Fcms%2Fmedia%2Fim-br-fiberform-de-17.pdf&usq=AOvVaw1poNdgptls027AOK2ud-S3> (Access date 03.02.2021)
- [52] LANXESS Deutschland GmbH: Anwendungsbeispiel: Airbaggehäuse in Composite-Sheet-Hybridtechnik, Internet Document: https://techcenter.lanxess.com/scp/emea/de/docguard/LANXESS_Durethan_DPBKV240_-_Takata_-_Airbag-Gehaeuse_-_CS_TI_2012-006_DE.pdf?docId=23296894 (Access date 03.02.2021)
- [53] W. Krause, F. Henning, S. Tröster, O. Geiger & P. Eyerer: *LFT-D – A Process Technology for Large Scale Production of Fiber Reinforced Thermoplastic Components*, Vol. 16, P. 289–302, 2003
- [54] H. Lee, M. Huh, S. Kang & S. Il Yun: Compressive behavior of automotive side impact beam with continuous glass fiber reinforced thermoplastics incorporating long fiber thermoplastics ribs, In: *Fibers and Polymers*, Vol. 18, P. 1609–1613, 2017
- [55] Dieffenbacher GmbH: *Hydraulische Pressensysteme und Direktverfahren für faserverstärkte thermoplastische und duroplastische Kunststoffe*, Internet Document: https://www.industrial-production.de/upload_weka/nwo/002/502/Dieffenbacher_2502277.pdf (Access date 03.02.2021)
- [56] N.A.: *The E-LFT process*, Internet Document: <https://en.weber-fibertech.eu/> (Access date 16.02.2021)
- [57] T. Kloska: *Leichtbaupotenziale im Fahrwerk - Multi-Material-Design durch simultane Umformung von Metallblechen und Urformung von langfaserverstärkten Thermoplasten (LFT)*, Dissertation, Universität Siegen, Siegen 2020
- [58] X. F. Fang & T. Kloska: *Hybrid forming of sheet metals with long fiber-reinforced thermoplastics (LFT) by a combined deep drawing and compression molding process*, In: *International Journal of Material Forming*, Vol. 13, P. 561–575, 2020
- [59] D. Heidrich, T. Kloska & X. F. Fang: *Abschlussbericht zum BMBF-Forschungsprojekt MultiForm*, universi - Universitätsverlag Siegen, Siegen 2019
- [60] D. Heidrich, T. Kloska & X. F. Fang: *Hybrid Forming - A Novel Manufacturing Technique for Metal-LFT Structural Parts*, In: *SAE Technical Paper*, Vol. 2020-01-0235, P. 1–10, 2020

-
- [61] D. Heidrich & X. F. Fang: Design of Automotive Structural Metal GFRP Hybrid Parts using the novel Manufacturing Technique “Hybrid forming”, In: NAFEMS World Congress 2019, In: Conference proceedings, NAFEMS, Quebec City, Canada, June 17-20, 2019
- [62] T. Kloska & X. F. Fang: Lightweight chassis components – The development of a hybrid automotive control arm from design to manufacture, In: International Journal of Automotive Technology, 2021 (To be published)
- [63] B. Klein: Leichtbau-Konstruktion, 10th ed., Springer, Berlin 2013
- [64] J. Starke: Carbon composites in automotive structural applications, In: EuCIA: Composites and Sustainability, In: Conference proceedings, Brussel, 19 March, 2016
- [65] Trinseo, Internet Document: <http://www.trinseo.com/News-And-Events/Trinseo-News/2015/May/Trinseo-Automotive-Launches-New-ENLITE-Product-Family> (Access date 11.12.2018)
- [66] Wikipedia: Sandwich material, Internet Document: <https://en.wikipedia.org/wiki/File:CompositeSandwich.png> (Access date 11.12.2018)
- [67] C. Dallner, J. Sandler, M. Hillebrecht & W. Reul: Faserverbundkonzept für ein Cabrio-Dachmodul, In: ATZproduktion, Vol. 5, P. 178–183, 2012
- [68] A. Droste, R. Janssen, P. Naughton & J. Röttger: Kunststoff-Metall- Hybridlösungen für Frontend-Modulträger., In: ATZ - Automobiltechnische Zeitschrift, Vol. 107, P. 1114–1117, 2005
- [69] H. Goldbach & J. Hoffner: Hybridbauteil in der Serienfertigung, Internet Document: https://techcenter.lanxess.com/scp/emea/de/docguard/TI_2006-003_DE_Hybridbauteile_in_der_Serienfertigung_.pdf?docId=63414 (Access date 01.06.2021)
- [70] M. Ahlers: Carbon Core - die neue BMW 7er Karosserie, In: Karosseriebautage, In: Conference proceedings, Hamburg, 2016
- [71] T. Muhr, J. Weber, A. Theobald & M. Hillebrecht: Wirtschaftliche Leichtbauweise für eine hybride B-Säule, In: ATZ - Automobiltechnische Zeitschrift, Vol. 117, P. 16–21, 2015
- [72] N.A.: Erlange Träger, Internet Document: <https://www.ikt.tf.fau.de/forschung/forschungsschwerpunkte/leichtbau-und-fvk/kunststoff-metall-hybridtechnik/> (Access date 04.02.2021)
- [73] G. W. Ehrenstein, S. Amesöder, L. Fernandez, H. Niemann & R. Deventer: Werkstoff- und prozessoptimierte Herstellung flächiger Kunststoff-Kunststoff und Kunststoff-Metall-Verbundbauteile, In: Berichts- und Industriekolloquium, In: Tagungsband: Robuste, verkürzte Prozessketten für flächige Leichtbauteile, Bamberg, October 15-16, 2003
- [74] L. Eckstein: Kunststoffe im Kraftfahrzeug - Vorlesungsumdruck, RWTH Aachen 2012
- [75] A. Jäschke & U. Dajek: Dachrahmen in Hybridbauweise, In: Sonderdruck aus VDI-Tagungsband, Vol. 4260, P. 25–45, 2004
- [76] U.S. department of transportation national highway traffic safety administration: Laboratory test procedure for FMVSS 216 Roof Crush Resistance November 16, 2006

-
- [77] A. al- Sheyyab: Light-weight hybrid structures - Process integration and optimized performance, Dissertation, Friedrich-Alexander-Universität Erlangen-Nürnberg, Erlangen 2008
- [78] T. Malek: Noch leichter, noch belastbarer, In: Plastverarbeiter, Vol. Mai, P. 38-39, 2010
- [79] N.A.: Audi Car - 2017 Audi 4 Door, Internet Document: <https://www.nicepng.com/maxp/u2e6t4t4r5u2i1t4/> (Access date 28.06.2021)
- [80] N.A.: Lamborghini Aventador LP700-4 rouge face, Internet Document: <https://www.v12-gt.com/Les-plus-belles-photos-de-GT-et-de-Classic/Photos-GT/Lamborghini/Lamborghini-Aventador-LP700-4-rouge-face-avant-portes-ouvertes> (Access date 28.06.2021)
- [81] N.A.: Fords Minivan B-Max bietet Komfort, Internet Document: <https://www.haz.de/Mehr/Auto-Verkehr/Uebersicht/Fords-Minivan-B-Max-bietet-Komfort> (Access date 28.06.2021)
- [82] N.A.: Tesla Model X, Internet Document: <https://steemit.com/introduceyourself/@yousep/sexy-tesla-model-y-2018-price-and-release-date> (Access date 28.06.2021)
- [83] E. Schulz: Türenbenchmark und Prüfstandkonstruktion, Bachelor thesis, Universität Siegen, Siegen 2013
- [84] L. Li: Entwicklung einer modularen Fahrzeugtür unter Berücksichtigung leichtbaugerechter Werkstoffe, Fügeverfahren und Integrationsmöglichkeiten, Master thesis, Universität Siegen, Siegen 2014
- [85] X. F. Fang: Kraftfahrzeugtechnik 1, Vorlesungsumdruck- Kapitel 6: Entwicklung von Türen und Klappen sowie Verglasung, Siegen 2021
- [86] E. Hilfrich, J. Maas & T. Flöth: Vergleich und Optimierung von Fahrzeugtüren Türen-Benchmark, In: ATZ - Automobiltechnische Zeitschrift, Vol. 109, P. 522–529, 2007
- [87] Porsche Engineering: ULSAC Validation Program Engineering Report, 2000
- [88] EuroNCAP: Pole side impact testing protocol, EuroNCAP, 2004
- [89] D. Wang, G. Dong, J. Zhang & S. Huang: Car side structure crashworthiness in pole and moving deformable barrier side impacts, In: Tsinghua Science and Technology, Vol. 11, P. 725–730, 2006
- [90] O. Hoffmann: Der innovative Lösungsbaukasten für die Automobilindustrie - InCar, 2009
- [91] A. Lösch, S. Drewes, I. Klüppel & L. Korves: Doors in the competition among materials, In: ATZ - Automobiltechnische Zeitschrift, Vol. 111; extra: Das InCar-Projekt von ThyssenKrupp, P. 72–83, 2009
- [92] N.A.: Audi Space Frame, Internet Document: <https://www.audi-technology-portal.de/de/karosserie/aluminiumkarosserien/audi-space-frame-asf> (Access date 16.02.2021)
- [93] P. E. Krajewski: Elevated Temperature Forming of Sheet Magnesium Alloys, In: SAE Technical Paper, Vol. 2001-01-3104, 2001

-
- [94] J. T. Carter, P. E. Krajewski & R. Verma: The hot blow forming of AZ31 Mg sheet: Formability assessment and application development, In: JOM, Vol. 60, P. 77–81, 2008
- [95] R. Verma & J. T. Carter: Quick Plastic Forming of a Decklid Inner Panel with Commercial AZ31 Magnesium Sheet, In: SAE Technical Paper, Vol. 2006-01-0525, 2006
- [96] R. Schmerberg: The aluminium hang-on parts in the new Audi Q7, In: Doors & closures in car body engineering 2015, In: Conference Proceedings, Bad Nauheim, Germany, November 17-18, 2015
- [97] A. Kirsch & R. Zimprich: New BMW 7 series door system, In: Doors & closures in car body engineering 2015, In: Conference Proceedings, Bad Nauheim, Germany, November 17-18, 2015
- [98] N. Sakamoto & T. Kawase: Doors and closures of the new Honda clarity fuel cell, In: Doors & closures in car body engineering 2016, In: Conference Proceedings, Bad Nauheim, Germany, November 15-16, 2016
- [99] L. Lckert, R. Henn, S. Gies, R. Göbbels & K. Fischer: CFK-Leichtbauteile für den Einsatz in einem Rennwagen und möglicher Einsatz in Serienfahrzeugen, In: 39. Fachtagung Prozesskette Karosserie, In: Conference Proceedings, Eisenach, Germany, 2008
- [100] M. Schulz & M. Thienel: Leicht und Modular: Ein CFK-Türsystem für den intelligenten Matrialmix, Brose Fahrzeugteile GmbH, 2012
- [101] Brose Fahrzeugteile GmbH: The future is lighter: Brose CFRP door, Internet Document: <https://www.brose.com/cz-en/press/2013/the-future-is-lighter-brose-cfrp-door.html> (Access date 07.01.2021)
- [102] M. Thienel: Organosheet - The future for Lightweight-Doors in Mass Production, In: Doors & closures in car body engineering 2015, In: Conference Proceedings, Bad Nauheim, Germany, November 17-18, 2015
- [103] M. Cetin & M. Thienel: Large-series production of thermoplastic door module carriers, In: Lightweight Design Worldwide, Vol. 12, P. 12–17, 2019
- [104] X. F. Fang & M. Grote: Development of a method for the identification and engineering design of endless fiber reinforced composites, In: International Journal of Automotive Technology, Vol. 18, P. 861–873, 2017
- [105] W. Hufenbach & F. Adam: Anwendungsperspektiven von multifunktionalen Hybridbauweisen und -komponenten im Mobilitätssektor, DLR – Wissenschaftstag 2014, Braunschweig, Germany, 2014
- [106] J. Rotheiser: Joining of plastics, 3rd ed., Hanser Publishers; Hanser Publications, Munich, Cincinnati, Ohio 2009
- [107] J. Vittinghoff & D. Drummer: Im Spritzguss stoffschlüssig verbunden, In: Adhaes Kleb Dicht, Vol. 56, P. 42–46, 2012
- [108] A. Yousefpour, M. Hojjati & J.-P. Immarigeon: Fusion Bonding/Welding of Thermoplastic Composites, In: Journal of Thermoplastic Composite Materials, Vol. 17, P. 303–341, 2004

-
- [109] T. Nguzenvo & P. Lenfeld: A review of studies on ultrasonic welding, In: International Journal of Engineering, Vol. 15, P. 81–89, 2017
- [110] J. Zhang, K.K. Chawla & U.K. Vaidya: Ultrasonic Welding of Glass Fiber Reinforced Polypropylene, In: Advanced Materials Research, Vol. 557-559, P. 1313–1316, 2012
- [111] M. Constantinou & M. Gehde: Neue Verfahrensvarianten zur Herstellung hochsteifer Hohlkörper aus Organoblechen mittels Infrarotschweißen, In: Technomer 2019: 26. Fachtagung über Verarbeitung und Anwendung von Polymeren, In: Conference proceedings, Chemnitz, November 7-8, 2019
- [112] A. Pereira da Costa, E. Cocchieri Botelho, M. Leali Costa, N. Eiji Narita & J. Ricardo Tarpani: A Review of Welding Technologies for Thermoplastic Composites in Aerospace Applications, In: J. Aerosp. Technol. Manag., Vol. 4, P. 255–265, 2012
- [113] PennEngineering: SI threaded inserts for plastics, Internet Document: https://www.pemnet.com/fastening_products/pdf/sidata.pdf (Access date 04.02.2021)
- [114] KVT: Tappex Gewindeeinsätze, Internet Document: <https://www.kvt-fastening.de/de/produkte/marken/tappex/> (Access date 04.02.2021)
- [115] M. Grujicic, V. Sellappan, M. A. Omar, N. Seyr, A. Obieglo, M. Erdmann & J. Holzleitner: An overview of the polymer-to-metal direct-adhesion hybrid technologies for load-bearing automotive components, In: Journal of Materials Processing Technology, Vol. 197, P. 363–373, 2008
- [116] K. Ramani & B. Moriarty: Thermoplastic bonding to metals via injection molding for macro-composite manufacture, In: Polymer Engineering & Science, Vol. 38, P. 870–877, 1998
- [117] K. Ramani & W. Zhao: The evolution of residual stresses in thermoplastic bonding to metals, In: International Journal of Adhesion and Adhesives, Vol. 17, P. 353–357, 1997
- [118] P. Mitschang, R. Velthuis, S. Emrich & M. Kopnarski: Induction Heated Joining of Aluminum and Carbon Fiber Reinforced Nylon 66, In: Journal of Thermoplastic Composite Materials, Vol. 22, P. 767–801, 2009
- [119] H. Paul: Bewertung von langfaserverstärkten Kunststoff-Metall-Hybridverbunden auf der Basis des Verformungs- und Versagensverhaltens, Dissertation, Karlsruher Institut für Technologie, Karlsruhe 2013
- [120] D. Flock: Wärmeleitungsfügen hybrider Kunststoff-Metall-Verbindungen, Dissertation, RWTH Aachen University, Aachen 2012
- [121] F. J. Boerio & P. Shah: Adhesion of Injection Molded PVC to Steel Substrates, In: The Journal of Adhesion, Vol. 81, P. 645–675, 2005
- [122] N. Modler, F. Adam, J. Maaß, P. Kellner, P. Knothe, M. Geuther & C. Irmiler: Intrinsic Lightweight Steel-Composite Hybrids for Structural Components, In: Materials Science Forum, Vol. 825-826, P. 401–408, 2015
- [123] K. Küsters: Hylight - Innovative Hybrid-Leichtbautechnologie für die Automobilindustrie, Hochschule trifft Mittelstand, IKV, Aachen, Germany, 2011
- [124] J. Schild: Verfahrensentwicklung zur integrierten Herstellung von Kunststoff/Metall-Strukturbauteilen im Spritzgießverfahren, Dissertation, RWTH Aachen University, Aachen 2017

-
- [125] T. Lindner, E. Saborowski, M. Scholze, B. Zillmann & T. Lampke: Thermal Spray Coatings as an Adhesion Promoter in Metal/FRP Joints, In: Metals, Vol. 8, P. 769, 2018
- [126] R. Wehmeyer: Herstellung von Kunststoff-Metall-Bauteilen mit integrierter Umformung im Spritzgießprozess, Dissertation, RWTH Aachen University, Aachen 2012
- [127] U. Kneiphoff: Gewichtsreduktion durch warm- und kaltumgeformte B-Säule, In: ATZextra-Das Projekt ThyssenKrupp InCar plus, P. 102–104, 2014
- [128] T. Gholami, J. Lescheticky & R. Passmann: Crashworthiness Simulation of Automobiles with ABAQUS / Explicit, In: ABAQUS Users' Conference, In: Conference proceeding, Munich, Germany, 2003
- [129] X. F. Fang, F. Zhang & P. Klaas: Developing a method for component design in vehicle body structure without availability of the complete vehicle data, In: NAFEMS World Congress 2015, In: Conference proceedings, NAFEMS, San Diego, USA, 2015
- [130] A. Teibinger, H. Marbler-Gores, G. Schönberger, B. Mlekusch & C. Dornberg: Methodical and integrated developing method with innovative solution strategy for virtual and real realization of concept studies, In: Graz Symposium Virtual Vehicle, In: Conference Proceedings, ViF, Graz, Austria, May, 2011
- [131] A. Teibinger: Entwicklung einer Validierungsmethode für Berechnungsmodelle hochfester Fahrzeugstrukturen, Dissertation, Technische Universität Graz, Graz 2015
- [132] F. Schmidt & M. Pitzer: Analysis of Component Based Modelling for Car Body Structures to Side Impact, In: ATZLive, P. 195–206, 2012
- [133] LSTC: LS-DYNA keyword user's manual volume I Version 971, 2007
- [134] LSTC: LS-DYNA keyword user's manual volume II material models Version 971, 2007
- [135] B. Koch, G. Knözinger, T. Pleschke & H. J. Wolf: Hybrid-Frontend als Strukturbauteil, In: Kunststoffe, P. 82–86, 1999
- [136] LANXESS Deutschland GmbH: Hybrid-Frontend Ford Focus, LANXESS Deutschland GmbH, 2008
- [137] LANXESS Deutschland GmbH: Anwendungsbeispiel Frontend in Hybridtechnik mit Organoblech, LANXESS Deutschland GmbH, 2010
- [138] I. Meskin & S. Da Costa-Pito: Composite solution for a lightweight front end module, In: ATZ Worldwide, Vol. 118, P. 52–55, 2016
- [139] ElringKlinger AG: Leichtbauteile aus Kunststoff., Internet Document: https://www.elringklinger.de/sites/default/files/brochures/downloads/elringklinger_lightweight_plastic_components_de_201708_kopierschutz.pdf (Access date 07.01.2021)
- [140] N.A.: EJOT FDS - The flow drill screw for high strength sheet metal joints, Internet Document: https://www.ejot.com/medias/sys_master/Industry_Flyer/Industry_Flyer/ha7/h33/9051736244254/EJOT-FDS-english-Flyer.pdf (Access date 04.02.2021)
- [141] N.A.: EJOT - Joining technology in multi material designs for lightweight applications, Internet Document: https://www.ejot.com/medias/sys_master/Industry_Flyer/Industry_Flyer/h24/h23/9051

- 738931230/EJOT-Multi-material-and-lightweight-design-Brochure-07.18.pdf (Access date 04.02.2021)
- [142] F. Henning: Leichtbau mit Faserverbundwerkstoffen, Vorlesungsumdruck - Kapitel 5: Fügenverfahren für den Leichtbau, KIT 2021
- [143] H. Friedrich, G. Kopp, F. Henning & A. Piller: Fügen von faserverstärkten Kunststoffen in Multi-Material-Fahrzeugsstrukturen - aktuelle Forschungsergebnisse, In: 11. Internationale AVK-Tagung, In: Conference Proceedings, DLR, Essen, Germany, September 22-23, 2008
- [144] D. Sun, P. Gumbsch, K. Steiner & D. Prätzel-Wolters: Entwicklung einer Methode zur Crashsimulation von langfaserverstärkten Thermoplast (LFT) Bauteilen auf Basis der Faserorientierung aus der Formfüllsimulation, FAT (Forschungsvereinigung Automobiltechnik e.V.) 2016
- [145] J. L. Thomason: The influence of fibre length and concentration on the properties of glass fibre reinforced polypropylene. 6. The properties of injection moulded long fibre PP at high fibre content, In: Composites Part A: Applied Science and Manufacturing, Vol. 36, P. 995–1003, 2005
- [146] J. L. Thomason: The influence of fibre length and concentration on the properties of glass fibre reinforced polypropylene: 7. Interface strength and fibre strain in injection moulded long fibre PP at high fibre content, In: Composites Part A: Applied Science and Manufacturing, Vol. 38, P. 210–216, 2007
- [147] T. P. Skourlis, S. R. Mehta, C. Chassapis & S. Manoochehri: Impact Fracture Behavior of Injection Molded Long Glass Fiber Reinforced Polypropylene, In: Polymer Engineering & Science, Vol. 38, P. 79-89, 1998
- [148] X.F. Wan, Y. Pan, X.D. Liu & Y. C. Shan: Influence of material anisotropy on long glass fiber reinforced thermoplastics composite wheel: Dynamic impact simulation, In: ASME 2015 International Mechanical Engineering Congress and Exposition, In: Conference Proceedings, Houston, Texas, U.S.A., November 13-19, 2015
- [149] M. J. Voelker: Low Temperature Impact Properties of Long Fiber Thermoplastic Composite Molding Materials, In: Polymer Composites, Vol. 12, 1991
- [150] J. L. Thomason: The influence of fibre length, diameter and concentration on the modulus of glass fibre reinforced polyamide 6,6, In: Composites Part A: Applied Science and Manufacturing, Vol. 39, P. 1732–1738, 2008
- [151] S. J.H. Kuhlman & S. I. Hill: High Strain Rate Mechanical Properties of Long Glass Fiber Filled Polypropylene and Nylon, In: SAE International 2014-01-1056, 2014
- [152] S. Duan, X. Yang & Y. Tao: Experimental study on strain-rate-dependent behavior and failure modes of long glass fiber-reinforced polypropylene composite, In: Journal of Reinforced Plastics and Composites, Vol. 34, P. 1261–1270, 2015
- [153] N.A.: Abaqus 6.13 User's Guide, Internet Document: <http://130.149.89.49:2080/v6.13/index.html> (Access date 04.02.2021)
- [154] Altair Engineering: Hyperworks 2017 - Desktop User Guides, Internet Document: https://altairhyperworks.com/hwhelp/Altair/2017/help/hwd/hwd.htm?hyperworks_desktop_applications.htm (Access date 04.02.2021)

-
- [155] L. Harzheim: Strukturoptimierung - Grundlagen und Anwendungen, 3. überarbeitete und erweiterte Auflage, Verlag Europa-Lehrmittel Nourney, Vollmer GmbH & Co. KG, Haan-Gruiten 2019
- [156] N.A.: posiwire Wegseil-Positionssensoren: WS31C, Internet Document: https://www.asm-sensor.com/files/asmTheme/pdf/asm_posiwire_ws31c_de.pdf (Access date 04.02.2021)
- [157] M. Grote: Entwicklung einer Methode zur anforderungsgerechten Werkstoffauswahl und Strukturauslegung von PKW-Karosserien im Multi-Material-Design, Dissertation, Universität Siegen, Siegen 2018
- [158] K. Durst: Beitrag zur systematischen Bewertung der Eignung anisotroper Faserverbundwerkstoffe im Fahrzeugbau, Dissertation, Universität Stuttgart, Stuttgart 2008
- [159] X. F. Fang, J. Li & S. Kurtenbach: Cost-effective body structure for an E-vehicle, In: ATZ Worldwide, Vol. 116, P. 10–15, 2014
- [160] N.A.: STABILUS: Ölhydraulische Dämpfer, Internet Document: https://www.stabilus.com/fileadmin/user_upload/04-Products/05-Dampers/stabilus_OEIhy.Daempfer_D__0408_final-komprimiert__1_.pdf (Access date 19.03.2020)
- [161] N.A.: FESTO: Pneumatischer Dämpfer, Internet Document: https://www.festo.com/cat/de_de/data/doc_de/PDF/DE/SHOCK-ABSORBER_DE.PDF (Access date 19.03.2020)
- [162] N.A.: G-M-P SHOP: Gummi Metall Puffer, Internet Document: <https://gummi-metall-puffer-shop.de/gummi-metall-puffer> (Access date 19.03.2020)
- [163] N.A.: STS Produkt-Katalog, Internet Document: <https://www.sts-schwingungstechnik.de/wp-content/uploads/katalog/2015> (Access date 19.03.2020)
- [164] United Nations: Addendum 94: Regulation No. 95 Revision 1 (ECE-95) 16.11.2011
- [165] M. Keuerleber, P. Eyerer, H. Schüle, A. Radtke, O. Altmann & W. P. Loh: Gestalten, Fügen, Berechnungsansätze und Simulation EDV-unterstützter Konstruktionen und Auslegung von Kunststoffbauteilen, In: Polymer Engineering, Springer Berlin Heidelberg, 2008
- [166] R. A. Malloy: Plastic Part Design for Injection Molding, Hanser, Carl, München 2012
- [167] X. F. Fang: Personal communication, Lehrstuhl für Fahrzeugleichtbau, 2020
- [168] O. Abdulhameed, A. Al-Ahmari, W. Ameen & S. Hammad Mian: Additive manufacturing: Challenges, trends, and applications, In: Advances in Mechanical Engineering, Vol. 11, P. 1-27, 2019
- [169] Proto3000 Inc.: FDM Nylon 12CF data sheet, Internet Document: https://proto3000.com/wp-content/uploads/2017/11/Nylon12_CF.pdf (Access date 27.04.2021)
- [170] Proto3000 Inc.: High-Performance Prototypes That Are Light-Weight And Carbon-Fiber Reinforced, Internet Document: <https://proto3000.com/materials/nylon-12cf/#performance> (Access date 27.04.2021)

-
- [171] S. Nowotny, A. Chadwick, G. Doll, O. Hellbach, S. Hümbert, L. Raps, I. Schiel & M. Simone: DLR Activities in the Field of Thermoplastic Fiber Placement and Additive Manufacturing, In: LCC-ANU Symposium, In: Conference proceeding, Munich, Germany, September 10, 2020
- [172] L. Eckstein: Structural design of vehicles, 4. edition, fka, Forschungsgesellschaft Kraftfahrwesen mbH, Aachen 2014
- [173] N.A.: High Performance Plastics, Internet Document: https://www.onlineplastics.com/products/high-performance-plastics-c-1_192.html#1-YToxOntzOjQ6lmdyaWQiO2k6MDt9 (Access date 04.02.2021)
- [174] X. F. Fang: Faserverbundkunststoffe im Fahrzeugbau, Vorlesungsumdruck Kapitel 10 - FVK in der Fahrzeugstruktur - Karosserie, Siegen 2021
- [175] P. Reithofer, B. Jilka, S. Hartmann, T. Erhart & A. Haufe: Short and long fiber reinforced thermoplastics – material models in LS-DYNA, In: 10th European LS-DYNA Conference, In: Conference proceedings, Würzburg, Germany, June 15-17, 2015
- [176] H. Zhang & M. Chen: Current recycling regulations and technologies for the typical plastic components of end-of-life passenger vehicles: a meaningful lesson for China, In: Journal of Material Cycles and Waste Management, Vol. 16, P. 187–200, 2014
- [177] G. Oliveux, L. O. Dandy & G. A. Leeke: Current status of recycling of fibre reinforced polymers: Review of technologies, reuse and resulting properties, In: Progress in Materials Science, Vol. 72, P. 61–99, 2015
- [178] G. Colucci, H. Simon, D. Roncato, B. Martorana & C. Badini: Effect of recycling on polypropylene composites reinforced with glass fibres, In: Journal of Thermoplastic Composite Materials, Vol. 30, P. 707–723, 2017
- [179] S. Das: Recycling and life cycle issues for lightweight vehicles, In: Materials, design and manufacturing for lightweight vehicles, CRC Press, 2011
- [180] P. Puri, P. Compston & V. Pantano: Life cycle assessment of Australian automotive door skins, In: The International Journal of Life Cycle Assessment, Vol. 14, P. 420–428, 2009
- [181] J. R. Duflou, Y. Deng, K. van Acker & W. Dewulf: Do fiber-reinforced polymer composites provide environmentally benign alternatives? A life-cycle-assessment-based study, In: MRS Bulletin, Vol. 37, P. 374–382, 2012

10 Appendix

10.1 Intrusion and intrusion velocity comparison of component development method

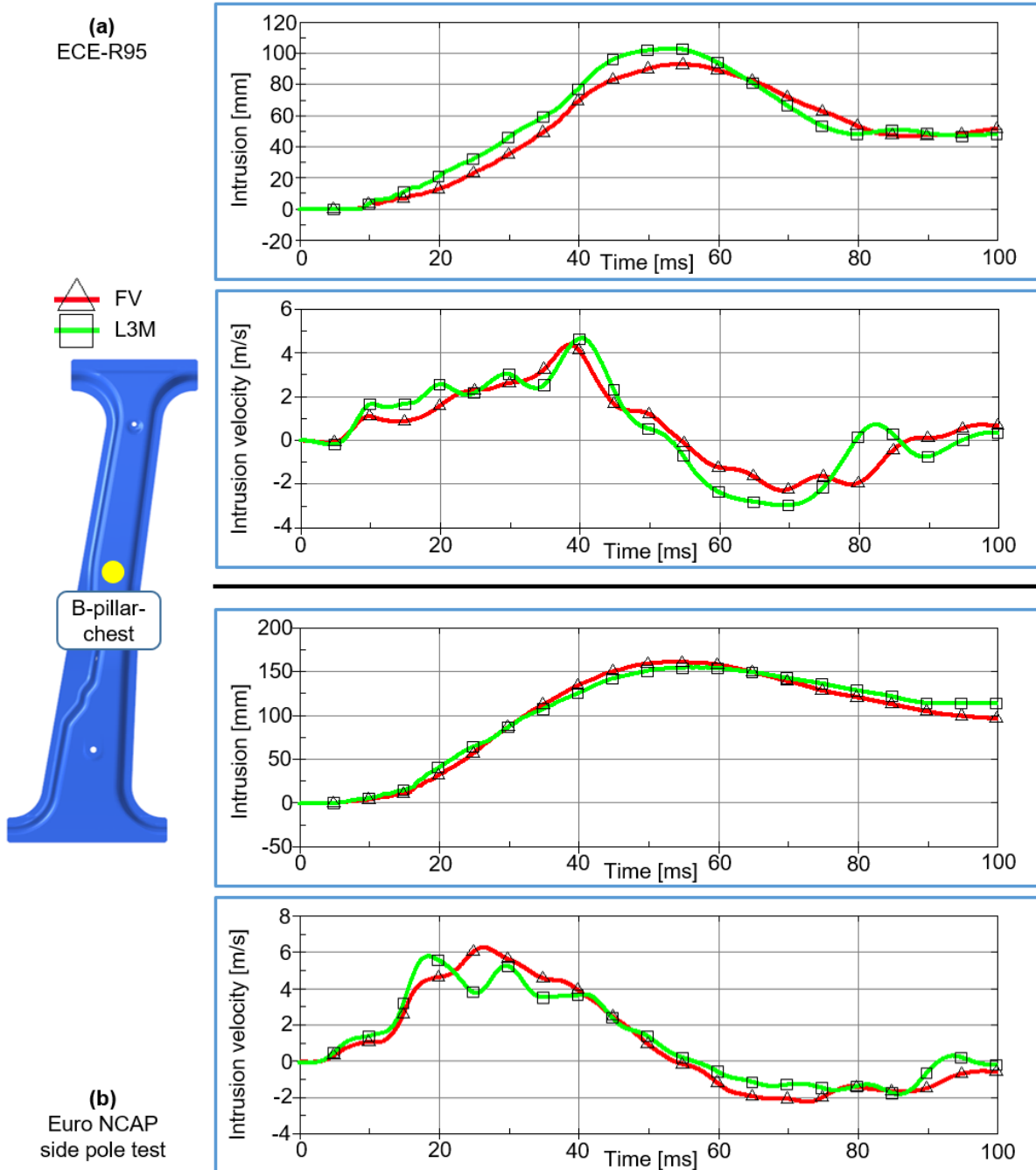


Figure 10-1 Small vehicle: the comparison of the intrusion and intrusion velocity between the full vehicle (FV) simulation and the component simulation with L3M at the measuring point "B-pillar-chest": (a) ECE-R95; (b) the Euro NCAP side pole test (version 2001)

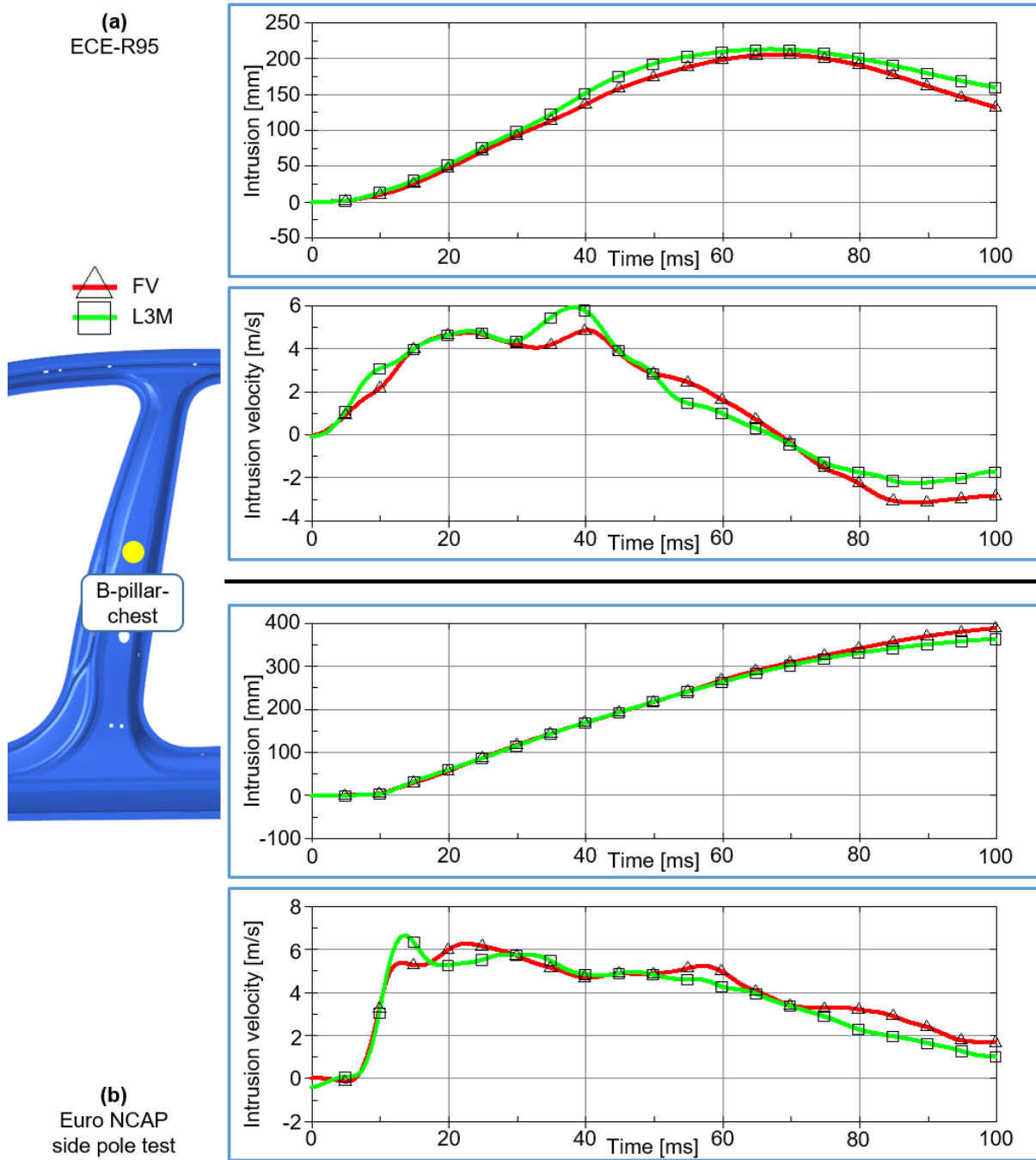










Figure 10-2 Mid-size vehicle: the comparison of the intrusion and intrusion velocity between the full vehicle (FV) simulation and the component simulation with L3M at measuring point “B-pillar-chest”: (a) ECE-R95; (b) Euro NCAP side pole test (version 2001)

10.2 Bill of material of the FLB-concept

No.	Component name	Material	Structure / Geometry
1	Door inner panel	PP-GF30	
2	Window frame 1	Aluminum (extrusion profile)	
3	Window frame connector	CFRP (Not specified)	
4	Window frame 2	Aluminum (extrusion profile)	
5	Belt reinforcement inner	Aluminum (extrusion profile)	
6	Hinge reinforcement (brick 1)	PP-GF30	
7	Hinge reinforcement (brick 2)	PP-GF30	
8	Hinge reinforcement (tube)	CFRP (Not specified)	

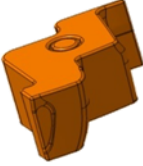

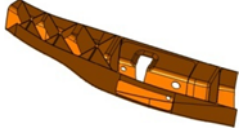


9	Hinge reinforcement (brick 3)	PP-GF30	
10	Side impact beam	Steel (DP1000, original component)	
11	Latch reinforcement (part 1)	CFRP (Not specified)	
12	Latch reinforcement (part 2)	CFRP (Not specified)	
13	Belt reinforcement outer	PP-GF30	

Table 10-1 FLB concept: bill of material (BOM)

10.3 Detail of the FE model for the crash simulation

10.3.1 Important modeling requirement for the full vehicle crash simulation

Property	Specific requirement
FE solver	<ul style="list-style-type: none"> • Ls-Dyna R 10.1.0
Element type	<ul style="list-style-type: none"> • Sheet components: Shell element • ELFORM in Ls-Dyna: 16 (fully integrated shell element (very fast))
Element size	<ul style="list-style-type: none"> • General component: 5mm • Component made of ultra-high-strength steel: 3mm
Contact	<p><u>Keywords in Ls-Dyna [133]</u></p> <ul style="list-style-type: none"> • *CONTACT_AUTOMATIC_SINGLE_SURFACE • *CONTACT_AUTOMATIC_SURFACE_TO_SURFACE
Welding	<p><u>Keywords in Ls-Dyna [133; 134]</u></p> <ul style="list-style-type: none"> • MIG welding: <ul style="list-style-type: none"> *CONSTRAINED_NODAL_RIGID_BODY • Spot welding: <ul style="list-style-type: none"> *SECTION_BEAM + *MAT_SPOTWELD + *CONTACT_SPOTWELD
Special connection	<p><u>Keywords in Ls-Dyna [133; 134]</u></p> <ul style="list-style-type: none"> • Door hinge <ol style="list-style-type: none"> 1) Hinge material: *MAT_RIGID 2) Rotation joint: *CONSTRAINED_JOINT_REVOLUTE

Table 10-2 Important modeling requirement for the crash simulation in this work

10.3.2 *Mat_24 in Ls-Dyna with the strain rate dependency

As shown in Figure 10-3, in Ls-Dyna, to active the strain-rate effect of materials, several “effective plastic strain versus yield stress” curves (also name as “flow curve”) in a strain-rate range should be given in the *Mat_24. Flow curves are achieving from material specimen testing, such as tensile tests under different speeds. Due to the difficulty of those testing, only limited flow curves can be defined. For this reason, intermediate values between flow curves are defined by the mathematic method “interpolation”. No extrapolation is applied if the strain rate value is out of the defined range. For this reason, to achieve possibly accurate crash simulation results, this range should be large enough to cover the strain rate values on most elements in chosen loading cases.

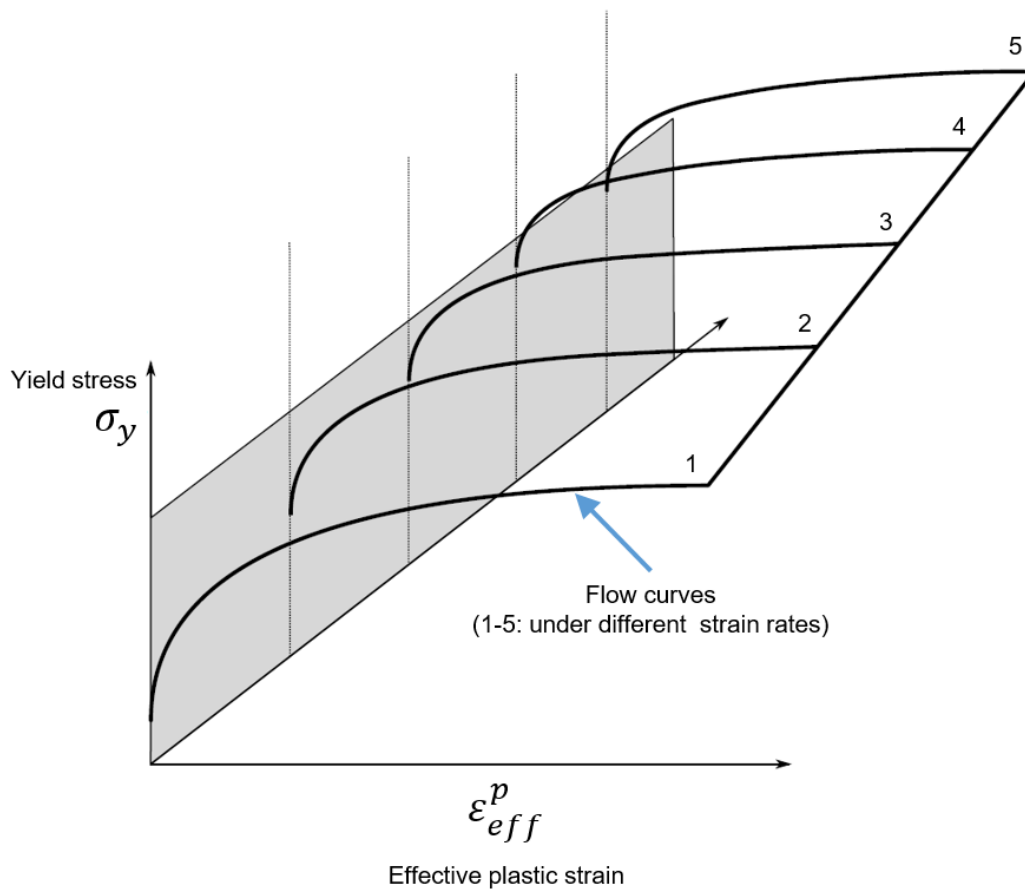


Figure 10-3 Schematic of strain-rate-dependent flow curves defined with a table in *Mat_24 (Curve 1 to 5 are flow curves under different strain rates from low to high) [134]

10.3.3 Modeling UD-Tape with *Mat_54 in Ls-Dyna

Parameter determination for UD-Tapes with *Mat_54

1) General situations and goals

- No failure criteria for the UD-Tape are planned to be considered in this work.

MID	RHO	EA	EB	EC	PRBA	PRCA	PRCB
GAB	GBC	GCA	KF	AOPT			
			A1	A2	A3	MANGLE	
V1	V2	V3	D1	D2	D3	DFAILM	DFAILS
TFAIL	ALPH	SOFT	FBRT	YCFAC	DFAILT	DFAILC	EFS
XC	XT	YC	YT	SC	CRIT	BETA	

Table 10-3 Typical parameters in *Mat_54 of Ls-Dyna [134]

2) Parameters in the green area of Table 10-3:

- Material properties related to elastic behavior
- Accurate values based on the provided data from the UD-Tape manufacturer.
- Specific values cannot be published due to the confidentiality agreement.

3) Parameters in the yellow area of Table 10-3:

- Enlarged material failure strain values were given to ensure a minimal / no failure situation on the UD Tapes based on coupon specimen tensile simulations
- Testing data related to these parameters are not available at this concept development phase.
- Specific used values in this work:

DFAILM (Maximum strain for matrix straining in tension or compression) = 0.1

DFAILS (Maximum tensorial shear strain) = 0.1

DFAILT (Maximum strain for fiber tension) = 1

DFAILC (Maximum strain for fiber compression) = -1

4) Parameters in the red area of Table 10-3:

- Enlarged material failure strength values were given to ensure a minimal / no failure situation on the UD Tapes based on coupon specimen tensile simulations
- Testing data related to these parameters are not available at this concept development phase.
- Specific used values in this work:

XC (Longitudinal compressive strength) = 0.5

XT (Longitudinal tensile strength) = 0.5

YC (Transverse compressive strength) = 0.3

YT (Transverse tensile strength) = 0.3

SC (Shear strength) = 0.3

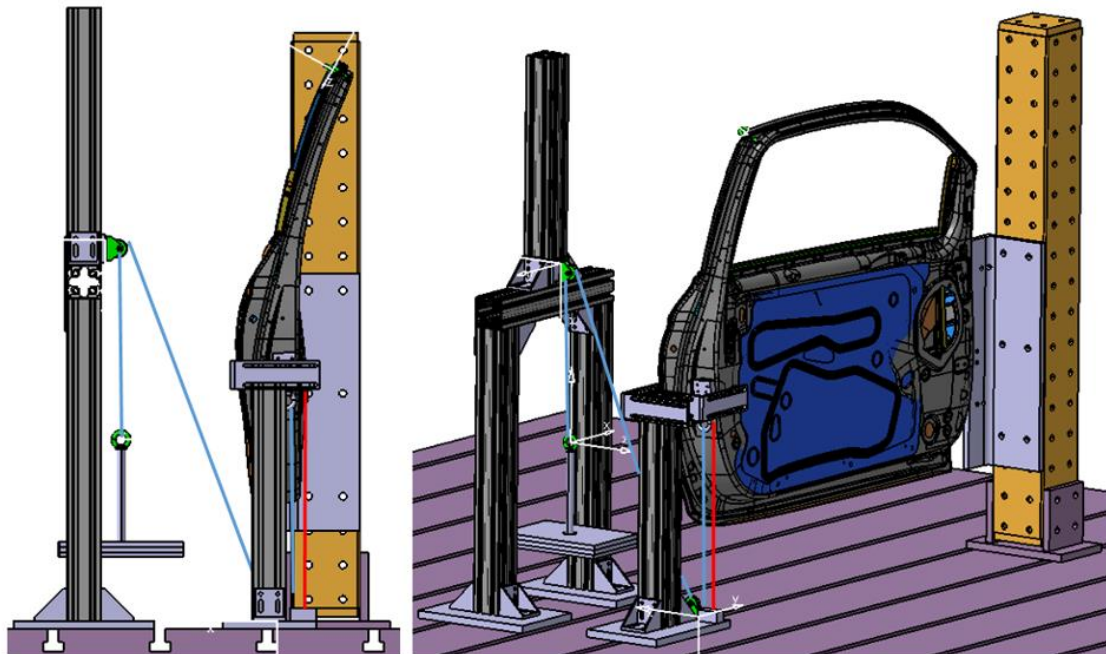
10.4 Bill of material of the reference door

No.	Name		Material	Thickness (mm)	Weight (kg)
1	Inner panel		Steel - CR	0.7	5.75
2	Outer panel		Steel - CR210	0.65	4.61
3	Frame reinforcement		Steel - CR	1	1.95
4	Mirror and upper hinge reinforcement	Sheet metal part	Steel - CR	1.5	0.6
		Reinforced plate	Steel - HR270	3.5	0.073
5	Door stopper and lower hinge reinforcement	Sheet metal part	Steel - CR	1.5	0.62
		Reinforced plate	Steel - HR270	3.5	0.073
6	Belt reinforcement outer		Steel - CR	0.65	0.864
7	Latch reinforcement		Steel - CR	1	0.046

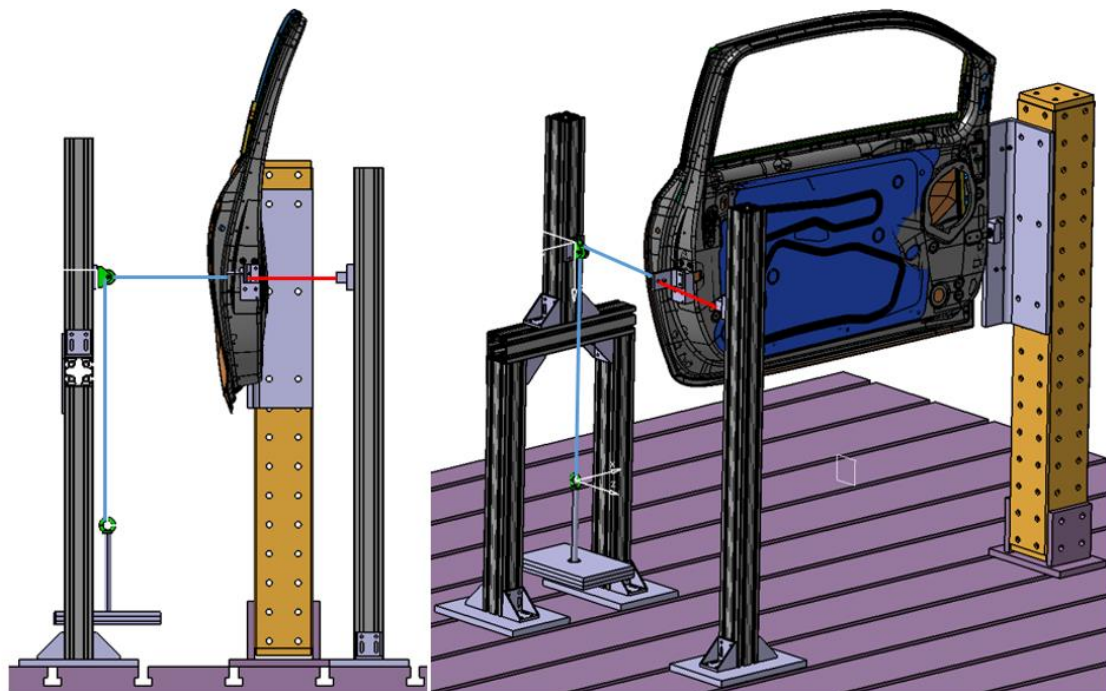
8	Side impact beam		Steel - HS1300T/950Y	1.65	1.491
9	Window guide	Rail	Steel - CR	0.8	0.221
		Connector upper	Steel - CR	0.8	0.06
		Connector bottom	Steel - CR	1.5	0.032
					Total weight: 16.39

Table 10-4 Reference door: bill of material (BOM)

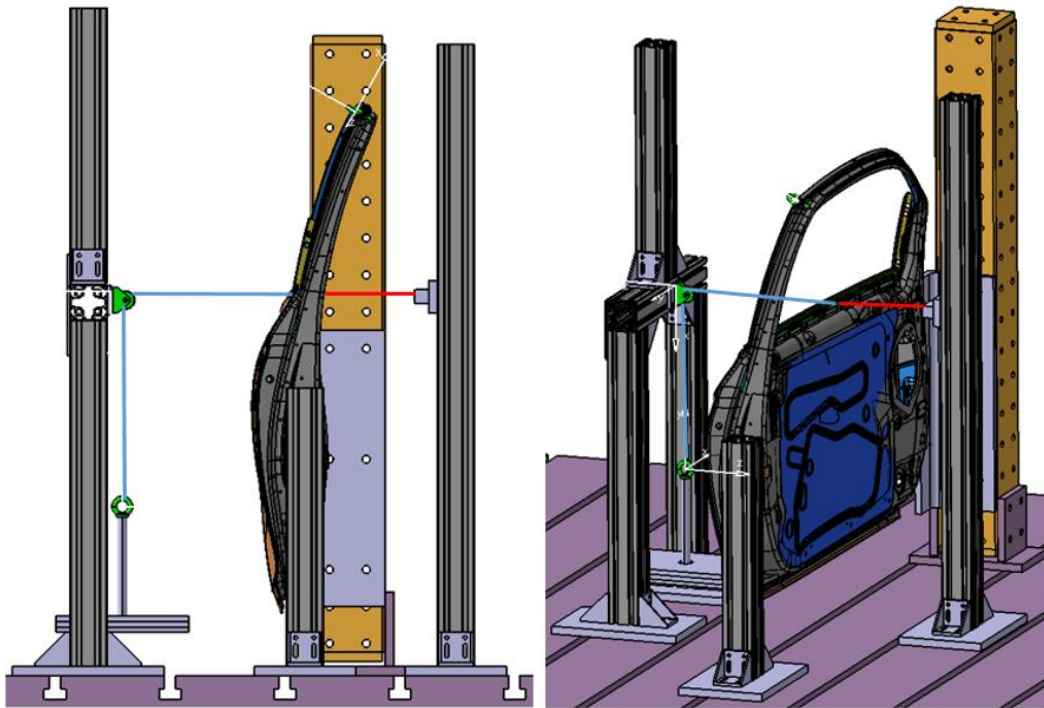
10.5 Schematics of the door static test bench (CAD)



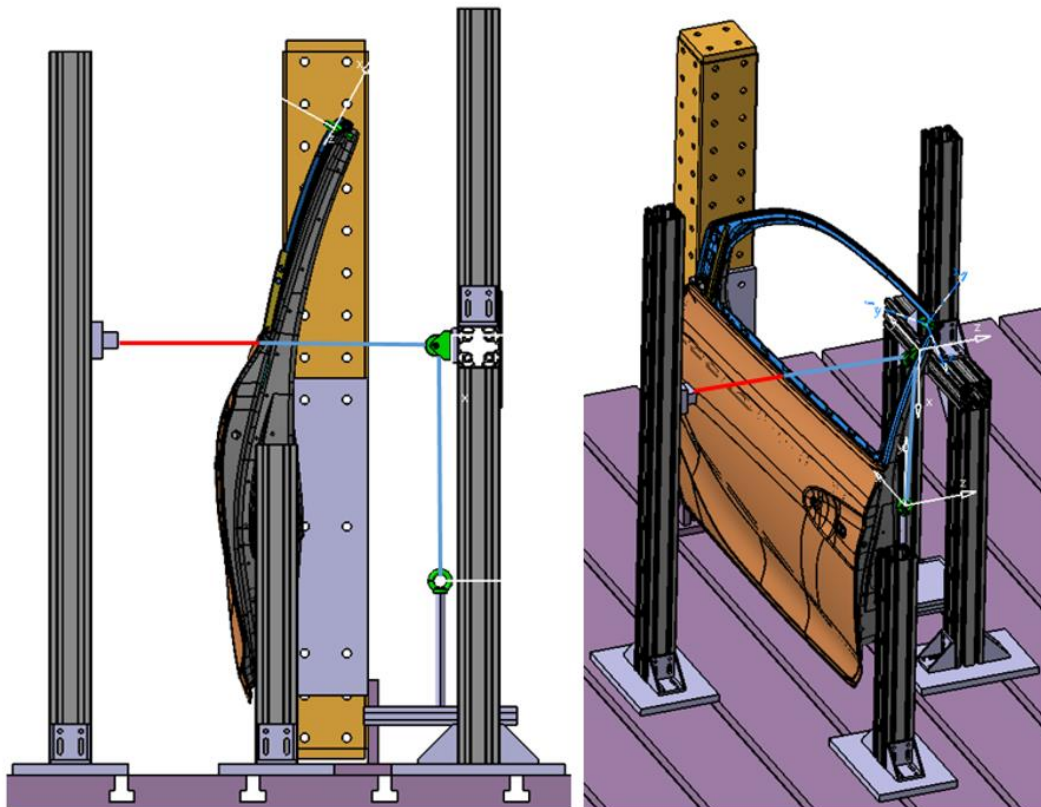
(a) Door sag



(b) Over opening



(c) Belt stiffness outer



(d) Belt stiffness inner

Figure 10-4 Schematics of door static test bench: door sag (a); over opening (b); belt stiffness outer (c); belt stiffness inner (d)

10.6 Maximal intrusion comparison between concept 1 and the reference

Maximal intrusion (mm)				
* - : concept < reference				
Measuring point number	Reference door	Concept door 1	Dif* (%)	Dif* (mm)
S1	49.5	44.1	-11%	-5.4
S2	62.6	54.3	-13%	-8.3
S3	25.5	25.9	2%	0.4
S4	22.4	21.1	-6%	-1.3
S5	19.6	21.2	8%	1.6
S6	20.6	22.2	8%	1.6
S7	28.6	29.4	3%	0.8
S8	29.1	28.5	-2%	-0.6
S9	25.1	24.6	-2%	-0.5
S10	51.4	50.5	-2%	-1
S11	75.4	71.9	-5%	-3.5
S12	142	136	-4%	-6
S13	110	121	10%	11
S14	81.3	96.2	18%	14.9

S15	80	94.2	18%	14.2
S16	74.1	88.4	19%	14.3
S17	54.3	59.7	10%	5.4
D1	67.9	76.9	13%	9
D2	86	78.7	-8%	-7.3
D3	52.3	54.1	3%	1.8
D4	46	47.7	4%	1.7
D5	43	41.6	-3%	-1.4
D6	41.7	39.5	-5%	-2.2
D7	40	42.9	7%	2.9
D8	45.6	44.7	-2%	-0.9
D9	52.1	48.3	-7%	-3.8
D10	77	79.3	3%	2.3
D11	159	165	4%	6
D12	236	270	14%	34
D13	177	201	14%	24
D14	122	147	20%	25
D15	120	143	19%	23

D16	122	138	13%	16
D17	75.4	90.9	21%	15.5
D18	167	176	5%	9
D19	168	174	4%	6
D20	84	85	1%	1
DP1	84.8	79.8	-6%	-5
DP2	202	202	0%	0
DP3	253	248	-2%	-5
DP4	270	254	-6%	-16
DP5	339	331	-2%	-8
DP6	221	252	14%	31

Table 10-5 Maximal intrusion comparison between concept 1 and the reference

10.7 Maximal intrusion comparison between concept 2 and the reference

Maximal intrusion (mm)				
* - : concept < reference				
Measuring point number	Reference door	Concept door 2	Dif* (%)	Dif* (mm)
S1	49.5	43.4	-12%	-6.1
S2	62.6	55.3	-12%	-7.3
S3	25.5	26.5	4%	1
S4	22.4	20.8	-7%	-1.6
S5	19.6	21.1	8%	1.5
S6	20.6	21.6	5%	1
S7	28.6	28.3	-1%	-0.3
S8	29.1	28.5	-2%	-0.6
S9	25.1	25.5	2%	0.4
S10	51.5	51.5	0%	0
S11	75.4	73	-3%	-2.4
S12	142	135	-5%	-7
S13	110	120	9%	10
S14	81.3	95.4	17%	14.1

S15	80	93	16%	13
S16	74.1	87.5	18%	13.4
S17	54.3	58.8	8%	4.5
D1	67.9	71.4	5%	3.5
D2	86	78.8	-8%	-7.2
D3	52.3	52.6	1%	0.3
D4	46	46.4	1%	0.4
D5	43	41.9	-3%	-1.1
D6	41.7	38.3	-8%	-3.4
D7	40	40	0%	0
D8	45.6	43.8	-4%	-1.8
D9	52.1	49.6	-5%	-2.5
D10	77	81.8	6%	4.8
D11	159	165	4%	6
D12	236	268	14%	32
D13	177	196	11%	19
D14	122	144	18%	22
D15	120	136	13%	16

D16	122	130	7%	8
D17	75.4	85.1	13%	9.7
D18	167	162	-3%	-5
D19	168	176	5%	8
D20	84	77.8	-7%	-6.2
DP1	84.8	78.8	-7%	-6
DP2	202	193	-4%	-9
DP3	253	242	-4%	-11
DP4	270	257	-5%	-13
DP5	339	331	-2%	-8
DP6	221	249	13%	28

Table 10-6 Maximal intrusion comparison between concept 2 and the reference

10.8 Door material cost calculation and comparison

Material	PP-LGF40	Steel	Aluminum	UD tapes
Cost (€/kg)	1.26	0.7	2.5	12
Estimated usage rate on door structure	90%	55%	Sheet: 55% Profile: 90% Casting: 90%	90%

Table 10-7 Raw material cost

Door type Material weight (kg)	Concept 1	Concept 2	Reference aluminum door (Sheet constructed)	Reference steel door (Sheet constructed)
PP-LGF40	6.557	7.455		
Steel	2.031	1.975		16.39
Alu (Sheet)	2.54	2.409	13.11	
Alu (Profile)	1.183	0		
Alu (Casting)	0.246	0		
UD-Tape	0.5548	1.269		
Total weight (kg)	13.11	13.11	13.11	16.39
Total material cost* (€)	34.7	40.8	59.6	20.9

*inclusive material waste

Table 10-8 Door material cost

10.9 Life cycle analysis on automotive door outer panel

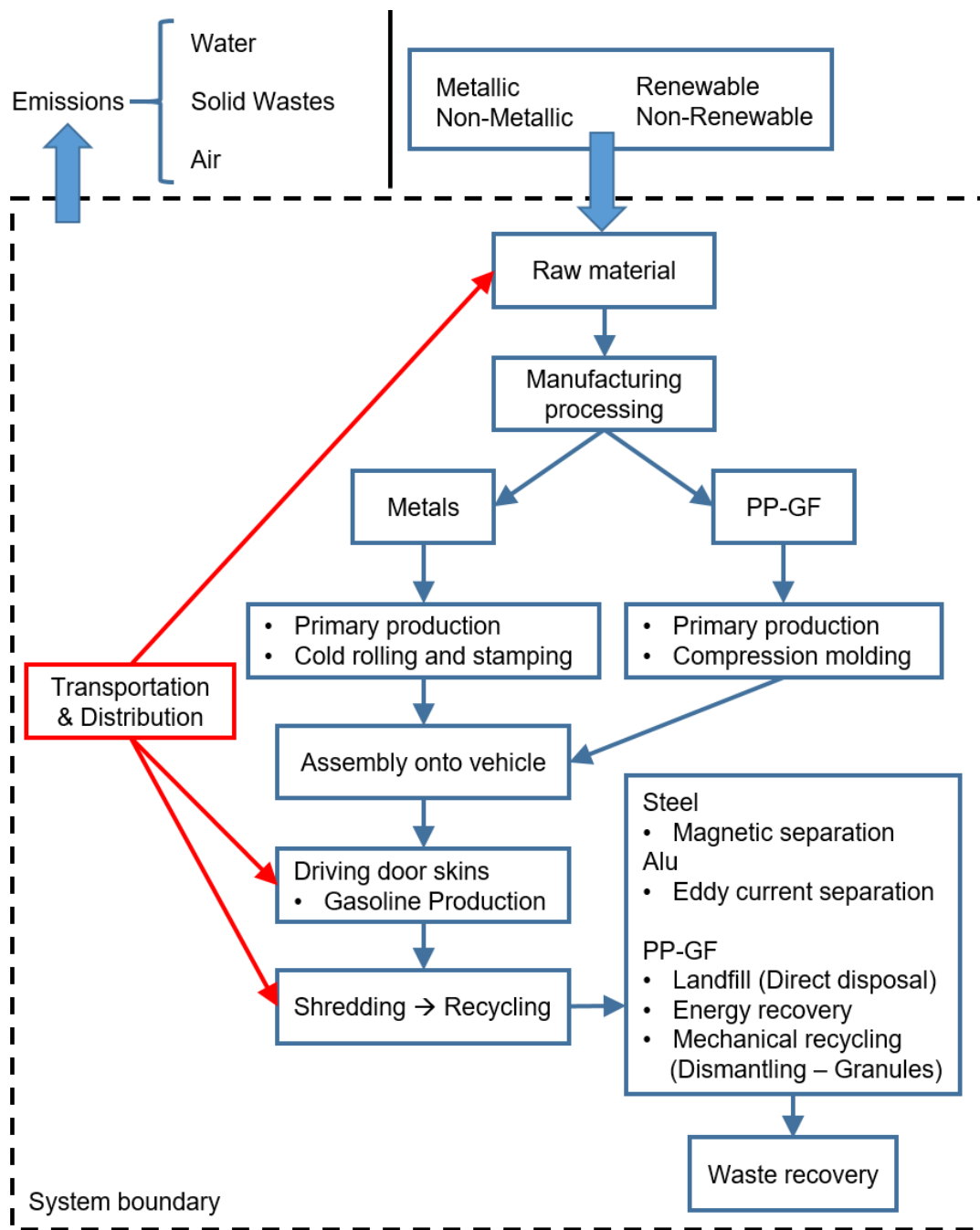


Figure 10-5 System boundary and impact categories for LCA of door outer panels [180]

Property	Steel	PP-GF
Material substitution factor	1	0.69
Mass of outer panels (4 doors) (kg)	17	11.7
Total mass of the car (kg)	1381	1376
Fuel efficiency (km/l)	11.31	11.56
Lifetime fuel consumed by car (l)	13264	12976
Lifetime fuel consumed by outer panels (l)	163	111

Table 10-9 Characteristics of door outer panels for LCA [180]

Die „Siegener Schriftenreihe Automobiltechnik“ präsentiert die Dissertationen des Lehrstuhls für Fahrzeugleichtbau (FLB) der Universität Siegen. Die Beiträge befassen sich mit der Entwicklung von Methoden und Prinzipien sowie neuen Leichtbautechnologien zur effizienten Gestaltung des Leichtbaus in Karosserie- und Fahrwerkstrukturen.

Die Reihe erscheint in unregelmäßigen Abständen.

**Mit neuen Methoden zu
leichten Lösungen**